IDENTIFICATION OF SUBSTRATE REQUIREMENTS FOR γ-SECRETASE CLEAVAGE OF THE AMYLOID PRECURSOR PROTEIN

Nadine Tamara Werner

Graduate School of Systemic Neurosciences

LMU Munich

Dissertation at the

Graduate School of Systemic Neurosciences

Ludwig-Maximilians-Universität München

February, 2022

To my parents.

Supervisor

Professor Dr. Harald Steiner

Biomedical Center (BMC), Division of Metabolic Biochemistry, Faculty of Medicine, LMU Munich, Germany

German Center for Neurodegenerative Diseases (DZNE) - Munich

First Reviewer: Prof. Dr. Harald Steiner

Second Reviewer: Prof. Dr. Moritz Rossner

External Reviewer Prof. Dr. Tobias Hartmann

Date of Submission: 20.02.2022

Date of Defense: 14.07.2022

Index

Summary

Intramembrane proteolysis is of vital importance for numerous cellular processes and its dysfunction has repeatedly been associated with various diseases, such as Alzheimer's disease (AD) and cancer. γ-Secretase is an intramembrane-cleaving protease complex involved in the production of the amyloid-β peptide (Aβ), one of the neuropathological hallmarks of AD. To date, a vast number of γ-secretase substrates have been identified with C99, the precursor of Aβ, being one of the best studied substrates. Yet, despite recent advances in the field, the factors determining substrate recognition and efficient cleavage remain largely elusive. No specific consensus sequence motif for the discrimination between substrates and non-substrates is currently known to exist. However, several lines of evidence suggested that the presence of a flexible region (e.g., a glycine-glycine (GG)-hinge motif) within the transmembrane domain (TMD) of a substrate might be critical for substrate recruitment and cleavage by γ-secretase and intramembrane proteases in general, although, conflicting data existed.

The cleavage of a γ-secretase substrate (substrate processing) can be divided into two stages: the initial cleavage and the subsequent trimming, also referred to as processivity. To illuminate the principles of substrate recognition and cleavage by γ-secretase, this thesis combined biophysical studies with biochemical data on the cleavability of various C99-based constructs. The work presented here, demonstrated that the GG-hinge motif in C99 conveys a flexibility necessary for the interaction with γ-secretase. A certain flexibility appears to be critical for the translocation from the exosites (distal binding sites) to the active site and correct positioning of the scissile bond at the active site. Indeed, the presence of a flexible motif in the N-terminal half of the TMD (TM-N) of C99 proved to be a sufficient substrate requirement for cleavage of C99 and may even be a substrate requirement for a subgroup of γ-secretase substrates. The cleavage region, in the C-terminal TMD (TM-C), turned out to be equally important for substrate cleavage by γ-secretase. It appears that specific interactions between the substrate's TM-C and the enzyme are far more important than a flexible motif in this region of C99. It is possible, that the TM-C is vital for docking of the scissile bond at the active center, as well as for the formation of a β-sheet, which has been shown to stabilize the substrate and to bring the scissile bond into position. Intriguingly, both the flexible motif and the cleavage region must cooperate to enable efficient cleavage of C99. After the initial cleavage, however, a helical TMD promoted further trimming. Altogether, these data indicate that cleavage of C99 is

determined by the presence of a flexible region in the TM-N, facilitating the translocation to the active site, and the cleavage region in the TM-C, crucial for the formation of a cleavage competent state, while a helical TMD is required for efficient trimming. Overall, this work further illuminated the principles of substrate recognition and cleavage by γ-secretase, helping to advance our understanding of the structurally and functionally most complex intramembrane protease known.

Zusammenfassung

Die Intramembranproteolyse ist für zahlreiche grundlegende zelluläre Prozesse von entscheidender Bedeutung. Eine Dysfunktion dieses Prozesses wurde bereits mehrfach mit verschiedenen Krankheiten, wie der Alzheimer-Krankheit (AK) und Krebs, in Verbindung gebracht. Die γ-Sekretase ist eine Intramembranprotease, welche an der Produktion von Aβ, Hauptbestandteil eines der neuropathologischen Merkmale der AK, beteiligt ist. Bis heute wurde eine Vielzahl von γ-Sekretase Substraten identifiziert, wobei C99, das Vorläuferprotein von Aβ, eines der am besten untersuchten Substrate darstellt. Jedoch sind, trotz der jüngsten Fortschritte auf dem Gebiet der γ-Sekretase Forschung, die Faktoren, die für die Erkennung und effiziente Spaltung der Substrate ausschlaggebend sind, nach wie vor weitgehend unbekannt. So wurde bisher kein spezifisches Erkennungsmotiv für die Unterscheidung von Substraten und Nicht-Substraten identifiziert. Diverse Hinweise deuten jedoch darauf hin, dass das Vorhandensein einer flexiblen Region (z. B.: ein Glycin-Glycin- (GG-) Scharnier-Motiv) innerhalb der Transmembrandomäne (TMD) eines Substrats entscheidend für die Spaltung durch die γ-Sekretase, und Intramembranproteasen im Allgemeinen, sein könnte. Die Datenlage bezüglich der Rolle einer flexiblen TMD für die Substratspaltung war allerdings nicht eindeutig.

Die Spaltung eines γ-Sekretase-Substrats (Prozessierung) kann in zwei Abschnitte unterteilt werden: die initiale endoproteolytische Spaltung und die anschließende carboxyterminale Spaltung. Um die Prinzipien der Substraterkennung und -spaltung durch die γ-Sekretase besser verstehen zu können, wurden in dieser Arbeit biophysikalische Analysen mit biochemischen Daten zur Spaltbarkeit verschiedener C99-basierter Konstrukte kombiniert. Die hier vorgestellten Ergebnisse machen deutlich, dass das GG-Motiv in C99 eine für die Interaktion zwischen dem Substrat und der γ-Sekretase notwendige Flexibilität vermittelt. Eine gewisse Flexibilität scheint für die Translokation von den „Exosites“ (Bindestellen abseits des aktiven Zentrums) hin zu dem aktiven Zentrum, sowie die korrekte Positionierung der zu spaltenden Peptidbindung in dem aktiven Zentrum der γ-Sekretase entscheidend zu sein. Tatsächlich erwies sich das Vorhandensein eines flexiblen Motivs in dem N-terminalen Teil der TMD (TM-N) von C99 als hinreichende Substratanforderung für die Spaltung durch die γ-Sekretase. Möglicherweise stellt ein solches Motiv sogar eine Substratanforderung für eine Untergruppe von γ-Sekretase Substraten dar. Der C-terminale Teil der Spaltregion, lokalisiert in der

C-terminalen Hälfte der TMD (TM-C), erwies sich als ebenso essenziell für die Spaltung durch die γ-Sekretase. Es scheint, dass spezifische Interaktionen zwischen dem TM-C von C99 und dem Enzym viel wichtiger sind als ein flexibles Motiv in dieser Region des Substrats. Möglicherweise ist die TM-C entscheidend für das Andocken der zu spaltenden Bindung an das aktive Zentrum, sowie für die Bildung eines β-Faltblattes, welches das Substrat stabilisiert und die zu spaltende Bindung in Position bringt. Interessanterweise war ein Zusammenspiel zwischen dem flexiblen Motiv und der natürlichen Spaltregion notwendig, um eine effiziente Spaltung von C99 zu ermöglichen. Die weitere carboxyterminale Spaltung des Substrats, die im Anschluss an die initiale Spaltung erfolgt, wurde hingegen durch eine helikale Konformation der TMD des Substrats begünstigt. Folglich wird die Spaltung von C99 durch das Vorhandensein einer flexiblen Region im TM-N, welche die Translokation zum aktiven Zentrum ermöglicht, und der natürlichen Spaltregion im TM-C, welche für die Positionierung des Substrats wichtig ist, bestimmt. Während eine helikale TMD für eine effiziente carboxyterminale Spaltung erforderlich ist. Insgesamt hat diese Arbeit dazu beigetragen, die Prinzipien der Substraterkennung und -spaltung durch die γ-Sekretase aufzuklären und unser Verständnis der strukturell und funktionell komplexesten, bekannten Intramembranprotease, voranzutreiben.

1 Introduction

1.1 Intramembrane Proteolysis

Intramembrane proteolysis is a fundamental mechanism involved in various cellular processes, including cell differentiation, neurite outgrowth, lipid metabolism and apoptosis (Wolfe, 2009, Lal and Caplan, 2011). Importantly, it has also been associated with severe diseases like Alzheimer's disease (AD), frontotemporal lobar degeneration (FTLD), Parkinson's disease (PD) and several forms of cancer (Rizzo et al., 2008, Brady et al., 2014, Sun et al., 2016). Intramembrane proteolysis typically describes the cleavage of type I and II transmembrane proteins, taking place within the hydrophobic environment of the membrane (Figure 1). This cleavage is catalyzed by so called intramembrane proteases (IMPs), polytopic membrane proteins whose active site is located in the transmembrane region (Wang et al., 2006b, Wu et al., 2006, Sun et al., 2016). Cleavage by IMPs results in the release of protein fragments and thus represents a possibility to regulate biological processes (Brown et al., 2000, Beard et al., 2019). In most cases, intramembrane proteolysis is preceded by ectodomain shedding (cleavage) of the transmembrane protein via so called sheddases (Kapeller et al., 1973, Black, 1980, Haass and Selkoe, 1993) (Figure 1).

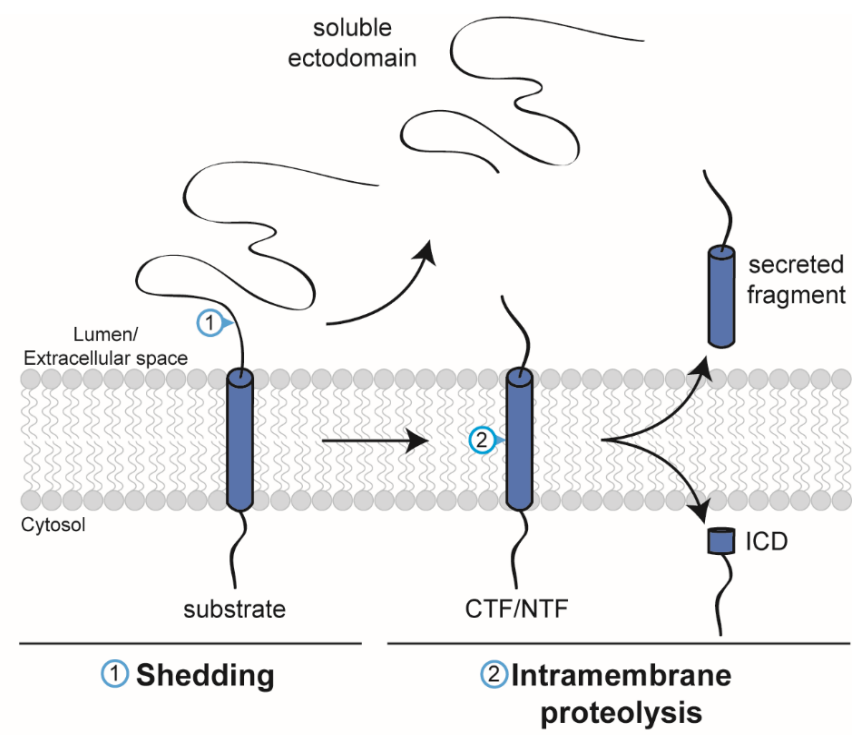

Figure 1: Intramembrane proteolysis. In a first step, a sheddase cleaves the substrate within its extracellular domain to release a soluble ectodomain (shedding). Next, the remaining membrane-bound C-terminal fragment (CTF) or N-terminal fragment (NTF) is cleaved by an intramembrane protease (IMP). This results in the generation of an intracellular domain (ICD) which is released into the cytosol and the secretion of a second fragment.

IMPs are essential for all kingdoms of life and can be divided into four families, grouped according to their catalytic mechanism (Langosch et al., 2015): aspartyl proteases (Wolfe et al., 1999, Weihofen et al., 2002), glutamyl proteases (Manolaridis et al., 2013), metalloproteases (Rawson et al., 1997), and serine (rhomboid) proteases (Urban et al., 2001). It was discovered only 25 years ago that proteolysis can also occur within the hydrophobic environment of the lipid membrane (Sakai et al., 1996). This was an entirely new and surprising concept since water is essential for the hydrolysis of a peptide bond, and it was unclear how water would reach the active site, which itself is buried in the membrane. Definite proof came from several crystal structure analyses clearly showing the active sites of IMPs deeply immersed in the lipid membrane bilayer (Wang et al., 2006b, Wu et al., 2006, Sun et al., 2016). At the same time, the structures and further biochemical experiments solved the riddle of how IMPs overcome this apparent obstacle: The active site of IMPs faces a solvent accessible cavity or a channel, thereby ensuring the availability of water for the hydrolysis (Sato et al., 2006, Tolia et al., 2006, Wang et al., 2006b, Ben-Shem et al., 2007, Feng et al., 2007, Manolaridis et al., 2013, Sun et al., 2016).

Proteolysis is an irreversible process and thus needs to be controlled. Since enzyme and substrate have to meet in order for proteolysis to occur, the proteolytic activity of IMPs is primarily regulated via the cellular localization of both, enzyme and substrate (Lee et al., 2001, Goldstein et al., 2002, Tsruya et al., 2007, Beel and Sanders, 2008, Lastun et al., 2016). The majority of substrates identified so far are single-pass type I and II membrane proteins. It seems, however, that polytopic membrane proteins may also be cleavable by IMPs (Fleig et al., 2012, Wan et al., 2012, Avci et al., 2014). The exception is the Ras and a-factor-converting enzyme 1 (Rce1), the only glutamyl protease identified so far which acts as a carboxypeptidase by removing the C-terminal anchor of CaaX (C: Cystein, a: aliphatic amino acids, X: other amino acid) proteins like Ras (rat sarcoma) (Boyartchuk et al., 1997, Hampton et al., 2018). Most strikingly, in contrast to soluble proteases most IMPs do not seem to recognize a certain substrate recognition motif, instead it was hypothesized that they might recognize a certain conformation of their substrates (Urban and Freeman, 2003, Hemming et al., 2008, Moin and Urban, 2012, Langosch et al., 2015, Langosch and Steiner, 2017). To date, the rhomboid proteases are the only IMPs for which a prevalent recognition motif has been identified (Strisovsky et al., 2009). However, this motif does not appear to be a universal requirement for all rhomboid proteases (Tatsuta et al., 2007, Strisovsky et al., 2009, Schäfer et al., 2010, Ha et

al., 2013). For the aspartyl protease signal peptide peptidase-like 3 (SPPL3) it appears that methionine or tyrosine occur frequently at the position directly N-terminal of the cleavage site (Kuhn et al., 2015). It remains unclear whether this represents a real sequence recognition motif for SPPL3 or whether certain properties of the amino acids at this position are being recognized instead (Mentrup et al., 2020).

1.1.1 The γ-Secretase Complex and its Role in Health and Disease

Structurally and functionally, γ-secretase is the most complex IMP known to date. It is an aspartyl protease comprised of four subunits (see chapter 1.1.1.1) for which no less than 149 substrates have been identified so far (Güner and Lichtenthaler, 2020). It is therefore not surprising that γ-secretase is involved in numerous biological processes, including cell fate and cell death, neurite outgrowth, synaptogenesis, as well as angiogenesis (Haapasalo and Kovacs, 2011, Jurisch-Yaksi et al., 2013). Consequently, the proper function of γ-secretase is essential during development but also in adulthood. Its involvement in development, cell differentiation and its role in cancer have made Notch-1 one of the best studied substrates of γ-secretase (Andersson et al., 2011). During Notch signaling γ-secretase cleaves Notch-1 within its transmembrane domain (TMD) to liberate the intracellular domain (NICD) into the cytosol (De Strooper et al., 1999, Steiner et al., 1999a, Okochi et al., 2002). Once released, the NICD is able to translocate to the nucleus and affect transcription of target genes (Struhl and Adachi, 1998, Schroeter et al., 1998). Abolishing γ-secretase activity in mice resulted in severe defects and has been linked to the loss of Notch-1 cleavage by γ-secretase (Shen et al., 1997, Wong et al., 1997). Some of the defects reported include severe morphological and developmental defects not just in the brain (Shen et al., 1997, Kim and Shen, 2008), problems in T- and B-cell maturation (Doerfler et al., 2001a, Hadland et al., 2001, Wong et al., 2004), as well as embryonic lethality (Shen et al., 1997, Donoviel et al., 1999).

An equally well-known substrate is the amyloid precursor protein (APP). The cleavage of APP by γ-secretase gives rise to the amyloid-β (Aβ) peptide (Golde et al., 1992, Haass et al., 1992b, Estus et al., 1992, Shoji et al., 1992, Busciglio et al., 1993, De Strooper et al., 1998, Herreman et al., 1999, Naruse et al., 1998, Herreman et al., 2000, Zhang et al., 2000) which is believed to be central to the pathogenesis of Alzheimer's disease (AD) (Hardy and Higgins, 1992, Selkoe and Hardy, 2016). Despite its involvement in pathological processes in AD, the Aβ peptide may also fulfill important physiological roles in the brain. These seem to include an antimicrobial

function (Soscia et al., 2010, Gosztyla et al., 2018), a role in the recovery from different brain injuries (Atwood et al., 2003, Brothers et al., 2018), as well as a role in the proper function of synapses (Dougherty et al., 2003, Kamenetz et al., 2003, Puzzo et al., 2011), and memory formation (Wu et al., 1995, Puzzo et al., 2008, Abramov et al., 2009). Some studies suggest that Aβ may be able to inhibit angiogenesis (Paris et al., 2004, Zhao et al., 2009). Similar to Notch, the cleavage of APP results in the release of the APP intracellular domain (AICD) (compare chapter 1.1.1.3.2). It is still under debate whether the AICD also translocates to the nucleus (Hébert et al., 2006, Müller et al., 2007) and activates transcription of several genes (Cao and Südhof, 2001, Gao and Pimplikar, 2001), including p53 (Checler et al., 2007), endothelial growth factor receptor (Zhang et al., 2007), and low-density lipoprotein-receptor related family proteins (Liu et al., 2007). Further, the AICD has been implicated in the regulation of apoptosis (Kinoshita et al., 2002, Nakayama et al., 2008, Ozaki et al., 2006) and cytoskeletal functions, like actin organization (Müller et al., 2007, Ward et al., 2010) and axonal transport (Gunawardena and Goldstein, 2001).

1.1.1.1 Assembly and Location of the γ-Secretase Complex

Initially, only presenilin (PS) has been directly associated with γ-secretase activity (Steiner et al., 1999a, Wolfe et al., 1999, Esler et al., 2000, Li et al., 2000). However, other components were soon identified (Yu et al., 2000, Francis et al., 2002, Goutte et al., 2002, Lee et al., 2002, Steiner et al., 2002) and it became clear that the active γ-secretase complex is composed of four membrane-spanning subunits: presenilin 1 or 2 (PS1 or PS2) which is the active subunit of γ-secretase (De Strooper et al., 1998, Naruse et al., 1998, Herreman et al., 1999, Steiner et al., 1999a, Wolfe et al., 1999, Herreman et al., 2000, Kimberly et al., 2000, Zhang et al., 2000), nicastrin (NCT), anterior pharynx defective-1 (APH-1), and presenilin enhancer-2 (PEN-2) (Edbauer et al., 2003, Kimberly et al., 2003, Takasugi et al., 2003). At least six distinct γ-secretase complexes co-exist in humans (Hébert et al., 2004, Shirotani et al., 2004b), as two homologous have been identified for PS (PS1 and 2) (Yu et al., 1998) and APH-1 (APH-1a and APH-1b). Additionally, two different splice variants have been found for APH-1a (APH-1a short (1aS) and long (1aL)). Independent of the different homologues and splice variants, the four subunits assemble in a 1:1:1:1 stoichiometry (Sato et al., 2007). The assembly occurs in a stepwise manner (LaVoie et al., 2003, Shirotani et al., 2004a, Capell et al., 2005, Fraering et al., 2004) and is believed to take place in the ER (Kim et al., 2004, Capell et al., 2005).

However, recent findings suggest that initial complex formation takes place in the ER but assembly is completed only after exit from the ER (Wouters et al., 2021).

The most important subunit is PS which harbors the active site, composed of two aspartate residues within its TMDs 6 and 7 (Wolfe et al., 1999, Steiner et al., 1999a, Kimberly et al., 2000) with one of its aspartate residues being part of a characteristic GxGD active site motif (Steiner et al., 2000). It seems that before the complex can become active, the catalytic component PS must undergo an endoproteolytic cleavage in the hydrophilic loop 2 between TMD6 and 7, generating the N-terminal and the C-terminal fragment of PS (PS-NTF, PS-CTF) (Thinakaran et al., 1996, Podlisny et al., 1997). This is an autocatalytic cleavage (Edbauer et al., 2003, Wolfe et al., 1999, Steiner et al., 1999a, Beher et al., 2001, Fukumori et al., 2010) occurring in a stepwise manner (Podlisny et al., 1997, Steiner et al., 1999b, Fukumori et al., 2010). After this cleavage, the newly generated fragments, the PS-NTF and -CTF, remain associated (Capell et al., 1998, Thinakaran et al., 1998, Yu et al., 1998). The subunit PEN-2 directly interacts with PS and is needed for endoproteolysis of PS, and for complex stability (Steiner et al., 2002, Takasugi et al., 2003, Luo et al., 2003, Prokop et al., 2004, Kim and Sisodia, 2005, Bammens et al., 2011). APH-1 is also necessary for assembly and stabilization of the complex (Gu et al., 2003, Takasugi et al., 2003). Whereas the largest subunit NCT was initially proposed to be a substrate receptor which actively recruits the substrate (Shah et al., 2005) it is currently believed to be more passively involved in substrate recognition and anchoring (Bolduc et al., 2016, Fukumori and Steiner, 2016, Petit et al., 2019, Zhou et al., 2019). Nevertheless, NCT has been shown to interact with the substrate (Shah et al., 2005, Fukumori and Steiner, 2016, Petit et al., 2019, Zhou et al., 2019). During the maturation of the complex, NCT is partially glycosylated in the ER and after reaching the Golgi it is further glycosylated (Yu et al., 2000, Edbauer et al., 2002, Leem et al., 2002). A complete glycosylation of NCT is discussed to be important for the activity of the γ-secretase complex (Yang et al., 2002, Shirotani et al., 2003, Moniruzzaman et al., 2018), however, this does not appear to be necessary (Herreman et al., 2003, López et al., 2015).

The fully mature and active γ-secretase complex is transported to different cellular locations. Functional sites of the γ-secretase are the plasma membrane (Kaether et al., 2002, Chyung et al., 2005) and the endosomal/lysosomal compartments of the secretory pathway (Pasternak et al., 2003, Zhang et al., 2006). Interestingly, the two PS1- and PS2-containing γ-secretase

complexes have distinct subcellular locations. While the PS1 associated complex is present at the cell surface (Kaether et al., 2002) and in the endosomal compartments (Pasternak et al., 2003), the PS2 complex, on the other hand, is preferentially located in the late endosomal/lysosomal compartments (Meckler and Checler, 2016, Sannerud et al., 2016).

1.1.1.2 Structure of the γ-Secretase Complex: the Apo- and Holo-State

The first high-resolution structure of the PS1/γ-secretase without a substrate (apo-state) permitted a first glimpse at the complex enzyme and revealed that the then identified 19 TMDs of the four subunits are arranged in a horseshoe-like shape (Lu et al., 2014). With higher-resolution structures, it became clear that the whole γ-secretase complex consists of 20 TMDs and that the two catalytic aspartates of PS are located on the convex side of the structure (Sun et al., 2015) (Figure 2). Initially, it was believed that the substrate would enter the enzyme from the cavity formed by the horseshoe-shape, the refined structure, however, suggested that the substrate accesses the active center from the convex side (Sun et al., 2015). Very interesting was also the structure of the subunit NCT. Its extracellular domain (ECD) makes up for about 94% of the entire subunit and extends out of the membrane to form a lid-like structure that covers the complex (Xie et al., 2014, Bai et al., 2015b). One group modeled the structure of PS2/γ-secretase and provided evidence that the two complexes (PS1 and PS2 containing γ-secretase) are overall very similar, except that the active site pocket seems to be expanded, which might affect the substrate specificity of the PS2 complex (Dehury et al., 2019a).

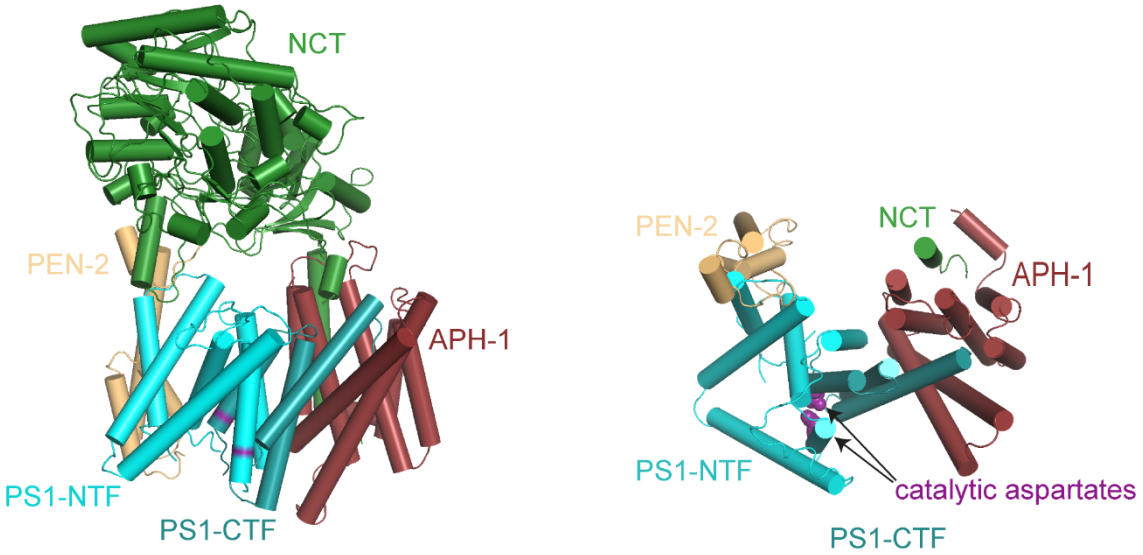

Figure 2: Cryo-EM Structure of the γ-Secretase Complex (apo-state) (PDB: 5NF3). The γ-secretase complex assumes a horseshoe-like structure (compare top view, right panel), with NCT forming a lid-like structure that covers the complex. The catalytic aspartates are located on the convex side of this horseshoe-like structure (highlighted in magenta). For better visualization, the helices of γ-secretase are depicted as cylinders (both panels), the ECD of NCT is not shown in the top view (right panel), and the sidechains of the catalytic aspartates are depicted as spheres (modified from Bai et al., 2015a).

The structures also uncovered the very dynamic nature of the γ-secretase (Li et al., 2014, Bai et al., 2015a, Elad et al., 2015). Several studies describe at least three conformational states of the complex (Escamilla-Ayala et al., 2020). It appears that the proteolytic activity depends on the conformation of the complex and certain conformations have been associated with the production of longer and more harmful Aβ species (Beher et al., 2004, Uemura et al., 2009, Wahlster et al., 2013, Elad et al., 2015, Dehury et al., 2019b). Importantly, γ-secretase inhibitors (GSIs) and modulators (GSMs) can affect the conformation of the γ-secretase and seem to favor different conformations of the complex (Lleó et al., 2004, Uemura et al., 2009, Li et al., 2014, Takeo et al., 2014, Bai et al., 2015a, Elad et al., 2015, Wang et al., 2015).

Very recently, the structures of γ-secretase in complex with either of its two most important substrates (holo-state), APP or Notch (Zhou et al., 2019, Yang et al., 2019) have been published. It is believed that both structures represent a conformation right before the cleavage of the substrate (Zhou et al., 2019). Compared to the apo-state, the binding of the substrate induced major conformational changes in the γ-secretase. The structure also revealed for the first time that the APP-based substrate C83 unfolds its C-terminal TMD (TM-C) around the initial cleavage site and the four residues downstream form a β-strand (β3). Most interestingly, this

β-strand engages with two newly formed β-strands of the PS-NTF (β1) and the PS-CTF (β2) to form a hybrid β-sheet (Figure 3). These two steps are crucial for the cleavage, since the scissile bond becomes accessible for cleavage only after the helix unfolds, while the formation of the β-sheet stabilizes the substrate and brings the scissile bond into position (Zhou et al., 2019). An interaction with another region of PS1, the PAL motif, that has already been associated with the active site conformation (Wang et al., 2004, Wang et al., 2006a, Sato et al., 2008, Tolia et al., 2008) and the activation of the catalytic site (Tolia et al., 2008), further stabilized the substrate (Zhou et al., 2019).

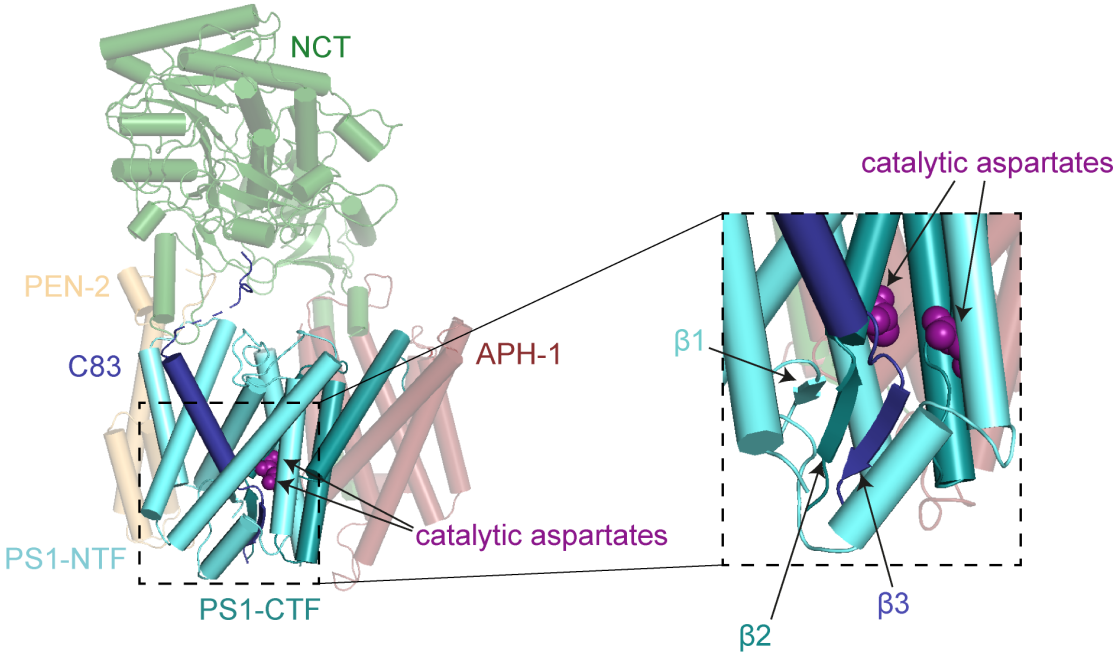

Figure 3: Cryo-EM Structure of γ-Secretase Bound to C83 (PDB: 6IYC). The left panel shows the cryo-EM structure of the γ-secretase bound to a C-terminal fragment of its substrate APP (C83) with the subunits APH-1, NCT, and PEN-2 being transparent. A zoom onto the newly formed β-sheet is depicted on the right. The β-sheet is formed by a β-strand from PS1-NTF (β1), a β-strand from PS1-CTF (β2), and a β-strand from C83 (β3). The catalytic aspartates are highlighted in magenta. For better visualization, the TMD2 of PS1-NTF is not shown here (modified from Zhou et al., 2019).

Similar to C83, an unfolding around the initial cleavage site and the formation of a β-sheet C-terminal of the cleavage region was also seen for Notch in complex with γ-secretase (Yang et al., 2019). Overall, the two structures of the γ-secretase in complex with APP or Notch were very similar and only minor differences could be identified (Zhou et al., 2019, Yang et al., 2019). However, to solve the holo-structure both studies had to introduce two changes: the substrate was covalently cross-linked to the enzyme and one of the active site aspartates has been mutated. These changes might have affected the structure and caused artefacts. Thus, the

exact structure should be interpreted with care. Recently, the same group published structures of γ-secretase in complex with GSIs and a GSM (Yang et al., 2021). The GSIs analyzed in this study occupied a very similar region which the β-strand of the substrate would occupy as well, while the GSM engaged with an allosteric site enabling it to fulfill a modulatory role rather than inhibiting γ-secretase activity (Yang et al., 2021). Overall, both, the GSIs and the GSM, induced structural changes comparable to those induced by the substrate, including the formation of the two β-strands β1 and β2 (Yang et al., 2021). For the γ-secretase structure with the GSM it needs to be considered, however, that a GSI was used to mimic a bound substrate (Yang et al., 2021).

1.1.1.3 A Key Player in Alzheimer's Disease

AD is an incurable neurodegenerative disease, first described in 1907 by Alois Alzheimer (Alzheimer, 1907). Today about 50 million people worldwide are suffering from a form of dementia and between 60 to 70% of them are affected by AD (WHO, 2020) (WHO, 2020). Patients suffering from AD develop mild memory problems that over time evolve into a massive impairment of cognitive functions (Burns et al., 1991, Morris et al., 2001, Wilson et al., 2012). γ-Secretase is a key enzyme in AD, as it cleaves APP to give rise to Aβ, a central peptide in the pathogenesis of AD (Hardy and Higgins, 1992). Since the discovery by Alzheimer in 1907, extracellular Aβ plaques (Glenner and Wong, 1984a, Glenner and Wong, 1984b, Masters et al., 1985, Hyman et al., 2012) and intracellular neurofibrillary tangles (NFTs), comprised of the Tau protein (Kidd, 1963, Terry, 1963, Kidd, 1964, Iqbal et al., 1974), are established neuropathological hallmarks of AD (Figure 4). Both are still critical for diagnosing AD (Hyman et al., 2012).

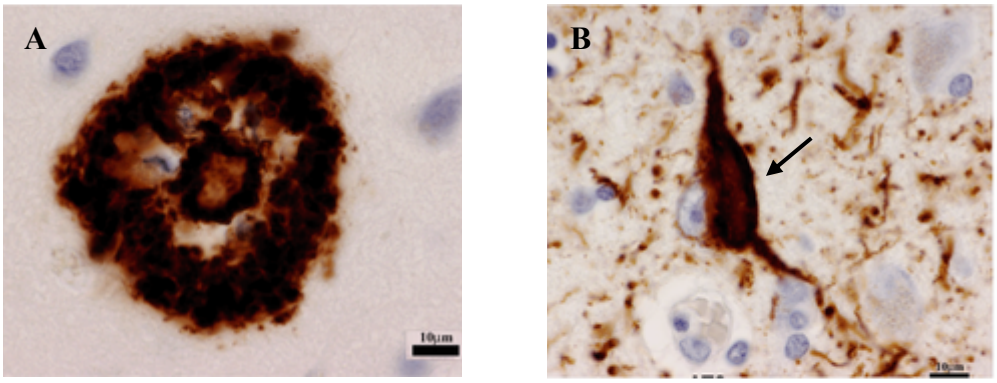

Figure 4: The two neuropathological hallmarks of AD. A: Extracellular Aβ plaque in a brain section of an AD patient stained with an antibody against Aβ. **B:** Intracellular neurofibrillary tangles (black arrow) comprised of hyperphosphorylated tau in a brain section from a patient stained with an antibody detecting hyperphosphorylated tau (from (Sengoku, 2020)).

Most of the AD cases can be attributed to the sporadic form of AD (SAD) occurring later in life, usually around an age of 65 (Terry, 1995), and accounting for about 99% of all AD cases. Only the remaining 1% is due to the genetic form of AD (FAD, familial AD) (Terry, 1995, Sims et al., 2020). The latter causing the patients to suffer from symptoms already between 30 and 60 years, or sometimes even earlier. FAD has been linked to mutations in three different genes *APP* (Chartier-Harlin et al., 1991, Goate et al., 1991, Murrell et al., 1991, Mullan et al., 1992), *PSEN1* encoding for PS1 (Sherrington et al., 1995) and *PSEN2* which encodes for PS2 (Levy-Lahad et al., 1995a, Levy-Lahad et al., 1995b, Rogaev et al., 1995). For SAD on the other hand several risk factors have been identified, with age (Brookmeyer et al., 1998, Evans et al., 1989, Lobo et al., 2000, Ossenkoppele et al., 2015), genetic factors like mutations or certain alleles (Gatz et al., 2006), and gender (Lobo et al., 2000, Chêne et al., 2015) being the main risk factors. Besides the strongest genetic risk factor Apolipoprotein E (ApoE) (Holtzman et al., 2011), many of the risk factors identified in the last few years (Hollingworth et al., 2011, Malik et al., 2015, Kunkle et al., 2019), seem to link microglia, the resident macrophages of the brain, and inflammation to AD (Hansen et al., 2018). TREM2, another well-known risk factor, enables microglia to respond to insults and change their activation status (Mazaheri et al., 2017, Gratuze et al., 2018). Activated microglia may fulfill a protective role by clearing Aβ (Frackowiak et al., 1992, Paresce et al., 1996), but constantly activated microglia might also become harmful, or dysfunctional (Long and Holtzman, 2019, Lewcock et al., 2020). However, the precise role of microglia for the pathology of AD is still not entirely resolved. Interestingly, in both forms of the disease patients present with the same disease course, and the same

neuropathological changes (Nochlin et al., 1993, Lippa et al., 1996), suggesting a common mechanism.

1.1.1.3.1 The Amyloid Cascade Hypothesis: Connecting the Two Hallmarks of AD

The most widely accepted hypothesis, linking Aβ and NFTs, and offering an explanation on how they might cause AD, is the amyloid cascade hypothesis postulated by J. A. Hardy and G. A. Higgins in 1992 (Hardy and Higgins, 1992, Selkoe and Hardy, 2016). The key player of this hypothesis is Aβ. In a healthy brain, there is a balance between the formation, a physiological process (Haass et al., 1992b, Seubert et al., 1992, Shoji et al., 1992, Haass and Selkoe, 1993), and the degradation of Aβ peptides. Whereas in AD, this homeostasis is disrupted (Hardy and Selkoe, 2002, Mawuenyega et al., 2010). If the Aβ metabolism is deregulated the Aβ peptides accumulate and form oligomers (Hardy and Selkoe, 2002), which eventually form amyloid plaques (Hardy and Allsop, 1991, Selkoe, 1991). According to the amyloid cascade hypothesis the deposition of Aβ, as well as the formation of longer Aβ peptides, are the central events in the course of the disease and a series of other events, like the formation of NFTs, vascular damage, the degeneration of neurons, and the dementia itself, are directly caused by this (Hardy and Higgins, 1992, Selkoe and Hardy, 2016). The amyloid hypothesis has not yet been definitively proven, but there is a substantial amount of good evidence. By far the most compelling argument in favor of the amyloid hypothesis comes from genetics. To date, about 223 mutations appear to be linked to AD that are located either on *APP* or on *PSEN1* and *2* (*Note: only mutations that are designated as 'likely pathogenic' or 'pathogenic' for AD (according to the Alzforum database) are included here*) (Alzforum). Interestingly, a mutation has been identified (Peacock et al., 1993) which protects against the development of AD and cognitive decline by reducing the production (Jonsson et al., 2012, Benilova et al., 2014, Maloney et al., 2014, Kimura et al., 2016) and aggregation of Aβ (Benilova et al., 2014, Maloney et al., 2014, Zheng et al., 2015). Moreover, a very recent study showed that high levels of Aβ38 in the CSF (cerebrospinal fluid) are associated with a reduced cognitive decline and a reduced risk for dementia (Cullen et al., 2021). Altogether, these and other data strongly support a central role of Aβ in the pathogenesis of AD.

Initially, it was believed that plaques are the toxic form of Aβ. However, evidence is accumulating that soluble oligomers may be the neurotoxic species (Shankar et al., 2008, Koffie et al., 2009, Esparza et al., 2013, Li and Selkoe, 2020). Interestingly, the presence of soluble

Aβ oligomers correlated more strongly with the synapse loss and disease progression than the presence of amyloid plaques (Lambert et al., 1998, Lue et al., 1999, McLean et al., 1999, Wang et al., 1999, Mc Donald et al., 2010). Nevertheless, the best correlate for cognitive decline is still the level of NFTs (Nelson et al., 2012).

1.1.1.3.2 APP and its Proteolytic Processing by γ-Secretase

APP is, like the amyloid precursor-like protein 1 and 2 (APLP1 and 2), part of the APP gene family all of which are type I membrane proteins that comprise a long glycosylated extracellular domain, a transmembrane domain (TMD), and a short cytoplasmic domain (Goldgaber et al., 1987, Kang et al., 1987, Robakis et al., 1987, Tanzi et al., 1987, Dyrks et al., 1988). The human gene encoding for APP is localized on chromosome 21 (Yoshikai et al., 1990). APP is ubiquitously expressed in the human body but most abundantly in the brain (Tanaka et al., 1989, Slunt et al., 1994, Lorent et al., 1995, Thinakaran et al., 1995). Three isoforms have been identified (APP695, APP751, and APP770), with the APP695 splice variant being the most abundant one in neurons (Tanzi et al., 1988, LeBlanc et al., 1991). After synthesis and glycosylation in the ER and the Golgi, APP is transported to the plasma membrane (PM) (Sisodia, 1992, Haass et al., 2012). Either it remains at the PM, or it is re-internalized rather rapidly via endocytosis and then resides in the endosomal compartment (Cook et al., 1997, Hartmann et al., 1997, Greenfield et al., 1999), or it is recycled back to the PM (Haass et al., 1992a, Nordstedt et al., 1993, Koo and Squazzo, 1994, Yamazaki et al., 1996).

The proteolytic processing of APP mainly involves three different enzymes, the α-, β-, and γ-secretase, and can be divided into two pathways: the non-amyloidogenic and the amyloidogenic processing pathway. The non-amyloidogenic processing pathway is the predominant pathway (Chow et al., 2010) and is initiated by the ectodomain shedding of APP via one of the α-secretases. The physiologically most relevant α-secretases are ADAM10 or ADAM17 (A Disintegrin And Metalloprotease domain family 10 or 17) (Parvathy et al., 1998, Lammich et al., 1999, Slack et al., 2001, Asai et al., 2003, Kuhn et al., 2010). This shedding event occurs after position L16 (Aβ numbering) of the Aβ domain (Esch et al., 1990), liberating the long extracellular domain sAPPα (soluble APPα) into the extracellular space (Buxbaum et al., 1998, Lammich et al., 1999). An 83 amino acid long protein, C83 or C-terminal fragment (CTFα), remains in the membrane to be further processed by γ-secretase, finally releasing the AICD and the p3 peptide (Haass et al., 1993, Gu et al., 2001, Sastre et al., 2001, Weidemann et

al., 2002) (Figure 5). As the α-secretases cleave within the Aβ domain, the non-amyloidogenic pathway prevents the formation of Aβ peptides (Esch et al., 1990, Sisodia et al., 1990). Increasing the non-amyloidogenic processing might therefore represent a way to reduce the formation of Aβ peptides (Haass et al., 2012). This strategy must, however, be treated with caution since an increased activity of ADAM10 has been shown to be involved in cancer progression in many ways (Tang, 2020).

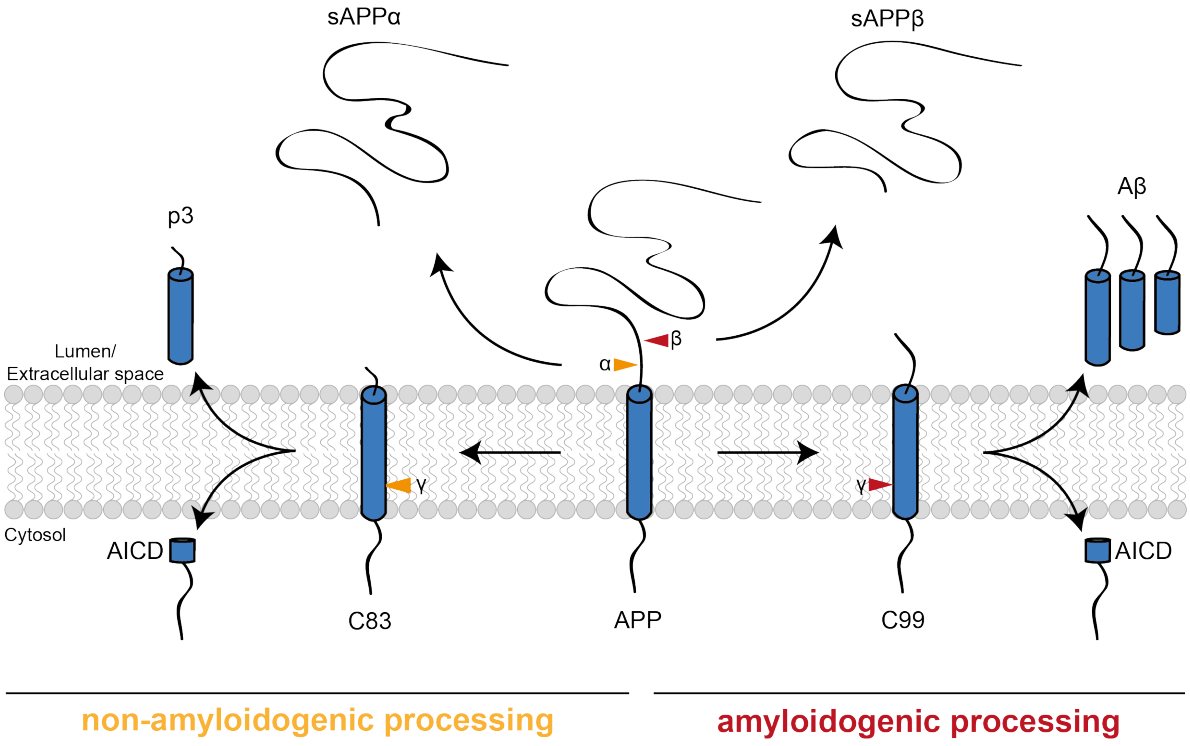

Figure 5: Proteolytic Processing of APP. The cleavage of APP can be divided in the non-amyloidogenic (orange arrowheads) and the amyloidogenic processing (red arrowheads). During the non-amyloidogenic processing, APP is cleaved first by an α-secretase (orange arrowhead labeled with 'α') which releases the soluble APPα (sAPPα). The remaining C83 fragment is subsequently cleaved by γ-secretase (γ) within its TMD, resulting in the generation of the AICD and the p3 fragment. The amyloidogenic processing, on the other hand, is initiated by the cleavage of β-secretase (β) which liberates the sAPPβ fragment. Next, the membrane bound C99 is processed by γ-secretase (γ) to generate an AICD, as well as Aβ peptides of different lengths.

The first step in the amyloidogenic processing, on the other hand, is carried out by the membrane-bound β-secretase BACE1 (β-site APP-cleaving enzyme) (Sinha et al., 1999, Vassar et al., 1999, Yan et al., 1999, Cai et al., 2001). BACE1 primarily cleaves at position D1 (Aβ numbering), releasing soluble APPβ (sAPPβ) into the extracellular space and leaving a slightly longer C99 (or CTFβ), in the membrane (Sinha et al., 1999, Vassar et al., 1999, Yan et al.,

1999). Alternatively, BACE1 can also cleave APP after position Y10 (Aβ numbering), resulting in shorter, N-terminally truncated Aβ11-x species (Haass et al., 1992b, Vassar et al., 1999). Similar to the non-amyloidogenic pathway, C99 is further processed by γ-secretase within its TMD, releasing the AICD into the cytosol and generating Aβ (Haass and Selkoe, 1993, Vassar et al., 1999) (Figure 5). This first cleavage performed by γ-secretase is also referred to as the ε-cleavage and occurs either at position 48 or 49 of the Aβ fragment (Sastre et al., 2001, Gu et al., 2001, Yu et al., 2001, Weidemann et al., 2002). Instead of releasing its substrate, however, γ-secretase carries on cleaving the still membrane-bound long Aβ fragment in a stepwise manner, trimming away small carboxyterminal peptides (Qi-Takahara et al., 2005, Takami et al., 2009, Zhao et al., 2005, Kakuda et al., 2006), and stopping only once the remaining Aβ peptide is short enough to be released from the membrane. This trimming (also referred to as processivity) usually occurs in steps of three to four amino acids resulting in the secretion of Aβ peptides ranging from 37 to 43 amino acids in length (Qi-Takahara et al., 2005, Takami et al., 2009, Zhao et al., 2004, Zhao et al., 2005). However, also longer penta- and hexa-peptides have been detected (Takami et al., 2009, Okochi et al., 2013). As the initial cleavage can occur either at position 48 or 49, two distinct Aβ product lines are formed: the major Aβ40 line (Aβ49 → Aβ46 → Aβ43 → Aβ40) and the minor Aβ42 line (Aβ48 → Aβ45 → Aβ42 → Aβ38), both named after their main product (Qi-Takahara et al., 2005) (Figure 6). Additionally, product line crossing can occur as well (Okochi et al., 2013, Matsumura et al., 2014, Olsson et al., 2014) resulting in a rather complex scheme of possible cleavages.

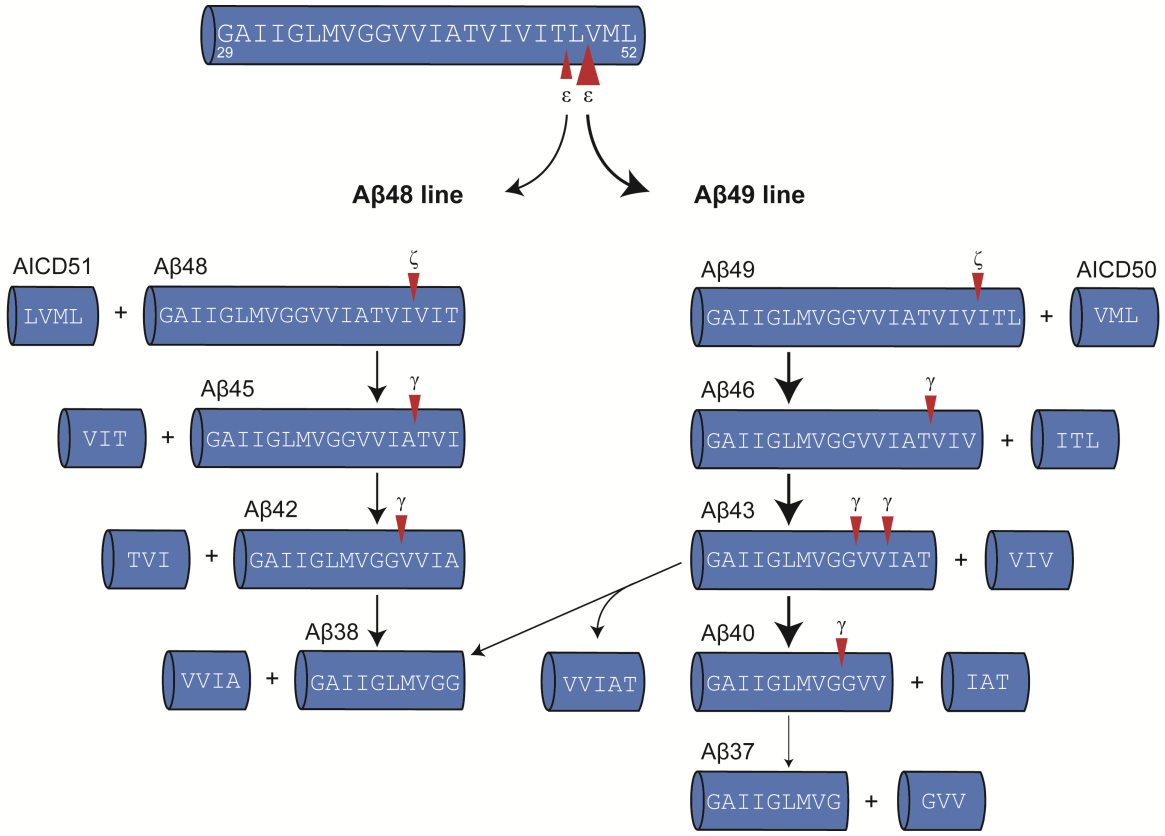

Figure 6: The Sequential Cleavage of the APP TMD by γ-Secretase. This graphic shows only the TMD of APP (from G29 until L52) and the resulting cleavage products. Initially, cleavage by γ-secretase releases an AICD and generates a membrane-bound Aβ. This ε-cleavage can take place either at T48 or at L49, resulting in the generation of two distinct Aβ product lines: the minor Aβ48 line and the major Aβ49 line. The major product line generates mainly Aβ40 via consecutive cleavage at position 49 (ε-site), 46 (ζ-site), and 43 (γ-site). The main product of the Aβ48 line is Aβ42, resulting from stepwise cleavage at 48 (ε-site) and 45 (ζ-site). The red arrowheads mark the exact cleavage sites, while the thickness of the black arrows reflects the frequency of cleavage site usage.

Accounting for about 80-90% of all the Aβ peptides produced, Aβ40 represents the major species, alongside only minor amounts of Aβ42 (10%) and Aβ38 (10%). Even lower amounts are produced of Aβ37 and Aβ43, with about only 1% each, or even less. Whilst not being the major product, Aβ42 is the main component of amyloid plaques (Iwatsubo et al., 1994). Its two additional amino acids render the Aβ42 peptide more hydrophobic than the shorter Aβ40. Therefore, it has a stronger tendency to form oligomers and is believed to be a highly pathogenic species (Jarrett et al., 1993, Iwatsubo et al., 1994, Suzuki et al., 1994, Mucke et al., 2000, Haass and Selkoe, 2007). Although neglected in many studies, several findings suggest a similar pathogenic role for Aβ43, as it too is a major component of amyloid plaques (Iwatsubo et al., 1994, Welander et al., 2009, Saito et al., 2011, Kretner et al., 2016, Jakel et al., 2019). It is now

widely believed that Aβ42 and Aβ43 are the pathologically relevant species in AD (Jarrett et al., 1993, Mucke et al., 2000, Saito et al., 2011). It was hypothesized that also longer Aβ species (Aβ45 and longer), are potentially pathogenic (Qi-Takahara et al., 2005, Devkota et al., 2021), however, further investigations are needed to clarify the role of such longer species. Nevertheless, it appears that an impaired processing or an insufficient degradation of the Aβ peptides are relevant for the pathogenesis of AD, as this increases the relative amounts of longer and potentially more pathogenic Aβ species. In line with this, 19 mutations have already been identified in the *APP* gene that have been linked to FAD (Alzforum), all affecting the generation of Aβ and its properties. In principle, APP FAD mutations can be divided into three groups: mutations at or around the BACE1 cleavage site which result in elevated levels of Aβ (Citron et al., 1992, Mullan et al., 1992, Haass et al., 1995, Di Fede et al., 2009, Kimura et al., 2016), two of these mutations also affect the aggregation properties of Aβ (Murray et al., 2016), and mutations at γ-secretase cleavage sites increase the relative amounts of longer and more aggregation prone Aβ species (Iwatsubo et al., 1994, Tamaoka et al., 1994, Suzuki et al., 1994, Scheuner et al., 1996, Weggen and Beher, 2012), while mutations within the Aβ sequence change the aggregation properties of Aβ (Nilsberth et al., 2001, Hori et al., 2007, Selkoe and Hardy, 2016, Hatami et al., 2017).

The processing of APP is regulated via the cellular localization of the substrate and the enzyme. APP and γ-secretase are both located at the PM and in the endosomal/lysosomal compartment (Sisodia, 1992, Cook et al., 1997, Hartmann et al., 1997, Greenfield et al., 1999, Kaether et al., 2002, Pasternak et al., 2003, Chyung et al., 2005, Lichtenthaler et al., 2011, Haass et al., 2012). As also ADAMs localize to the PM, the non-amyloidogenic processing mainly occurs at the surface of the cell (Sisodia, 1992, Haass et al., 2012, Ikezu et al., 1998, Lammich et al., 1999), but also the trans-Golgi network is involved (Sambamurti et al., 1992, Golde et al., 1992, De Strooper et al., 1993, Kuentzel et al., 1993, Tomita et al., 1998). BACE1 on the other hand, is predominantly found in the endosomal compartment (Vassar et al., 1999) and the amyloidogenic processing primarily occurs within the endosomal/lysosomal system (Golde et al., 1992, Haass et al., 1992a, Koo and Squazzo, 1994) and at the PM (Haass et al., 1993, Chyung and Selkoe, 2003, Kaether et al., 2006).

1.1.1.3.3 Therapy Strategies for AD: Targeting γ-Secretase Activity

Despite the enormous progress that has been made in the field, unfortunately no cure is available to date. The current therapies are only symptomatic treatments, utilizing acetylcholinesterase inhibitors and NMDA receptor antagonists aiming to slow down or delay the cognitive decline and antidepressants as well as antipsychotics to reduce psychological and behavioral symptoms. However, they are not able to stop the disease progression. Nevertheless, a wide range of potentially disease-modifying approaches, targeting Aβ, and inflammation via different β- and γ-secretase inhibitors or antibodies, have been and still are being tested (Cummings et al., 2019, Long and Holtzman, 2019). Many therapy strategies target the production, accumulation, and deposition of Aβ (Aβ targeting therapies) and aim to slow down or even stop the disease progression (Panza et al., 2019). However, most drug candidates developed in the past have failed (Cummings et al., 2014). This was the case for initial strategies trying to influence the production of Aβ peptides via the inhibition of γ-secretase (Wolfe et al., 1998, Siemers et al., 2006, Galasko et al., 2007, Siemers et al., 2007), which had to be discontinued due to severe side effects (Doody et al., 2013, Coric et al., 2015). The majority of the observed side effects, caused by such GSIs, are believed to be due to the inhibition of the Notch signaling (Doerfler et al., 2001b, Hadland et al., 2001, Geling et al., 2002, Wong et al., 2004). This was the starting point for the development of GSMs. Instead of inhibiting γ-secretase activity, these drugs enhance the carboxyterminal trimming activity of γ-secretase (Weggen et al., 2001, Weggen et al., 2003a, Weggen et al., 2003b). Thus, GSMs lower the generation of the longer and potentially more toxic Aβ42 species and of the Aβ40 species, while increasing the levels of the shorter species (Aβ37 and Aβ38) (Weggen et al., 2001, Crump et al., 2013). They act only on the trimming of APP, without affecting the initial ε-cleavage of γ-secretase substrates (Weggen et al., 2003a, Kounnas et al., 2010, Crump et al., 2013, Dimitrov et al., 2013). Shorter species, like Aβ38, seem to be non-toxic and might even be protective (Moore et al., 2017). Further, GSMs have been shown to influence the conformation of PS (Lleó et al., 2004, Takeo et al., 2014) and increase the stability of the enzyme-substrate-complex (Szaruga et al., 2017). This might explain the prolonged residence time of Aβ42 at the enzyme (Okochi et al., 2013) and the consequently increased production of shorter Aβ species observed with GSMs. A positive effect of GSMs on Aβ pathology and cognition has already been demonstrated in mice (Imbimbo et al., 2010, Mitani et al., 2012, Rogers et al., 2012). Moreover, a reduction of Aβ40 and/or Aβ42 paired with an increase in shorter species (Aβ37 and Aβ38) could be demonstrated

in mice and rats (Rynearson et al., 2021), as well as in healthy human individuals (Yu et al., 2014, Toyn et al., 2016) supporting the potential of GSMs as a therapy strategy (Cullen et al., 2021). Some GSMs still need some refinement to be used safely to treat patients with AD (Bursavich et al., 2016). However, the GSM (compound 2) recently presented by Rynearson and colleagues appears to be a more promising candidate (Rynearson et al., 2021). Thus, GSMs still represent a promising therapy option for patients suffering from FAD as well as SAD (Long and Holtzman, 2019, Trambauer et al., 2020, Cullen et al., 2021). New hope also arises from the recent approval of the first Aβ-targeting therapy based on the Aβ-directed antibody aducanumab (FDA, 2021).

1.1.1.4 Substrate Recruitment and Processing by γ-Secretase

Substrate recruitment and processing by γ-secretase is rather complex and involves multiple steps (Figure 7). First, a putative substrate needs to be recognized as such. As shown for C99, the substrate binds first to so called exosites, these are binding sites distal from the active site. Subsequently, the substrate has to translocate from one exosite to another, as the γ-secretase features several exosites (Esler et al., 2002, Tian et al., 2002, Beher et al., 2003, Kornilova et al., 2005, Fukumori and Steiner, 2016). Until the substrate can finally access the active site for cleavage both, the enzyme and the substrate, undergo a conformational change (Li et al., 2014, Scharnagl et al., 2014, Bai et al., 2015b, Bai et al., 2015a, Langosch et al., 2015, Fukumori and Steiner, 2016, Zhou et al., 2019, Yang et al., 2019). It was hypothesized that a certain flexibility of the substrate is required for it to reach the active site of the γ-secretase complex (Tian et al., 2002, Scharnagl et al., 2014, Langosch et al., 2015, Stelzer et al., 2016). Once at the active site, the substrate is finally cleaved. Interestingly, after this initial cleavage, γ-secretase carries on cleaving the substrate repeatedly in a consecutive fashion (Okochi et al., 2006, Yanagida et al., 2009, Fukumori et al., 2010, Ran et al., 2017) and only then the products are released.

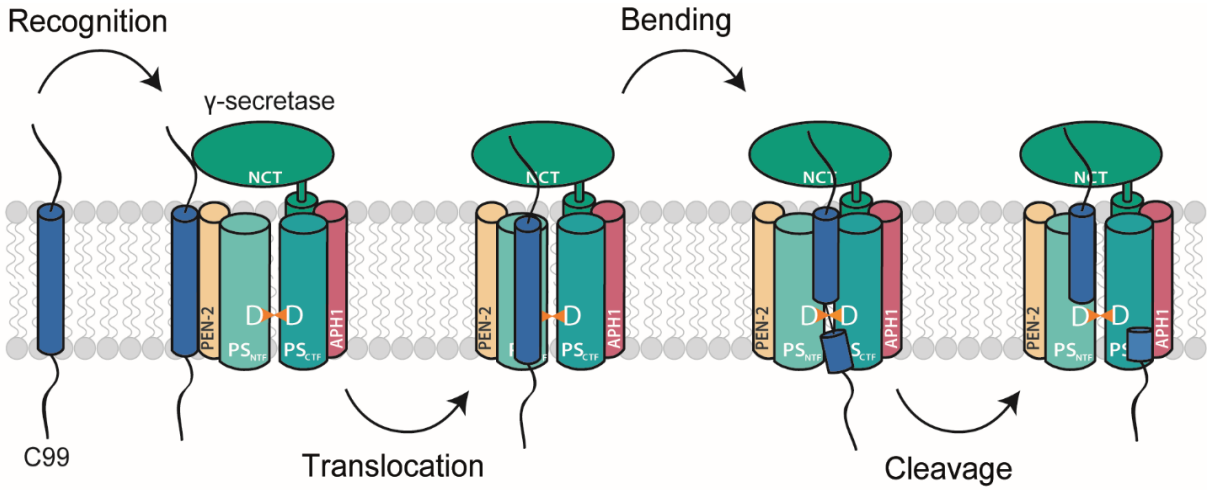

Figure 7: Recruitment and Processing of C99 is a Stepwise Mechanism. Initially, C99 needs to be recognized as a substrate by the γ-secretase complex. Next, it binds to an exosite (distal binding site) and further translocates from one exosite to the another. In order to enter the active site, C99 has to undergo a conformational change, possibly by bending its TMD. Once it has reached the active site, C99 is cleaved by γ-secretase. The catalytic aspartates are depicted as orange arrowheads.

1.1.1.4.1 Recognition and Translocation to the Active Site

Until today, already 149 proteins have been identified as substrates of the γ-secretase (Güner and Lichtenthaler, 2020). However, no specific consensus sequence motifs have been discovered for the discrimination between substrates and non-substrates so far (Beel and Sanders, 2008). Despite our knowledge about the structure of the γ-secretase complex, the mechanism by which it recognizes its substrates remains largely elusive. Only a few general substrate requirements have been established. Typically, γ-secretase substrates are type I membrane proteins (Xia and Wolfe, 2003) with a short ectodomain (ECD), which is either naturally short or a result of prior shedding by α- or β-secretases (Struhl and Adachi, 2000, Hemming et al., 2008, Laurent et al., 2015, Bolduc et al., 2016). Additionally, they feature a permissive transmembrane and intracellular domain (Hemming et al., 2008).

The N-terminal region of γ-secretase substrates, the ECD, has been implicated in substrate recognition and recruitment (Zhang et al., 2002, Ren et al., 2007, Kukar et al., 2011, Xu et al., 2016). While the ECD of C99, especially two amino acids within this region, S26 and K28 (Aβ numbering), have been shown to affect the cleavage specificity and processivity of γ-secretase (Ren et al., 2007, Page et al., 2010, Kukar et al., 2011, Ousson et al., 2013, Jung et al., 2014, Petit et al., 2019). Further, the substrate's TMD, as well as the intracellular domain (ICD) are

important for the recognition of a substrate (Hemming et al., 2008, Fukumori and Steiner, 2016). The length of the ECD, however, appears to be the most critical feature for the recognition and the cleavage of a substrate. Typically, the ECD of γ-secretase substrates is around 10 to 30 amino acids long. It was demonstrated that the cleavability increased the shorter the ECD is, while increasing the length above 50 amino acids increasingly hindered cleavage by γ-secretase (Struhl and Adachi, 2000, Funamoto et al., 2013, Bolduc et al., 2016). It is believed that due to its structure, the subunit NCT acts like a gate-keeper and sterically hinders proteins with a too long ECD from accessing the active site of γ-secretase (Bolduc et al., 2016). This already represents a first step of substrate selection. However, a short ECD is not a sufficient substrate requirement since also non-substrates of γ-secretase have been identified that are type I proteins with an artificially short ECD (Hemming et al., 2008). Moreover, NCT appears to be involved in the substrate recruitment as it has been demonstrated to directly interact with C99 (Shah et al., 2005, Zhang et al., 2012, Fukumori and Steiner, 2016, Petit et al., 2019), or C83 (Zhou et al., 2019) and Notch (Shah et al., 2005). One study further revealed that the direct interaction of NCT and the substrate C99 stabilizes the enzyme-substrate-complex, thereby affecting processivity (Petit et al., 2019).

After the initial recognition, the substrate does not directly access the active site. Instead, multiple lines of evidence point towards the involvement of at least one substrate-binding site in guiding the substrate towards the active site (Esler et al., 2002, Tian et al., 2002, Beher et al., 2003). For the cleavage of C99, Fukumori and Steiner could show that this is indeed a stepwise process in which the substrate interacts in a rather complex sequence of binding events with several exosites before it finally accesses the active site for cleavage (Fukumori and Steiner, 2016). In their study, they could identify PS1-NTF, NCT, and PEN-2 as exosite-providing subunits of γ-secretase, with PS1-NTF being the major substrate-binding site. They showed that C99 initially interacts with exosites in NCT and PEN-2. In the next two steps, the substrate is released, binds to exosites in the PS1-NTF and finally accesses the active site — formed by PS1-NTF and CTF —, for cleavage. They found that the most prominent exosite-interactions of C99 are H6 (Aβ numbering), interacting with NCT, A30 engaging with PEN-2, and E3 which contacts the PS1-NTF. Many of the interactions of C99 with PS1-NTF and -CTF identified by Fukumori and Steiner were also detected in the structure of γ-secretase in complex with C99 (Zhou et al., 2019). Fukumori and Steiner suggested that exosites provide a means of identifying flexible substrates and thus play an important role in the recognition of γ-secretase substrates

(Fukumori and Steiner, 2016). However, binding to exosites may also be circumvented since peptides containing almost only the TMD of APP have been shown to be cleaved by γ-secretase (Yin et al., 2007, Yan et al., 2017).

Exactly which path the substrate takes to get from the exosites to the active site is not yet entirely clear. It seems that an entry via an opening formed by TMDs 2 and 6 is the most likely one (Bai et al., 2015b, Kong et al., 2015, Somavarapu and Kepp, 2017, Yang et al., 2019, Fukumori et al., 2020). Alternatively, it has been proposed that the substrate may enter through the open space between TMDs 2 and 3 (Bai et al., 2015a), or between TMDs 6 and 9 (Fukumori and Steiner, 2016, Hitzenberger and Zacharias, 2019a). Clear is, however, that the process by which the substrate gains access to the active site involves major conformational changes on the side of the enzyme, as either way is blocked at some point by one of the many TMDs or loops of the γ-secretase (Bai et al., 2015a, Fukumori et al., 2020).

After the substrate reached the active site, there still seems to be another substrate selection step carried out by the highly conserved GxGD motif in TMD 7 of PS1, harboring one of the catalytic aspartates. While the activity and the processivity of γ-secretase depends on the two glycines (Steiner et al., 2000, Pérez-Revuelta et al., 2010), the Leucine at position x in this motif confers a certain substrate selectivity (Yamasaki et al., 2006, Kretner et al., 2013). The GxGD motif might thus be important for the correct positioning of the substrate's scissile bond (Steiner et al., 2018).

However, before the cleavage can finally take place, the local helical structure around the cleavage sites needs to unwind so that the scissile bond is accessible for cleavage (Ye et al., 2000, Clemente et al., 2018, Brown et al., 2018, Yang et al., 2019, Zhou et al., 2019). Typically, proteases recognize and bind their substrates in an extended β-strand conformation (Tyndall et al., 2005). In line with this, cleavage sites of soluble proteases, residing in α-helices (Timmer et al., 2009, Belushkin et al., 2014), are known to readily unfold (Robertson et al., 2016). For IMPs it has been suggested that helix-breaking residues close to the cleavage site or a certain conformational flexibility are needed for the exposure of the scissile bond (Ye et al., 2000, Lemberg and Martoglio, 2002, Lu et al., 2011, Brown et al., 2018, Clemente et al., 2018, Steiner et al., 2020). Unwinding of the helix around the initial cleavage sites has been confirmed by recent cryogenic electron microscopy (cryo-EM) structures of γ-secretase in complex with two of its substrates, APP and Notch-1 (Yang et al., 2019, Zhou et al., 2019).

1.1.1.4.2 General Cleavage Mechanism of γ-Secretase: Lessons from APP-Processing

The cleavage mechanism itself is best understood so far for the γ-secretase substrate APP (compare paragraph 1.1.1.3.2). It is well established now that γ-secretase cleaves APP not only once within its TMD, but repeatedly in succession. This sequential cleavage (trimming) usually occurs in steps of three to four amino acids (Takami et al., 2009, Okochi et al., 2013). A possible explanation of how and why γ-secretase preferentially cleaves in a tri-peptide-releasing way was given by Bolduc and colleagues in 2016. They could show that γ-secretase features three amino-acid-binding pockets (S1', S2', and S3') in the active site region which are able to stabilize the enzyme-substrate scission complex. In their model, the substrate engaged with these three pockets by fitting its P1' - P3' positions (three amino acids C-terminal of the cleavage site) into the binding pockets of γ-secretase. They proposed that this is repeated for each cleavage step and that it ensures proper positioning of the scissile bond. After the P1' - P3' residues of the substrate are bound to the pockets of the enzyme, the substrate is cleaved directly upstream of the P1' position. Their data further suggests that the S1' and S3' pockets are rather large, allowing for more bulky side chains to be accommodated, but the S2' pocket is smaller and thus seems to be restrictive towards the access of bulky aromatic amino acids at P2'. They concluded that the binding pockets explain the preferred tri-peptide cleavage pattern of γ-secretase and are further decisive for the Aβ product line selection. An interaction of the APP-based substrate C83 with three binding pockets in γ-secretase is supported by the recent structure of γ-secretase in complex with C83 (Zhou et al., 2019). Another study provided further evidence for the existence of such binding pockets (Hitzenberger and Zacharias, 2019b). However, the data from this study suggest that the S1' and S3' pocket form one large binding pocket (Hitzenberger and Zacharias, 2019b). It was further proposed that each cleavage destabilizes the TMD of the substrate, resulting in an unfolding of the cleavage region (Szaruga et al., 2017, Petit et al., 2019). This might enable the P1' to P3' residues to engage with the binding pockets. With each cleavage also the enzyme-substrate-complex is destabilized, finally resulting in the release of the products (Szaruga et al., 2017).

To date, it is not clear whether all substrates of γ-secretase are cleaved repeatedly in a consecutive fashion. Nevertheless, data on the cleavage of other substrates suggest that APP is not the only substrate cleaved in such a way. Cleavage data obtained by Gu *et al.* suggest a continued successive trimming after the initial cleavage for APLP1 (Gu et al., 2001). Indeed,

even Aβ-like peptides have been identified for APLP1 (Yanagida et al., 2009). Likewise, an ICD (Schroeter et al., 1998) and Aβ-like peptides of varying lengths have also been detected for Notch-1 (Okochi et al., 2002, Okochi et al., 2006, Ran et al., 2017) and CD44 (Lammich et al., 2002, Ran et al., 2017). Interestingly, it was demonstrated that these Aβ-like peptides of Notch-1 and APLP1 could also serve as substrates of γ-secretase, suggesting that APLP1 and Notch-1 are both cleaved repeatedly in a stepwise fashion (Okochi et al., 2013). Recently, multiple cleavage sites have also been identified for several other γ-secretase substrates, including the three other Notch receptors (Notch-2, 3, and 4) and vascular endothelial growth factor receptor 1 (VEGFR1), suggesting a stepwise trimming mechanism also for these substrates (Ran et al., 2017). Most interestingly, also the autoproteolytic cleavage of PS1 has been shown to follow a stepwise three amino acid-spaced cleavage mechanism (Fukumori et al., 2010).

1.1.1.4.3 The Conformational Flexibility of the Substrate and its Role for Substrate Recruitment and Processing

A certain conformational flexibility of the substrate has been proposed as an important factor for cleavage by IMPs (Langosch et al., 2015, Langosch and Steiner, 2017). Multiple findings demonstrating an effect of helix-destabilizing residues within substrates of other IMPs on proteolysis (Ye et al., 2000, Lemberg and Martoglio, 2002, Urban and Freeman, 2003, Fluhrer et al., 2012, Moin and Urban, 2012, Chen et al., 2014, Spitz et al., 2020), support this idea. Amino acids that are known to destabilize the α-helical conformation of a TMD are glycine (G), and proline (P), while alanine (A), and leucine (L) are potentially helix-forming residues (Chou and Fasman, 1974, O'Neil and DeGrado, 1990, Li and Deber, 1994). On the one hand, flexibility seems important for the unwinding of the helix prior to cleavage as described above, and several findings support this idea. It has been demonstrated that stabilizing or destabilizing the cleavage region of C99 via mutational analysis decreased or increased the cleavage of C99, respectively (Fernandez et al., 2016, Sato et al., 2009). Similarly, cleavage of Notch-1 was decreased when the glycines close to the cleavage site have been mutated (Vooijs et al., 2004, Xu et al., 2016). Interestingly, earlier data suggest that unfolding of the TM-C of C99 caused by the APP FAD mutation L52P affects the cleavage specificity of the initial cleavage by γ-secretase (Dimitrov et al., 2013). Contrary to these findings, however, Pester and colleagues showed that, in comparison to several non-substrate TMDs, the TMD of APP is rather rigid in

the vicinity of the cleavage site (Pester et al., 2013b). Findings from other studies demonstrating the stability of the TM-C of C99 further support this (Stelzer et al., 2016, Götz et al., 2019a). Additionally, studies analyzing the cleavability of mutant C99 substrates showed a decrease in cleavability when introducing a flexible glycine tripeptide C-terminal of the cleavage region (Sato et al., 2009). Analysis of the APP FAD mutant V46G within the cleavage region showed a reduced cleavage in two studies (Munter et al., 2010, Xu et al., 2016), while one study also showed an increased AICD production (Devkota et al., 2021). The cleavability of substrates of other aspartate IMPs was also not increased when helix-destabilizing residues were introduced at or near the cleavage site (Yücel et al., 2019, Spitz et al., 2020). Thus, it remains to be clarified, whether the unwinding and cleavage of a substrate requires the region close to the cleavage site to be flexible or not.

On the other hand, flexibility may already be crucial for the interaction with the enzyme, for the access to the active site, and for the presentation of the scissile bond (Tian et al., 2002, Scharnagl et al., 2014, Langosch et al., 2015, Stelzer et al., 2016). Substrates could adopt different interconverting shapes, and if only specific shapes can bind to the enzyme and access its active site, the occurrence of those shapes would affect the recruitment and processing of a given substrate. Thus, flexible substrate TMDs may be more easily recognized and cleaved. This would be in line with multiple groups reporting that both, γ-secretase and substrate, undergo conformational changes upon binding and during substrate cleavage (Li et al., 2014, Scharnagl et al., 2014, Bai et al., 2015b, Bai et al., 2015a, Langosch et al., 2015, Fukumori and Steiner, 2016, Zhou et al., 2019, Yang et al., 2019). Several groups suggested that the TMD of a substrate needs to be flexible in order to bend and access the active site of the IMP (Tian et al., 2002, Strisovsky et al., 2009, Scharnagl et al., 2014, Langosch et al., 2015). The necessary flexibility could be conveyed by motifs containing helix-destabilizing residues, like a glycine-glycine (GG)-hinge motif or a short asparagine-proline motif as they are found in substrates of other IMPs (Ye et al., 2000, Lemberg and Martoglio, 2002, Urban and Freeman, 2003, Akiyama and Maegawa, 2007, Fluhrer et al., 2012, Moin and Urban, 2012, Linser et al., 2015). Multiple lines of evidence suggest that the γ-secretase substrate APP harbors a GG-hinge (Miyashita et al., 2009, Nadezhdin et al., 2011, Pester et al., 2013a, Dominguez et al., 2014, Lemmin et al., 2014, Dominguez et al., 2016), which might provide the flexibility needed for recruitment and cleavage (Pester et al., 2013a, Dominguez et al., 2014, Lemmin et al., 2014, Langosch et al., 2015, Langosch and Steiner, 2017, Scharnagl et al., 2014). Thus, it has been

proposed that also APP needs a hinge which may enable the TMD to bend and access the active site (Langosch et al., 2015, Scharnagl et al., 2014, Tian et al., 2002).

1.2 Aims of the Thesis: Understanding Substrate Recruitment and Processing by γ-Secretase

Despite our knowledge about the function and the structure of all IMPs, how γ-secretase recognizes and efficiently cleaves its substrates is a major question that has remained unanswered for more than two decades of basic research in this field. Insights into this process are, however, urgently needed to advance our understanding of γ-secretase, one of the key enzymes in AD, and to gain further insights into IMPs in general. Thus, the overall aim of my thesis was to identify the principles of substrate recruitment and processing by γ-secretase.

One feature that has been suggested to play an important role for substrate recruitment and cleavage by γ-secretase is the conformational flexibility of the substrate. Its role for substrate recruitment and cleavage, however, remained inconclusive. Hence, one aim of my thesis was to investigate how helix-stabilizing and -destabilizing residues in the TMD of APP influence its initial cleavage as well as the stepwise trimming by γ-secretase. Combining this biochemical analysis with different biophysical approaches to analyze the flexibility and *in silico* modeling of initial contact sites of substrate and γ-secretase should help to clarify the role of the potentially helix-destabilizing GG-motif for substrate recruitment and processing by γ-secretase.

Another main goal of my thesis was to identify substrate determinants for γ-secretase by generating a non-substrate and reintroducing different motifs of C99 to regain cleavability. Specifically, I aimed to uncover the significance of a flexible TM-N for the initial cleavage and further trimming by analyzing different C99-based substrates. Additionally, I sought to elucidate whether flexibility is crucial also in the C-terminal half of a substrate's TMD. A flexible TM-C might facilitate the unwinding of the helix prior to cleavage, however, previous studies yielded diverging results on the importance of helix-destabilizing residues within the TM-C for the cleavability of a substrate. Analyzing the conformational flexibility of other γ-secretase substrates should clarify whether more substrates feature a certain conformational flexibility within their TMD. Finally, I aimed to explore whether both parts of the TMD (TM-N and TM-C), and potential substrate requirements within them, are equally important and if they cooperate for efficient cleavage by γ-secretase. A better understanding of substrate requirements for γ-secretase will help to unravel the secret of the highly specific cleavage by γ-secretase in the absence of sequence recognition motifs.

2 Results

2.1 Publication 1: 'Modulating Hinge Flexibility in the APP Transmembrane Domain Alters γ-Secretase Cleavage.'

This paper has been published in a peer-reviewed journal:

Götz A, **Mylonas N.** Högel P, Silber M, Heinel H, Menig S, Vogel A, Feyrer H, Huster D, Luy B, Langosch D, Scharnagl C, Muhle-Goll C, Kamp F, Steiner H. Modulating Hinge Flexibility in the APP Transmembrane Domain Alters γ-Secretase Cleavage. *Biophys J.* 2019 Jun 4;116(11):2103-2120. doi: 10.1016/j.bpj.2019.04.030.

Summary

This first publication focused on the role of the helix-destabilizing GG-hinge motif in the TMD of APP for cleavage and recognition by γ-secretase. To this end, one of the glycines (G38, Aβ numbering) of this motif has been exchanged by either a helix-destabilizing proline (P) or by a helix-stabilizing leucine (L). Circular dichroism spectroscopy and nuclear magnetic resonance spectroscopy of TMD peptides confirmed that the G38L mutation indeed increased the helicity, while the G38P mutation reduced the helical conformation of the construct when compared to the wild type (WT). Further, molecular dynamics (MD) simulations of TMD peptides proved that the mutations also affected the flexibility of the TMD. The substrate containing the G38L mutation was overall less flexible and motions (bending and twisting) around the hinge were more restricted compared to the WT, whereas the G38P construct proved to be more flexible, with motions around the hinge being more likely to occur. The analysis of the intrahelical H-bond strength of TMD peptides further supported the overall reduced conformational flexibility for the G38L mutation and the increased flexibility for the G38P construct. Additionally, this analysis revealed that the flexibility was changed mainly around the hinge motif, but neither of the mutations altered the conformational flexibility at the ε-sites. Interestingly, the region around the ε-sites proved to be in a stable helical conformation for all the constructs analyzed in this study. Surprisingly, both mutations reduced the overall cleavability of recombinant C99-based constructs and resulted in reduced levels of AICD and Aβ. A detailed analysis of the generated Aβ species via mass spectrometry revealed an increased processivity for the G38L mutation, even though its ε-cleavage was reduced. The processivity of the G38P construct, however, was reduced in comparison to the WT substrate.

In silico modeling of the initial contact of the substrate TMD with the γ-secretase complex did not uncover any differences and thus could not explain the observed differences in the cleavability of the mutants. However, the molecular dynamics simulations uncovered that both mutations affected the relative orientation of the TM-C harboring the ε-site, which is likely to affect the presentation of the scissile bond and thus the cleavage of the different constructs. Altogether, the results of this study clearly show that a certain flexibility of the APP TMD is critical for substrate processing and that the GG-hinge present in the TMD of APP enables specific motions needed for a correct positioning of the scissile bond at the active site. Further, the results suggest that conformational flexibility is key for the interaction with the enzyme, and thus for recognition and cleavage. It seems γ-secretase uses some kind of conformational sampling to differentiate between substrates and non-substrates.

My contribution to this publication

For this interdisciplinary study, I performed the *in vitro* (cell-free) cleavage assays, analyzed, and quantified the levels of the cleavage products generated. Further, I carried out the mass spectrometry analysis of the different Aβ species generated for each substrate. Figure 1 (B-F) comprises all the data I have generated for this publication. (For details, please see author contributions, pp. 178-182).

Biophysical *Journal*
Article

Modulating Hinge Flexibility in the APP Transmembrane Domain Alters γ-Secretase Cleavage

Alexander Götz,[1] Nadine Mylonas,[2,5] Philipp Högel,[3] Mara Silber,[4] Hannes Heinel,[6] Simon Menig,[1] Alexander Vogel,[6] Hannes Feyrer,[4] Daniel Huster,[6] Burkhard Luy,[4] Dieter Langosch,[3] Christina Scharnagl,[1,*] Claudia Muhle-Goll,[4,*] Frits Kamp,[2] and Harald Steiner[2,5,*]

[1]Physics of Synthetic Biological Systems (E14), Technical University of Munich, Freising, Germany; [2]Biomedical Center (BMC), Metabolic Biochemistry, Ludwig-Maximilians-University, Munich, Germany; [3]Center for Integrated Protein Science Munich at the Lehrstuhl Chemie der Biopolymere, Technical University Munich, Freising, Germany; [4]Institute of Organic Chemistry and Institute for Biological Interfaces 4, Karlsruhe Institute of Technology, Karlsruhe, Germany; [5]German Center for Neurodegenerative Diseases (DZNE), Munich, Germany; and [6]Institute for Medical Physics and Biophysics, Leipzig University, Leipzig, Germany

ABSTRACT Intramembrane cleavage of the β-amyloid precursor protein C99 substrate by γ-secretase is implicated in Alzheimer's disease pathogenesis. Biophysical data have suggested that the N-terminal part of the C99 transmembrane domain (TMD) is separated from the C-terminal cleavage domain by a di-glycine hinge. Because the flexibility of this hinge might be critical for γ-secretase cleavage, we mutated one of the glycine residues, G38, to a helix-stabilizing leucine and to a helix-distorting proline. Both mutants impaired γ-secretase cleavage and also altered its cleavage specificity. Circular dichroism, NMR, and backbone amide hydrogen/deuterium exchange measurements as well as molecular dynamics simulations showed that the mutations distinctly altered the intrinsic structural and dynamical properties of the substrate TMD. Although helix destabilization and/or unfolding was not observed at the initial ε-cleavage sites of C99, subtle changes in hinge flexibility were identified that substantially affected helix bending and twisting motions in the entire TMD. These resulted in altered orientation of the distal cleavage domain relative to the N-terminal TMD part. Our data suggest that both enhancing and reducing local helix flexibility of the di-glycine hinge may decrease the occurrence of enzyme-substrate complex conformations required for normal catalysis and that hinge mobility can thus be conducive for productive substrate-enzyme interactions.

INTRODUCTION

Proteolysis in the hydrophobic core of membranes is a fundamental cellular process that mediates critical signaling events as well as membrane protein turnover (1). Intramembrane proteases are polytopic membrane proteins carrying their active-site residues in transmembrane helices (2). Apart from the fact that they typically cleave their substrates within the transmembrane domain (TMD), little is still known about the substrate determinants of intramembrane proteases because they typically do not recognize consensus sequences, as observed with most soluble proteases. Soluble proteases are known to cleave their substrates within extended sequences (i.e., β-strands) or loops (3), and cleavage sites that reside in α-helices (4,5) are assumed to be intrinsically prone to unfolding (6). Therefore, rather than sequence motifs, the innate dynamics of substrate TMD helices is now increasingly discussed as a critical factor for substrate recognition and/or the cleavage reaction (7,8). Helix flexibility could be induced by, e.g., glycine residues in case of substrates of signal peptide peptidase (SPP) (9), the related SPP-like protease SPPL2b (10), and rhomboid (11). In the case of the site-2 protease SREBP substrate, a short helix-distorting asparagine-proline motif is thought to affect substrate recognition and/or cleavage (12,13).

γ-Secretase is a pivotal intramembrane protease complex (14,15) that cleaves a plethora of type I membrane protein substrates, including signaling proteins essential for life such as Notch1 as well as the β-amyloid precursor protein (APP), which is central to the pathogenesis of Alzheimer's disease (16,17). It is widely believed that an aberrant generation and accumulation of amyloid β-peptide (Aβ) in the brain triggers the disease (18,19). Aβ is a heterogeneous

Submitted October 30, 2018, and accepted for publication April 15, 2019.

*Correspondence: christina.scharnagl@tum.de or claudia.muhle@kit.edu or harald.steiner@med.uni-muenchen.de

Nadine Mylonas, Philipp Högel, and Mara Silber contributed equally to this work.

Editor: Alan Grossfield.

https://doi.org/10.1016/j.bpj.2019.04.030

mixture of secreted small peptides of 37–43 amino acids. Besides the major form Aβ_{40}, the highly aggregation-prone longer forms Aβ_{42} and Aβ_{43} are pathogenic Aβ variants (18,19). Aβ species are generated by γ-secretase from an APP C-terminal fragment (CTF; C99) that originates from an initial APP cleavage by β-secretase (15,20). C99 is first endoproteolytically cleaved in its TMD by γ-secretase at the ε-sites close to the cytoplasmic TMD border to release the APP intracellular domain (AICD) and then processed stepwise by tripeptide-releasing C-terminal trimming in two principal product lines, thereby releasing the various Aβ species from the membrane (21,22). Mutations in presenilin, the catalytic subunit of γ-secretase, are the major cause of familial forms of Alzheimer's disease (FAD) and are associated with increased Aβ_{42} to total Aβ ratios (15,23). Rare mutations in the cleavage region of the C99 TMD also shift Aβ profiles and represent another cause of FAD (15,23).

The molecular properties of substrates that are recognized by γ-secretase are still largely enigmatic. Established general substrate requirements are not only the presence of a short ectodomain (24,25), which is typically generated by sheddases such as α- or β-secretase, but, equally important, also permissive transmembrane and intracellular substrate domains (26). Recent studies suggest that the recruitment of C99 to the active site occurs in a stepwise process involving initial binding to exosites (i.e., substrate-binding sites outside the active site) in the nicastrin, PEN-2, and presenilin-1 (PS1) N-terminal fragment subunits of γ-secretase (27). Finally, before catalysis, interactions of C99 with the S2′ subsite pocket of the enzyme are critical for substrate cleavage and Aβ product line selection (22).

Kinetic studies have shown that intramembrane proteolysis is a surprisingly slow process in the minute range, i.e., much slower than cleavage by soluble proteases (28–30). The basis for the slow kinetics is not yet understood. With regard to C99 cleavage by γ-secretase, one reason could be that slow unwinding of the TMD helix at the initial ε-sites is rate limiting. This view is in line with biophysical studies demonstrating that the helical structure of the C99 TMD is extremely stable, particularly in its C-terminal region harboring the ε-sites (31). Indeed, a detailed recent analysis showed that di-glycine motifs introduced near the ε-sites enhance the initial cleavage, supporting the view that the helix must be locally destabilized to allow the cleavage reaction to occur (32). On the other hand, several reports also indicated that other regions than that harboring the cleavage sites of C99 play an important role for γ-secretase cleavage. For instance, mutations introduced at the luminal juxtamembrane boundary (33,34), as well as within the N-terminal part of the TMD (i.e., at sites distant from the cleavage region), can alter cleavage efficiency and shift cleavage sites (35,36). Furthermore, local destabilization and the length of the membrane-anchoring domains at the cytosolic juxtamembrane boundary, as well as β-sheet segments within the extracellular domain of C99, have been reported as important players for γ-secretase cleavage of C99 (37–39). Interestingly, NMR structures in detergent micelles (40,41) and molecular dynamics (MD) simulations in membrane bilayers (42–46) suggested that the C99 TMD also contains a flexible hinge region at the $G_{37}G_{38}$ residues, which may provide the necessary flexibility for the interaction with the enzyme (7,8,43,45,46). Remarkably, although most C99-related FAD mutations are in the vicinity of the cleavage sites (15), these mutations do not destabilize H-bonds at the ε-sites but have a major impact on upstream H-bond stability, including the region around the $G_{37}G_{38}$ hinge (47,48). The latter biophysical studies indicate that the $G_{37}G_{38}$ motif may play a crucial role in coordinating large-scale bending movements of the C99 TMD, which might facilitate the C-terminal part of the helix to move into the active site of γ-secretase (7,49,50). Interestingly, earlier studies with a different focus found that certain mutations at the $G_{37}G_{38}$ hinge can diversely affect γ-secretase cleavage efficiency (27,51).

Because it is thus possible that the innate flexibility of the C99 TMD enabled by the $G_{37}G_{38}$ hinge could play a role for γ-secretase cleavage and because a link of biochemical assays of substrate cleavage with biophysical studies of backbone dynamics is still missing, we aimed to address the following questions: 1) how intrinsic structural and dynamic properties of different domains of the TMD, such as local conformation, H-bond instability, bending propensity and relative spatial orientation, are interrelated; 2) whether conformational changes of the C99 TMD allowed by its intrinsic properties play a role in the initial encounter with the enzyme, its fitting into the active site, and/or the subsequent catalytic event; and 3) whether the local unfolding of the helix required for initial substrate cleavage depends on the intrinsic structural and dynamic properties of the domain harboring the ε-sites or is rather determined by the interaction of the latter domain with the enzyme.

To modulate $G_{37}G_{38}$ hinge bending, we generated two mutations of the C99 TMD. A G38L mutation was introduced to reduce helix flexibility and a G38P mutation to increase bending, considering the classical helix-breaking potential of proline in soluble (52) and membrane proteins (53). Assuming that a less flexible $G_{37}G_{38}$ hinge would impair the presentation of the cleavage domain to the active site, we hypothesized that the G38L mutation would reduce γ-secretase cleavage, whereas the G38P mutation would have the opposite effect. Additionally, we expected contrary effects of the G38L and G38P mutations on the dynamic properties of the C99 TMD, such as the intrinsic H-bond stability and relative spatial orientation of the distal region harboring the ε-sites.

In an interdisciplinary approach, we combined γ-secretase cleavage assays of recombinant full-length C99-derived substrates with biophysical measurements and MD simulations of peptides comprising the TMD of C99 to study its

intrinsic structural and dynamical properties in model membranes composed of POPC, i.e., before binding to the enzyme. In addition, we used a trifluoroethanol/water (TFE/H_2O) mixture, a well-established α-helix-stabilizing hydrophobic yet hydrated solvent that has been used previously to mimic the interior of proteins (54,55), as well as the catalytic cleft of γ-secretase (31,46–49,56,57). In particular, we asked whether cleavability could be correlated with $G_{37}G_{38}$ hinge-linked structural and dynamical properties of the TMD per se and, if so, what kind of properties would be functionally relevant.

Surprisingly, γ-secretase cleavage of both the G38L and particularly the G38P mutant of C99 was decreased compared to the wild type (WT), although the biophysical studies of the C99 TMD peptides corroborated the expected "stiffening" and "loosening" effects of the G38L and G38P mutants, respectively. Furthermore, effects of the G38 mutations on H-bond stability in the C99 TMD were observed only in the vicinity of the hinge and did not extend to residues around the ε-cleavage sites. MD simulations demonstrated that altered hinge flexibility leads to mutant specific distortions of the relative orientations of the helical turn harboring the ε-sites, which may consequently alter the interaction of the substrate with the active site of the enzyme, thereby impairing efficiency of the initial cleavage of both mutants. Our data thus suggest that complex global motions of the C99 TMD, controlled by the $G_{37}G_{38}$ hinge, may determine proper positioning of the substrate at the active site of the enzyme.

MATERIALS AND METHODS

Materials

1-Palmitoyl-2-oleoyl-*sn*-glycero-3-phosphocholine (POPC) as well as *sn*-1 chain perdeuterated POPC-d_{31} were purchased from Avanti Polar Lipids (Alabaster, AL). 1,1,1-3,3,3-Hexaflouroisopropanol (HFIP) and 2,2,2-TFE were purchased from Sigma-Aldrich (St. Louis, MO).

Peptides

For all circular dichroism (CD), solution NMR, solid-state NMR (ssNMR), and D/H exchange (DHX) experiments, $C99_{26–55}$, a 30-amino-acid-long peptide comprising residues 26–55 of C99 (C99 numbering; see Fig. 1 *A*) with N-terminal acetylation and C-terminal amidation was used. WT peptide and G38L and G38P mutants thereof (Table 1) were purchased from Peptide Specialty Laboratories, Heidelberg, Germany and from the Core Unit Peptid-Technologien, University of Leipzig, Germany. For electron transfer dissociation (ETD) measurements, to enhance fragmentation efficiency, we substituted the N-terminal SNK sequence of $C99_{26–55}$ with KKK. In all cases, purified peptides were >90% purity, as judged by mass spectrometry (MS).

γ-Secretase in vitro assay

C99-based WT and mutant substrates were expressed in *Escherichia coli* as C100-His_6 constructs (C99 fusion proteins containing an N-terminal methionine and a C-terminal His_6 tag) (58) and purified by Ni-NTA affinity chromatography. To analyze their cleavability by γ-secretase, 0.5 μM of the purified substrates was incubated overnight at 37°C with 3-([3-cholamidopropyl]dimethylammonio)-2-hydroxy-1-propanesulfonate (CHAPSO)-solubilized HEK293 membrane fractions containing γ-secretase as described (59). Incubations in the presence of the γ-secretase inhibitor L-685,458 (60) (Merck Millipore, Burlington, MA) or at 4°C served as controls. Generated Aβ and AICD were analyzed by immunoblotting using antibody 2D8 (61) and Penta-His (Qiagen, Hilden, Germany), respectively, and quantified by measuring the chemiluminescence signal intensities with the LAS-4000 image reader (Fujifilm Life Science, USA). Analysis of γ-secretase activity was repeated with three independent substrate purifications in three technical replicates for each of the constructs.

MS analysis of Aβ species

Aβ species generated in the γ-secretase vitro assays were immunoprecipitated with antibody 4G8 (Covance) and subjected to MS analysis on a 4800 MALDI-TOF (matrix-assisted laser desorption/ionization-time of flight)/TOF Analyzer (Applied Biosystems, Foster City, CA/MDS SCIEX, Framingham, MA) as described previously (62,63).

CD and UV spectroscopy

$C99_{26–55}$ WT and G38L and G38P mutant peptides were incorporated into large unilamellar vesicles (LUVs) composed of POPC at a lipid/protein molar ratio of 30:1. First, 500 μg peptide and 3.72 mg POPC were comixed in 1 mL HFIP. After evaporation of the HFIP, the mixture was dissolved in 1 mL cyclohexane and lyophilized. The resulting fluffy powder was dissolved in 977 μL buffer (10 mM sodium phosphate (pH 7.4)). After 10 freeze-thaw cycles, LUVs were prepared by extrusion using a 100-nm polycarbonate membrane and a LipoFast extruder device (Armatis, Mannheim, Germany). CD spectra were recorded with a Jasco 810 spectropolarimeter. A cuvette with a 1 mm pathlength was filled with 200 μL of the LUV-$C99_{26–55}$ preparation in which the final peptide concentration was 83 μM and the lipid concentration 2.5 mM. Mean molar residue ellipticities ([Θ]) were calculated based on the peptide concentrations. The ultraviolet (UV) absorbance at 210 nm of the WT peptide was used as a reference to normalize the final concentration of the reconstituted mutant peptides. Alternatively, for the peptides dissolved in TFE/H_2O (80/20 v/v), the concentrations were determined using the UV absorbance of the peptide bond at 205 nm. The calculated extinction coefficient at 205 nm was the same (ε_{205} = 87.5 × 10^3 M^{-1} cm^{-1}) for the WT and G38 mutants based on the sequences for the $C99_{26–55}$ WT and mutant peptides (64). Additionally, an experimental value of ε_{205} = 73.6 × 10^3 M^{-1} cm^{-1} for a homologous peptide (InsW-$C99_{26–55}$, Table 1) dissolved in TFE/H_2O was determined calibrating with ε_{280} = 5600 mol^{-1} cm^{-1} of the additional tryptophan.

Solution NMR

Dry $C99_{26–55}$ WT ($^{15}N/^{13}C$-labeled at positions G29, G33, G37, G38, I41, V44, M51, and L52) and G38L and G38P mutant peptides were dissolved in 500 μL 80% TFE-d3 and 20% H_2O, respectively. pH was adjusted to 5.0 by adding the corresponding amount of NaOH. Peptide concentrations ranged between 50 and 500 μM. The NMR spectra of the peptides were obtained on a 600 MHz AVANCE III spectrometer (Bruker BioSpin, Rheinstetten, Germany) equipped with a TXI cryoprobe at a temperature of 300 K. To assign ^1H and ^{13}C resonances of the peptides, a set of two-dimensional spectra was recorded: ^1H-^1H-TOCSY with a mixing time of 60 ms, ^1H-^1H-NOESY with a mixing time of 200 ms, and ^1H-^{13}C-HSQC. Spectra were recorded with 24 scans and 1000 data points in the indirect dimension. The NMR spectra were analyzed using NMRViewJ (One Moon Scientific).

For H/D exchange (HDX) measurements (NMR-HDX), dry peptides were dissolved in 80% TFE-d3 and 20% D_2O. Measurements were done at at least three different pH values to access all exchangeable protons, using the correlation of exchange rate and pH value. pH was adjusted using NaOD and DCl. 11 TOCSY or ClipCOSY (65) spectra with an experimental time of 3 h 26 min each (mixing time 30 ms, 24 scans, 300 data points in the indirect dimension) were acquired sequentially. Additionally, 11 ^{1}H-^{15}N-HSQC spectra of the WT were recorded (two scans, 128 points in the indirect dimension) in between.

The exchange of the first five to six and the last two residues was too fast to measure. M35 and A42 cross peak intensities were significantly lower than those of other amino acids. The HDX rate constant ($k_{exp,HDX}$) was obtained fitting the crosspeak intensities over time to Eq. 1:

$$y = c + a \times e^{\left(-k_{exp,HDX} \times t\right)}, \quad (1)$$

where t is time and a and c are constants. Rate constants were calculated for all three pH values and then scaled to pH 5.

ssNMR

For ssNMR, A30, G33, L34, M35, V36, G37, A42, and V46 were labeled in the $C99_{26–55}$ WT peptide with ^{13}C and ^{15}N. In the two mutant peptides, only A30, L34, V36, and G37 were labeled as a compromise between expensive labeling and the highest information impact to be expected. Multilamellar vesicles were prepared by cosolubilizing POPC and the selected $C99_{26–55}$ peptide in HFIP at a 30:1 molar ratio. After evaporation of the solvent in a rotary evaporator, the sample film was dissolved by vortexing in cyclohexane. Subsequently, the samples were lyophilized to obtain a fluffy powder. The powder was hydrated with buffer (100 mM NaCl, 10 mM Hepes (pH 7.4)) to achieve a hydration level of 50% (w/w) and homogenized by 10 freeze-thaw cycles combined with gentle centrifugation. Proper reconstitution of the $C99_{26–55}$ WT and G38 mutants into the POPC membranes was confirmed by an analysis of the $^{13}C_{\alpha}$ chemical shifts of A30.

^{13}C magic-angle-spinning (MAS) NMR experiments were performed on a Bruker Avance III 600 MHz spectrometer (resonance frequency 600.1 MHz for ^{1}H, 150.9 MHz for ^{13}C) using 4 and 3.2 mm double-resonance MAS probes. The cross-polarization contact time was 700 μs, and typical lengths of the 90° pulses were 4 μs for ^{1}H and 4–5 μs for ^{13}C. For heteronuclear two-pulse phase modulation decoupling, a ^{1}H radio frequency field of 62.5 kHz was applied. ^{13}C chemical shifts were referenced externally relative to tetramethylsilane. ^{1}H-^{13}C dipolar couplings were measured by constant-time DIPSHIFT experiments using frequency-switched Lee-Goldburg for homonuclear decoupling (80 kHz decoupling field) (66). The ^{1}H-^{13}C dipolar coupling was determined by simulating dipolar dephasing curves over one rotor period. These dipolar couplings were divided by the known rigid limit as reported previously (67). MAS experiments for the site-dependent order parameter were carried out at an MAS frequency of 3 kHz and a temperature of 30°C. DIPSHIFT ^{1}H-^{13}C order parameters were analyzed with a variant of the established GALA model (68) to evaluate RMSD values for combinations of tilt and azimuthal angles of the TMD helix, explained in detail in the Supporting Materials and Methods.

MS experiments of DHX

All mass spectrometric experiments were performed on a Synapt G2 high definition mass spectrometer (Waters, Milford, MA). A 100 μL Hamilton gas-tight syringe was used with a Harvard Apparatus 11 plus, and the flow rate was set to 5 μL/min. Spectra were acquired in a positive-ion mode with one scan for each second and 0.1 s interscan time.

Solutions of deuterated peptide (100 μM in 80% (v/v) d1-TFE in 2 mM ND_4-acetate) were diluted 1:20 with protiated solvent (80% (v/v) TFE in 2 mM NH_4-acetate (pH 5.0)) to a final peptide concentration of 5 μM (at which the helices remain monomeric (46)) and incubated at a temperature of 20°C in a thermal cycler (Eppendorf, Hamburg, Germany). Incubation times were 0, 1, 2, 5, 10, 20, 30, 40, and 50 min and 1, 2, 3, 4, 6, 8, 12, 24, 48, and 72 h. Exchange reactions were quenched by placing the samples on ice and adding 0.5% (v/v) formic acid, resulting in a pH $\approx$ 2.5. Mass/charge ratios were recorded and evaluated as previously described (69,70), including a correction for the dilution factor. For ETD, we preselected the 5+ charged peptides via MS/MS and used 1,4-dicyanobenzene as a reagent. The fragmentation of peptides was performed as described (69). Briefly, ETD MS/MS scans were accumulated over 10 min scan time, smoothed (Savitzky-Golay, 2 × 4 channels), and centered (80% centroid top, heights, three channels). MS-ETD measurements were performed after 13 different incubation periods (from 1 min to 3 d) in which exchange took place at pH 5.0. Shorter (0.1 min, 0.5 min) and longer (5 d, 7 d) incubation periods were simulated by lowering the pH to 4.0 or elevating pH to 6.45, respectively, using matched periods. The differences to pH 5.0 were considered when calculating the corresponding rate constants. We note that base-catalyzed exchange is responsible for at least 95% of total deuteron exchange at pH 4.0 and above. The resulting ETD c and z fragment spectra were evaluated using a semiautomated procedure (MassMap_2017-11-16_LDK Software; MassMap KG, Freising, Germany) (47). The extent of hydrogen scrambling could not be calculated with the ammonia loss method (71) because of the blocked N-termini. However, previous experiments with similar peptides showed scrambling to be negligible under our conditions (72). During all MS-DHX experiments, a gradual shift of monomodal shaped isotopic envelopes toward lower mass/charge values was observed. This is characteristic of EX2 kinetics with uncorrelated exchange of individual deuterons upon local unfolding (73,74).

MD simulations

The $C99_{26–55}$ WT, $C99_{26–55}$ G38L, and $C99_{26–55}$ G38P model peptide (for sequences, see Table 1) were investigated in a fully hydrated POPC bilayer and in a mixture of 80% TFE with 20% TIP3 water (v/v). Because no experimental structures were available for the G38 mutants, we used a stochastic sampling protocol to generate a set of 78 initial start conformations (for details, see (75)).

All-atom simulations in 80% TFE and 20% TIP3 (v/v) were set up as described previously (75). Each start conformation was simulated for 200 ns using settings as described in (46). Production runs were performed in an NPT ensemble (T = 293 K, p = 0.1 MPa) using NAMD 2.11 (76). Frames were recorded every 10 ps. The last 150 ns of each simulation were subjected to analysis, leading to an effective aggregated analysis time of 11.7 μs for each peptide.

For all-atom simulations in POPC bilayers, the stochastically sampled conformations were hierarchically clustered, and the centroid of the cluster with the highest population was placed in a symmetric bilayer, consisting of 128 POPC lipids, using protocols as provided by CHARMM-GUI (77). Simulations of 2.5 μs (T = 303.15 K, p = 0.1 MPa) were performed using NAMD 2.12 (76). Frames were recorded every 10 ps. Only the last 1.5 μs of the trajectory were subjected to analysis. All atomistic simulations use the CHARMM36 force field (78). Analysis of the H-bond occupancies, tilt, and azimuthal angles, as well as bending and twisting motions, is explained in detail in the Supporting Materials and Methods.

For the analysis of substrate TMD encounter with γ-secretase, we apply the DAFT approach (79) with a coarse-grained description of POPC lipids, water, $C99_{26–55}$ TMD, and γ-secretase. The use of >750 replicas per TMD starting from unbiased noninteracting initial states, sampling for at least 1 μs per replicate, and inclusion of low-amplitude backbone dynamics of γ-secretase (80) provided exhaustive sampling of potential contact sites and exceeds previous assessments of C99 binding sites with respect to both the number of replicates and simulation time (81,82). For further details, see the Supporting Materials and Methods and (83).

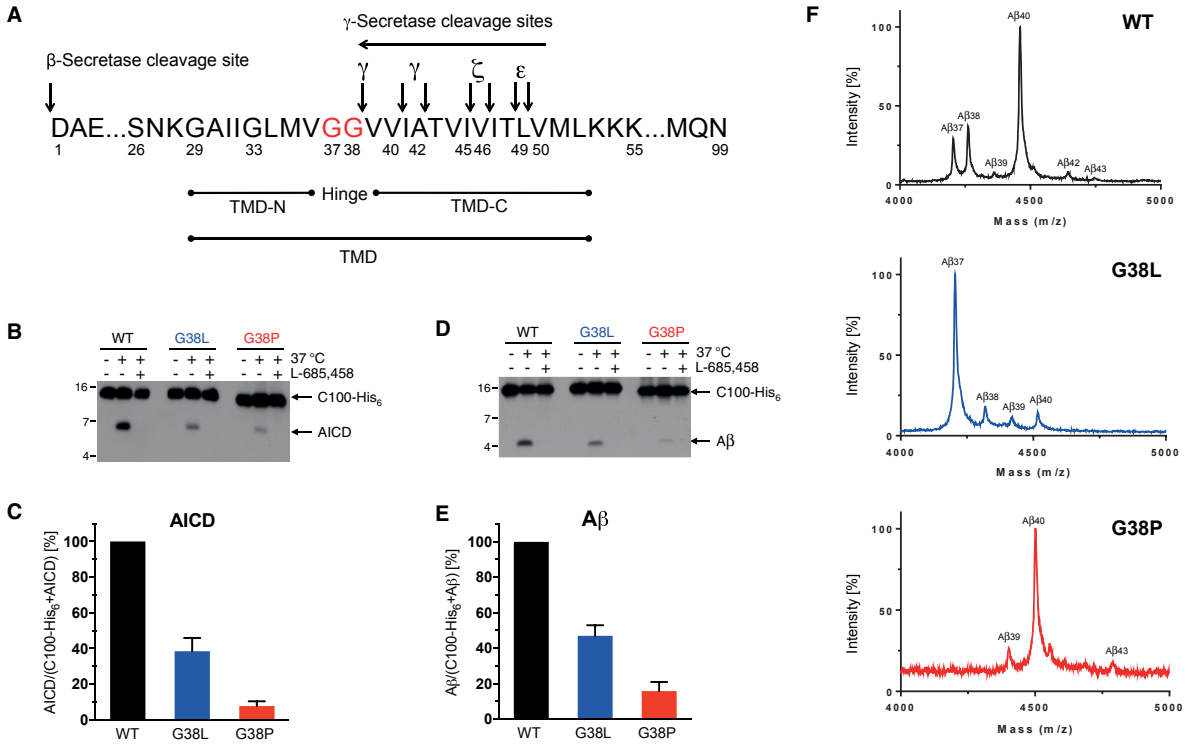

FIGURE 1 C99 G38P and G38L mutants distinctly alter γ-secretase cleavage and processivity. (*A*) The primary structure of C99 (Aβ numbering) and its major γ-secretase cleavage sites are shown. (*B*) Levels of AICD were analyzed by immunoblotting after incubation of C100-His_6 WT and mutant constructs with CHAPSO-solubilized HEK293 membrane fractions at 37°C. As controls, samples were incubated at 4°C or at 37°C in the presence of the γ-secretase inhibitor L-685,458 (60). (*C*) Quantification of AICD levels from (*B*) is shown. Values are shown as a percentage of the WT, which was set to 100%. Data are represented as mean ± standard error of the mean (n = 3, each n represents the mean of three technical replicates). (*D* and *E*) Corresponding analysis of Aβ is shown. (*F*) Representative MALDI-TOF spectra of the different Aβ species generated for WT and the G38 mutants are shown. The intensities of the highest Aβ peaks were set to 100% in the spectra.

RESULTS

G38L and G38P mutations in the C99 TMD differently impair γ-secretase cleavage

To examine whether and how leucine and proline mutations in the $G_{37}G_{38}$ hinge in the TMD of C99 affect the cleavage by γ-secretase (Fig. 1 *A*), G38L and G38P mutants of the C99-based recombinant substrate C100-His_6 (58) were purified and used to assess their cleavability in an established in vitro assay (59). As expected, AICD generation resulting from the initial ε-cleavage was reduced to ∼38% for the G38L mutant compared to WT (Fig. 1, *B* and *C*). Surprisingly, contrary to our hypothesis, ε-cleavage of the G38P mutant was even more reduced to only ∼8%. Concomitantly, Aβ levels were reduced for both G38L and G38P mutants to ∼47 and ∼16%, respectively (Fig. 1, *D* and *E*). To also investigate the impact of the mutations on the C-terminal trimming activity of γ-secretase, i.e., its processivity, we analyzed the distribution of the lengths of the Aβ species by MALDI-TOF MS (Fig. 1 *F*). Strikingly, although Aβ40 was, as expected, the predominant species for the cleavage of the WT substrate, Aβ37 was the major cleavage product for the G38L mutant. Thus, although the initial ε-cleavage was impaired for the G38L mutant, its processivity was enhanced. Aβ40 remained the major cleavage product for the G38P mutant, but in contrast to the WT, no Aβ37 and Aβ38 species were produced. Additionally, Aβ43 was also detected for this mutant. Remarkably, for both mutants, the unusual Aβ39 species was detected, which was barely

TABLE 1 Sequences of Investigated Peptides

Name	Sequence
$C99_{26–55}$	Ac-SNKGAIIGLMVGGVVI ATVIVITLVMLKKK-NH_2
$C99_{26–55}$ G38L	Ac-SNKGAIIGLMVGLVVI ATVIVITLVMLKKK-NH_2
$C99_{26–55}$ G38P	Ac-SNKGAIIGLMVGPVVI ATVIVITLVMLKKK-NH_2
KKK-$C99_{26–55}$	Ac-KKKGAIIGLMVGGVVI ATVIVITLVMLKKK-NH_2
InsW-$C99_{26–55}$	Ac-SNKWGAIIGLMVGGVVI ATVIVITLVMLKKK-NH_2

detected for the WT. Thus, for both mutants in the $G_{37}G_{38}$ hinge, γ-secretase cleavage was decreased, and the processivity was markedly and distinctly affected. We next sought to investigate the underlying basis of these observations.

G38 mutants do not alter contact probabilities with γ-secretase

Because the G38 mutations are localized close to potential TMD-TMD interaction interfaces (i.e., $G_{29}XXXG_{33}$, $G_{33}XXXG_{37}$, and $G_{38}XXXA_{42}$ motifs (43,46)), a possible explanation for the impaired γ-secretase cleavage of the G38 mutants could be altered contact preferences with γ-secretase. To screen for contact interfaces of the C99 TMD with γ-secretase, we set up an in silico docking assay for transmembrane components (DAFT (79)) using a coarse-grained description of POPC lipids, water, C99 TMD ($C99_{26–55}$), and γ-secretase. This protocol was previously shown to reliably reproduce experimentally verified protein-protein interaction sites in a membrane (79,84).

Our calculations showed that the $C99_{26–55}$ WT and both mutant peptides could principally interact with the surface of the γ-secretase complex and contact all four complex components (Fig. 2 *A*). In agreement with previous substrate cross-linking experiments (27), the $C99_{26–55}$ showed the highest binding preference for the PS1 N-terminal fragment (NTF) (Fig. 2 *A*). The normalized $C99_{26–55}$ proximities for each residue of γ-secretase (Fig. 2 *B*) indicated that the presenilin TMD2 may represent a major exosite of γ-secretase and revealed that contacts with the highest probabilities were formed between the juxtamembrane $S_{26}NK_{28}$ residues of $C99_{26–55}$ and the two threonine residues T119 and T124 in the hydrophilic loop 1 between TMD1 and TMD2 of PS1 (Fig. S1). Interactions between PS1 TMD2 and the C99 TMD could mainly be attributed to contacts of the A30, G33, G37, and V40 of the C99 TMD with residues L130, L134, A137, and S141 of PS1 TMD2 (Figs. 2 *C* and S1). Additional contact sites of the C99 TMD at V44 and I47 are located on the same face of the C99 TMD helix as the main contact sites (Fig. 2 *C*). However, the probabilities of the observed dominant contacts with the enzyme were

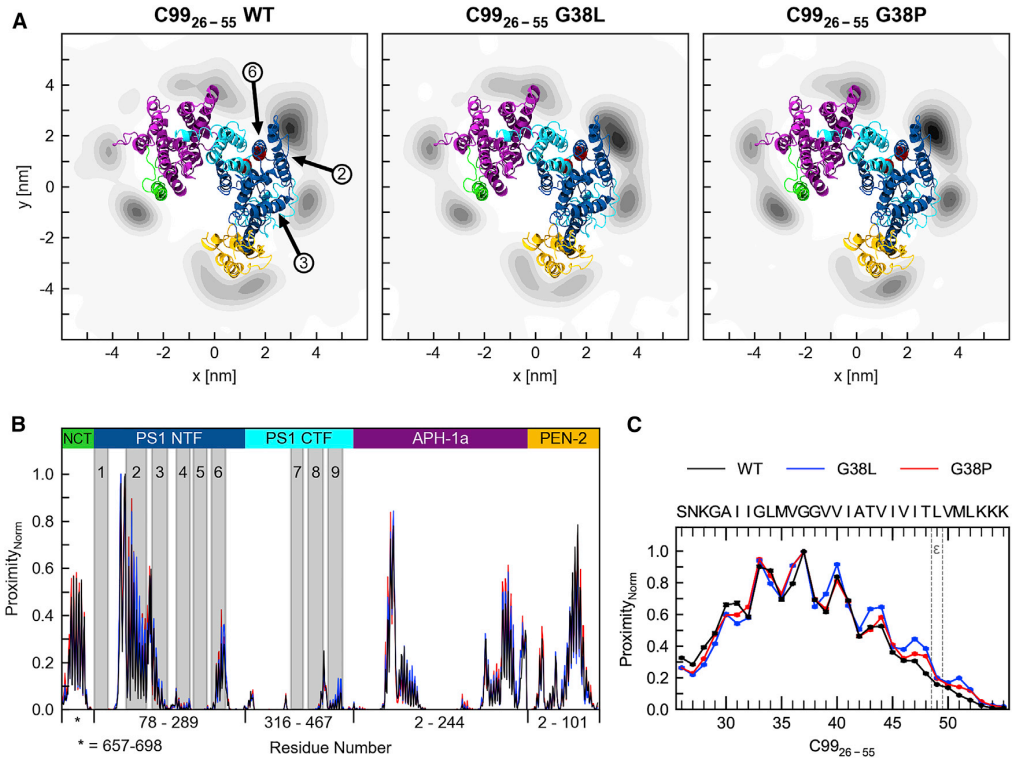

FIGURE 2 Probability of initial contacts of $C99_{26–55}$ peptides with γ-secretase is not altered for G38 mutants compared to WT, as revealed by in silico modeling of the encounter complex. (*A*) Kernel densities of the center-of-mass location of the $C99_{26–55}$ peptide are shown. Darker colors indicate higher contact probabilities. The representation shows the parts of γ-secretase that are embedded in the membrane, pertaining to the subunits nicastrin (*green*), PS1 NTF (*blue*), PS1 CTF (*cyan*), APH-1a (*purple*), and PEN-2 (*yellow*). Black arrows highlight TMD2, TMD3, and TMD6 of PS1, and the active-site aspartate residues in PS1 TMD6 and TMD7 are indicated by red spheres. (*B*) Normalized proximities between residues of γ-secretase subunits and the $C99_{26–55}$ peptide are shown. Gray areas indicate residues that are part of the indicated TMDs of PS1. (*C*) Normalized proximities between $C99_{26–55}$ residues and TMD2 of PS1 are shown.

not significantly altered by the G38 mutations. Thus, based on our substrate docking simulations, the structural alterations of the C99 G38 mutant TMD helices may not cause gross alterations in initial substrate-enzyme interactions.

G38 hinge mutations cause structural changes of the C99 TMD helix

We thus next investigated how the G38 mutations affect structural and dynamical properties of the C99 TMD. To compare the effects of the G38L and G38P mutants on the helical conformation of the C99 TMD, WT, and mutant $C99_{26–55}$ peptides were incorporated into LUVs composed of POPC. As shown in Fig. 3 *A*, CD spectroscopy measurements demonstrated that the peptides contain a high content of α-helical conformation in the lipid bilayer. As expected, the helical conformation was stabilized for the G38L (indicated by the more negative ellipticity at 220 nm) and destabilized for the G38P mutant. Similar effects were found when the peptides were analyzed in TFE/H_2O (80/20 v/v) (Fig. 3 *B*). In this solvent, ellipticity and the shape of the spectra was different compared to POPC, but the minima at 208 and 220 nm were nevertheless indicative of a high degree of helicity.

The high helical content of the WT and mutant C99 TMDs was corroborated by solution NMR, in which structural information was derived from secondary chemical shifts ($\Delta\delta$) (Fig. 3 *C*; for complete data set, see Fig. S2) and nuclear overhauser effect (NOE) patterns (Fig. S2). Over the entire TMD sequence, $C99_{26–55}$ WT showed cross peaks that are typical for an ideal α-helix (containing 3.6 residues per turn; Fig. S2). $\Delta\delta(^{13}C_\alpha)$ and $\Delta\delta(^{1}H_\alpha)$ chemical shifts in particular, as well as $\Delta\delta(^{13}C_\beta)$, indicated a strong helicity for the C-terminal domain (TMD-C) ranging from V39 to L52 (Fig. 3 *C*; Fig. S2). In contrast, the N-terminal domain (TMD-N), ranging from G29 up to V36, seemed to form a less stable helix. At positions G37 and G38, the helical pattern appeared to be disturbed, which is obvious from the reduced $\Delta\delta(^{1}H_\alpha)$ values at these residues. This observed pattern of TMD-N and TMD-C domains flanking the short $G_{37}G_{38}$ segment of lower stability is consistent with previous results (40,46,48,49).

With regard to the G38 mutants, no major overall changes in the NOE patterns and secondary chemical shifts were

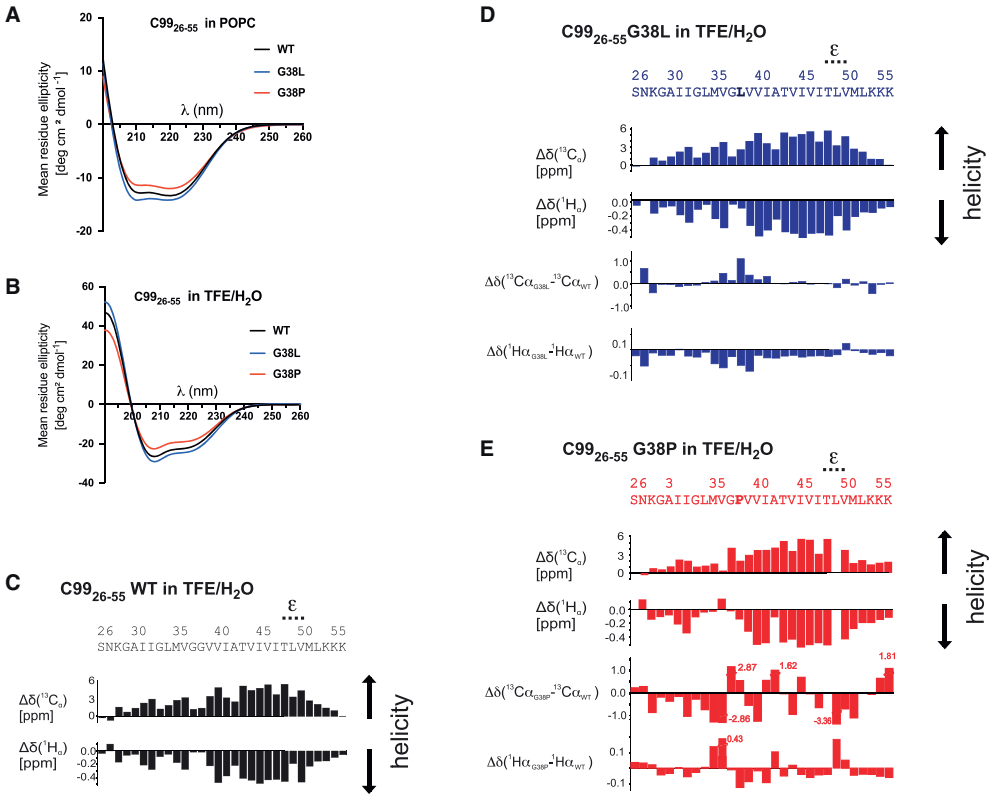

FIGURE 3 Helicity of $C99_{26–55}$ TMD peptides is increased by the G38L and distorted by the G38P mutation. (*A*) CD spectra of $C99_{26–55}$ WT and G38L and G38P mutant peptides reconstituted in POPC model membranes and (*B*) dissolved in TFE/H_2O are shown. (*C*) Chemical shift indices ($\Delta\delta$) for $^{13}C_\alpha$ and $^{1}H_\alpha$ atoms of each residue of $C99_{26–55}$ WT obtained from solution NMR in TFE/H_2O are shown. (*D* and *E*) Results of solution NMR measurements as in (*C*) of the G38L and G38P mutants, respectively, are shown, in which the differences between $\Delta\delta$ values of mutants and WT are also depicted.

observed. However, a detailed view showed small but distinct differences in secondary chemical shifts both for G38L and G38P. G38L appeared slightly stabilized compared to the WT. Chemical shift changes were restricted to the two helical turns around L38 (M35–I41) and the immediate termini (Fig. 3 *D*). For G38P, the high number of differences in both $\Delta\delta(^{13}C_\alpha)$ and $\Delta\delta(^{1}H_\alpha)$ shifts compared to those of the WT values (Fig. 3 *E*) indicated changes in structure or stability induced by the mutation that, however, were too subtle to also result in altered NOE patterns (Fig. S2). This stems from the fact that NOEs for dynamic helices are dominated by the most stable conformation, whereas the highly sensitive chemical shifts are affected even by minuscule changes. Particularly, the helicity of the N-terminal part up to V36 had decreased for G38P according to the chemical shift pattern, but also the remaining C-terminal part showed significant and irregular deviations compared to the WT. Concomitantly, for G38P, we observed an overall increase of H_N resonance line widths, which is indicative of an increased global conformational exchange (Fig. S3). Here, also, several minor alternative conformations were visible that resulted in more than one H_N/H_α resonance for many residues (up to four for some residues) (Fig. S3). The overall helical conformation was also confirmed by the profile of mean-squared fluctuations obtained from the MD simulations (Fig. S4). The w-shape is a fingerprint of the large-amplitude bending motion (48), which is characteristic for helices. In POPC as well as in TFE/H_2O, the G38 mutations impacted mainly local flexibility in the helix center but conserved below-average fluctuations in the cleavage domain (Fig. S4).

Taken together, consistent with the CD data, the solution NMR data and MD simulations show that the $C99_{26–55}$ peptide has a high propensity to form a helical structure that is only slightly reduced in the $G_{37}G_{38}$ hinge region. Interestingly, the TMD-C, i.e., the region in which the cleavages by γ-secretase occur, has a much stronger helicity compared to the TMD-N. The G38L mutation caused a stabilization of the helix around the $G_{37}G_{38}$ hinge, albeit small, whereas the G38P mutation disturbed the helix both in its TMD-N and TMD-C parts.

G38 mutant TMD helices display altered hydrogen-bond stability around the $G_{37}G_{38}$ hinge

To further investigate the impact of the G38 mutations on conformational flexibility of the C99 TMD, we next analyzed the stability of intrahelical H-bonds of the $C99_{26–55}$ WT and mutant helices. To this end, we performed backbone amide DHX experiments in TFE/H_2O using MS (MS-DHX) as well as HDX using NMR (NMR-HDX). Determining amide exchange in POPC membranes was not feasible because the bilayer effectively shields central parts of the TMD helix (69,70). Generally, although exchange rate constants also depend on the local concentration of hydroxyl ions (i.e., the exchange catalyst) and are influenced by side-chain chemistry (73), the reduced stability of backbone amide H-bonds associated with more flexible helices results in faster amide exchange. Fig. 4 *A* shows the overall MS-DHX of >98% deuterated $C99_{26–55}$ WT and mutant peptides (5 μM) in TFE/H_2O. Consistent with previous results (31,46,49), overall DHX kinetics was characterized by rapid deuteron exchange within minutes, followed by a relatively fast exchange over 60 min (Fig. 4 *A*, *inset*) and a subsequent very slow process. Near complete exchange was seen after 3 days. Relative to the WT, the G38L mutation slowed hydrogen exchange, whereas an apparent slight enhancement of exchange was observed for G38P. This enhancement is, however, largely ascribed to the fact that proline does not contribute an amide deuterium, thus reducing the number of exchangeable deuterons in DHX (Fig. 4 *A*, *inset*).

To obtain insight into local amide H-bond strength, we next measured residue-specific amide DHX rate constants ($k_{exp,DHX}$) using ETD of our TMD peptides in the gas phase after various periods of exchange (MS-ETD-DHX) (47,72). To enhance fragmentation efficiency, we substituted the N-terminal SNK sequence of the $C99_{26–55}$ TMD by KKK (75). The rate constants shown in Fig. 4 *B* reveal that DHX occurred within minutes for residues up to M35 within TMD-N and at the C-terminal KKK residues for all three peptides. Rate constants gradually decreased by up to two orders of magnitude in the region harboring the $G_{37}G_{38}$ motif. Compared to the WT, both G38 mutants perturbed exchange downstream of the mutation site in the region around the γ-40 cleavage site. Although the G38L mutation decreased $k_{exp,DHX}$ significantly between V39 and T43, G38P increased $k_{exp,DHX}$, mainly for V39 and V40. Very slow exchange was observed in the TMD-C, containing the ε-cleavage sites, which was not affected by the G38 mutants. Additionally, we measured HDX by NMR spectroscopy. The shape of the NMR-HDX profile (Fig. 4 *C*) roughly matched the MS-ETD-DHX profile in that exchange within the TMD-N was faster than within the TMD-C (Fig. 4 *B*). NMR confirmed the locally reduced exchange rates for the G38L mutant and the locally enhanced rates for G38P, although the experimental errors prevented clear assignments of the differences to individual residues. As for MS-ETD-DHX, the G38 mutants did not affect the NMR-HDX in the vicinity of the ε-cleavage sites. The generally lower H/D rate constants, relative to the respective D/H values, are ascribed to the intrinsically slower chemical HDX as compared to DHX (75,85).

DHX rate constants reconstructed from the fraction of open H-bonds and the local water concentration as calculated from the MD simulations could reproduce the overall MS-DHX kinetics well ($0.400 \leq \chi^2 \leq 1.493$, Fig. S5). In accordance with the ETD-derived rate profile, the calculated site-specific k_{DHX} exchange rate constants (Fig. 4 *D*) revealed fast exchange at both termini and very slow exchange

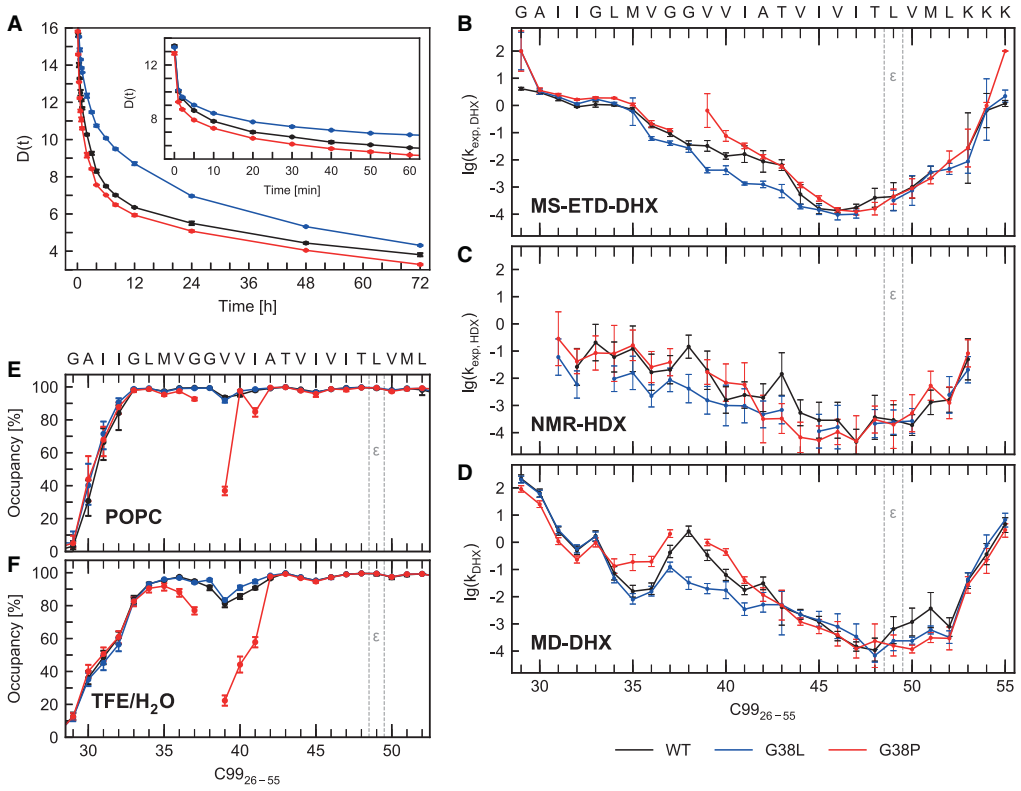

FIGURE 4 DHX rates along the TMD of $C99_{26-55}$ reveal an impact of the G38 mutations on H-bond stability around the mutation sites but not at the ε-sites. (*A*) Overall DHX kinetics of $C99_{26-55}$ WT and G38L and G38P mutant peptides measured with MS-DHX is shown. Complete deuteration was followed by back-exchange in TFE/H_2O (pH 5.0), T = 20°C. Exchange kinetics during the first 60 min (*inset*) and 72 h were measured (n = 3, error bars showing SD are smaller than the size of the symbols). Note that the lower deuterium content in G38P mainly resulted from the lack of one amide deuteron at the cyclic side chain of proline. (*B*) Site-specific DHX rate constants ($k_{exp,DHX}$ (min^{-1})) of $C99_{26-55}$ WT and G38L and G38P mutants dissolved in TFE/H_2O are shown, as determined by MS-ETD (error bars show 95% CI). (*C*) Site-specific HDX rate constants ($k_{exp,HDX}$ (min^{-1})) determined by NMR are shown (n = 3, error bars show SD). (*D*) Site-specific k_{DHX} (min^{-1}) computed from MD simulations are shown (error bars show 95% CI). (*E*) Backbone H-bond occupancy of the individual residues of $C99_{26-55}$ WT and its G38L and G38P mutants in POPC and (*F*) in TFE/H_2O is shown, calculated by MD simulations (error bars show 95% CI). An amide H-bond is counted as closed if either the α- or 3_{10}-H-bond is formed. Note that G38P cannot form H-bonds at residue 38 because of the chemical nature of proline.

in the TMD-C. Additionally, the slow exchange at the ε-sites, without significant differences between WT and the G38 mutants, was confirmed. Taken together, for all peptides, local amide exchange rates determined by three different techniques consistently reported reduced H-bond strength in the helix-turn downstream to the G38 mutation site in the γ-cleavage site region compared to very strong H-bonds around the ε-sites.

To gain further insight into the distribution of backbone flexibility along the $C99_{26-55}$ peptides, we focused on the site-specific population of α-H-bonds (NH(i)…O (i–4)) and 3_{10}-H-bonds (NH(i)…O (i–3)). The population of both H-bonds is of significant interest because switching between α- and 3_{10}-H-bonds allows for conformational flexibility of the TMD helix without inducing a permanent structural change (86). As such behavior was detected previously for $C99_{28-55}$ (46,48,49) as well as for other TMDs (72,86), we calculated both α- and 3_{10}-H-bond occupancies for each residue of $C99_{26-55}$ in POPC and TFE/H_2O, respectively, from the MD simulations (Fig. S6). In POPC, for the WT and G38L peptides, but not for G38P, a 10% lower occupancy of α-H-bonds emanating from backbone amides of V39 was largely compensated through the formation of 3_{10}-H-bonds (Fig. S6). In TFE/H_2O, a larger-stretch of H-bonds spanning from the G33 carbonyl-oxygen to the amide-hydrogen at I41 was destabilized (Fig. S6). In this segment, for all peptides, a maximal drop in α-helicity by 40% was only partially compensated by the formation of 3_{10}-H-bonds, indicating enhanced conformational variability. Note that the HDX reflects the combined occupancies (Fig. 4, *E* and *F*), in which an amide is regarded as protected from exchange if either the α- or the 3_{10}-H-bond is formed. As shown in Fig. 4, *E* and *F*, intrahelical H-bonds were distorted only around the $G_{37}G_{38}$ sites, which correlated with

the flexibility at the $G_{37}G_{38}$ hinge where H-bonds on the opposite face of the hinge have to stretch to allow for bending. This distortion around the $G_{37}G_{38}$ hinge for WT and the expected effects of the G38 mutations were consistent with the above-described DHX experiments (Fig. 4, *B* and *C*).

With regard to the cleavage domain, of all $C99_{26–55}$ peptides both in POPC and TFE/H_2O, we found a 5–10% population of 3_{10}-H-bonds around the amides of T43/V44 and T48/L49 as well as enhanced 3_{10}-H-bond propensity at the border to the C-terminal juxtamembrane residues (Fig. S6). However, neither shifting between α- and 3_{10}-H-bonds nor helix distortions involving the carbonyl-oxygen at the ε-sites or other signs of helix distortions could be detected for the G38 mutants (Fig. 4, *E* and *F*; Fig. S6). Remarkably, the occupancies of 3_{10}-H-bonds in the cleavage domain did not change when changing solvent from POPC to the hydrophilic environment in the TFE/H_2O solution (Fig. S6). This demonstrates that the ε-sites are in a rather stable helical conformation, regardless of the solvent, that is not perturbed by the G38 mutations. In summary, the MD simulation findings and the H/D experiments indicate that alterations of the flexibility of the $G_{37}G_{38}$ hinge caused by the G38 mutations do not result in altered backbone dynamics at the ε-sites.

G38 mutants alter the spatial orientation of the ε-cleavage site region

In addition to local variations of the structure and stability of the C99 TMD, global orientation of the TMD helix in the bilayer may play an important role in substrate recognition and cleavage. TMD helices usually tilt to compensate hydrophobic mismatching between the length of the hydrophobic domain of the TMD and the hydrophobic thickness of the lipid bilayer (87,88). Additionally, azimuthal rotations of the tilted helix around its axis are not randomly distributed but reflect preferential side-chain interactions with the individual components of the phospholipid bilayer (88–90). To explore a potential influence of the G38 mutations on these properties, we investigated the distribution of tilt (τ) and concomitant azimuthal rotation (ρ) angles (Fig. S7 *A*) of $C99_{26–55}$ embedded in a POPC bilayer by ssNMR and MD simulations. The C_α-H_α order parameters of residues A30, L34, M35, V36, G37, A42, and V46 of $C99_{26–55}$ (Table S1), chosen to represent the helical wheel with C_α-H_α bond vectors pointing in many different directions, were derived from DIPSHIFT experiments, which also confirmed the proper reconstitution of the peptides in the POPC bilayer (Fig. S8). To estimate τ and ρ of the TMD helix in $C99_{26–55}$, a variant of the GALA model (68) was used (see Supporting Materials and Methods).

In Fig. 5 *A*, the normalized inverse of the root mean-square deviation ($RMSD_{Norm}$) between data and model is shown as function of tilt and azimuthal rotation angles. For all three peptides, relatively broad τ,ρ landscapes with several possible orientations were found. Reliable helix orientations comprising helix tilt angles on the order of $\tau < 30°$ were found for all three peptides, although the G38P landscape deviated from the similar landscapes of WT and the G38L mutant. A tilt angle below 30° for the WT C99 TMD was also reported by others (91), although in the latter study a very heterogeneous picture with different orientation and dynamics of several helix parts was drawn. As shown in Fig. 5 *B*, the calculated probability distributions of (τ,ρ) combinations from MD simulations were in agreement with the ssNMR observations. Average tilt angles were also below 30° (WT: 23.1° with 95% CI (20.2, 26.2°), in agreement with previous results (43), G38L: 21.8° (18.7, 25.2°), and G38P: 25.9° (22.2, 29.9°)). A precise average ρ angle could not be calculated from the order parameters obtained from ssNMR nor obtained from the MD simulation but only a range of possible orientations, which is indicative of high TMD helix dynamics in liquid-crystalline membranes. In fact, all possible angles of ρ are observed in the MD simulations with considerable probability (Fig. 5 *B*). Consistent with only small mutation-induced variations in helix tilt and rotation angles, no significant differences of the mean residue insertion depths in the POPC bilayer were observed in the MD simulations, indicating quite similar vertical z-position of the cleavable bonds in the membrane for the WT and mutants (Fig. S9).

Helices not only tilt and rotate in the membrane as a rigid body but are able to reorient intrahelical segments relative to each other, which in the case of the C99 TMD is enabled by the $G_{37}G_{38}$ hinge (46–48). We thus next sought to investigate the impact of the G38 mutations on the relative orientation of the helical turn carrying the ε-sites in the TMD-C to that of the TMD-N by analyzing the probability distributions of bending and swivel angles. The bending angle (θ) is defined as the angle between the axes through segment A (residues I31–M35) in the TMD-N and segment B (containing the ε-sites) in the TMD-C (residues I47–M51, Fig. S7 *B*). The swivel angle (ϕ) is defined by the horizontal rotation of domain B relative to the C_α atom of G33 as reference in domain A (Fig. S7 *B*). Positive ϕ-angles represent counterclockwise rotation. We analyzed the bend and swivel conformational sampling from the MD simulations for the $C99_{26–55}$ WT and G38 mutant peptides in POPC and TFE/H_2O (Table S2). In POPC, domain B of the WT and G38L peptides exhibited bending rarely exceeding 30° with a mean value of ~12° (Fig. 5 *C*). For the G38P mutant, an increased population of conformations with θ even larger than 40°, lack of conformations with $\theta < 15°$, and an average bending of ~32° reveal a persistent reorientation of the ε-sites (Fig. 5 *C*, *D*, and *F*). The range of bending angles sampled around their average value was similar ($\pm 30°$) for all peptides. Generally, we observed that C99 TMD bending is anisotropic. Notably, the horizontal rotation (i.e., swivel angle) of the ε-site orientation was sensitively

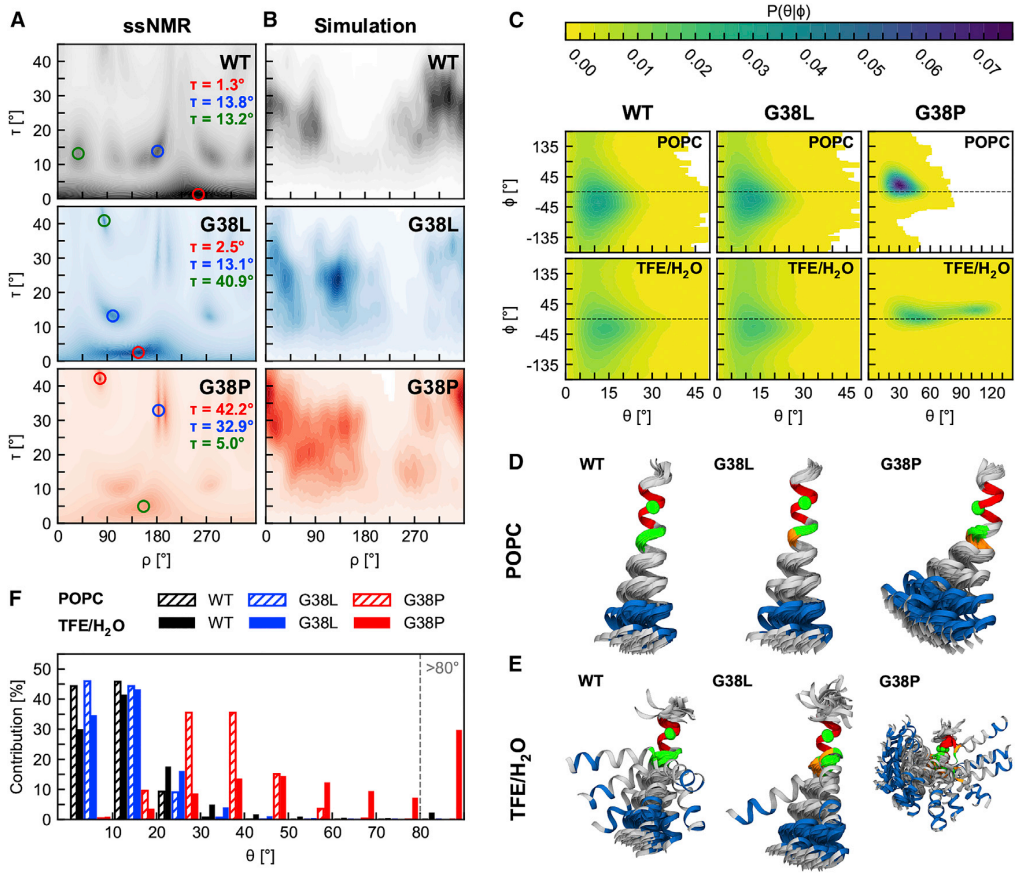

FIGURE 5 G38 mutations of the $C99_{26–55}$ peptide do not significantly alter its global membrane orientation but change the relative orientation of the ε-sites region. (*A*) Heat maps of tilt (τ) and azimuthal rotation (ρ) angle combinations of $C99_{26–55}$ WT and G38L and G38P mutant peptides in a POPC bilayer are given as determined by ssNMR. The colors represent the $RMSD_{Norm}$ of the given (τ,ρ) pair. Maxima (*dark areas*) represent possible orientations. The circles represent the likeliest (*red*), second likeliest (*blue*), and third likeliest (*green*) solutions. (*B*) Probability distributions P (τ,ρ) of τ and ρ angle combinations of $C99_{26–55}$ WT and G38L and G38P mutants in a POPC bilayer are shown, calculated from MD simulations. Dark areas represent high probabilities. (*C*) Probability distributions of bending (θ) and swivel (ϕ) angle combinations characterizing the orientation of ε-sites in $C99_{26–55}$ WT and G38L and G38P mutants in POPC and in TFE/H_2O are shown, calculated from MD simulations. (*D* and *E*) Representative conformations for WT and G38 mutants in (*D*) POPC and (*E*) TFE/H_2O determined by K-means clustering of (θ,ϕ) combinations in cos-sin space are shown. Domains colored in red (domain A) represent the TMD-N segment I31-M35 and were also used to overlay the structures. Domains colored in blue (domain B) indicate the TMD-C segment I47-M51 carrying the ε-sites. The $G_{37}G_{38}$ hinge is colored in green. For the G38 mutants, the L and P residues are depicted in orange. Green spheres represent the C_α atom of G33 used as reference for the determination of swivel angles. (*F*) Distribution of conformations according to their bending angles θ are shown. The last class summarizes all conformations with $\theta > 80°$.

influenced by the mutations with respect to both direction and extent of fluctuations (Fig. 5 *C*). Thus, both G38 mutations imparted a counterclockwise shift of the sampled swivel angles compared to WT. The average ϕ angle shifted by 10° for the G38L mutant and by 40° for the G38P mutant with respect to the WT (Table S2). Furthermore, compared to WT and G38L peptides, which sampled a swivel angle range of $\pm 60°$, the G38P mutation favored a much narrower range ($\pm 30°$) (Fig. 5 *C*). Changing from the POPC membrane to TFE/H_2O did not shift the preference of the peptides for the particular range of swivel angles (Fig. 5, *C* and *E*). However, in TFE/H_2O, we generally noted an increase in the fraction of conformations with larger bending angles (Fig. 5 *F*). In the case of the G38P peptide, we even noticed excursions to a population with large bending angles $\theta > 80°$ (Fig. 5 *F*; Table S2).

The comparison of the bend and swivel behavior of ε-site orientations revealed that the preference for specific helix conformations depends on the mutation at G38. The G38P mutation alters both bend and swivel angles, i.e., vertical and horizontal position of the ε-cleavage site region with respect to TMD-N. In contrast, the G38L mutation mainly impacts the swivel angles and thus misdirects the ε-cleavage region horizontally. Taken together, we found that compared

to the WT, the relative orientation of the domain containing the ε-sites is misdirected for both mutants. The latter could explain the reduced cleavage of both mutants by γ-secretase, as will be discussed below.

G38 mutations relocate hinge sites and alter extent of hinge bending and twisting

The results obtained so far revealed that the impact of the $G_{37}G_{38}$ hinge mutations on H-bond stability is confined to a small number of residues in the hinge region. Although H-bonding around the ε-sites was not altered, we noticed that sampling of ε-site orientations is distorted in the mutants. Because TMD helices generally bend and twist around various flexible sites, leading to changes in the helical pitch or the direction of the helix axis (92–95), we next asked whether such helix motions could contribute to the relative orientation of the ε-cleavage site region. MD simulations allow for analyzing the fundamental types of helix motions, i.e., bending or twisting around a single hinge (referred to as types B and T) and combined bending and/or twisting around a pair of hinges (referred to as types BB, BT, TB, and TT) (48,72). These six types of subdomain motions are exemplified in Fig. 6 *A* for $C99_{26–55}$ WT.

To understand the impact of the G38 mutations on the variability of the relative orientations of the ε-cleavage site region, we investigated the subdomain motions in WT and mutant peptides. Hinge sites are detected as flexible joints, coordinating the motions of quasi-rigid flanking segments (48,72,75,96). The individual contribution of each

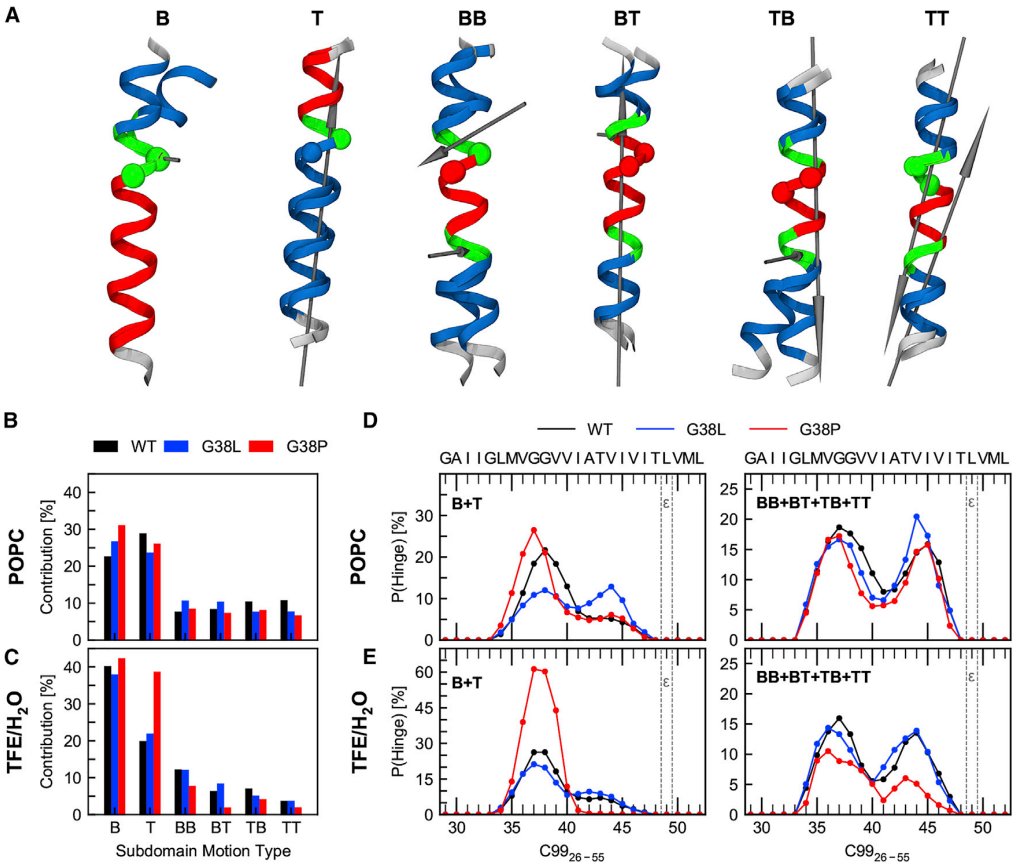

FIGURE 6 G38 mutations alter global bending and twisting motions. (*A*) The fundamental motions of helices exemplified for the $C99_{26–55}$ WT peptide are shown. Motion types are bending (B) and twisting (T) coordinated by a single hinge, as well as combinations of bending and twisting (types BB, BT, TB, and TT) coordinated by a pair of hinges. Helical segments moving as quasi-rigid domains are colored in blue and red. Residues that act as flexible hinges are colored in green. Spheres represent C_α atoms of G37 and G38 and are colored according to the domain in which they are located. Screw axes passing the hinge regions are shown in gray. A screw axis perpendicular to the helix axis indicates a bending-like motion, whereas a screw axis parallel to the helix axis indicates a twisting-like motion. For mixed bending and twisting motions, a larger projection of the screw axis with respect to the helix axis indicates a higher percentage of twisting. (*B*) Probability of all six types of hinge bending and twisting motions in POPC and (*C*) TFE/H_2O is shown. (*D* and *E*) Probability of each residue to act as a hinge site in the single-hinge (B + T) and double-hinge motions (BB + BT + TB + TT) for peptides in (*D*) POPC and (*E*) TFE/H_2O is shown.

type of subdomain motion to the overall dynamics is depicted in Fig. 6, *B* and *C*. More than 90% of the sampled conformations deviated from a straight helix. In the POPC bilayer, bending and twisting around a single hinge (types B + T) contributed ~55% to overall backbone flexibility, and motions around a pair of hinges (types BB, BT, TB, and TT) contributed ~35%. Note that the same residues are able to provide bending as well as twisting flexibility. The loss of packing constraints from lipids as well as enhanced H-bond flexibility in TFE/H_2O (Fig. 4, *E* and *F*) correlated with favored helix bending (types B and BB) in WT and G38L. Remarkably, for G38P, both single bending (type B) as well as twisting (type T) around the $G_{37}G_{38}$ motif were enhanced at the expense of all other hinge motions. The marked helix bending indicates that the broader distributions of tilt and azimuthal rotation angles observed for G38P and the slightly narrower distributions for G38L compared to the WT, as found in the MD simulations and also experimentally by ssNMR (Fig. 5 *A*), might not only indicate differences between these mutants in their intrinsic membrane orientation but could also reflect the increased bending of G38P.

Because of their reduced H-bond stabilities, combined with extensive shifting between α- and 3_{10}-H-bonding (Fig. S6) and the absence of steric constraints, the $V_{36}GGV_{39}$ sites in the C99 TMD are optimally suited to act as hinges, an observation discussed already previously (40,43,45,48,49). Interestingly, a second hinge located in the TMD-C, upstream of the ε-sites appearing around residues $T_{43}VI_{45}$, was revealed (Fig. 6, *D* and *E*), consistent with previous results (48,75). When acting in combination (motion types BB, BT, TB, and TT), both hinges coordinate bending/twisting of the flanks (domains A and B) with respect to the middle part of the helix (residues V36–V46). A change of local H-bond flexibility (Fig. S6) is able to alter the location of the flexible joints coordinating the motions of the flanking segments (Fig. 6, *D* and *E*) (72). In POPC, the hinge propensities of G38P, compared to WT and G38L, clearly shifted from G38 to G37 for all types of motions (Fig. 6 *D*). The shift of a hinge site by one residue correlates with the counterclockwise reorientation of the ε-sites, as also documented in Fig. 5 *C*, by a shift of the swivel angle distribution toward more positive values (also see Table S2). The most severe impact on single-hinge location was noticed for the G38L mutant in POPC. Restricted rotational freedom around L38 in the tightly packed lipid environment eliminates preference for single-hinge bending and twisting around the $G_{37}G_{38}$ hinge and enhances bending around the second $T_{43}VI_{45}$ hinge (Fig. 6 *D*). Most importantly, although WT and G38L peptides sample ε-site orientations characterized by similar bend and swivel angles (Fig. 5 *C*), the backbone conformations contributing to the orientation variability were different. In TFE/H_2O, anisotropic bending over the $G_{37}G_{38}$ hinge was confirmed by the equal hinge propensity of these two residues in the WT peptide, whereas both mutants slightly preferred bending over G37 (Fig. 6 *E*).

In conclusion, the simulations show that the heterogeneous distribution of flexibility in the C99 TMD results from several residues coordinating bending and twisting motions. These hinge motions are favored by the absence of steric constraints as well as by flexible H-bonds shifting between i,i + 3 and i,i + 4 partners. Furthermore, the helix deformations associated with these motions and the location of the hinges are determined by sequence (WT versus G38L or G38P) as well as by packing constraints imposed by the environment (POPC membrane versus TFE/H_2O). Thus, although the ε-sites reside in a stable helical domain, they possess mobility because of a variety of backbone motions enabled by two flexible regions acting as hinges, the $V_{36}GGV_{39}$ region and the $T_{43}VI_{45}$ region. The kind and relative contributions of these motions are distinctly altered by both G38 mutations, leading to a shift of the predominant relative spatial orientation of the ε-sites.

DISCUSSION

To investigate the hypothesis that the flexibility of the TMD helix induced by the $G_{37}G_{38}$ hinge could possibly play an important role for the cleavage of the C99 γ-secretase substrate, the G38 hinge residue was mutated to leucine or proline. CD and solution NMR experiments, as well as MD simulations, confirmed our rationale that exchanging G38 with leucine leads to a globally more stable helix, whereas the G38P mutation reduces overall helicity. Unexpectedly, both mutants strongly reduced cleavage efficiency in the C99 γ-secretase cleavage assay. Moreover, the processivity of γ-secretase was also changed. These observations show that the G38 mutations have a dramatic impact on both the initial cleavage at the ε-site and the subsequent C-terminal trimming by γ-secretase.

One possibility to explain the impaired cleavage of the mutant substrates could be an altered encounter with γ-secretase due to changes of the global orientation of mutant C99 within the membrane. For instance, the different profile in mean-squared fluctuations, as well as the altered average bending angle for the G38P TMD, could alter the initial binding of this mutant with the enzyme. However, the ssNMR measurements and corresponding MD simulations revealed no significant differences of the tilt angles of the TMD of WT and the G38 mutants in a POPC bilayer. Additionally, MD simulations of the initial contact between the $C99_{26–55}$ peptide and γ-secretase in a POPC bilayer did not disclose major differences between the G38 mutants and WT. Consistent with previous studies (27), the PS1 NTF subunit of γ-secretase was found as most prominent contact region. However, substrate contacts with the catalytic cleft of the γ-secretase complex were not observed in these simulations. It is likely that relaxations of the enzyme-substrate complex after binding as well as the

substrate transfer to the active site take more time than the ~370 μs total simulation time per peptide used in this analysis. Apparently, the differences between WT and mutant substrates become relevant at a stage beyond these initial contacts in the substrate recruitment process.

We also assessed whether modified backbone dynamics in the proximity of the ε-sites might explain the altered cleavability of the mutants. Backbone amide DHX experiments showed that, compared to the WT, the overall exchange kinetics was slower for G38L and somewhat faster for G38P. A more detailed residue-specific analysis revealed that effects only occurred near the $G_{37}G_{38}$ hinge, whereas residues around the ε-sites were not affected. Near these sites, MS-ETD-DHX, NMR-HDX, and MD simulations consistently reported low exchange rates and stable intrahelical H-bonds. Neither weaker H-bonds nor interchanging populations of α- and 3_{10}-H-bonds were observed at these sites. Although these results confirm previous studies (31,46,49), they seem to be in contrast with a recent study by Cao et al. (97), who calculated D/H fractionation factors from ratios of exchange rates to determine H-bond strengths in the cleavage domain of C99 in lysomyristoyl-phosphatidyl glycerol micelles. However, as explained elsewhere (75), H-bond strengths derived by the approach of Cao et al. (97) describe the preference for deuterium in an amide-to-solvent H-bond rather than the properties of the intrahelical amide-to-carbonyl H-bonds. Thus, altered backbone dynamics at the ε-sites cannot explain the reduced cleavage by γ-secretase of both the G38L and the G38P mutants. Apparently, breaking the H-bonds in the vicinity of the ε-sites might be the major hurdle for substrate cleavage that can be overcome only by interactions with the enzyme. Interestingly, also at the γ-cleavage sites of the $C99_{26–55}$ peptide, DHX rates were decreased for the G38L mutation and slightly increased for G38P compared to the WT. However, these findings do not necessarily explain the altered processivity of the mutants because the backbone dynamics of the shortened C99 TMD is likely to change after the AICD has been cleaved off.

Advanced models for enzyme catalysis provide evidence that the intrinsic conformational dynamics of substrates and enzymes play a key role for recognition and catalytic steps (98–101). Large-scale shape fluctuations might be selected to enable recognition, whereas lower-amplitude, more localized motions help to optimize and stabilize the enzyme-bound intermediate states (98–102). The chemical reaction is thought to be a rare, yet rapid, event (103) that occurs only after sufficient conformational sampling of the enzyme-substrate complex to generate a configuration that is conducive to the chemical reaction. For the complex between γ-secretase and the substrate, this sampling could be at the level of substrate transfer from exosites to the active site as well as at the level of substrate fitting into the active site. After the initial binding, a series of relaxations and mutual adaptation steps of the substrate's TMD and the enzyme might be required before the scissile bond fits into the active site. In such a way, multiple conformational selection steps may play a decisive role in whether cleavage can take place (100). With regard to C99, the organization of rigidity and flexibility along the helix backbone rather than local flexibility at the ε-cleavage sites alone might be the essential property. Residues enjoying higher flexibility can act as hinges, coordinating the motions of more rigid flanking segments. These flexible hinges might provide the necessary bending and twisting flexibility for orienting the reaction partners properly. Our simulations and previously reported MD simulations reveal that the residues $T_{43}VI_{45}$ upstream of the ε-sites provide additional hinge flexibility that may be of importance for conformational adaptation of the TMD to interactions with the enzyme, where large-scale bending around the $G_{37}G_{38}$ hinge is obstructed (48,75). In addition to bending around the $G_{37}G_{38}$ sites, twisting and more complex motions, including combinations of bending and twisting around the pair of hinges, can occur. The resulting distribution of conformations translates into a diversity of ε-site orientations. The perturbation of this distribution found in our MD simulations might provide plausible explanations of the reduced cleavability of both the G38L and the G38P mutant. Particularly, the counterclockwise shifts of the orientation of the ε-sites for both G38L and G38P mutants in POPC and the absence of small bending angles for G38P indicate that presentation of the scissile bond to the active site of presenilin can be misdirected for each mutant in its own way and differently compared to WT.

Notably, the TMD of Notch1 as well as the TMD of the insulin receptor, two other substrates of γ-secretase (16), have conformations very different from that of the C99 TMD as determined from solution NMR of single-span TM helices in membrane mimics (104,105). In particular, Notch1 appears to be a straight helix, whereas the TMD helix of the insulin receptor is S-shaped, resembling the minor population of double-hinge conformations of the C99 TMD in a POPC bilayer found in our study. These observations seem to challenge the model assuming a central hinge as an integral step for the passage of the substrate toward the active site. Nevertheless, the conformational repertoire of the TMD of the substrates is determined by the α-helical folding, in which helices bend and twist around several sites. The relative importance of the individual conformations reflects sequence-specific differences in local flexibility. Functionally relevant conformational states are not necessarily among the highest-populated ones. Rather, conformations for which the protein has a low intrinsic propensity might be selected for productive interactions with the enzyme regulating or coordinating mechanistic stages preceding catalysis. These so-called "hidden," "invisible," or "dark" states are amenable by NMR or MD methods (102,106–108). Thus, although missing a central flexible hinge, Notch1 and insulin receptor (and even other substrates of γ-secretase) might

nevertheless provide the repertoire of functionally important motions necessary to adapt to interactions with the enzyme at different stages of the catalytic cycle. Furthermore, binding and conformational relaxation steps of different substrates might follow different pathways to optimize the catalytically competent state (99,100).

CONCLUSIONS

Taken together, our study reveals that helix-flexibility-modulating G38L and G38P mutations have a severe impact on cleavage efficiency and processivity of the C99 substrate by γ-secretase. Notably, the G38 mutations do not have an impact on the H-bond stability around the ε-cleavage. We therefore conclude that necessary conformational relaxations required to facilitate the proteolytic event at the active site are not necessarily due to intrinsically enhanced flexibility of the C99 substrate around its ε-cleavage site but must be induced by interactions of the substrate with the enzyme. This interpretation of our data is in line with conclusions from recent vibrational spectroscopy and NMR studies of enzyme-substrate interactions of PSH, an archaeal homolog of presenilin. These studies provided evidence that PSH can induce local helical unwinding toward an extended β-strand geometry in the center of the TMD of the substrate Gurken (109), as well as in the ε-cleavage site region of a C99-TMD-derived substrate (110). Strong evidence for the local unfolding of the substrate TMD helix was also recently provided by cryogenic electron microscopy structural data for γ-secretase in complex with Notch1 or C83 (111,112). For both substrates, unfolding at the ε-cleavage sites was induced and stabilized by the formation of a hybrid β-sheet composed of β-strands of PS1 and a β-strand comprising amino acids near the substrate's TMD C-terminus. Our study suggests that, before the catalytic event, intrinsic conformational flexibility of the substrate in regions remote from the initial cleavage site is also necessary to prepare access to the active site and orient the reaction partners properly. Because conformational adaptability of the C99 substrate TMD is provided by flexible regions coordinating motions of helical segments, subtle changes of H-bond flexibility induced around the $G_{37}G_{38}$ hinge by the G38L and G38P mutations alter the local mechanical linkage to other parts of the helix. As a consequence, irrespective of whether the mutation at the $G_{37}G_{38}$ hinge is helix-stabilizing or helix-destabilizing, the orientation of the distal initial cleavage sites can be distorted in such a way that the probability of productive orientations with the active site of γ-secretase is decreased, thereby leading to impaired cleavage and altered processivity.

SUPPORTING MATERIAL

Supporting Material can be found online at https://doi.org/10.1016/j.bpj.2019.04.030.

AUTHOR CONTRIBUTIONS

D.H., B.L., D.L., C.S., C.M.-G., and H.S. conceived the study, designed experiments, analyzed and interpreted data, and supervised research. A.G. performed all-atom and S.M. coarse-grained MD simulations. F.K. performed CD spectroscopy. N.M. performed cleavage assays. P.H. performed HDX experiments, and M.S., H.H., A.V., and H.F. performed NMR spectroscopy. A.G., S.M., F.K., N.M., P.H., M.S., H.H., A.V., and H.F. analyzed and interpreted data. F.K. coordinated the drafting and writing of the manuscript. F.K., C.M.-G., A.G., C.S., and H.S. wrote the manuscript with contributions of all authors.

ACKNOWLEDGMENTS

We thank Martin Zacharias for providing results of all-atom simulations of γ-secretase and Marius Lemberg for critical reading of the manuscript.

This work was supported by the Deutsche Forschungsgemeinschaft (FOR2290) (D.H., B.L., D.L., C.S., and H.S.) and in part by the VERUM Foundation (F.K.). The Gauss Centre for Supercomputing and the Leibniz Supercomputing Center provided computing resources through grants pr48ko and pr92so (C.S.).

REFERENCES

1. Wolfe, M. S. 2009. Intramembrane-cleaving proteases. *J. Biol. Chem.* 284:13969–13973.
2. Sun, L., X. Li, and Y. Shi. 2016. Structural biology of intramembrane proteases: mechanistic insights from rhomboid and S2P to γ-secretase. *Curr. Opin. Struct. Biol.* 37:97–107.
3. Madala, P. K., J. D. Tyndall, …, D. P. Fairlie. 2010. Update 1 of: proteases universally recognize β strands in their active sites. *Chem. Rev.* 110:PR1–PR31.
4. Timmer, J. C., W. Zhu, …, G. S. Salvesen. 2009. Structural and kinetic determinants of protease substrates. *Nat. Struct. Mol. Biol.* 16:1101–1108.
5. Belushkin, A. A., D. V. Vinogradov, …, M. D. Kazanov. 2014. Sequence-derived structural features driving proteolytic processing. *Proteomics.* 14:42–50.
6. Robertson, A. L., S. J. Headey, …, S. P. Bottomley. 2016. Protein unfolding is essential for cleavage within the α-helix of a model protein substrate by the serine protease, thrombin. *Biochimie.* 122:227–234.
7. Langosch, D., C. Scharnagl, …, M. K. Lemberg. 2015. Understanding intramembrane proteolysis: from protein dynamics to reaction kinetics. *Trends Biochem. Sci.* 40:318–327.
8. Langosch, D., and H. Steiner. 2017. Substrate processing in intramembrane proteolysis by γ-secretase - the role of protein dynamics. *Biol. Chem.* 398:441–453.
9. Lemberg, M. K., and B. Martoglio. 2002. Requirements for signal peptide peptidase-catalyzed intramembrane proteolysis. *Mol. Cell.* 10:735–744.
10. Fluhrer, R., L. Martin, …, C. Haass. 2012. The α-helical content of the transmembrane domain of the British dementia protein-2 (Bri2) determines its processing by signal peptide peptidase-like 2b (SPPL2b). *J. Biol. Chem.* 287:5156–5163.
11. Moin, S. M., and S. Urban. 2012. Membrane immersion allows rhomboid proteases to achieve specificity by reading transmembrane segment dynamics. *eLife.* 1:e00173.
12. Ye, J., U. P. Davé, …, M. S. Brown. 2000. Asparagine-proline sequence within membrane-spanning segment of SREBP triggers intramembrane cleavage by site-2 protease. *Proc. Natl. Acad. Sci. USA.* 97:5123–5128.
13. Linser, R., N. Salvi, …, G. Wagner. 2015. The membrane anchor of the transcriptional activator SREBP is characterized by intrinsic

conformational flexibility. *Proc. Natl. Acad. Sci. USA.* 112:12390–12395.

14. De Strooper, B., T. Iwatsubo, and M. S. Wolfe. 2012. Presenilins and γ-secretase: structure, function, and role in Alzheimer Disease. *Cold Spring Harb. Perspect. Med.* 2:a006304.
15. Steiner, H., A. Fukumori, …, M. Okochi. 2018. Making the final cut: pathogenic amyloid-β peptide generation by γ-secretase. *Cell Stress.* 2:292–310.
16. Haapasalo, A., and D. M. Kovacs. 2011. The many substrates of presenilin/γ-secretase. *J. Alzheimers Dis.* 25:3–28.
17. Jurisch-Yaksi, N., R. Sannerud, and W. Annaert. 2013. A fast growing spectrum of biological functions of γ-secretase in development and disease. *Biochim. Biophys. Acta.* 1828:2815–2827.
18. Holtzman, D. M., J. C. Morris, and A. M. Goate. 2011. Alzheimer's disease: the challenge of the second century. *Sci. Transl. Med.* 3:77sr1.
19. Selkoe, D. J., and J. Hardy. 2016. The amyloid hypothesis of Alzheimer's disease at 25 years. *EMBO Mol. Med.* 8:595–608.
20. Lichtenthaler, S. F., C. Haass, and H. Steiner. 2011. Regulated intramembrane proteolysis–lessons from amyloid precursor protein processing. *J. Neurochem.* 117:779–796.
21. Takami, M., and S. Funamoto. 2012. γ-Secretase-dependent proteolysis of transmembrane domain of amyloid precursor protein: successive tri- and tetrapeptide release in amyloid β-Protein production. *Int. J. Alzheimers Dis.* 2012:591392.
22. Bolduc, D. M., D. R. Montagna, …, D. J. Selkoe. 2016. The amyloid-beta forming tripeptide cleavage mechanism of γ-secretase. *eLife.* 5:e17578.
23. Weggen, S., and D. Beher. 2012. Molecular consequences of amyloid precursor protein and presenilin mutations causing autosomal-dominant Alzheimer's disease. *Alzheimers Res. Ther.* 4:9.
24. Bolduc, D. M., D. R. Montagna, …, M. S. Wolfe. 2016. Nicastrin functions to sterically hinder γ-secretase-substrate interactions driven by substrate transmembrane domain. *Proc. Natl. Acad. Sci. USA.* 113:E509–E518.
25. Struhl, G., and A. Adachi. 2000. Requirements for presenilin-dependent cleavage of notch and other transmembrane proteins. *Mol. Cell.* 6:625–636.
26. Hemming, M. L., J. E. Elias, …, D. J. Selkoe. 2008. Proteomic profiling of γ-secretase substrates and mapping of substrate requirements. *PLoS Biol.* 6:e257.
27. Fukumori, A., and H. Steiner. 2016. Substrate recruitment of γ-secretase and mechanism of clinical presenilin mutations revealed by photoaffinity mapping. *EMBO J.* 35:1628–1643.
28. Kamp, F., E. Winkler, …, H. Steiner. 2015. Intramembrane proteolysis of β-amyloid precursor protein by γ-secretase is an unusually slow process. *Biophys. J.* 108:1229–1237.
29. Arutyunova, E., P. Panwar, …, M. J. Lemieux. 2014. Allosteric regulation of rhomboid intramembrane proteolysis. *EMBO J.* 33:1869–1881.
30. Dickey, S. W., R. P. Baker, …, S. Urban. 2013. Proteolysis inside the membrane is a rate-governed reaction not driven by substrate affinity. *Cell.* 155:1270–1281.
31. Pester, O., A. Götz, …, D. Langosch. 2013. The cleavage domain of the amyloid precursor protein transmembrane helix does not exhibit above-average backbone dynamics. *Chembiochem.* 14:1943–1948.
32. Fernandez, M. A., K. M. Biette, …, M. S. Wolfe. 2016. Transmembrane substrate determinants for γ-secretase processing of APP CTFβ. *Biochemistry.* 55:5675–5688.
33. Kukar, T. L., T. B. Ladd, …, T. E. Golde. 2011. Lysine 624 of the amyloid precursor protein (APP) is a critical determinant of amyloid β peptide length: support for a sequential model of γ-secretase intramembrane proteolysis and regulation by the amyloid β precursor protein (APP) juxtamembrane region. *J. Biol. Chem.* 286:39804–39812.
34. Ren, Z., D. Schenk, …, I. P. Shapiro. 2007. Amyloid β-protein precursor juxtamembrane domain regulates specificity of γ-secretase-dependent cleavages. *J. Biol. Chem.* 282:35350–35360.
35. Higashide, H., S. Ishihara, …, S. Funamoto. 2017. Alanine substitutions in the GXXXG motif alter C99 cleavage by γ-secretase but not its dimerization. *J. Neurochem.* 140:955–962.
36. Oestereich, F., H. J. Bittner, …, L. M. Munter. 2015. Impact of amyloid precursor protein hydrophilic transmembrane residues on amyloid-β generation. *Biochemistry.* 54:2777–2784.
37. Sato, T., T. C. Tang, …, S. O. Smith. 2009. A helix-to-coil transition at the ε-cut site in the transmembrane dimer of the amyloid precursor protein is required for proteolysis. *Proc. Natl. Acad. Sci. USA.* 106:1421–1426.
38. Hu, Y., P. Kienlen-Campard, …, S. O. Smith. 2017. β-Sheet structure within the extracellular domain of C99 regulates amyloidogenic processing. *Sci. Rep.* 7:17159.
39. Ousson, S., A. Saric, …, D. Beher. 2013. Substrate determinants in the C99 juxtamembrane domains differentially affect γ-secretase cleavage specificity and modulator pharmacology. *J. Neurochem.* 125:610–619.
40. Barrett, P. J., Y. Song, …, C. R. Sanders. 2012. The amyloid precursor protein has a flexible transmembrane domain and binds cholesterol. *Science.* 336:1168–1171.
41. Nadezhdin, K. D., O. V. Bocharova, …, A. S. Arseniev. 2011. Structural and dynamic study of the transmembrane domain of the amyloid precursor protein. *Acta Naturae.* 3:69–76.
42. Miyashita, N., J. E. Straub, …, Y. Sugita. 2009. Transmembrane structures of amyloid precursor protein dimer predicted by replica-exchange molecular dynamics simulations. *J. Am. Chem. Soc.* 131:3438–3439.
43. Dominguez, L., S. C. Meredith, …, D. Thirumalai. 2014. Transmembrane fragment structures of amyloid precursor protein depend on membrane surface curvature. *J. Am. Chem. Soc.* 136:854–857.
44. Dominguez, L., L. Foster, …, D. Thirumalai. 2016. Impact of membrane lipid composition on the structure and stability of the transmembrane domain of amyloid precursor protein. *Proc. Natl. Acad. Sci. USA.* 113:E5281–E5287.
45. Lemmin, T., M. Dimitrov, …, M. Dal Peraro. 2014. Perturbations of the straight transmembrane α-helical structure of the amyloid precursor protein affect its processing by γ-secretase. *J. Biol. Chem.* 289:6763–6774.
46. Pester, O., P. J. Barrett, …, D. Langosch. 2013. The backbone dynamics of the amyloid precursor protein transmembrane helix provides a rationale for the sequential cleavage mechanism of γ-secretase. *J. Am. Chem. Soc.* 135:1317–1329.
47. Stelzer, W., C. Scharnagl, …, D. Langosch. 2016. The impact of the 'Austrian' mutation of the amyloid precursor protein transmembrane helix is communicated to the hinge region. *ChemistrySelect.* 1:4408–4412.
48. Götz, A., and C. Scharnagl. 2018. Dissecting conformational changes in APP's transmembrane domain linked to ε-efficiency in familial Alzheimer's disease. *PLoS One.* 13:e0200077.
49. Scharnagl, C., O. Pester, …, D. Langosch. 2014. Side-chain to main-chain hydrogen bonding controls the intrinsic backbone dynamics of the amyloid precursor protein transmembrane helix. *Biophys. J.* 106:1318–1326.
50. Tian, G., C. D. Sobotka-Briner, …, B. D. Greenberg. 2002. Linear non-competitive inhibition of solubilized human γ-secretase by pepstatin A methylester, L685458, sulfonamides, and benzodiazepines. *J. Biol. Chem.* 277:31499–31505.
51. Yan, Y., T. H. Xu, …, H. E. Xu. 2017. Defining the minimum substrate and charge recognition model of γ-secretase. *Acta Pharmacol. Sin.* 38:1412–1424.
52. Altmann, K. H., J. Wójcik, …, H. A. Scheraga. 1990. Helix-coil stability constants for the naturally occurring amino acids in water. XXIII. Proline parameters from random poly (hydroxybutylglutamine-co-L-proline). *Biopolymers.* 30:107–120.

53. von Heijne, G. 1991. Proline kinks in transmembrane α-helices. *J. Mol. Biol.* 218:499–503.

54. Buck, M. 1998. Trifluoroethanol and colleagues: cosolvents come of age. Recent studies with peptides and proteins. *Q. Rev. Biophys.* 31:297–355.

55. Schutz, C. N., and A. Warshel. 2001. What are the dielectric "constants" of proteins and how to validate electrostatic models? *Proteins.* 44:400–417.

56. Sato, C., Y. Morohashi, …, T. Iwatsubo. 2006. Structure of the catalytic pore of γ-secretase probed by the accessibility of substituted cysteines. *J. Neurosci.* 26:12081–12088.

57. Tolia, A., L. Chávez-Gutiérrez, and B. De Strooper. 2006. Contribution of presenilin transmembrane domains 6 and 7 to a water-containing cavity in the γ-secretase complex. *J. Biol. Chem.* 281:27633–27642.

58. Edbauer, D., E. Winkler, …, C. Haass. 2003. Reconstitution of γ-secretase activity. *Nat. Cell Biol.* 5:486–488.

59. Kretner, B., J. Trambauer, …, H. Steiner. 2016. Generation and deposition of Aβ43 by the virtually inactive presenilin-1 L435F mutant contradicts the presenilin loss-of-function hypothesis of Alzheimer's disease. *EMBO Mol. Med.* 8:458–465.

60. Shearman, M. S., D. Beher, …, J. L. Castro. 2000. L-685,458, an aspartyl protease transition state mimic, is a potent inhibitor of amyloid β-protein precursor γ-secretase activity. *Biochemistry.* 39:8698–8704.

61. Shirotani, K., M. Tomioka, …, H. Steiner. 2007. Pathological activity of familial Alzheimer's disease-associated mutant presenilin can be executed by six different γ-secretase complexes. *Neurobiol. Dis.* 27:102–107.

62. Page, R. M., K. Baumann, …, C. Haass. 2008. Generation of Aβ38 and Aβ42 is independently and differentially affected by FAD-associated presenilin 1 mutations and γ-secretase modulation. *J. Biol. Chem.* 283:677–683.

63. Winkler, E., S. Hobson, …, H. Steiner. 2009. Purification, pharmacological modulation, and biochemical characterization of interactors of endogenous human γ-secretase. *Biochemistry.* 48:1183–1197.

64. Anthis, N. J., and G. M. Clore. 2013. Sequence-specific determination of protein and peptide concentrations by absorbance at 205 nm. *Protein Sci.* 22:851–858.

65. Koos, M. R. M., G. Kummerlöwe, …, B. Luy. 2016. CLIP-COSY: a clean in-phase experiment for the rapid acquisition of COSY-type correlations. *Angew. Chem. Int.Engl.* 55:7655–7659.

66. Munowitz, M. G., R. G. Griffin, …, T. H. Huang. 1981. Two-dimensional rotational spin-echo nuclear magnetic resonance in solids: correlation of chemical shift and dipolar interactions. *J. Am. Chem. Soc.* 103:2529–2533.

67. Huster, D., L. Xiao, and M. Hong. 2001. Solid-state NMR investigation of the dynamics of the soluble and membrane-bound colicin Ia channel-forming domain. *Biochemistry.* 40:7662–7674.

68. van der Wel, P. C., E. Strandberg, …, R. E. Koeppe, II. 2002. Geometry and intrinsic tilt of a tryptophan-anchored transmembrane α-helix determined by (2)H NMR. *Biophys. J.* 83:1479–1488.

69. Stelzer, W., B. C. Poschner, …, D. Langosch. 2008. Sequence-specific conformational flexibility of SNARE transmembrane helices probed by hydrogen/deuterium exchange. *Biophys. J.* 95:1326–1335.

70. Poschner, B. C., S. Quint, …, D. Langosch. 2009. Sequence-specific conformational dynamics of model transmembrane domains determines their membrane fusogenic function. *J. Mol. Biol.* 386:733–741.

71. Rand, K. D., M. Zehl, …, T. J. Jørgensen. 2010. Loss of ammonia during electron-transfer dissociation of deuterated peptides as an inherent gauge of gas-phase hydrogen scrambling. *Anal. Chem.* 82:9755–9762.

72. Högel, P., A. Götz, …, D. Langosch. 2018. Glycine perturbs local and global conformational flexibility of a transmembrane helix. *Biochemistry.* 57:1326–1337.

73. Konermann, L., J. Pan, and Y.-H. Liu. 2011. Hydrogen exchange mass spectrometry for studying protein structure and dynamics. *Chem. Soc. Rev.* 40:1224–1234.

74. Xiao, H., J. K. Hoerner, …, I. A. Kaltashov. 2005. Mapping protein energy landscapes with amide hydrogen exchange and mass spectrometry: I. A generalized model for a two-state protein and comparison with experiment. *Protein Sci.* 14:543–557.

75. Götz, A., P. Högel, …, D. Langosch. 2019. Increased H-bond stability relates to altered ε-efficiency and Aβ levels in the I45T familial Alzheimer's disease mutant of APP. *Sci. Rep.* 9:5321.

76. Phillips, J. C., R. Braun, …, K. Schulten. 2005. Scalable molecular dynamics with NAMD. *J. Comput. Chem.* 26:1781–1802.

77. Lee, J., X. Cheng, …, W. Im. 2016. CHARMM-GUI input generator for NAMD, GROMACS, AMBER, OpenMM, and CHARMM/OpenMM simulations using the CHARMM36 additive force field. *J. Chem. Theory Comput.* 12:405–413.

78. Best, R. B., X. Zhu, …, A. D. Mackerell, Jr. 2012. Optimization of the additive CHARMM all-atom protein force field targeting improved sampling of the backbone φ, ψ and side-chain $\chi(_1)$ and $\chi(_2)$ dihedral angles. *J. Chem. Theory Comput.* 8:3257–3273.

79. Wassenaar, T. A., K. Pluhackova, …, R. A. Böckmann. 2015. High-throughput simulations of dimer and trimer assembly of membrane proteins. The DAFT approach. *J. Chem. Theory Comput.* 11:2278–2291.

80. Poma, A. B., M. Cieplak, and P. E. Theodorakis. 2017. Combining the MARTINI and structure-based coarse-grained approaches for the molecular dynamics studies of conformational transitions in proteins. *J. Chem. Theory Comput.* 13:1366–1374.

81. Audagnotto, M., A. Kengo Lorkowski, and M. Dal Peraro. 2018. Recruitment of the amyloid precursor protein by γ-secretase at the synaptic plasma membrane. *Biochem. Biophys. Res. Commun.* 498:334–341.

82. Li, S., W. Zhang, and W. Han. 2017. Initial substrate binding of γ-secretase: the role of substrate flexibility. *ACS Chem. Neurosci.* 8:1279–1290.

83. Hitzenberger, M., and M. Zacharias. 2019. γ-Secretase studied by atomistic molecular dynamics simulations: global dynamics, enzyme activation, water distribution and lipid binding. *Front. Chem.* 6:640.

84. Altwaijry, N. A., M. Baron, …, A. Townsend-Nicholson. 2017. An ensemble-based protocol for the computational prediction of helix-helix interactions in G protein-coupled receptors using coarse-grained molecular dynamics. *J. Chem. Theory Comput.* 13:2254–2270.

85. Teilum, K., B. B. Kragelund, and F. M. Poulsen. 2005. Application of hydrogen exchange kinetics to studies of protein folding. Protein Folding Handbook. Wiley-VCH, pp. 634–672.

86. Cao, Z., and J. U. Bowie. 2012. Shifting hydrogen bonds may produce flexible transmembrane helices. *Proc. Natl. Acad. Sci. USA.* 109: 8121–8126.

87. Killian, J. A. 1998. Hydrophobic mismatch between proteins and lipids in membranes. *Biochim. Biophys. Acta.* 1376:401–415.

88. Strandberg, E., S. Esteban-Martín, …, J. Salgado. 2012. Hydrophobic mismatch of mobile transmembrane helices: merging theory and experiments. *Biochim. Biophys. Acta.* 1818:1242–1249.

89. Strandberg, E., S. Esteban-Martín, …, A. S. Ulrich. 2009. Orientation and dynamics of peptides in membranes calculated from 2H-NMR data. *Biophys. J.* 96:3223–3232.

90. Esteban-Martín, S., and J. Salgado. 2007. The dynamic orientation of membrane-bound peptides: bridging simulations and experiments. *Biophys. J.* 93:4278–4288.

91. Itkin, A., E. S. Salnikov, …, B. Bechinger. 2017. Structural characterization of the amyloid precursor protein transmembrane domain and its γ-cleavage site. *ACS Omega.* 2:6525–6534.

92. Bugge, K., K. Lindorff-Larsen, and B. B. Kragelund. 2016. Understanding single-pass transmembrane receptor signaling from a structural viewpoint-what are we missing? *FEBS J.* 283:4424–4451.

93. Wilman, H. R., J. Shi, and C. M. Deane. 2014. Helix kinks are equally prevalent in soluble and membrane proteins. *Proteins.* 82:1960–1970.

94. Hall, S. E., K. Roberts, and N. Vaidehi. 2009. Position of helical kinks in membrane protein crystal structures and the accuracy of computational prediction. *J. Mol. Graph. Model.* 27:944–950.

95. Hayward, S. 1999. Structural principles governing domain motions in proteins. *Proteins.* 36:425–435.

96. Hayward, S., and R. A. Lee. 2002. Improvements in the analysis of domain motions in proteins from conformational change: DynDom version 1.50. *J. Mol. Graph. Model.* 21:181–183.

97. Cao, Z., J. M. Hutchison, …, J. U. Bowie. 2017. Backbone hydrogen bond strengths can vary widely in transmembrane helices. *J. Am. Chem. Soc.* 139:10742–10749.

98. Henzler-Wildman, K. A., M. Lei, …, D. Kern. 2007. A hierarchy of timescales in protein dynamics is linked to enzyme catalysis. *Nature.* 450:913–916.

99. Nashine, V. C., S. Hammes-Schiffer, and S. J. Benkovic. 2010. Coupled motions in enzyme catalysis. *Curr. Opin. Chem. Biol.* 14:644–651.

100. Ma, B., and R. Nussinov. 2010. Enzyme dynamics point to stepwise conformational selection in catalysis. *Curr. Opin. Chem. Biol.* 14:652–659.

101. Boehr, D. D., R. Nussinov, and P. E. Wright. 2009. The role of dynamic conformational ensembles in biomolecular recognition. *Nat. Chem. Biol.* 5:789–796.

102. Agarwal, P. K., N. Doucet, …, C. Narayanan. 2016. Conformational sub-states and populations in enzyme catalysis. *Methods Enzymol.* 578:273–297.

103. Warshel, A., and R. P. Bora. 2016. Perspective: defining and quantifying the role of dynamics in enzyme catalysis. *J. Chem. Phys.* 144:180901.

104. Deatherage, C. L., Z. Lu, …, C. R. Sanders. 2017. Structural and biochemical differences between the Notch and the amyloid precursor protein transmembrane domains. *Sci. Adv.* 3:e1602794.

105. Li, Q., Y. L. Wong, and C. Kang. 2014. Solution structure of the transmembrane domain of the insulin receptor in detergent micelles. *Biochim. Biophys. Acta.* 1838:1313–1321.

106. Lezon, T. R., and I. Bahar. 2010. Using entropy maximization to understand the determinants of structural dynamics beyond native contact topology. *PLoS Comput. Biol.* 6:e1000816.

107. Palmer, A. G., III 2015. Enzyme dynamics from NMR spectroscopy. *Acc. Chem. Res.* 48:457–465.

108. Anthis, N. J., and G. M. Clore. 2015. Visualizing transient dark states by NMR spectroscopy. *Q. Rev. Biophys.* 48:35–116.

109. Brown, M. C., A. Abdine, …, I. Ubarretxena-Belandia. 2018. Unwinding of the substrate transmembrane helix in intramembrane proteolysis. *Biophys. J.* 114:1579–1589.

110. Clemente, N., A. Abdine, …, C. Wang. 2018. Coupled transmembrane substrate docking and helical unwinding in intramembrane proteolysis of amyloid precursor protein. *Sci. Rep.* 8:12411.

111. Yang, G., R. Zhou, …, Y. Shi. 2019. Structural basis of Notch recognition by human γ-secretase. *Nature.* 565:192–197.

112. Zhou, R., G. Yang, …, Y. Shi. 2019. Recognition of the amyloid precursor protein by human γ-secretase. *Science.* 363:eaaw0930.

2.2 Publication 2: 'Cooperation of N- and C-Terminal Substrate Transmembrane Domain Segments in Intramembrane Proteolysis by γ-Secretase.'

This manuscript has been submitted to Cell Reports recently.

Werner NT[§], Högel P[§], Güner G[§], Stelzer W, Lichtenthaler SF, Steiner H, and Langosch D.

[§]These authors contributed equally.

Summary

This study went one step further and identified features within the APP TMD necessary for cleavage by γ-secretase. Based on the first publication, we hypothesized that a C99-based construct with a TMD consisting only of leucines (polyLeu-TMD) would form a stable and thus very rigid TMD helix that should not be cleaved by γ-secretase. This potential non-substrate served as a basis for reintroducing different motifs into the polyLeu-TMD to define the minimal substrate and to identify substrate requirements. Measurements of the H-bond strength indicated that this C99-based construct with a polyLeu-TMD was indeed very stable. Analyzing the cleavability of this construct confirmed that it is a non-substrate of γ-secretase, since virtually no AICD or Aβ peptides could be detected. These results again underlined the importance of flexibility for substrate cleavage by γ-secretase. Further evidence was provided by the analysis of two other constructs in which the G37/G38-hinge motif has been reintroduced into the polyLeu-TMD. One of these constructs contained only the GG-motif and a second one also contained the two flanking residues V_{36} and V_{39} which may promote bending around the GG-hinge as it has been shown previously to promote conformational dynamics of a TMD (Quint et al., 2010). Indeed, introducing the GG-motif increased the flexibility in the TM-N, as indicated by a reduction in the H-bond stability. This effect was slightly more pronounced for the construct which also featured the flanking valines. Both constructs were cleaved to a rather similar extent, the additional valines only marginally increased the cleavability further, proving that the highly flexible GG-hinge alone is sufficient to render a non-substrate into a substrate of γ-secretase. Further analysis also revealed flexible regions in the TM-N of other γ-secretase substrates, suggesting that this might be a common requirement for γ-secretase.

To clarify whether increasing the flexibility within the cleavage region really increases the cleavability an additional polyLeu-TMD construct with the G37/G38-hinge, harboring a second

helix-destabilizing GG-hinge motif at the ε-cleavage sites, has been included in this study. Introducing this second hinge did indeed result in an increased flexibility in the TM-C, however, without further increasing the cleavability. These results did not support a role for TM-C flexibility in substrate cleavage. Instead, they suggest a more prominent role for specific interactions of the TM-C with the enzyme for this process. Reintroducing a C-terminal part of the cleavage region (V44 - L52), surrounding the ε-cleavage sites, into the non-substrate, on the other hand, was enough to restore cleavability to a similar extent as the hinge motif. Remarkably, combining both, the hinge and the C-terminal cleavage region, on the polyLeu-TMD backbone, was sufficient to restore cleavability of the natural TMD sequence almost completely. This suggests that the flexible region (GG-hinge) in the TM-N and the natural APP cleavage domain in TM-C cooperated for efficient cleavage. Additionally, the findings obtained from the cell-free system could be recapitulated in a cellular model, thus supporting the conclusions drawn from the cell-free system.

A detailed analysis of the cleavage products generated in the cell-free system revealed that, in contrast to the natural TMD of APP, all polyLeu-TMD-based substrates shifted the initial ε-cleavage from position 49 towards cleavage at 48. This suggested that the hinge and the C-terminal cleavage region are important for cleavability but are not decisive for ε-site specificity. Interestingly, the processivity of all generated substrates was greatly enhanced, indicating that once the substrate has reached the active site a helical TMD may promote its trimming, or it may cause γ-secretase to skip the γ- and ζ-cleavage sites. To conclude, the cleavability of a γ-secretase substrate is determined by a certain flexibility in its TM-N allowing the translocation to the active center, by specific interactions of its TM-C with the enzyme crucial for docking to the active site and the formation of a β-sheet, and by the cooperation of the TM-N and TM-C during these steps.

My contribution to this publication

As one of the first authors, I performed the *in vitro* (cell-free) cleavage assays, analyzed, and quantified the levels of the cleavage products generated. I carried out the detailed mass spectrometry analysis of the cleavage products generated (AICD and Aβ) for each substrate. Further, I interpreted the data and helped to write the manuscript. All the data I have contributed can be found in figures 2-4, B-G. (For details, please see author contributions, pp. 178-182).

Cooperation of N- and C-terminal substrate transmembrane domain segments in intramembrane proteolysis by γ-secretase

Nadine T. Werner[1§], Philipp Högel[2§], Gökhan Güner[3§], Walter Stelzer[2], Stefan F. Lichtenthaler[3,4,5*], Harald Steiner[1,3*], and Dieter Langosch[2*]

[1] Biomedical Center (BMC), Division of Metabolic Biochemistry, Faculty of Medicine, LMU Munich, Germany

[2] Chair of Biopolymer Chemistry, Technical University of Munich, Freising, Germany

[3] German Center for Neurodegenerative Diseases (DZNE), Munich, Germany

[4] Neuroproteomics, School of Medicine, Klinikum rechts der Isar, Technical University of Munich, Munich, Germany

[5] Munich Cluster for Systems Neurology (SyNergy), Munich, Germany

[§]These authors contributed equally

[*]Corresponding authors: HS (harald.steiner@med.uni-muenchen.de), SFL (stefan.lichtenthaler@dzne.de), DL (langosch@tum.de)

For editorial review, send correspondence to:

D. Langosch, Lehrstuhl für Chemie der Biopolymere, Technische Universität München, Weihenstephaner Berg 3, 85354 Freising, Germany. Tel.: +49-8161-71-3500; Fax: +49-8161-71-4404; E-mail: langosch@tum.de

Abstract

Intramembrane proteases play a pivotal role in biology and medicine, but how these proteases decode cleavability of a substrate transmembrane domain (TMD) remains unclear. Here, we studied the role of conformational flexibility of a TMD, as determined by deuterium/hydrogen exchange, on substrate cleavability by γ-secretase *in vitro* and *in cellulo*. By comparing hybrid TMDs based on the natural amyloid precursor protein TMD and an artificial poly-Leu non-substrate, we found that substrate cleavage requires conformational flexibility within the N-terminal half of the TMD helix (TM-N). Robust cleavability also requires the C-terminal TMD sequence (TM-C) containing the substrate cleavage sites. Since flexibility of TM-C does not correlate with cleavage efficiency, the role of the TM-C may be defined mainly by its ability to form a cleavage-competent state near the active site, together with parts of presenilin, the enzymatic component of γ-secretase. In sum, cleavability of a γ-secretase substrate depends on cooperating TMD segments, which deepens our mechanistic understanding of intramembrane proteolysis.

Introduction

Understanding the mechanism of intramembrane proteolysis presents a formidable challenge as cleavage occurs within the plane of a lipid membrane. The aspartate protease γ-secretase cleaves the transmembrane domain (TMD) of C99, a shedded form of the amyloid precursor protein (APP) being causally linked to Alzheimer's disease. Cleavage of C99 by γ-secretase generates ~4 kDa amyloid-β (Aβ) peptides, longer forms of which are harmful and believed to trigger the disease [1,2]. In addition to C99, γ-secretase has been reported to cleave the TMDs of ~150 other proteins [3]. Having small extracellular domains is one requirement for cleavage by γ-secretase. Also, all currently known substrates share a type I, i.e. N_{out}, transmembrane topology, yet they represent only a small fraction of this class of single span membrane proteins. Their TMDs do not share an apparent consensus motif [4]. Nonetheless, substrate cleavage shows site specificity which is influenced by many disease-associated and artificial point mutations [1,5].

The sequence-specificity of substrate cleavage in the absence of common sequence patterns presents a conundrum, which led to the view that the presence of certain structural features of a substrate may determine its cleavability by γ-secretase. In seminal studies, the NMR structures of C99 revealed a bend at the $G_{37}G_{38}$ (Aβ numbering) motif within TM-N, the N-terminal half of its transmembrane (TM) helix [6,7]. Considerable conformational flexibility at the bend was confirmed by deuterium/hydrogen exchange (DHX) experiments and molecular dynamics (MD) simulations [8,9]. Indeed, mutations altering helix flexibility at $G_{37}G_{38}$ affect the efficiency and specificity of cleavage [9,10]. It had therefore been suggested that substrate TM helices might share a flexible TM-N (reviewed in [11-13]).

Another potential mechanism governing substrate selection has been proposed to rely on helix flexibility around the cleavage sites. In the case of soluble proteases, the part of a substrate that is docked into a protease's active site exists in an extended conformation exposing the scissile bond to the catalytic residues [14]. Accordingly, substrates of soluble proteases tend to exhibit enhanced conformational flexibility around the scissile peptide bonds. Therefore, cleavage sites are abundant in loop regions as well as in helical regions that are predicted to unfold easily [15]. That an intramembrane protease also requires partial substrate unfolding has only recently been demonstrated by the cryo-EM structures of γ-secretase in complex with the APP fragment C83 or with a fragment of Notch1, another major γ-secretase substrate. Both structures reveal helix unfolding around the residues forming the initial cleavage sites [16]. Similarly, interaction with a homolog of presenilin, the catalytic subunit of γ-secretase, had resulted in extended substrate

conformation [17,18]. Therefore, one might expect that substrate TMD helices are highly flexible near their scissile bonds and that further mutational destabilization would promote cleavage. In line with this, γ-secretase cleavage of TREM2 has been reported recently to be located within a presumably flexible part of its TMD [19]. However, mutational studies have not established a clear link between the impact of mutations on helix flexibility near the scissile sites and the efficiency of their cleavage [20-24].

Here, we initially compared the flexibility profiles of the C99 TMD to those of other well-established γ-secretase substrates. Focusing on C99, we then employed a gain-of-function approach to systematically explore the relationship between its TM helix flexibility and its cleavability with a view to delineate the mechanism of substrate/non-substrate discrimination. To this end, we first designed a non-substrate based on a rigid TM helix. Grafting different motifs of the natural C99 TMD onto this template identified sequence motifs being crucial for flexibility and/or cleavability. Indeed, the $V_{36}G_{37}G_{38}V_{39}$ motif within TM-N conferred partial cleavability along with pronounced helix flexibility in DHX experiments. However, flexibility within the natural cleavage region of TM-C appeared not to govern substrate selection although TM-C is required for full cleavability. Our data suggest that a cooperation of N- and C-terminal TMD segments is critical for presentation of the cleavage site region to the active site and formation of a cleavage-competent state.

Results

Biphasic DHX kinetics diagnose highly flexible regions within the TM helices of γ-secretase substrates. In order to examine the role of local helix flexibility for γ-secretase cleavage, we determined the stability of amide H-bonds by DHX in different TMD model constructs and correlated them to their cleavage efficiency and sequence-specificity *in vitro* and *in cellulo*. For DHX analysis, we used synthetic peptides where the hydrophobic TMD residues are flanked by Lys triplets (Table S1). Similar to our previous analysis of various substrate TMD peptides [8-10,25,26], DHX kinetics of exhaustively (> 95%) deuterated peptides were measured at 20°C and pH 5 in 80% trifluoroethanol (TFE). The polarity of TFE roughly matches that within the solvated interior of a protein [27] and is therefore thought to mimic the aqueous environment within presenilin [28]. Gas-phase fragmentation after different periods of DHX [25], yielded residue-specific DHX kinetics. From the DHX kinetics we derived the corresponding amide exchange rate constants k_{exp} leading to the distributions of the respective free energy changes ΔG that are associated with the disruption of amide H-bonds. These distributions are designated 'flexibility profiles'.

Previously, the flexibility profile of the C99 TMD was obtained by fitting residue-specific DHX kinetics with a monoexponential decay function [9]. Here, a critical re-examination of the C99 kinetics, that were supplemented with additional data, revealed that the exchange kinetics from G37 to A42 and near both helix termini are fitted more appropriately with a biexponential function (Figs. 1 and S1). For each of these amides, we thus obtained a high $k_{exp,A}$ and a low $k_{exp,B}$ value that give rise to the corresponding ΔG_A and ΔG_B values. For example, Fig. 1 B shows biphasic exchange at G38 at logarithmic (upper panel) or linear (lower panel) time scales. We propose that ΔG_A and ΔG_B values describe the free energy change of H-bond opening at a given amide ('single opening') or of the simultaneous opening of two neighboring H-bonds ('double opening), respectively, as detailed in the Supplemental Discussion and schematized in Fig. S2.

Fig. 1 A shows that single openings from G37 to A42, containing the helix bend, are described by very low ΔG_A values of <1.5 kcal/mol. In particular, $k_{exp,A}$ at V39 is similar to the DHX rate constant of an unprotected amide (Fig. S1), thus yielding a negative ΔG_A signifying a mainly open state. Single openings at many other residues correspond to $\Delta G \approx$ 4-5.5 kcal/mol (as obtained by monoexponential curve fitting). Biphasic DHX at amides near both helix termini (Figs. 1 A and S1) suggest frequent double H-bond openings as a hallmark of helix fraying. Due to the uncertainty of ΔG_A at M51, C-terminal helix fraying may either start downstream of M51 or downstream of T48, in which case biphasic exchange at L49 and V50 would appear independent of fraying (see also pL-

VGGV/εGG and pL-VGGV/cr described below). In order to relate the exchange behavior to helix geometry, we compared the DHX data to the lengths and angles of H-bonds within the TM helix in the C99 NMR structure [6]. Fig. S3 shows that none of the amides from G38 through I41 exhibits strong H-bonding. G37 and A42 bordering this segment appear to form strong α-helical H-bonds in the structure. Biphasic exchange at these positions may reflect double H-bond openings together with amides of G38 or I41, respectively.

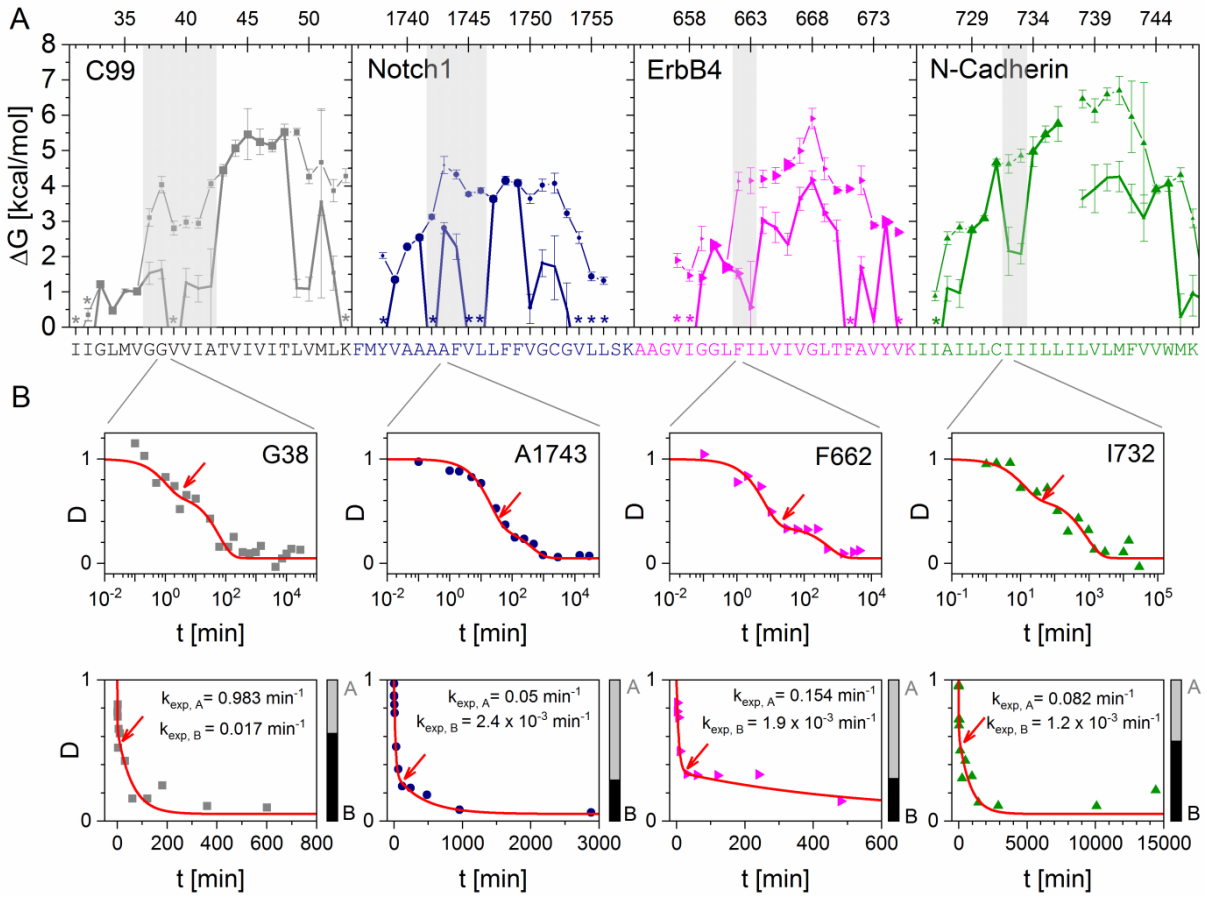

Figure 1. Comparing helix flexibilities of various γ-secretase substrate TMDs. (A) Comparison of amide H-bond stabilities ΔG calculated from k_{exp} values given in Fig. S1. The complete peptide sequences are given in Table S1. Within areas of biphasic DHX, lower and higher values correspond to ΔG_A and ΔG_B, respectively. Thick or thin lines connect the values characterizing single or double H-bond openings, respectively. The sizes of the data points approximate the deuteron populations A and B (data points are obscured by the lines in some cases). Asterisks denote residues where the calculated $\Delta G_A<0$ or where the apparent $k_{exp,A}$ exceeds the chemical exchange rate, thus reflecting extremely facile single H-bond opening (see: Supplemental Discussion). Shading highlights flexible TM-N domains exhibiting biphasic DHX. Aβ numbering is used for C99. Error bars correspond to standard confidence intervals (calculated from the errors of fit in k_{exp} determination, in some cases smaller than the symbols, N=3 independent DHX reactions). No values can be shown for N-Cadherin I737 due to poor fragmentation efficiency and/or overlap of isobaric fragments. N=3 independent DHX reactions. **(B)** Exemplary

DHX kinetics fitted with a biexponential decay function. Upper panels: time axes at a logarithmic scale; lower panels: linear time axes that were truncated such as to better visualize the intersections between fast and slow regimes of exchange (arrows). Bars next to the panels visualize the sizes of the amide populations exchanging with different kinetics (A, fast; B, slow). Data are reproduced from Figs. S1.

In order to examine the potential occurrence of highly flexible regions within the TM helices from γ-secretase substrates other than C99, we also investigated well established substrate TMDs with different primary structures and biological roles [29] by DHX. The flexibility profiles of the TMD helices of ErbB4 and N-Cadherin were determined and compared to those of C99 and Notch1 [26] (Fig. 1 A). In all cases, the respective TM-Ns contain regions with weak amide H-bonds exhibiting biphasic exchange kinetics (grey shading in Fig. 1 A). Biphasic DHX also extended across additional internal residues and at the termini where they indicate helix fraying.

Taken together, biphasic DHX kinetics appear to diagnose very weak amide H-bonding at massively deformed sites within the C99 TM helix, such as at the bend at the $V_{36}G_{37}G_{38}V_{39}$ motif, as well as at frayed helix termini. By analogy, the analysis of other γ-secretase substrate TMDs suggests highly flexible regions including their TM-N helices that may thus be a widespread feature of γ-secretase substrates.

Introducing a hinge into the N-terminal half of a non-substrate poly-Leu TMD facilitates its cleavage. Assuming that a substrate TMD helix must be conformationally flexible [11,12], we reasoned that a rigid poly-Leu sequence [30], denoted in the following for the constructs used as pL, may resist cleavage. The helix-stabilizing effect of Leu [31] at position (i) is ascribed to favorable interactions of its large and flexible side chain with side chains of its (i±3,4) neighbors along an α-helix [32]. Our attempts to assign site-specific exchange rates to a pL helix tagged with Lys triplets failed due to massively overlapping fragment patterns generated by ETD of this symmetric sequence. However, H-bond stability within the oligo-Leu regions of peptides pL-GG or pL-VGGV (Fig. 2 A) approaches ~6 kcal/mol, thus attesting to the rigidity of a pL helix, as previously demonstrated by very slow overall DHX [30].

To assess the potential cleavability of a rigid pL helix by γ-secretase, we used recombinant C99 constructs based on the C100-His_6 protein [33]. We first compared wt C99 to the pL construct, a corresponding chimera holding a 24-residue poly-Leu sequence in place of the natural TMD using a well-established *in vitro* assay [34]. The generated AICD and Aβ peptides (we also refer to Aβ peptides for peptides generated by the pL variants) were analyzed via immunoblotting (Fig. 2 B - E) and by MALDI-TOF mass spectrometry (MS) (Fig. 2 F, G) [35]. Generation of both AICD and Aβ from pL was

strongly reduced to levels of ~6% or ~3% of wt, respectively (Fig. 2 B - E), suggesting that pL is effectively a non-substrate of γ-secretase.

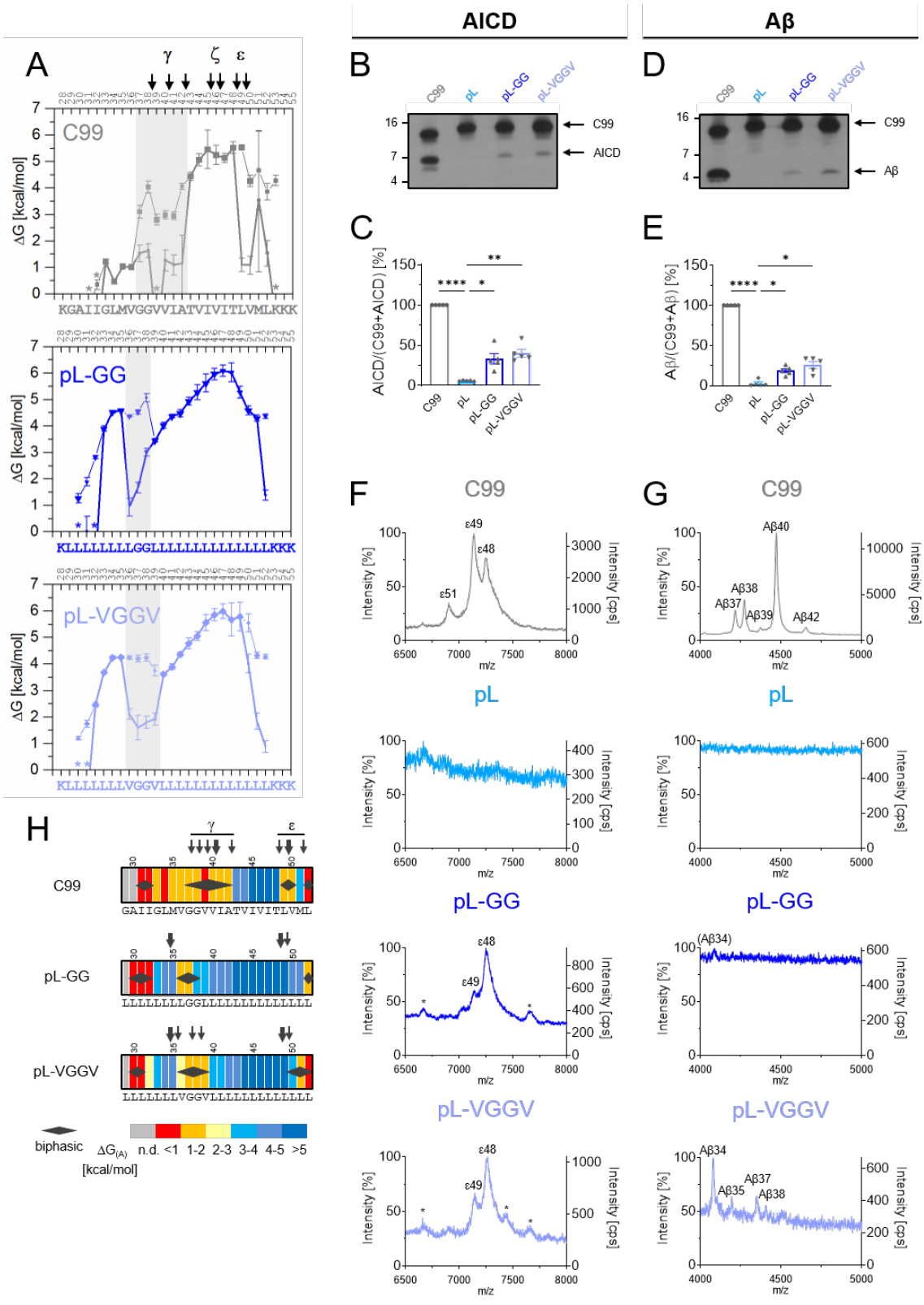

Figure 2. Improving helix flexibility within the N-terminal half of a non-substrate poly-Leu TMD partially restores cleavage. (A) Amide H-bond stabilities ΔG calculated from k_{exp} values given in Fig. S5. Canonical cleavage sites are indicated. C99 data are reproduced from Fig. 1 for comparison.N=3. **(B, D)** Cleavage efficiency of the different constructs after incubation with CHAPSO-solubilized HEK293 membrane fractions at

37°C. Levels of AICD **(B)** and Aβ **(D)** were subsequently analyzed by immunoblotting. The TMD sequences of C99-based constructs are given in part **(A)**. Quantification of AICD **(C)** and Aβ **(E)** levels, values shown as percent of wt C99, which was set to 100%. Data are represented as means ± SEM, (N=5). Statistical significance was assessed using one-way ANOVA with Dunnett's multiple comparison test and pL as a control condition (*: $p < 0.05$, **: $p < 0.01$, ***: $p < 0.001$, ****: $p < 0.0001$). **(F)** Representative MALDI-TOF spectra from three independent measurements show the different AICD fragments generated for the various constructs. The intensities of the highest AICD peaks were set to 100%. Additionally, the counts per second (cps) are shown on the right y-axis. * Unspecific peak. Calculated and observed masses for each peak can be found in Table S2. **(G)** Representative MALDI-TOF spectra from two independent measurements show the different Aβ fragments generated for the various constructs. The intensities of the highest Aβ peaks were set to 100%. Additionally, the counts per second (cps) are shown on the right y-axis. Calculated and observed masses for each peak can be found in Table S3. **(H)** Heat maps summarizing the color-coded ΔG and ΔG_A values of single H-bond openings (n.d. = not determined), the occurrence of presumptive double openings (diamonds) and experimentally determined γ-secretase cleavage sites (arrows).

C99 cleavage is a sequential process starting at alternative ε-sites and then proceeding to ζ-sites and γ-sites. Depending on the chosen ε48 or ε49 site, cleavage produces a 51- or 50-residue long APP intracellular domain (AICD) plus various Aβ peptides, typically ranging from Aβ37-Aβ42, as end products of the stepwise cleavages, including Aβ40 as predominant form [1,36]. For wt C99, the MS pattern of AICD products showed the two characteristic major cleavage products with the predominance of the ε49-cleaved (AICD50) over the ε48-cleaved (AICD51) form, thus confirming the known preferential cleavage at ε49 (Fig. 2 F). In line with this, the intensity of the MS signal for Aβ40 exceeded that of Aβ42 and of a number of smaller cleavage products (Fig. 2 G). Importantly, neither AICD nor Aβ was detected in the case of pL, thus establishing the poly-Leu TMD as a non-substrate TMD.

Using pL as a template for examining the importance of C99-derived sequence motifs, we next asked to which extent the reintroduction of the $G_{37}G_{38}$ or $V_{36}G_{37}G_{38}V_{39}$ hinge motifs would confer both conformational flexibility and cleavability to pL. DHX analysis of the hybrid pL-GG and pL-VGGV peptides revealed biphasic DHX within TM-N (Fig. 2 A). Compared to C99, the occurrence of biphasic DHX is shifted towards the N-terminus, restricted to fewer amides and characterized by somewhat higher ΔG_A and ΔG_B values (Fig. 2 A). The hinge region thus appears to be more pronounced within pL-VGGV than in pL-GG.

Interestingly, cleavage of the corresponding C99-based pL-GG and pL-VGGV constructs produced AICD and Aβ fragments at levels of 33% and 40% (AICD) and 19% and 26% (Aβ) of wt, respectively

(Fig. 2 B - E). Thus, introducing a hinge into the poly-Leu TMD partially restores cleavability. For both constructs, pL-GG and pL-VGGV, initial cleavage remained highly site-specific with ε48-cleaved and ε49-cleaved AICDs predominating, albeit the site of preferential cleavage was shifted from ε49 to ε48 (Fig. 2 F). Surprisingly, abundant Aβ species, such as Aβ40, were not detected with these constructs. For the somewhat better cleavable pL-VGGV, the only species found were peptides ≤Aβ38, with Aβ34 as the major form (Fig. 2 G). Compared to wt C99, this indicates a much more efficient processing of pL-GG and pL-VGGV proteins across the canonical γ-sites.

Fig. 2 H summarizes the data by connecting the strengths of single H-bond opening (ΔG, ΔG_A), as encoded by heat maps, to areas with biphasic DHX and the location and usage of the cleavage sites. It illustrates how introducing a hinge region into TM-N enhances cleavability, albeit with altered cleavage site usage, of an otherwise rigid and uncleavable poly-Leu TMD.

Elevating flexibility within the C-terminal half of a TMD does not promote cleavage. Having shown that the flexibility-conferring diglycine hinge motifs in a poly-Leu TM-N can partially restore cleavage, we next probed the potential impact of enhancing flexibility in the C-terminal half. To this end, we replaced two Leu residues in pL-VGGV by Gly at positions 48 and 49 that are equivalent to the C99 ε-cleavage sites. On the one hand, the resulting pL-VGGV/εGG construct exhibits extended biphasic DHX from positions 46 through 50 (Fig. 3 A). The highly flexible region around both glycines appears to be distinct from a region of C-terminal fraying, as in C99 wt (Fig. 3 A). On the other hand, *in vitro* cleavage of the corresponding C99 chimera did not indicate enhanced AICD or Aβ production relative to the parental pL-VGGV (Fig. 3 B - E) indicating that artificially enhancing helix flexibility around the initial cleavage sites does not promote cleavage. Further, the AICD mass spectrum obtained from pL-VGGV/εGG was similar to that of pL-VGGV with a major peak resulting from cleavage at ε48 (Fig. 3 F). The analysis of the Aβ species revealed minor amounts of Aβ35, Aβ37, and Aβ38 peptides in addition to Aβ34, again being reminiscent of pL-VGGV (Fig. 3 G). Again, Fig. 3 H summarizes the relationships between DHX profiles and cleavage specificity.

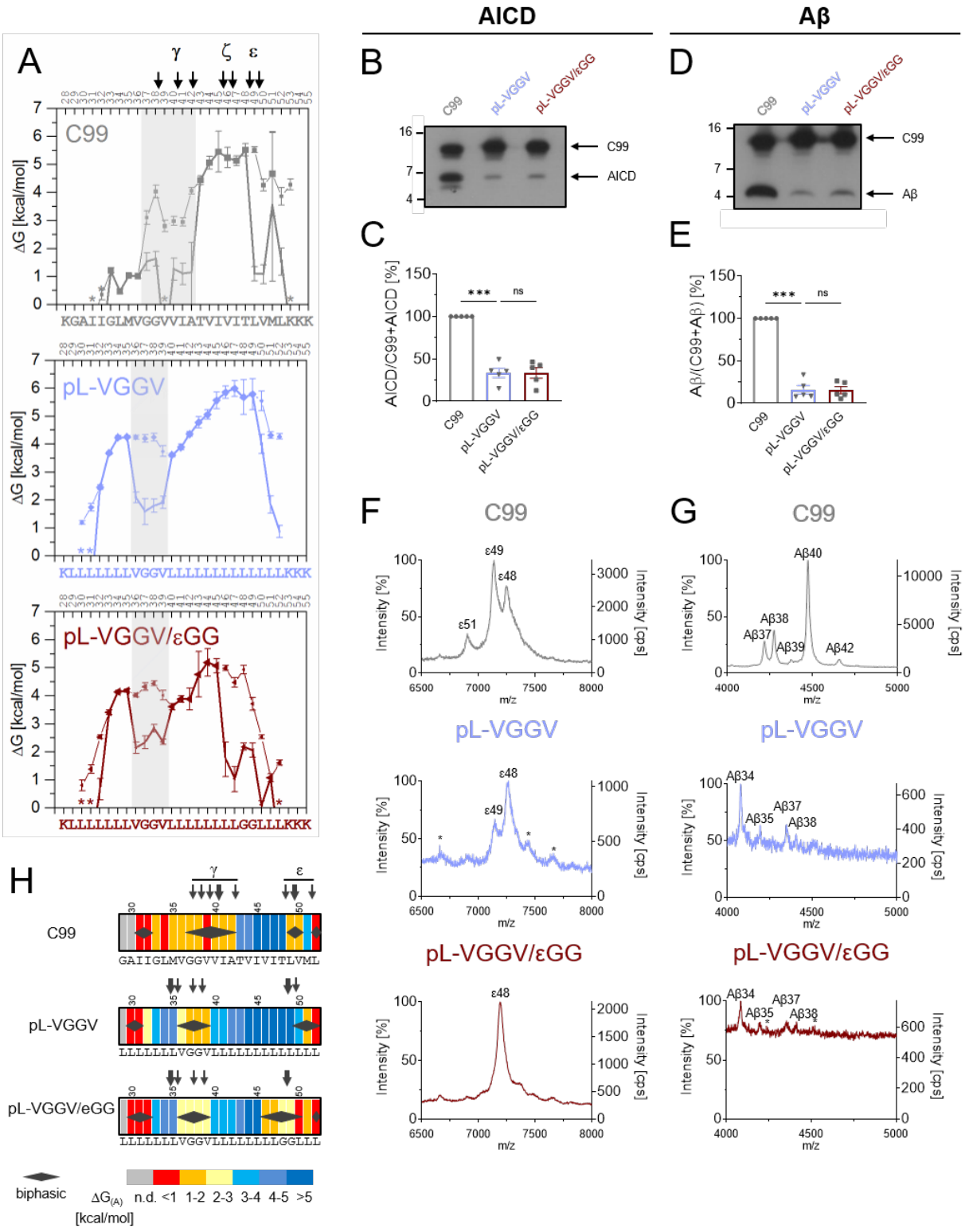

Figure 3. The flexibility of the cleavage region does not determine cleavage efficiency. (A) Amide H-bond stabilities ΔG calculated from k_{exp} values given in Fig. S5. N=3. C99 and pL-VGGV data are reproduced from Fig. 2 for comparison. **(B, D)** Cleavage efficiency of the different constructs after incubation with CHAPSO-solubilized HEK293 membrane fractions at 37°C. Levels of AICD **(B)** and Aβ **(D)** were subsequently analyzed by immunoblotting. The TMD sequences of C99-based constructs are given in part **(A)**. Quantification of AICD **(C)** and Aβ **(E)** levels, values shown as percent of wt C99, which was set to 100%. Data are represented as means ±

SEM, (N=5). Statistical significance was assessed using one-way ANOVA with Dunnett's multiple comparison test and pL-VGGV as a control condition (*: p <0.05, **: p < 0.01, ***: p < 0.001, ****: p < 0.0001). **(F, G)** Data for C99 and pL-VGGV are reproduced from Fig. 2 for comparison. **(F)** Representative MALDI-TOF spectra from three independent measurements show the different AICD fragments generated for the various constructs. The intensities of the highest AICD peaks were set to 100%. Additionally, the counts per second (cps) are shown on the right y-axis. * denotes unspecific peaks. **(G)** Representative MALDI-TOF spectra from two independent measurements show the different Aβ fragments generated for the various constructs. The intensities of the highest Aβ peaks were set to 100%. Additionally, the counts per second (cps) are shown on the right y-axis. * Unspecific peak. **(H)** Heat maps summarizing the color-coded ΔG and ΔG_A values of single H-bond openings (n.d. = not determined), the occurrence of presumptive double openings (diamonds) and experimentally determined γ-secretase cleavage sites (arrows).

That enhancing helix flexibility around the initial cleavage sites does not promote cleavage of C99 by γ-secretase seems to contradict earlier observations where the double mutation I47G/T48G elevated initial C99 cleavage, whereas I47L/T48L strongly inhibited cleavage [22]. The kinetic analysis of the cleavage of these substrates had suggested that those changes resulted from altered reaction velocities (V_{max}) of the bound substrates, rather than from changes in binding affinity (K_m). As those results had suggested an apparent link between helix flexibility of TM-C and cleavability, we studied the conformational flexibility of these mutant helices by DHX. As expected, I47G/T48G increased helix flexibility around the mutated positions and lead to biphasic DHX *viz.* double H-bond openings. Interestingly, this double mutation also extended the occurrence of biphasic DHX across the entire TM-N (Fig. S6). Contrary to our expectation, however, I47L/T48L also slightly destabilizes the mutated sites, for potential reasons discussed below. Additionally, the I47L/T48L mutation abolishes biphasic DHX at V40 and I41 (Fig. S6), suggesting reduced helix flexibility within TM-N. These findings again challenge the idea that helix flexibility around the ε-cleavage sites scales with C99 cleavability [22]. Rather, the mutations might alter cleavability by affecting the flexibility of TM-N.

Combining the N-terminal hinge with the natural cleavage region restores cleavability. In another attempt to restore C99-level cleavage competence, we reintroduced V44 to L52 encompassing the ε-cleavage sites (termed cr). DHX showed that TM-N helix flexibility of pL-VGGV/cr roughly matched that of pL-VGGV (Fig. 4 A). Helix flexibility within the cleavage region greatly exceeded that of the corresponding oligo-Leu sequence. Compared to wt C99, we even detected additional sites of biphasic exchange at I47 and T48 (Fig. 4 A). Interestingly, cleavage assays of pL-VGGV/cr clearly showed an increase in AICD and Aβ production relative to pL-VGGV, up to a level of 82% or 68%, respectively, of the wt construct (Fig. 4 B - E). Including the cleavage region, however, did not restore the wt pattern of AICD fragments. Rather, the usage of ε-sites was similar to that of pL-VGGV, i.e.

mainly at ε48 (Fig. 4 F). The Aβ pattern of pL-VGGV/cr also did not match that of the wt (Fig. 4 G). Again, a mixture of shorter Aβ peptides indicated an increased processivity reminiscent of pL-VGGV and pL-VGGV/εGG. The cleavage efficiency of pL-cr, a derivative lacking the VGGV motif, was similar to that of pL-VGGV (Fig. 4 B - E). Thus, the cleavage region exhibits limited cleavability even without the VGGV hinge (see Fig. 2 B - E). While the patterns of pL-cr AICD fragments matched those of pL-VGGV, it produced mainly Aβ36 (Fig. 4 F, G). Unfortunately, we were unable to interpret DHX data of the pL-cr peptide as we could not identify a sufficient number of fragments after gas phase fragmentation.

Taken together, grafting residues V44 to L52 including both ε-sites onto the oligo-Leu TMD markedly enhanced cleavage. Only in cooperation with the VGGV hinge, however, does this region confer cleavability that is close to that of wt C99. The rank order of cleavability (wt C99 > pL-VGGV/cr > pL-VGGV) again does not match the rank order of helix flexibility of the cleavage region (pL-VGGV/cr > wt C99 > pL-VGGV) (Fig. 4 H).

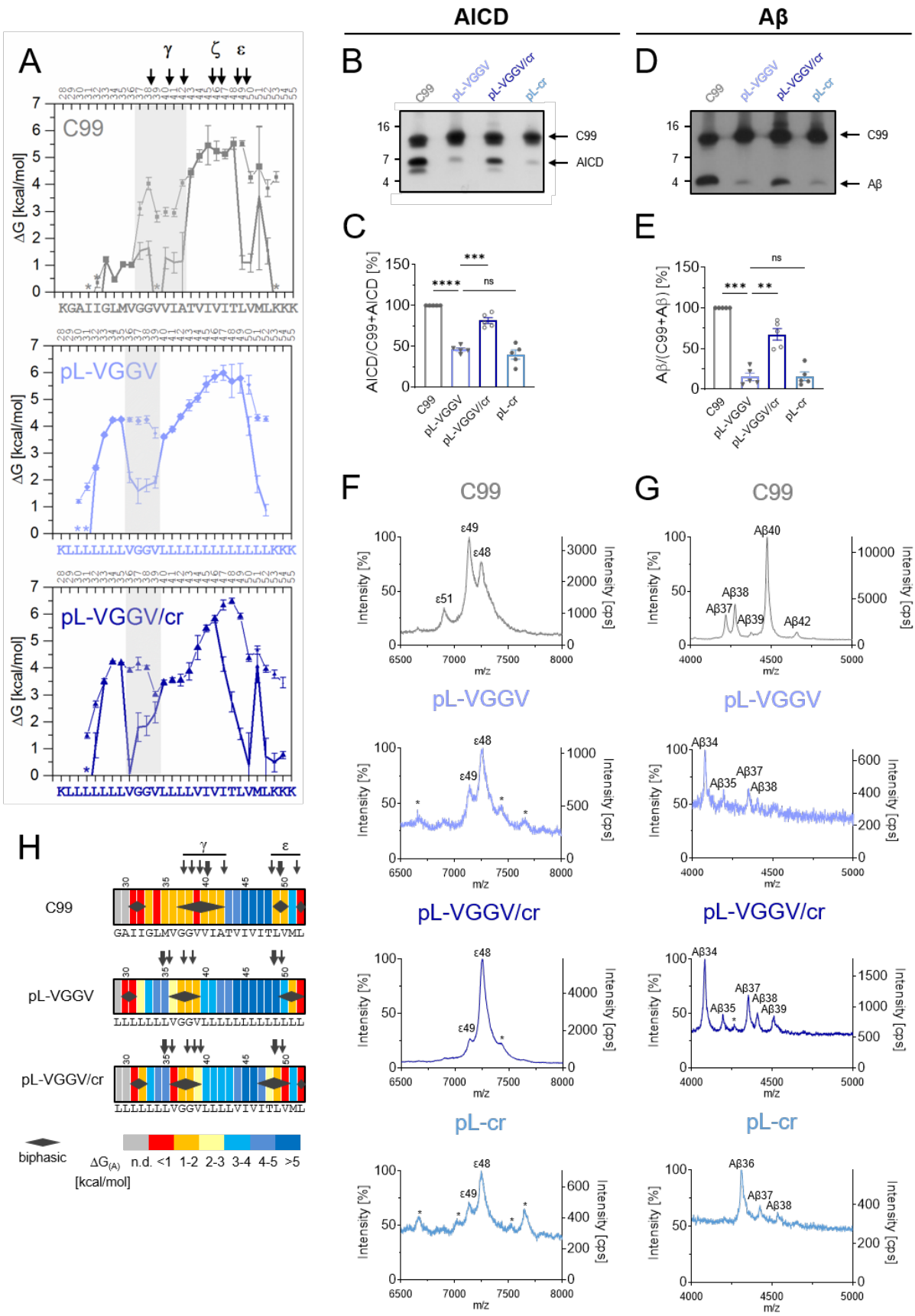

Figure 4. The native sequence around ε-sites cooperates with the hinge to restore cleavability. (A) Amide H-bond stabilities ΔG of pL-VGGV/cr calculated from k_{exp} values given in Fig. S5. N=3. C99 and pL-VGGV data

reproduced from Fig. 2 for comparison. **(B, D)** Cleavage efficiency of the different constructs after incubation with CHAPSO-solubilized HEK293 membrane fractions at 37°C. Levels of AICD **(B)** and Aβ **(D)** were subsequently analyzed by immunoblotting. The TMD sequences of C99-based constructs are given in part **(A)**. Quantification of AICD **(C)** and Aβ **(E)** levels, values shown as percent of wt C99, which was set to 100%. Data are represented as means ± SEM, N=5. Statistical significance was assessed using one-way ANOVA with Dunnett's multiple comparison test and pL-VGGV as a control condition (*: $p < 0.05$, **: $p < 0.01$, ***: $p < 0.001$, ****: $p < 0.0001$). **(F, G)** Data for C99 reproduced from Fig. 2 for comparison **(F)** Representative MALDI-TOF spectra from three independent measurements show the different AICD fragments generated for the various constructs. The intensities of the highest AICD peaks were set to 100%. Additionally, the counts per second (cps) are shown on the right y-axis. **(G)** Representative MALDI-TOF spectra from two independent measurements show the different Aβ fragments generated for the various constructs. The intensities of the highest Aβ peaks were set to 100%. Additionally, the counts per second (cps) are shown on the right y-axis. **(H)** Heat maps summarizing the color-coded ΔG and ΔG_A values of single H-bond openings (n.d. = not determined), the occurrence of double openings (diamonds) and experimentally determined γ-secretase cleavage sites (arrows).

C99 cleavage *in cellulo* supports conclusions drawn from *in vitro* analysis. In order to investigate the role of the different sequence motifs in a cellular membrane with its complex mixture of natural lipids and proteins, we also performed cleavage assays in HEK293 cells transfected with the corresponding C99 derivatives. The extent of γ-cleavage by the cell's endogenous γ-secretase was assessed by determining the levels of secreted Aβ peptides via immunoblotting. As shown in Fig. 5, replacing the C99 TMD by the poly-Leu sequence virtually abolished Aβ secretion in the cell-based assay, corroborating the poly-Leu TMD as a non-substrate. Further, inserting the $G_{37}G_{38}$ or $V_{36}G_{37}G_{38}V_{39}$ motifs again partially restored cleavage to levels of 13% to 22%, respectively, thus confirming the importance of the TM-N hinge region. A similar increase in Aβ production was also seen upon grafting the cleavage region (V44 to L52) onto poly-Leu. Importantly, a further elevation of Aβ secretion, up to a level similar to C99, was achieved by combining the hinge and the cleavage region in the pL-VGGV/cr construct. Similar to the situation in the cell-free assays, a GlyGly pair in the TM-C (pL-VGGV/εGG) did not promote Aβ production above that of pL-VGGV.

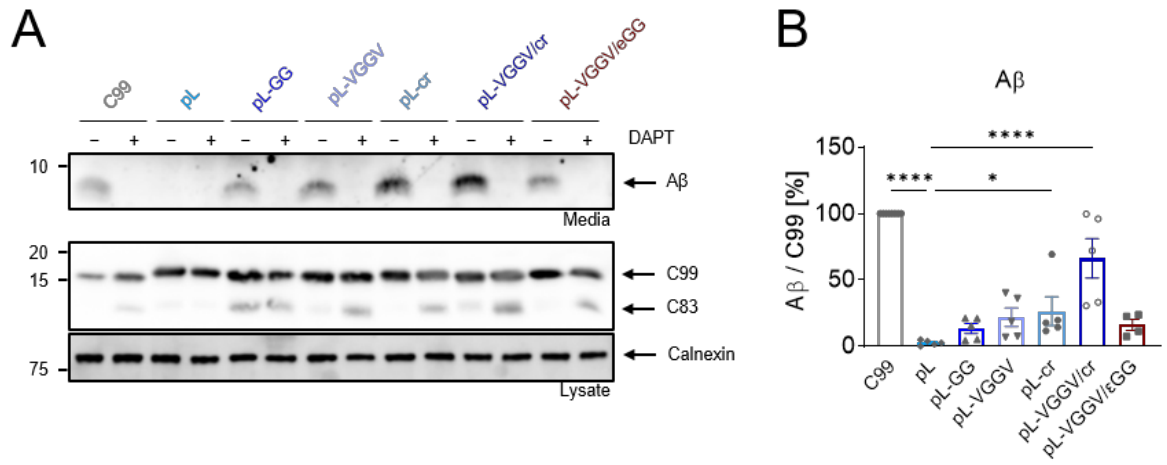

Figure 5. Influence of TMD sequence on Aβ production recapitulated *in cellulo*. HEK293 cells were transiently transfected with the indicated wt and pL-based C99 constructs containing an N-terminal HA- and a C-terminal 2xFlag-tag. To control for specificity, transfected cells were treated with γ-secretase inhibitor DAPT (or vehicle DMSO) for 24 hrs. **(A)** HA-tagged Aβ secreted into the culture media, was detected via immunoblotting against HA. The cellular levels of the full length, tagged C99, as well as α-secretase cleavage product C83, were detected via immunoblotting against Flag. Calnexin was used as a loading control. **(B)** Quantification of HA-Aβ blots, like the exemplary one shown in **(A)**. Only vehicle conditions were quantified since no signals were detected with DAPT. The values represented were normalized to wt C99. Data are represented as means ± SEM, N=4 for pL-VGGV/εGG, and N=5 for the rest. One-way ANOVA with Dunnett's multiple comparison test was performed by taking pL as the control condition (*: $p < 0.05$, **: $p < 0.01$, ***: $p < 0.001$, ****: $p < 0.0001$, F ratio = 29.04, degrees of freedom = 36).

Together, the *in cellulo* cleavage data confirm that a poly-Leu TMD is a non-substrate for γ-secretase. Importantly, the impacts of the hinge and the cleavage region on processing by γ-secretase are similar in cell-based and cell-free assays.

Discussion

The main objective of this study was to illuminate the role and cooperative behaviour of different parts of a TMD in defining its cleavability by γ-secretase. Our overarching aim was to better understand how γ-secretase discriminates substrates from non-substrates, this is also a major unresolved issue with other intramembrane proteases. To this end, we examined hybrid sequences between C99 and an artificial non-substrate, denoted pL, holding a rigid and featureless poly-Leu TMD. pL is virtually uncleaved *in vitro* and *in cellulo,* despite its permissively short extracellular domain and the presence of the C99 juxtamembrane domains. This non-substrate served as a template to identify critical features of a substrate TMD.

First, grafting the C99-derived $G_{37}G_{38}$ or $V_{36}G_{37}G_{38}V_{39}$ motifs onto pL introduced a highly flexible site within TM-N, as indicated by low H-bond strengths and biphasic DHX kinetics reminiscent of the di-glycine hinge within the wt C99 TMD. Biphasic amide exchange is composed of fast and slow regimes that occur in parallel and are proposed to reflect single and correlated double H-bond openings at neighboring amides, respectively. As such, they complement the observation of low H-bond strength in diagnosing massive helix deformations. To our knowledge, this is the first report of biphasic DHX within TM helices. Biphasic DHX had previously been associated with multiple sub-conformations of soluble proteins [37]. While grafting $G_{37}G_{38}$ onto pL partially restores cleavability, the $V_{36}G_{37}G_{38}V_{39}$ motif confers not only stronger flexibility than $G_{37}G_{38}$ but also more effective cleavage. This gain-of-function complements previous mutational studies where mutating G38 had impaired cleavage [9] and provides further proof that a conformationally flexible TM-N is important for C99 cleavage by γ-secretase. MD simulations of the enzyme/C99 complex had suggested previously that TM-N bending enables the C99 TM helix to enter presenilin and access its catalytic cleft [7,38]. By analogy to C99, helix bending may promote the translocation of other substrate TMDs from sites of initial contact towards the catalytic center of γ-secretase. This is supported by the detection of weak H-bonding and biphasic DHX within the TMDs of well-known γ-secretase substrates other than C99. In the case of Notch1, the region exhibiting correlated H-bond openings overlaps partially with the tetra-Ala motif that is distorted in the γ-secretase/Notch1 structure [16]. Although NMR spectroscopy in the helix-stabilizing hydrophobic environment of a detergent micelle had previously indicated a rather straight Notch1 TM helix, MD simulations had suggested helix unwinding at L1747, which is part of the flexible region detected here [39]. With ErbB4 and N-Cadherin, the identification of correlated H-bond openings coincides with the abundance of helix-destabilizing Gly and/or β-branched residues. Altogether, these findings let us propose that substantial conformational flexibility within TM-N, possibly associated with dynamic helix bending, may be one crucial requirement for γ-secretase substrates. Conformational flexibility may also facilitate the processing

of substrates of other intramembrane proteases including site-2-protease, signal peptide peptidase (SPP) and signal peptide peptidase-like (SPPL) proteases, as well as of rhomboid proteases (reviewed in [11,12]). Recent examples include the SPP substrate Xbp1u where stabilizing the TM helix by Leu abolished cleavage [25]. Biphasic DHX kinetics was also detected at several sites within the Xbp1u TMD (our unpublished observations). NMR spectroscopy recently uncovered a slight bend at the $A_{42}G_{43}A_{44}$ motif in the center of the TM helix of tumor necrosis factor α (TNFα), an SPPL2a substrate. Replacing $A_{42}G_{43}A_{44}$ by Leu stabilized the helix and strongly decreased cleavage at a downstream site of the TMD [40]. Although the TNFα TMD bend is less pronounced than that of C99 as shown by NMR spectroscopy [40], biphasic DHX is also apparent at a number of residues including $A_{42}G_{43}A_{44}$ (our unpublished observations).

A second crucial finding reported here relates to a hypothetical role of conformational flexibility within TM-C. One the one hand, biphasic DHX identified significant flexibility at C99 L49 and V50 that appears distinct from helix fraying seen downstream of M51. This flexible region had not been discovered in previous DHX analyses of the C99 TMD where kinetics had been approximated by a monoexponential process [9]. Conformational flexibility within the C99 TM-C is not surprising, though, as it contains an overabundance of β-branched residues that are known to destabilize helices [31,32]. We found that TM-C is important as residues V44 - L52 confer a level of cleavability in pL-cr comparable to that conferred by the $V_{36}G_{37}G_{38}V_{39}$ motif in pL-VGGV. Does the importance of TM-C for cleavage efficiency rest on its conformational flexibility? We consider this an unlikely szenario since a di-glycine pair within the TM-C of pL-VGGV/εGG strongly enhances flexibility but not cleavability. Moreover, we cannot confirm the previously presumed opposite impact of two C99 double mutations (I47G/T48G, I47L/T48L) on conformational flexibility around the ε-sites, thus challenging a proposed dependence of cleavability on local helix flexibility [22]. While the Gly residues indeed destabilize the I47G/T48G TMD near the mutated sites, as shown here [22], they also expand the flexible region within its TM-N. Unexpectedly, the Leu residues of I47L/T48L also have a slight local destabilizing effect which may result from removing the side-chain/main-chain H-bond that extends from T48 to V44 and stabilizes the helix [41]. What is more, the I47L/T48L mutation has a stabilizing effect on TM-N. Conceivably, therefore, the reported opposite effects of both double mutations on C99 cleavability [22] might indeed stem from their opposite long-range impacts on TM-N flexibility. That TM-C helix flexibility does not determine the efficiency of initial cleavage is also suggested by previous findings on other substrate/enzyme systems. In the case of Notch1, the initial S3 cleavage site is formed by G1743 and V1744. Exchanging V1744 by either Leu or Gly strongly compromised cleavage [24]. Also, helix-destabilizing C49P or H52P mutations directly at the cleavage site of the TNFα TMD did not enhance its cleavage by SPPL2a [40]. The finding that increasing the level of helix flexibility

within TM-C does not scale with cleavability is initially surprising given that the region from I47 to V50 of the C99 TMD is unfolded within γ-secretase and residues M51-K54 form a hybrid β-sheet with presenilin [16]. This suggests that TM-C unfolding around the scissile site is indeed required for cleavage. Since, however, TM-C flexibility does not correlate with cleavability of the substrate TMDs investigated here, helix unfolding around cleavage sites may not constitute a rate-limiting step in intramembrane proteolysis. Indeed, helices in aqueous solution unfold at nanosecond timescales [42], which is orders of magnitude faster than notoriously slow intramembrane proteolysis [43-45].

Our third crucial finding is that initial cleavage within the oligo-Leu sequence of pL-GG and pL-VGGV takes place at the canonical positions 48 and 49, although cleavage of our constructs predominated at residue 48 while wt C99 is mainly cut at ε49. It appears therefore, as if the specificity of ε-cleavage is largely independent of the natural C99 sequence. Rather, the presentation of the scissile sites to the catalytic residues may mainly be defined by the overall geometry of the substrate/enzyme complex. Further, the formation of smaller Aβ species at the expense of major ones, such as Aβ40, from our model substrates may indicate that the sites of carboxyterminal trimming are shifted towards the N-terminus. Once the initial cleavage has taken place, the conformational rigidity of the oligo-Leu sequence in between cleavage region and $V_{36}G_{37}G_{38}V_{39}$ hinge may induce skipping of the γ- and ζ-cleavage sites that are characteristic of wt C99, thus producing the shorter Aβ fragments observed here. In an alternative model, the processivity of carboxyterminal trimming of our hybrid constructs may be greatly enhanced such that Aβ40 and Aβ42 are efficiently turned over to a range of shorter Aβ species. Similarly, C99 mutants containing stretches of Phe residues were preferentially cleaved at G38 in previous work [45].

What are the implications of our results for the mechanism of substrate selection? Intramembrane proteolysis takes minutes to hours, as indicated by low catalytic constants [43-45]. Catalytic constants comprise the kinetics of all reaction steps downstream of initial substrate binding [46]. We propose that at least two reaction steps limit cleavage after binding. One rate-limiting process may correspond to translocation of a substrate from an exosite at the interface of the lipid bilayer and presenilin towards its catalytic cleft were the water molecules required for proteolysis are sequestered within the interior of the protein. Translocation beyond sterically obstructing TMDs of presenilin and the loops connecting them is expected to be facilitated by the conformational flexibility of a substrate TM-N. Another rate-limiting process might correspond to the formation of a cleavage-competent state once the TMD has reached the catalytic cleft. Although the flexibility of the TM helix around the ε-site does not determine cleavability, as outlined above, one may envision that the C99 V44 – L52 region is crucial for the combined process of docking the unfolded sequence near

the catalytic residues followed by formation of the tripartite β-sheet with residues near the presenilin TMD7 N-terminus and within the TMD6/TMD7 connecting loop [16]. Although the formation of β-sheet from covalently connected strands takes only tens of microseconds [47], the assembly of sheet from disconnected strands may take minutes, as exemplified by aggregation-driven sheet formation in lysozyme [48]. In sum, at least two slow processes that involve substrate TM-N and TM-C, respectively, appear to limit the kinetics of intramembrane proteolysis. The presence of a conducive TM-N and TM-C as well as their functional cooperation may thus distinguish substrate TMDs from non-substrate TMDs.

Methods

Peptide synthesis. Peptides were synthesized by Fmoc chemistry by PSL, Heidelberg, Germany and purified to >90% purity as judged by mass spectrometry. All other chemicals were purchased from Sigma-Aldrich Co. (St. Louis, Missouri, USA).

Deuterium-hydrogen exchange by MS/MS. All mass spectrometric experiments were performed on a Synapt G2 HDMS (Waters Co., Milford, MA) and measurements were taken from distinct samples. Samples were injected from a 100 µL Hamilton gas-tight syringe via a Harvard Apparatus 11 Plus with a flow rate of 5 µL/min. Spectra were acquired in a positive-ion mode with one scan per second and a 0.1 s interscan time. Solutions of deuterated peptide (100 µM in 80% (v/v) d1-trifluoroethanol (d1-TFE) in 2 mM ND_4-acetate) were diluted 1:20 with protonated solvent (80% (v/v) TFE in 2 mM NH_4-acetate, pH 5.0) to a final peptide concentration of 5 µM and incubated at 20.0°C. Exchange reactions were quenched by cooling on ice and lowering the pH to 2.5 by adding 0.5% (v/v) formic acid. Mass/charge ratios were recorded and evaluated as previously described [49]. For electron transfer dissociation (ETD), we used 1,4-dicyanobenzene as an electron donor and preselected 5+ charged peptides via MS/MS. Fragmentation of peptides was performed as described [10]. Briefly, ETD MS/MS scans were accumulated over a 10 min scan time. ETD-measurements were performed after 13 different incubation periods (from 1 min to 3 d) where exchange had taken place at pH 5.0. Shorter (0.1 min, 0.5 min) and longer (5 d, 7 d) incubation periods were simulated by lowering the pH to 4.0 or elevating pH to 6.45, respectively, using matched time periods. The differences to pH 5.0 were taken into account when calculating the corresponding rate constants. We note that base-catalysed exchange is responsible for at least 95% of the total deuteron exchange at ≥ pH 4.0. The resulting ETD c' and z fragment spectra were evaluated using a semi-automated procedure (ETD FRAGMENT ANALYZER module of MassMap_2019-01_28_LDK Software [25]). The free energies ΔG required for H-bond opening were calculated from $k_{exp,DHX}$ and k_{ch} based on equation (1) based on Linderstrøm-Lang theory [50], assuming EX2 conditions and a predominantly folded state [25].

$$\Delta G = -R\,T\,\ln\left(\frac{k_{exp,DHX}}{k_{ch}-k_{exp,DHX}}\right) \qquad (1)$$

where k_{ch} represents the sequence-specific chemical rate constants that were calculated using the program SPHERE (http://landing.foxchase.org/research/labs/roder/sphere/) (under the set conditions: D-to-H-exchange, reduced Cys, pH =5.0, T = 20.0°C).

Monoexponential fitting of the data was done with equation (2) to calculate $k_{exp,DHX}$, which accounts for the concentration of deuterated solution in the DHX-ETD assay of 5% (v/v)

$$D(t) = 0.95 \cdot e^{-k_{exp,DHX}t} + 0.05 \quad (2)$$

while biexponential fitting was done with equation (3):

$$D(t) = A \cdot e^{-k_{exp,DHX,A}t} + B \cdot e^{-k_{exp,DHX,B}t} + 0.05 \quad (3)$$

Where A and B are the population sizes of the deuterons with slower and faster exchange rates, $k_{exp, DHX, A}$ and $k_{exp, DHX, B}$ respectively and A + B = 0.95.

C99 substrate constructs. All poly-L C99 constructs were generated by GenScript with a N-terminal signal sequence followed by a single N-terminal HA-tag and two C-terminal FLAG-tags in expression vector pcDNA3.1 to allow their direct use in cell-based assays. For cell-free assays, the constructs were initially recloned as PCR fragments into pQE60 (Qiagen) as described for wt C100-His_6 [33] to contain an N-terminal Met (M1 in C100) and a C-terminal His6 tag connected via a GSRS linker and then further recloned as NcoI/HindIII fragments into pET-21d(+) (Novagen) to increase expression yields.

Production of recombinant proteins and γ-secretase *in vitro* cleavage assay. Wt and pL-based C99 constructs were expressed in *E.coli* BL21$(DE3)_{RIL}$ or Rosetta(DE3) cells, respectively. All constructs were purified by Ni-NTA-agarose affinity chromatography. Briefly, induced cells were incubated for 3.5h at 37°C and sonicated. Following overnight urea-lysis [20 mM Tris/HCl (pH 8.5), 6 M urea, 1 mM $CaCl_2$, 100 mM NaCl, 1% Triton X-100, 1% SDS, with protease inhibitors], Ni^{2+}-NTA-agarose was added and the samples were incubated for 2h at room temperature with shaking. Following three washing steps, the substrate proteins were eluted with a buffer containing imidazole [50 mM Tris/HCl (pH 8.5), 300 mM NaCl, 0.2% SDS, 100 mM imidazole (pH 8.5)]. Purified constructs were incubated overnight at 37°C together with detergent-solubilized HEK293 membrane fractions containing γ-secretase and cleavage efficiency was analyzed as outlined previously [34]. Samples incubated at 4°C or at 37°C and in the presence of 0.5 µM of the γ-secretase specific inhibitor L-685,458 (Merck Millipore) [51] served as controls (Fig. S7). The *in vitro* generated cleavage products (AICD and Aβ) were analyzed by immunoblotting using antibody 2D8 and Y188, respectively, and quantified by measuring the chemiluminescence signal intensities with the LAS-4000 image reader (Fujifilm Life Science, USA). Quantification of cleavage products for each of the tested substrates was obtained from five independent assays (N=5). Measurements were taken from distinct samples.

Mass spectrometric analysis of substrate cleavage products. For analysis of the different AICD and Aβ species produced by γ-secretase mass spectrometry analysis was performed as previously described [35]. In brief, after incubation of purified substrate with detergent-solubilized membrane fractions containing γ-secretase, an immunoprecipitation step using the antibodies Y188 (AICD) and 4G8 (Aβ) was performed. Samples were diluted using IP-MS buffer [0.1% N-octyl glucoside, 140 mM NaCl, and 10 mM Tris (pH 8.0)] and incubated with the Y188 antibody and Protein A-Sepharose or with 4G8 and Protein G-Sepharose overnight at 4°C. The immunoprecipitates were washed three times with IP-MS buffer and distilled water and finally eluted (0.1% trifluoroacetic acid in 50% acetonitrile, saturated with a-cyano-4-hydroxy cinnamic acid). Subsequently, samples were subjected to mass spectrometry analysis on a 4800 MALDI-TOF/TOF Analyzer (Applied Biosystems/MDS SCIEX).

Statistics – mass spectrometry. Residue-specific DHX kinetics (equations (2) and (3)) originate from time-dependent deuteron contents D_{mean} averaged from the corrected masses of different fragment ions. In brief, the rate constants $k_{exp,\ DHX}$ were determined by a non-linear least squares fitting routine. Standard errors of $\log k_{exp,DHX}$ result from the errors of the fits. The limits of the standard confidence interval of ΔG are calculated by means of the standard error of $\log k_{exp,DHX}$. A detailed account of the procedure is presented in Supplemental Statistics.

For mass spectrometric analysis of AICD and Aβ generated in the *in vitro* cleavage assays, the cleavage products were immunoprecipitated and subsequently analyzed via MALDI-TOF mass spectrometry. One such assay represents one independent experiment. The AICD and Aβ spectra were generated from separate assays. The AICD spectra were measured from three (N=3) and the Aβ spectra from two independent experiments (N=2). In both cases, representative MALDI-TOF spectra are shown.

Statistics – cleavage assays. For one *in vitro* cleavage assay each of the constructs analyzed in this study was incubated together with detergent-solubilized γ-secretase. One such assay represents one independent experiment. Cleavage efficiency was analyzed for each assay separately and quantifications were done from five independent cleavage assays (N=5). Statistical significance was assessed using one-way ANOVA with Dunnett's multiple comparison test (*: $p < 0.05$, **: $p < 0.01$, ***: $p < 0.001$, ****: $p < 0.0001$). Two group comparisons were done using pL (Fig. 2) or pL-VGGV (Fig. 3 and 4) as a control group for a multiple comparison against all other constructs. Data are represented as means ± SEM. For *in cellulo* assays, the cleavage efficiencies of the constructs were tested in five independent experiments (N=5), with the exception of pL-VGGV/cr construct that was quantified in four independent experiments (N=4). Statistical significance was assessed using one-

way ANOVA with Dunnett's multiple comparison test (*: p <0.05, **: p < 0.01, ***: p < 0.001, ****: p < 0.0001). One group comparison was done using pL as a control group for a multiple comparison against all other constructs. Data are represented as means ± SEM.

***In cellulo* cleavage assays.** The HEK293 cells were cultured in DMEM media (Gibco) supplemented with 10%FCS in BioCoat™ Poly-D-Lysine 24-well (Corning) plates. The constructs were generated as mentioned in the section on C99 substrate constructs. Transfection of the indicated constructs was performed by Lipofectamine™ 2000 (Invitrogen), according to manufacturer's instructions. After overnight incubation with transfection solution, following 1x PBS wash, 500 µL of fresh media containing 1 µM DAPT (or vehicle DMSO) were added to the transfected cells. Conditioned media and cell lysates were collected after 24 h incubation. The conditioned media were centrifuged (1 h, 180000 x g, 4°C) to pellet cell debris and exosomes. Immunoblotting was performed to measure the Aβ release into the conditioned media from the transiently transfected HEK293 cells. Cell lysates were prepared as described [52] with STET lysis buffer (150 mM NaCl, 50 mM Tris pH 7.5, 2 mM EDTA, 1% Triton X-100) with protease inhibitor (Roche). For protein analysis by immunoblotting, samples were prepared as described [52]. Measurements were taken from distinct samples. Following antibodies were used in the immunoblots in given dilutions, anti-HA.11 (1:1000) (Covance, MMS-101P), anti-FLAG (1:2000) (Sigma-Aldrich, F1804), anti-Calnexin (1:2000) (Enzo, ADI-SPA-860).

Biological material availability. Plasmids encoding recombinant proteins can be obtained from the authors upon request.

Reporting summary. Further information on research design is available in the Nature Research Reporting Summary linked to this article.

Data availability. All data associated with this study are present in the paper and in the Supplementary Information. Source data are provided upon request.

Code availability. Computer code associated with this study can be obtained from the authors upon request.

References

1 Steiner, H., Fukumori, A., Tagami, S. & Okochi, M. Making the final cut: pathogenic amyloid-β peptide generation by γ-secretase. *Cell Stress* **2**, 292 - 310 (2018).

2 Hardy, J. & Selkoe, D. J. The amyloid hypothesis of Alzheimer's disease: progress and problems on the road to therapeutics. *Science* **297**, 353-356 (2002).

3 Güner, G. & Lichtenthaler, S. F. The substrate repertoire of γ-secretase/presenilin. *Seminars in Cell and Developmental Biology* **105**, 27-42, doi:10.1016/j.semcdb.2020.05.019 (2020).

4 Beel, A. J. & Sanders, C. R. Substrate specificity of γ-secretase and other intramembrane proteases. *Cellular and Molecular Life Sciences* **65**, 1311-1334 (2008).

5 Wolfe, M. S. Processive proteolysis by γ-secretase and the mechanism of Alzheimer's disease. *Biological Chemistry* **393**, 899-905, doi:10.1515/hsz-2012-0140. PMID: 22944690. (2012).

6 Barrett, P. J. *et al.* The amyloid precursor protein has a flexible transmembrane domain and binds cholesterol. *Science* **336**, 1168-1171, doi:10.1126/science.1219988 (2012).

7 Silber, M., Hitzenberger, M., Zacharias, M. & Muhle-Goll, C. Altered hinge conformations in APP transmembrane helix mutants may affect enzyme-substrate interactions of γ-secretase. *ACS Chemical Neuroscience* **11**, 4426-4433, doi:10.1021/acschemneuro.0c00640 (2020).

8 Pester, O. *et al.* The backbone dynamics of the amyloid precursor protein transmembrane helix provides a rationale for the sequential cleavage mechanism of γ-secretase. *Journal of the American Chemical Society* **135**, 1317-1329 (2013).

9 Götz, A. *et al.* Increased H-bond stability relates to altered ε-cleavage efficiency and Aβ levels in the I45T familial Alzheimer's disease Mutant of APP. *Scientific Reports* **9**, 5321, doi:10.1038/s41598-019-41766-1 (2019).

10 Stelzer, W., Scharnag, C., Leurs, U., Rand, K. D. & Langosch, D. The impact of the 'Austrian' mutation of the amyloid precursor protein transmembrane helix is communicated to the hinge region. *Chemistry Select* **1**, 4408-4412 (2016).

11 Langosch, D., Scharnagl, C., Steiner, H. & Lemberg, M. K. Understanding intramembrane proteolysis: from protein dynamics to reaction kinetics. *Trends in Biochemical Sciences* **40**, 318-327, doi:10.1016/j.tibs.2015.04.001 (2015).

12 Langosch, D. & Steiner, H. Substrate processing in intramembrane proteolysis by γ-secretase - the role of protein dynamics. *Biological Chemistry* **398**, 441-453, doi:10.1515/hsz-2016-0269 (2017).

13 Hitzenberger, M. *et al.* The dynamics of γ-secretase and its substrates. *Seminars in Cell and Developmental Biology* **105**, 86-101, doi:10.1016/j.semcdb.2020.04.008 (2020).

14 Madala, P. K., Tyndall, J. D., Nall, T. & Fairlie, D. P. Update 1 of: Proteases universally recognize β strands in their active sites. *Chemical Reviews* **110**, PR1-31, doi:10.1021/cr900368a (2010).

15 Belushkin, A. A. *et al.* Sequence-derived structural features driving proteolytic processing. *Proteomics* **14**, 42-50, doi:10.1002/pmic.201300416 (2014).

16 Yang, G. *et al.* Structural basis of Notch recognition by human γ-secretase. *Nature* **565**, 192-197, doi:10.1038/s41586-018-0813-8 (2019).

17 Brown, M. C. *et al.* Unwinding of the Substrate Transmembrane Helix in Intramembrane Proteolysis. *Biophysical Journal* **114**, 1579-1589, doi:10.1016/j.bpj.2018.01.043 (2018).

18 Clemente, N., Abdine, A., Ubarretxena-Belandia, I. & Wang, C. Coupled transmembrane substrate docking and helical unwinding in intramembrane proteolysis of amyloid precursor protein. *Scientific Reports* **8**, 12411, doi:10.1038/s41598-018-30015-6 (2018).

19 Steiner, A. *et al.* γ-Secretase cleavage of the Alzheimer risk factorTREM2 is determined by its intrinsic structural dynamics. *EMBO Journal*, 17, doi:10.15252/embj.2019104247 (2021).

20 Kwok, J. B. *et al.* Novel Leu723Pro amyloid precursor protein mutation increases amyloid β42(43) peptide levels and induces apoptosis. *Annals of Neurology* **47**, 249-253 (2000).

21 Bocharov, E. V. *et al.* Familial L723P mutation can shift the distribution between the alternative APP transmembrane domain cleavage cascades by local unfolding of the ε-cleavage site suggesting a straightforward mechanism of Alzheimer's disease pathogenesis. *ACS Chemical Biology* **14**, 1573-1582, doi:10.1021/acschembio.9b00309 (2019).

22 Fernandez, M. A. *et al.* Transmembrane substrate determinants for γ-secretase processing of APP CTFβ. *Biochemistry* **55**, 5675-5688, doi:10.1021/acs.biochem.6b00718 (2016).

23 Xu, T. H. *et al.* Alzheimer's disease-associated mutations increase amyloid precursor protein resistance to γ-secretase cleavage and the Aβ42/Aβ40 ratio. *Cell Discovery* **2**, 16026, doi:10.1038/celldisc.2016.26 (2016).

24 Vooijs, M., Schroeter, E. H., Pan, Y., Blandford, M. & Kopan, R. Ectodomain shedding and intramembrane cleavage of mammalian Notch proteins are not regulated through oligomerization. *Journal of Biological Chemistry* **279**, 50864-50873 (2004).

25 Yucel, S. S. *et al.* The metastable XBP1u transmembrane domain defines determinants for intramembrane proteolysis by signal peptide peptidase. *Cell Reports* **26**, 3087 - 3099, doi:10.1016/j.celrep.2019.02.057 (2019).

26 Stelzer, W. & Langosch, D. Conformationally flexible sites within the transmembrane helices of amyloid precursor protein and Notch1 receptor. *Biochemistry* **58**, 3065-3068, doi:10.1021/acs.biochem.9b00505 (2019).

27 Schutz, C. N. & Warshel, A. What are the dielectric "constants" of proteins and how to validate electrostatic models? *Proteins* **44**, 400-417 (2001).

28 Tolia, A., Chavez-Gutierrez, L. & De Strooper, B. Contribution of presenilin transmembrane domains 6 and 7 to a water-containing cavity in the γ-secretase complex. *Journal of Biological Chemistry* **281**, 27633-27642, doi:10.1074/jbc.M604997200 (2006).

29 Chavez-Gutierrez, L. *et al.* The mechanism of γ-Secretase dysfunction in familial Alzheimer disease. *EMBO Journal* **31**, 2261-2274, doi:10.1038/emboj.2012.79 (2012).

30 Högel, P. *et al.* Glycine perturbs local and global conformational flexibility of a transmembrane helix. *Biochemistry* **57**, 1326-1337, doi:10.1021/acs.biochem.7b01197 (2018).

31 Doig, A. J., Errington, N. & Iqbalsyah, T. M. in *Handbook of Protein Folding* Vol. 1 (ed Kiefhaber Buchner) 247-313 (Wiley, 2005).

32 Quint, S., Widmaier, S., Minde, D., Langosch, D. & Scharnagl, C. Residue-specific side-chain packing determines the backbone dynamics of transmembrane model helices. *Biophysical Journal* **99**, 2541-2549 (2010).

33 Edbauer, D. *et al.* Reconstitution of γ-secretase activity. *Nature Cell Biology* **5**, 486-488 (2003).

34 Kretner, B. *et al.* Generation and deposition of Aβ43 by the virtually inactive presenilin-1 L435F mutant contradicts the presenilin loss-of-function hypothesis of Alzheimer's disease. *EMBO Molecular Medicine* **8**, 458-465, doi:10.15252/emmm.201505952 (2016).

35 Page, R. M. *et al.* Generation of Aβ38 and Aβ42 is independently and differentially affected by familial Alzheimer disease-associated presenilin mutations and γ-secretase modulation. *Journal of Biological Chemistry* **283**, 677-683, doi:10.1074/jbc.M708754200 (2008).

36 Wolfe, M. S. Substrate recognition and processing by γ-secretase. *Biochimica et Biophysica Acta - Biomembranes* **1862**, 183016, doi:10.1016/j.bbamem.2019.07.004 (2020).

37 Qian, H. & Chan, S. I. Hydrogen exchange kinetics of proteins in denaturants: a generalized two-process model. *Journal of Molecular Biology* **286**, 607-616, doi:10.1006/jmbi.1998.2484 (1999).

38 Hitzenberger, M. & Zacharias, M. Structural modeling of γ-secretase Aβ n complex formation and substrate processing. *ACS Chemical Neuroscience* **10**, 1826-1840, doi:10.1021/acschemneuro.8b00725 (2019).

39 Deatherage, C. L. *et al.* Structural and biochemical differences between the Notch and the amyloid precursor protein transmembrane domains. *Science Advances* **3**, doi:10.1126/sciadv.1602794 (2017).

40 Spitz, C. *et al.* Non-canonical shedding of TNF alpha by SPPL2a is determined by the conformational flexibility of Its transmembrane helix. *Iscience* **23**, doi:10.1016/j.isci.2020.101775 (2020).

41 Scharnagl, C. *et al.* Side-chain to main-chain hydrogen bonding controls the intrinsic backbone dynamics of the amyloid precursor protein transmembrane helix. *Biophysical Journal* **106**, 1318-1326 (2014).

42 Jesus, C. S. H., Cruz, P. F., Arnaut, L. G., Brito, R. M. M. & Serpa, C. One peptide reveals the two faces of alpha-helix unfolding-folding dynamics. *Journal of Physical Chemistry B* **122**, 3790-3800, doi:10.1021/acs.jpcb.8b00229 (2018).

43 Dickey, S. W., Baker, R. P., Cho, S. & Urban, S. Proteolysis inside the membrane is a rate-governed reaction not driven by substrate affinity. *Cell* **155**, 1270-1281, doi:10.1016/j.cell.2013.10.053 (2013).

44 Kamp, F. *et al.* Intramembrane proteolysis of β-amyloid precursor protein by γ-secretase is an unusually slow process. *Biophysical Journal* **108**, 1229-1237, doi:10.1016/j.bpj.2014.12.045 (2015).

45 Bolduc, D. M., Montagna, D. R., Gu, Y., Selkoe, D. J. & Wolfe, M. S. Nicastrin functions to sterically hinder γ-secretase-substrate interactions driven by substrate transmembrane domain. *Proceedings of the National Academy of Sciences* **113**, E509-518, doi:10.1073/pnas.1512952113 (2016).

46 Fersht, A. *Structure and mechanism in protein science*. (Freeman, 2006).

47 Jager, M., Nguyen, H., Crane, J. C., Kelly, J. W. & Gruebele, M. The folding mechanism of a β-sheet: the WW domain. *Journal of Molecular Biology* **311**, 373-393, doi:10.1006/jmbi.2001.4873 (2001).

48 Sethuraman, A., Vedantham, G., Imoto, T., Przybycien, T. & Belfort, G. Protein unfolding at interfaces: slow dynamics of alpha-helix to β-sheet transition. *Proteins* **56**, 669-678, doi:10.1002/prot.20183 (2004).

49 Stelzer, W., Poschner, B. C., Stalz, H., Heck, A. J. & Langosch, D. Sequence-specific conformational flexibility of SNARE transmembrane helices probed by hydrogen/deuterium exchange. *Biophysical Journal* **95**, 1326-1330 (2008).

50 Zheng, J., Strutzenberg, T., Pascal, B. D. & Griffin, P. R. Protein dynamics and conformational changes explored by hydrogen/deuterium exchange mass spectrometry. *Current Opinion in Structural Biology* **58**, 305-313, doi:10.1016/j.sbi.2019.06.007 (2019).

51 Shearman, M. S. *et al.* L-685,458, an aspartyl protease transition state mimic, is a potent inhibitor of amyloid β-protein precursor γ-secretase activity. *Biochemistry* **39**, 8698-8704, doi:10.1021/bi0005456 (2000).

52 Pigoni, M. *et al.* Seizure protein 6 controls glycosylation and trafficking of kainate receptor subunits GluK2 and GluK3. *EMBO Journal* **39**, e103457, doi:10.15252/embj.2019103457 (2020).

Acknowledgments

We thank Dr. Manfred Wozny for kindly providing and extending the ETD FRAGMENT ANALYZER module of MassMap, Dr. Axel Imhof for providing access to the mass spectrometers within the Protein Analysis Unit of the LMU, Dr. Christina Scharnagl for helpful discussions, Manuel Hitzenberger for a script to analyze NMR structures, and Fabian Schmidt and Martin Ortner for critically reading the manuscript. This work was funded by the Deutsche Forschungsgemeinschaft (DFG, German Research Foundation) 263531414 / FOR 2290 (HS, SL, and DL) and the Munich Cluster

for Systems Neurology (EXC 2145 SyNergy - ID 390857198). Nadine Werner was funded by a stipend from the Hans and Ilse Breuer Foundation.

Author contributions

NW performed *in vitro* cleavage assays, PH and WS did DHX assays, GG performed *in cellulo* cleavage assays. DL, SL, and HS designed and supervised the project. DL wrote the manuscript together with the co-authors. All authors analysed their data, created their figures and have given approval to the final version of the manuscript.

Additional information

Supporting Information: Supporting information contains Tables S1, S2, S3 and Figures S1, S2, S3, S4, S5, S6, S7.

Competing interests: The authors declare no competing interests.

Supplementary Information

Cooperation of N- and C-terminal substrate transmembrane domain segments in intramembrane proteolysis by γ-secretase

Nadine T. Werner[1§], Philipp Högel[2§], Gökhan Güner[3§], Walter Stelzer[2], Stefan F. Lichtenthaler[3,4,5*], Harald Steiner[1,3*], and Dieter Langosch[2*]

[1] Biomedical Center (BMC), Division of Metabolic Biochemistry, Faculty of Medicine, LMU Munich, Germany

[2] Chair of Biopolymer Chemistry, Technical University of Munich, Freising, Germany

[3] German Center for Neurodegenerative Diseases (DZNE), Munich, Germany

[4] Neuroproteomics, School of Medicine, Klinikum rechts der Isar, Technical University of Munich, Munich, Germany

[5] Munich Cluster for Systems Neurology (SyNergy), Munich, Germany

[§]These authors contributed equally

[*]Corresponding authors:

D. Langosch, langosch@tum.de

H. Steiner, harald.steiner@med.uni-muenchen.de

S. Lichtenthaler, stefan.lichtenthaler@dzne.de

Supplemental Discussion

The origin of biphasic DHX. To explain the origin of biexponential, or biphasic, DHX, we assume that exchange at a given amide within a population of TMDs can follow one of two different kinetic regimes. The fast regime yields a high $k_{exp,A}$ while the slow regime leads to a low $k_{exp,B}$ value. These exchange rate constants are transformed into ΔG_A and ΔG_B values. We propose that the pairs of $k_{exp,A}/\Delta G_A$ and $k_{exp,B}/\Delta G_B$ values describe DHX at a given open amide ('single opening') or at simultaneously open neighboring amide pairs ('double opening'), respectively. Even in the latter case, i.e., after simultaneous opening of two H-bonds, less than one exchange events can occur per opening on average, given that open/close transitions of an H-bond are much more frequent than the chemical amide exchange reaction of an unfolded peptide in the EX2 mode [1] that characterizes DHX under our conditions [2].

To illustrate the point, H-bond opening at G38 may result in local DHX with a fast $k_{exp,A}$ and/or facilitate a second H-bond opening at G37 or V39. That second opening may enable DHX at G37 or V39, albeit with a slow $k_{exp,B}$, as a double opening is likely a rare event (see: Fig. S2). Exchange from the same doubly open state may also occur at G38, provided that a previous opening at G38 had not resulted in DHX. Accordingly, we propose that ΔG_A represents frequent single openings while ΔG_B may describe correlated double openings occurring at lower frequencies.

This proposition is based on the expectation that isolated openings are more frequent than reactions leading to two simultaneously open amides. We cannot rule out an inverse mechanism, however, where fast DHX occurs at two simultaneously open amides and slow DHX at isolated openings. This alternative interpretation would hold true if the decrease in the closing rate from a doubly open state would overcompensate a decrease in the opening rate leading to it. In this case, the aggregate lifetime of a doubly open state might exceed the aggregate lifetime of isolated openings.

Potential impact of experimental conditions on calculated H-bond strength. Exchange rate constants are transformed into ΔG_A and ΔG_B values by relating them to the rates k_{ch} of chemical exchange of unfolded peptides. In general, amides where k_{ch} exceeds the k_{exp} values from the literature [3] are protected from exchange depending on their H-bond strength. At some positions in TMDs investigated here, $k_{exp,A}$ exceeds k_{ch}, in those cases the latter appears to be lower under our conditions than the standard values for several potential reasons: (i) The molarity of water in 80% (v/v) TFE solvent is only 20% of the bulk molarity used for the determination of the reference chemical exchange rates k_{ch}; (ii) the hydration of residues in the hydrophobic core of a TMD dissolved in 80% TFE may be reduced relative to bulk water; (iii) k_{ch} values determined for model tripeptides in the unfolded state may not correctly represent sterical hindrance of exchange in the helical state; and (iv) TFE might have an impact on the autoionization constant of water and k_{ch} [4]. As a result, our calculated ΔG values might be underestimating the true values to some extent.

Supplemental Statistics in the Analysis of Amide Exchange Kinetics. It is assumed that exchange data are available for N exchange periods t_n (n=1, 2, …, N). To analyze the exchange kinetics of the amide hydrogen of amino acid m, the first step consists in the determination of the mean numbers D_{mean} (m,n) of the D numbers D_m obtained for all the fragment types analyzed for time point n.

The main model employed for the analysis of the kinetics predicts a first order reaction that leads from the starting value D_{start} of the D number to the asymptotic D number $D_{asymptotic}$. The experimental rate constant $k_{exp,m}$ for the exchange of amide hydrogen m is determined by a non-linear least squares fitting routine that minimizes the quantity χ^2 of equation (1a):

$$\chi^2 = \sum_{n=1}^{N} \left(\chi_{m,n}\right)^2 \text{ with } \chi_{m,n} := D_{mean}(m,n) - D_{fit}(m,n) \text{ and}$$
$$D_{fit}(m,n) := D_{asymptotic} + \left(D_{start} - D_{asymptotic}\right) \cdot \exp\left(-k_{exp,m} \cdot t_n\right). \quad (1a)$$

For amide hydrogens exhibiting a biphasic exchange dynamics, the quantity χ^2 of equation (1b) is minimized to determine the rate constants $k_{1\ exp,m}$, $k_{2\ exp,m}$ and the ratio A of the conformation exhibiting the rate constant $k_{1\ exp,m}$:

$$\chi^2 = \sum_{n=1}^{N} \left(\chi_{m,n}\right)^2 \text{ with } \chi_{m,n} := D_{mean}(m,n) - D_{fit}(m,n) \text{ and}$$
$$D_{fit}(m,n) := D_{asymptotic} + \left(D_{start} - D_{asymptotic}\right) \cdot E, \quad (1b)$$
$$E = A \cdot \exp\left(-k_{1\ exp,m} \cdot t_n\right) + (1-A) \cdot \exp\left(-k_{2\ exp,m} \cdot t_n\right).$$

For H/D and D/H exchange, the number D_{start} amounts to 0 and 1, respectively. In case some of the numbers D_{mean}(m,n) are not available due to missing fragments for certain time points, the fitting procedure is restricted to the time points with available D numbers. For the fitting to be performed, the number of time points with D numbers must not be smaller than three and six for monophasic and biphasic behavior, respectively.

To estimate the standard errors of the fitted quantities (monophasic behavior: $k_{exp,m}$, biphasic behavior: $k_{1\ exp,m}$, $k_{2\ exp,m}$ and A), the standard deviation σ_m is calculated for the residuals $\chi_{m,n}$ obtained for the best fit. The standard deviation σ_m is then used to perform the fitting defined in (1a) or (1b) for additional 2N sets of D numbers:

Set 1-1:	$D_{mean}(m,1)+\sigma_m$	$D_{mean}(m,2)$	...	$D_{mean}(m,N-1)$	$D_{mean}(m,N)$
Set 1-2:	$D_{mean}(m,1)-\sigma_m$	$D_{mean}(m,2)$	...	$D_{mean}(m,N-1)$	$D_{mean}(m,N)$
...	...	...	...	...	...
Set n-1:	$D_{mean}(m,1)$	...	$D_{mean}(m,n)+\sigma_m$	...	$D_{mean}(m,N)$
Set n-2:	$D_{mean}(m,1)$	...	$D_{mean}(m,n)-\sigma_m$	...	$D_{mean}(m,N)$
...	...	...	...	...	...
Set N-1:	$D_{mean}(m,1)$	$D_{mean}(m,2)$	...	$D_{mean}(m,N-1)$	$D_{mean}(m,N)+\sigma_m$
Set N-2:	$D_{mean}(m,1)$	$D_{mean}(m,2)$	...	$D_{mean}(m,N-1)$	$D_{mean}(m,N)-\sigma_m$

The uncertainty $\Delta_{m,n}$ of the decimal logarithm of the rate constant $k_{exp,m}$ that is caused by the uncertainty σ_m of the numbers $D_{mean}(m,n)$ is estimated as the mean of the two numbers $|\log[k_{exp,m}]-\log[k(\text{Set n-1})]|$ and $|\log[k_{exp,m}]-\log[k(\text{Set n-2})]|$. The quantities k(Set n-1) and k(Set n-2) stand for the best fit rate constants obtained with the sets of D-numbers Set n-1 and Set n-2, respectively. By error propagation, the standard error $\Delta\log(k_{exp,m})$ of the decimal logarithm of the experimental rate constant $k_{exp,m}$ is calculated in the following way:

$$\Delta \log\left(k_{exp,m}\right) = \sum_{n=1}^{N} \Delta_{m,n}. \tag{2a}$$

In case of a biexponential fit, the uncertainties $\Delta_{1\,m,n}$ and $\Delta_{2\,m,n}$ of the decimal logarithms of the rate constants $k_{1\,exp,m}$ and $k_{2\,exp,m}$, respectively, are estimated in full analogy to the estimation of $\Delta_{m,n}$. The standard errors $\Delta\log(k_{1\,exp,m})$ and $\Delta\log(k_{2\,exp,m})$ are calculated in the following way:

$$\Delta \log\left(k_{1\,exp,m}\right) = \sum_{n=1}^{N} \Delta_{1\,m,n},\ \Delta \log\left(k_{2\,exp,m}\right) = \sum_{n=1}^{N} \Delta_{2\,m,n}. \tag{2b}$$

To estimate the uncertainty of the relative abundance of the conformation with the rate constant $k_{1\,exp,m}$, the means $\Delta A_{m,n}$ of the two numbers $|A_{,m}- A(\text{Set n-1})|$ and $|A_{,m}- A(\text{Set n-2})|$ are calculated with A(Set n-1) and A(Set n-2) standing for the ratios obtained with the sets of D-numbers Set n-1 and Set n-2, respectively. By error propagation, the standard error $\Delta A_{,m}$ of the experimental ratio $A_{,m}$ is calculated as follows:

$$\Delta A_m = \sum_{n=1}^{N} \Delta A_{m,n}. \tag{3c}$$

In cases where $k_{ch,m}$ is available, the experimental rate constant $k_{exp,m}$ can be used to calculate the difference ΔG_m of the Gibbs Free Energy associated with the equilibrium between the effectively folded and the effectively unfolded situation for amide hydrogen m. If the rate constant of the unfolding reaction of the peptide, which leads to an exchange competent state of amide hydrogen m, is denoted by $k_{m,+}$, and if the rate constant of the reverse reaction that makes the amide hydrogen m not exchange competent is denoted by $k_{m,-}$, ΔG_m is given by equation (4):

$$\Delta G_m = -RT \cdot \ln\left(K_m\right) = -RT \cdot \ln\left(\frac{k_{m,+}}{k_{m,-}}\right). \tag{4}$$

According to equation (5), the fraction $k_{m,+}/(k_{m,+}+k_{m,-})$ can be determined from the experimental rate constant $k_{exp,m}$ and the chemical rate constant $k_{ch,m}$:

$$\frac{k_{m,+}}{k_{m,+}+k_{m,-}} = \frac{k_{exp,m}}{k_{ch,m}}. \tag{5}$$

Thus, the fraction of rate constants needed for the calculation of ΔG_m by means of equation (4) can be calculated from the experimental rate constant $k_{exp,m}$ and the chemical rate constant $k_{ch,m}$ according to equation (6):

$$\frac{k_{exp,m}}{k_{ch,m}} = \frac{k_{m,+}}{k_{m,+}+k_{m,-}} = \frac{\frac{k_{m,+}}{k_{m,-}}}{\frac{k_{m,+}}{k_{m,-}}+1} \rightarrow \frac{k_{m,+}}{k_{m,-}} \cdot \left(1-\frac{k_{exp,m}}{k_{ch,m}}\right) = \frac{k_{exp,m}}{k_{ch,m}} \rightarrow \tag{6}$$

$$\rightarrow \frac{k_{m,+}}{k_{m,-}} = \frac{k_{exp,m}}{k_{ch,m}-k_{exp,m}}.$$

The limits of the standard confidence interval of ΔG_m are calculated by means of the standard error $\Delta\log(k_{exp,m})$ of the decimal logarithm of $k_{exp,m}$ using equations (7):

$$\Delta G_{m,min} = -RT \cdot \ln\left(\frac{k_{+,m}}{k_{-,m}}\right)_{max} \text{ with } \left(\frac{k_{+,m}}{k_{-,m}}\right)_{max} = \frac{k_{exp,m} \cdot 10^{\Delta\log\left(k_{exp,m}\right)}}{k_{ch,m}-k_{exp,m} \cdot 10^{\Delta\log\left(k_{exp,m}\right)}},$$

$$\Delta G_{m,max} = -RT \cdot \ln\left(\frac{k_{+,m}}{k_{-,m}}\right)_{min} \text{ with } \left(\frac{k_{+,m}}{k_{-,m}}\right)_{min} = \frac{k_{exp,m} \cdot 10^{-\Delta\log\left(k_{exp,m}\right)}}{k_{ch,m}-k_{exp,m} \cdot 10^{-\Delta\log\left(k_{exp,m}\right)}}. \tag{7}$$

In case of a biexponential fit, instead of being performed with $k_{exp,m}$, the calculation of ΔG_m, $\Delta G_{m,min}$ and $\Delta G_{m,max}$ is based on the smaller of the two rate constants $k_{1\,exp,m}$ and $k_{2\,exp,m}$.

Table S1. Sequences of synthetic peptides investigated in this study

Peptide	Sequence
wt C99	Ac-KK**KGAIIGLMVGGVVIATVIVITLVMLKKK**-NH_2[1]
C99 I47G/T48G	Ac-KK**KGAIIGLMVGGVVIATVIV**GG**LVMLKKK**-NH_2
C99 I47L/T48L	Ac-KK**KGAIIGLMVGGVVIATVIV**LL**LVMLKKK**-NH_2
pL-GG	Ac-KKKLLLLLLLLGGLLLLLLLLLLLLLLKKK-NH_2
pL-VGGV	Ac-KKKLLLLLLLVGGVLLLLLLLLLLLLLKKK-NH_2
pL-VGGV/εGG	Ac-KKKLLLLLLLVGGVLLLLLLLLGGLLLKKK-NH_2
pL-VGGV/cr	Ac-KKKLLLLLLLVGGVLLLL**VIVITLVMLKKK**-NH_2
ErbB4	Ac-KKK**LIAAGVIGGLFILVIVGLTFAVYV**KKK-NH_2
N-Cadherin	Ac-KKK**GAIIAILLCIIILLILVLMFVVWM**KKK-NH_2
Notch1	Ac-KKK**LHFMYVAAAAFVLLFFVGCGVLLS**KKK-NH_2

[1] Termini were blocked by acetylation (N-terminus) or amidation (C-terminus) in order to remove non-natural charges. The natural parts of the sequences shown are in bold face type. Two N-terminal Lys residues were appended to C99 derivatives to enhance solubility and gas phase fragmentation by ETD [5]. Lys tags similar to those of C99 derivatives were appended to ErbB4, N-Cadherin, and Notch1 sequences in order to ensure similar conditions, such as hydration, to all TMDs compared here. We note that similarly constructed C99 TMD peptides were previously shown to be good substrates for γ-secretase [6].

Table S2. Mass and sequence of AICD peptides generated in the cell-free assay as detected by MALDI-TOF MS (panel F in Figs. 2 - 4). Da, Dalton.

Construct	Sequence	Peptide	Calculated mass [Da]	Observed mass [Da]
C99				
	LVMLKKKQYTSIHHGVVEVDAAVTPEERHLSKMQQNGYENPTYKFFEQMQNGSRSHHHHHH	ε48	7235.10	7236.44
	VMLKKKQYTSIHHGVVEVDAAVTPEERHLSKMQQNGYENPTYKFFEQMQNGSRSHHHHHH	ε49	7121.94	7124.44
	LKKKQYTSIHHGVVEVDAAVTPEERHLSKMQQNGYENPTYKFFEQMQNGSRSHHHHHH	ε51	6891.61	6887.77
pL-GG				
	LLLLKKKQYTSIHHGVVEVDAAVTPEERHLSKMQQNGYENPTYKFFEQMQNGSRSHHHHHH	ε48	7231.09	7232.41
	LLLKKKQYTSIHHGVVEVDAAVTPEERHLSKMQQNGYENPTYKFFEQMQNGSRSHHHHHH	ε49	7117.93	7116.61
pL-VGGV				
	LLLLKKKQYTSIHHGVVEVDAAVTPEERHLSKMQQNGYENPTYKFFEQMQNGSRSHHHHHH	ε48	7231.09	7227.85
	LLLKKKQYTSIHHGVVEVDAAVTPEERHLSKMQQNGYENPTYKFFEQMQNGSRSHHHHHH	ε49	7117.93	7121.17
pL-cr				
	LVMLKKKQYTSIHHGVVEVDAAVTPEERHLSKMQQNGYENPTYKFFEQMQNGSRSHHHHHH	ε48	7235.10	7234.45
	VMLKKKQYTSIHHGVVEVDAAVTPEERHLSKMQQNGYENPTYKFFEQMQNGSRSHHHHHH	ε49	7121.94	7122.59
pL-VGGV/cr				
	LVMLKKKQYTSIHHGVVEVDAAVTPEERHLSKMQQNGYENPTYKFFEQMQNGSRSHHHHHH	ε48	7235.10	7236.18
	VMLKKKQYTSIHHGVVEVDAAVTPEERHLSKMQQNGYENPTYKFFEQMQNGSRSHHHHHH	ε49	7121.94	7120.86
pL-VGGV/ εGG				
	GLLLKKKQYTSIHHGVVEVDAAVTPEERHLSKMQQNGYENPTYKFFEQMQNGSRSHHHHHH	ε48	7174.98	7175.70

Table S3. Mass and sequence of Aβ peptides generated in the cell-free assay as detected by MALDI-TOF MS (panel G in Figs. 2 - 4). Da, Dalton.

Construct	Sequence	Peptide	Calculated mass [Da]	Observed mass [Da]
C99				
	MDAEFRHDSGYEVHHQKLVFFAEDVGSNK GAIIGLMVG	Aβ37	4207.73	4207.75
	MDAEFRHDSGYEVHHQKLVFFAEDVGSNK GAIIGLMVGG	Aβ38	4264.79	4263.75
	MDAEFRHDSGYEVHHQKLVFFAEDVGSNK GAIIGLMVGGV	Aβ39	4363.92	4366.16
	MDAEFRHDSGYEVHHQKLVFFAEDVGSNK GAIIGLMVGGVV	Aβ40	4463.05	4462.96
	MDAEFRHDSGYEVHHQKLVFFAEDVGSNK GAIIGLMVGGVVIA	Aβ42	4647.29	4646.17
pL-GG				
	MDAEFRHDSGYEVHHQKLVFFAEDVGSNK LLLLLL	Aβ34	4074.65	4075.64
pL-VGGV				
	MDAEFRHDSGYEVHHQKLVFFAEDVGSNK LLLLLL	Aβ34	4074.65	4073.86
	MDAEFRHDSGYEVHHQKLVFFAEDVGSNK LLLLLLL	Aβ35	4187.81	4188.24
	MDAEFRHDSGYEVHHQKLVFFAEDVGSNK LLLLLLLVG	Aβ37	4343.99	4345.07
	MDAEFRHDSGYEVHHQKLVFFAEDVGSNK LLLLLLLVGG	Aβ38	4401.05	4400.33
pL-cr				
	MDAEFRHDSGYEVHHQKLVFFAEDVGSNK LLLLLLLL	Aβ36	4300.97	4301.11
	MDAEFRHDSGYEVHHQKLVFFAEDVGSNK LLLLLLLLL	Aβ37	4414.13	4414.79
	MDAEFRHDSGYEVHHQKLVFFAEDVGSNK LLLLLLLLLL	Aβ38	4527.29	4526.49
pL-VGGV/cr				
	MDAEFRHDSGYEVHHQKLVFFAEDVGSNK LLLLLL	Aβ34	4074.65	4073.94
	MDAEFRHDSGYEVHHQKLVFFAEDVGSNK LLLLLLL	Aβ35	4187.81	4187.43
	MDAEFRHDSGYEVHHQKLVFFAEDVGSNK LLLLLLLVG	Aβ37	4343.99	4344.49
	MDAEFRHDSGYEVHHQKLVFFAEDVGSNK LLLLLLLVGG	Aβ38	4401.05	4401.04
	MDAEFRHDSGYEVHHQKLVFFAEDVGSNK LLLLLLLVGGV	Aβ39	4500.18	4500.78

Construct	Sequence	Peptide	Calculated mass [Da]	Observed mass [Da]
pL-VGGV/ εGG				
	MDAEFRHDSGYEVHHQKLVFFAEDVGSNK LLLLLL	Aβ34	4074.65	4072.93
	MDAEFRHDSGYEVHHQKLVFFAEDVGSNK LLLLLLL	Aβ35	4187.81	4188.19
	MDAEFRHDSGYEVHHQKLVFFAEDVGSNK LLLLLLLVG	Aβ37	4343.99	4343.20
	MDAEFRHDSGYEVHHQKLVFFAEDVGSNK LLLLLLLVGG	Aβ38	4401.05	4403.19

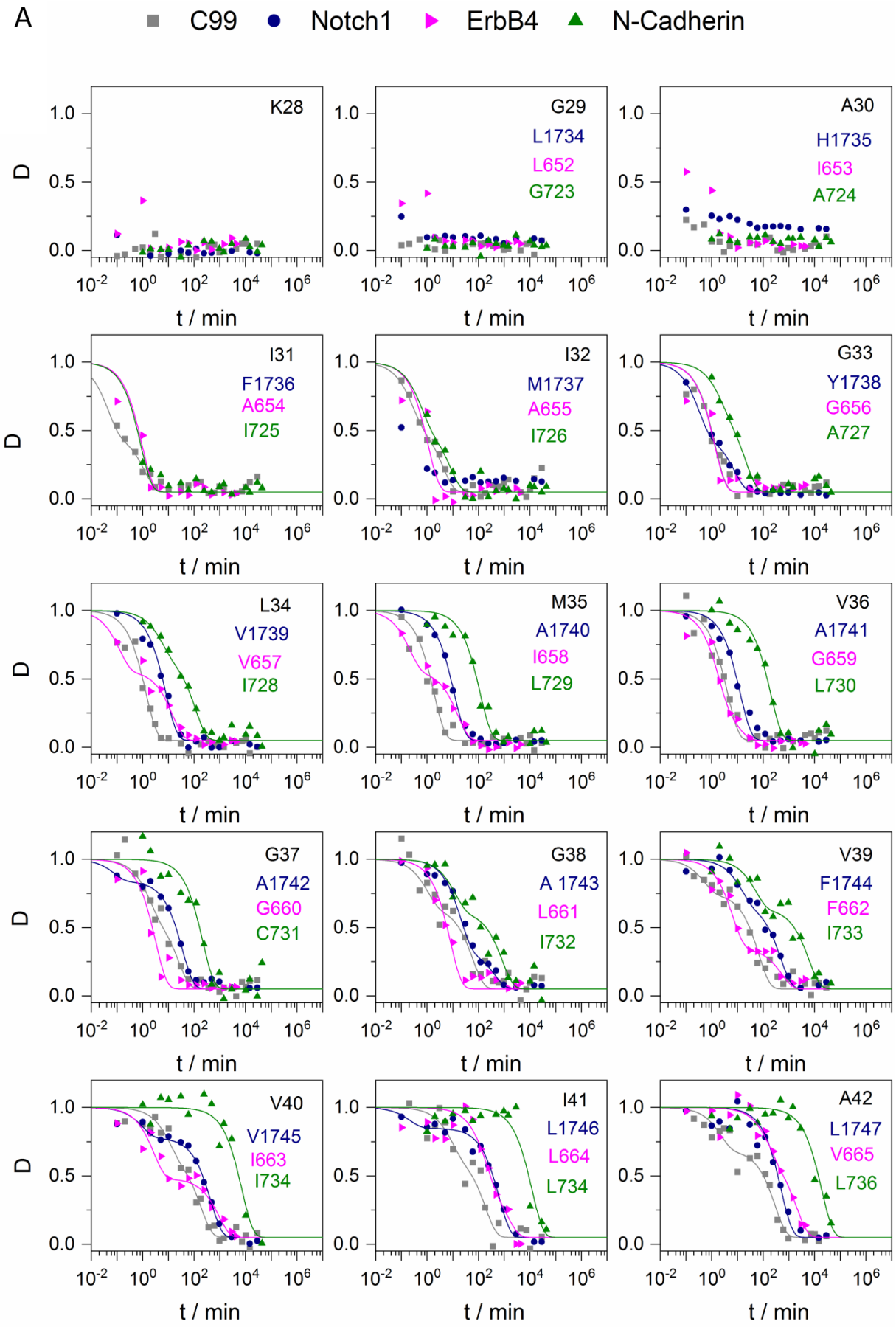
A
C99
Notch1
ErbB4
N-Cadherin
D
t / min
K28
G29
L1734
L652
G723
A30
H1735
I653
A724
I31
F1736
A654
I725
I32
M1737
A655
I726
G33
Y1738
G656
A727
L34
V1739
V657
I728
M35
A1740
I658
L729
V36
A1741
G659
L730
G37
A1742
G660
C731
G38
A 1743
L661
I732
V39
F1744
F662
I733
V40
V1745
I663
I734
I41
L1746
L664
L734
A42
L1747
V665
L736

100

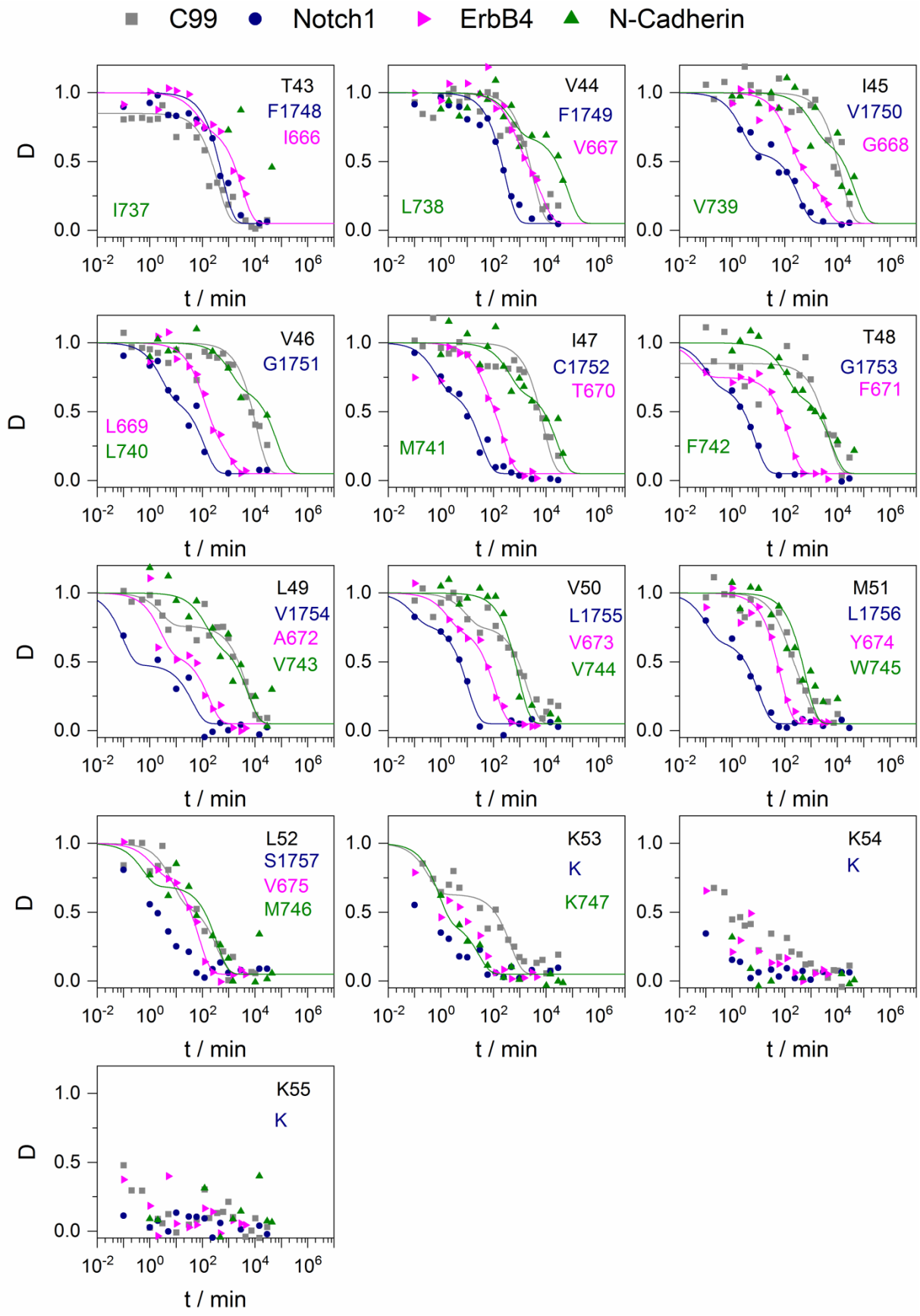
C99
Notch1
ErbB4
N-Cadherin
T43
F1748
I666
I737
V44
F1749
V667
L738
I45
V1750
G668
V739
V46
G1751
L669
L740
I47
C1752
T670
M741
T48
G1753
F671
F742
L49
V1754
A672
V743
V50
L1755
V673
V744
M51
L1756
Y674
W745
L52
S1757
V675
M746
K53
K
K747
K54
K
K55
K
D
t / min

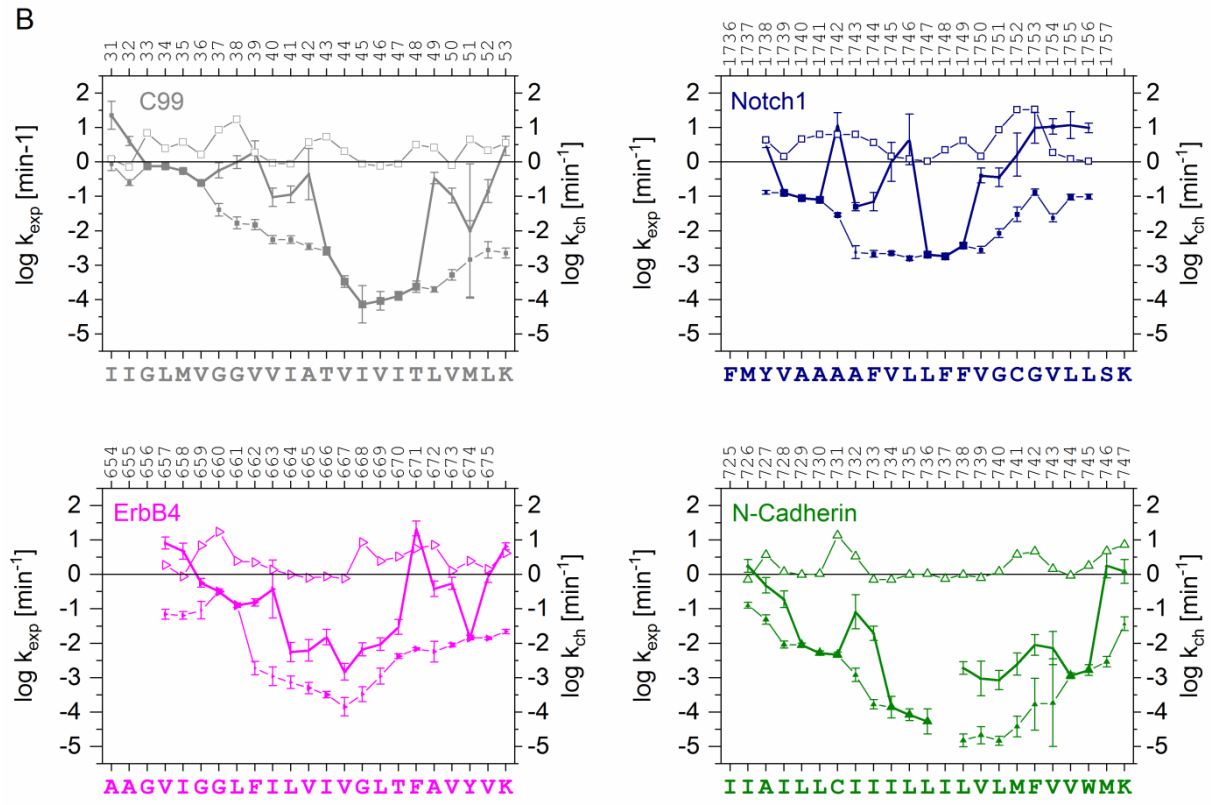

Figure S1. DHX of C99, Notch1, ErbB4, and N-Cadherin TMDs. (A) Residue-specific amide DHX kinetics where the calculated deuterium contents D of the respective amides are plotted against the exchange period t. The kinetics are overlayed after aligning the sequences at the terminal Lys-tags. **(B)** Exchange rate constants k_{exp} of individual amide deuterons (filled symbols, N = 3, log k_{exp} ± error of fit) and chemical exchange rate constants k_{ch} (emtpy symbols). Values of C99 and Notch1 were obtained after reevaluating data from refs. [5,7,8] after supplementing them with additional measurements to increase the density of the data points.

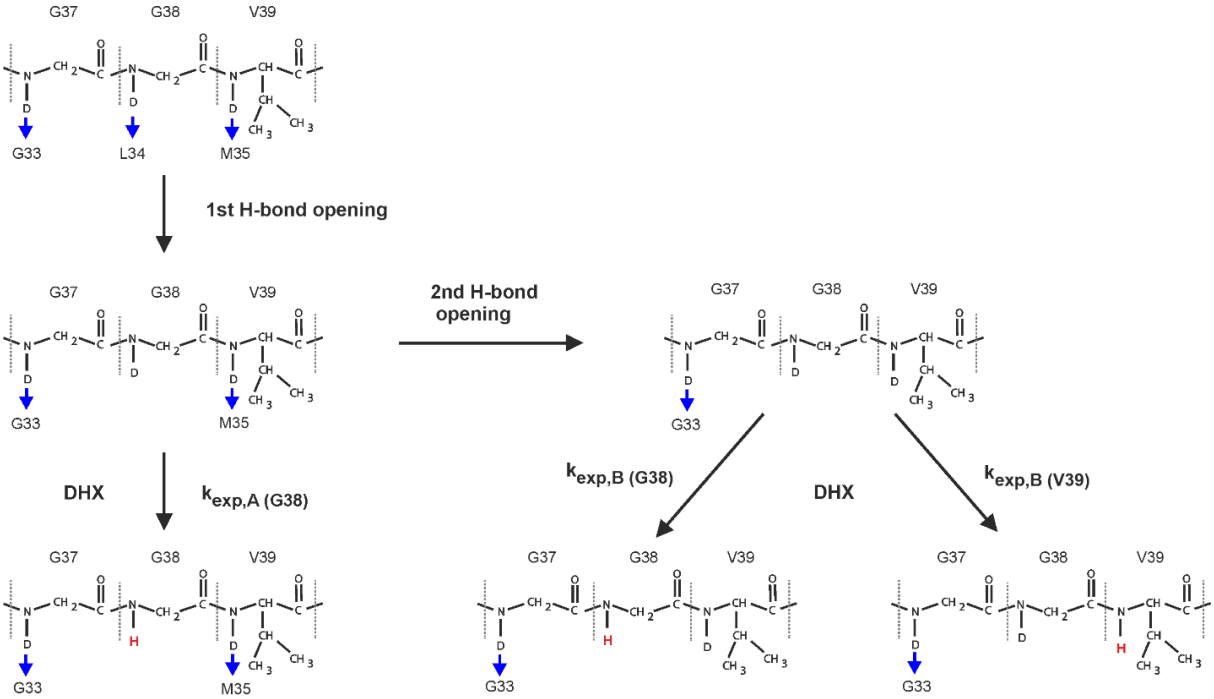

Figure S2 Putative origin of biphasic DHX. The scheme illustrates how the loss of an (i,i-4) amide H-bond (blue arrows) at G38 might allow fast DHX at G38. Alternatively, H-bond loss at G38 might lead to loss of a neighboring amide H-bond, e.g. at V39, followed by slower DHX at either V39 or G38.

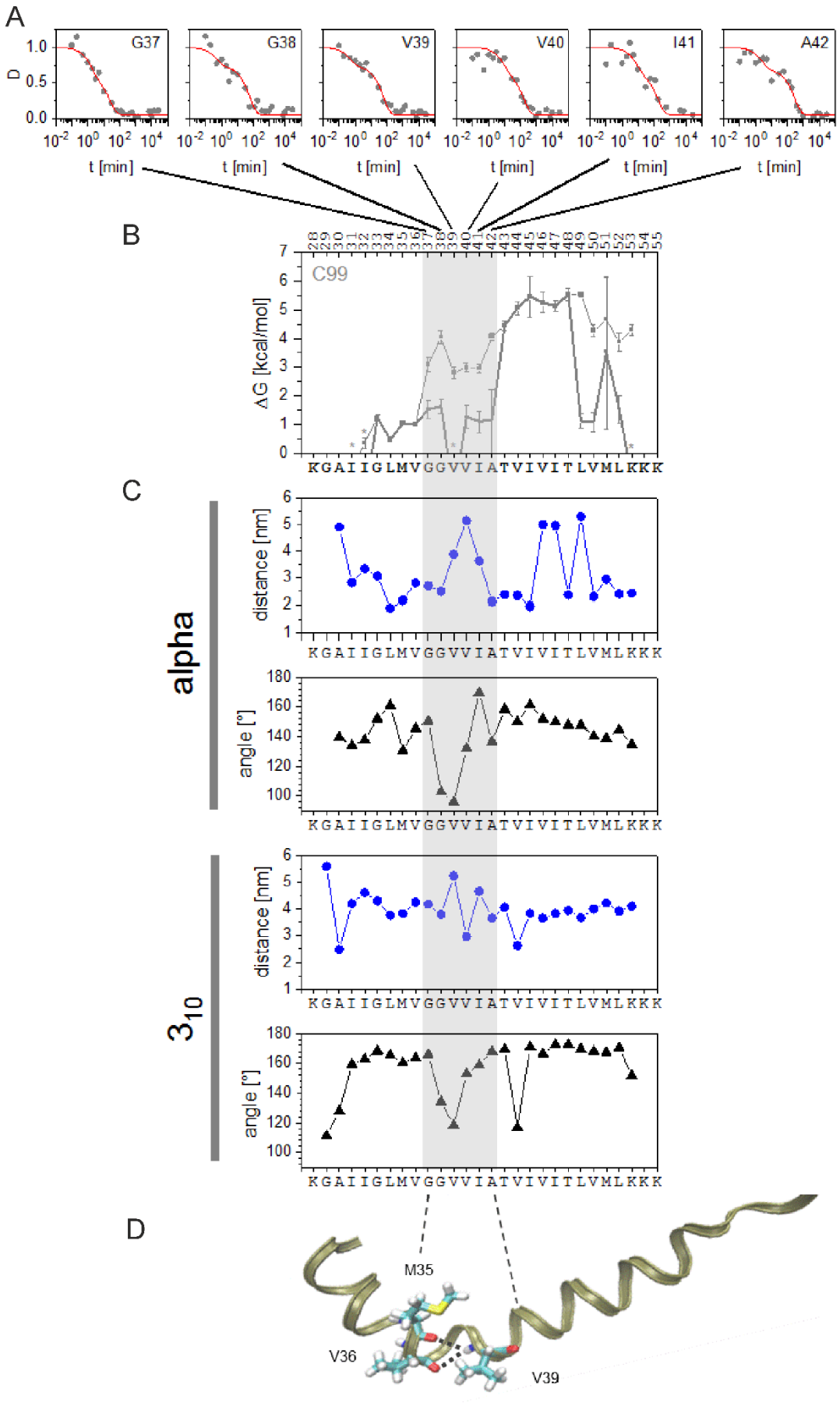
A
G37
G38
V39
V40
I41
A42
D
t [min]
B
C99
ΔG [kcal/mol]
KGAIIGLMVGGVVIATVIVITLVMLKKK
C
alpha
distance [nm]
angle [°]
3₁₀
D
M35
V36
V39

Figure S3. Biexponential DHX and amide H-bonding of wt C99. (A) Exemplary biphasic DHX kinetics near the hinge region (reproduced from Fig. S1). **(B)** H-bond stabilities ΔG (reproduced from Fig. 1). **(C)** Potential α (i,i-4) and 3_{10} (i,i-3) helical amide H-bond geometries calculated from the first model of NMR structure pdb 2lp1 [9]. Yellow shading marks residues giving rise to biphasic DHX, as illustrated in part (A). **(D)** First model of pdb 2lp1 from K28 to K55. Note that the N-H ... O=C distances (broken lines) and angles between V39 and M35 (d=3.88 Å, Θ= 96°) or V36 (d=5.23 Å, Θ= 118°), respectively, indicate extremely weak potential amide H-bonds originating from V39 that exhibits the most pronounced biphasic DHX (model generated with VMD [10]).

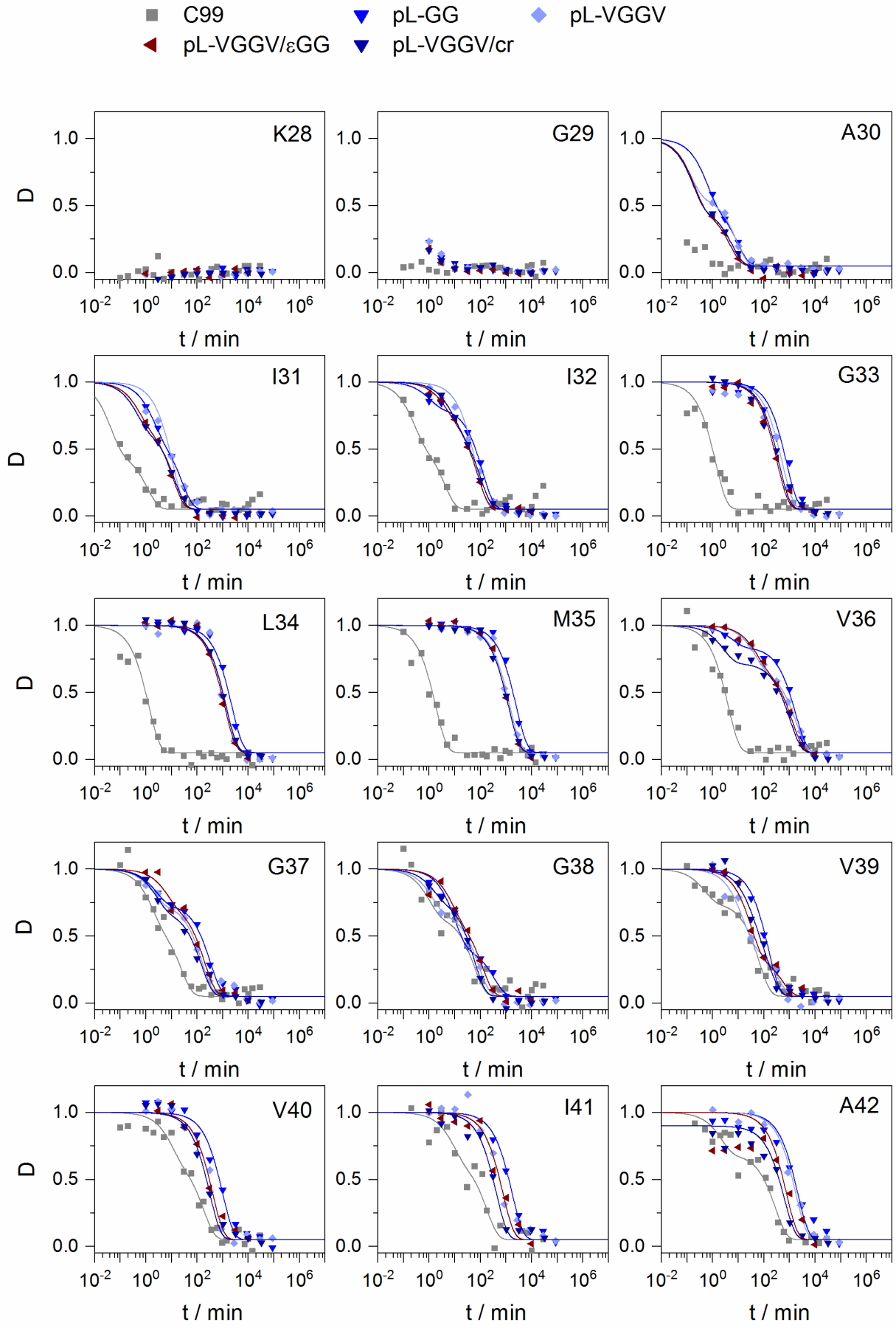
C99
pL-GG
pL-VGGV
pL-VGGV/εGG
pL-VGGV/cr
K28
G29
A30
I31
I32
G33
L34
M35
V36
G37
G38
V39
V40
I41
A42
D
t / min
1.0
0.5
0.0
10-2
100
102
104
106

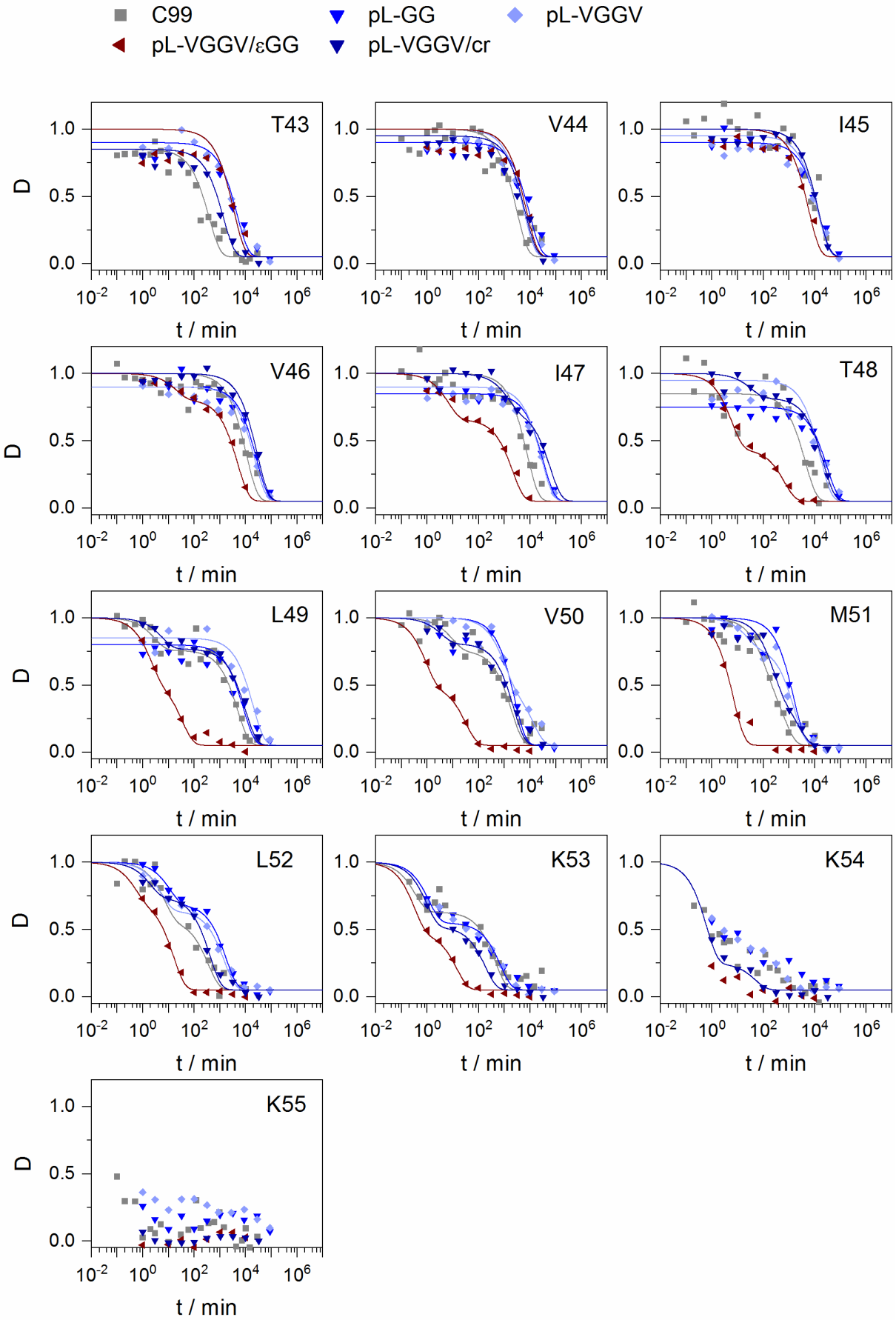
C99
pL-GG
pL-VGGV
pL-VGGV/εGG
pL-VGGV/cr
T43
V44
I45
V46
I47
T48
L49
V50
M51
L52
K53
K54
K55
D
t / min

Figure S4 Residue-specific amide DHX kinetics of C99 derivatives. The calculated deuterium contents D (mean values, N = 3) of the respective amides are plotted against the exchange period t. The shown kinetics were used to calculate the respective k_{exp} values after data fitting with monoexponential or biexponential decay functions. Fitting was only performed for those kinetics that were deemed complete enough for calculating k_{exp}. Sequence positions (Aβ numbering) are given in the insets; the amino acid type at a given position corresponds to the wt C99 sequence. C99 data are taken from Fig. S1.

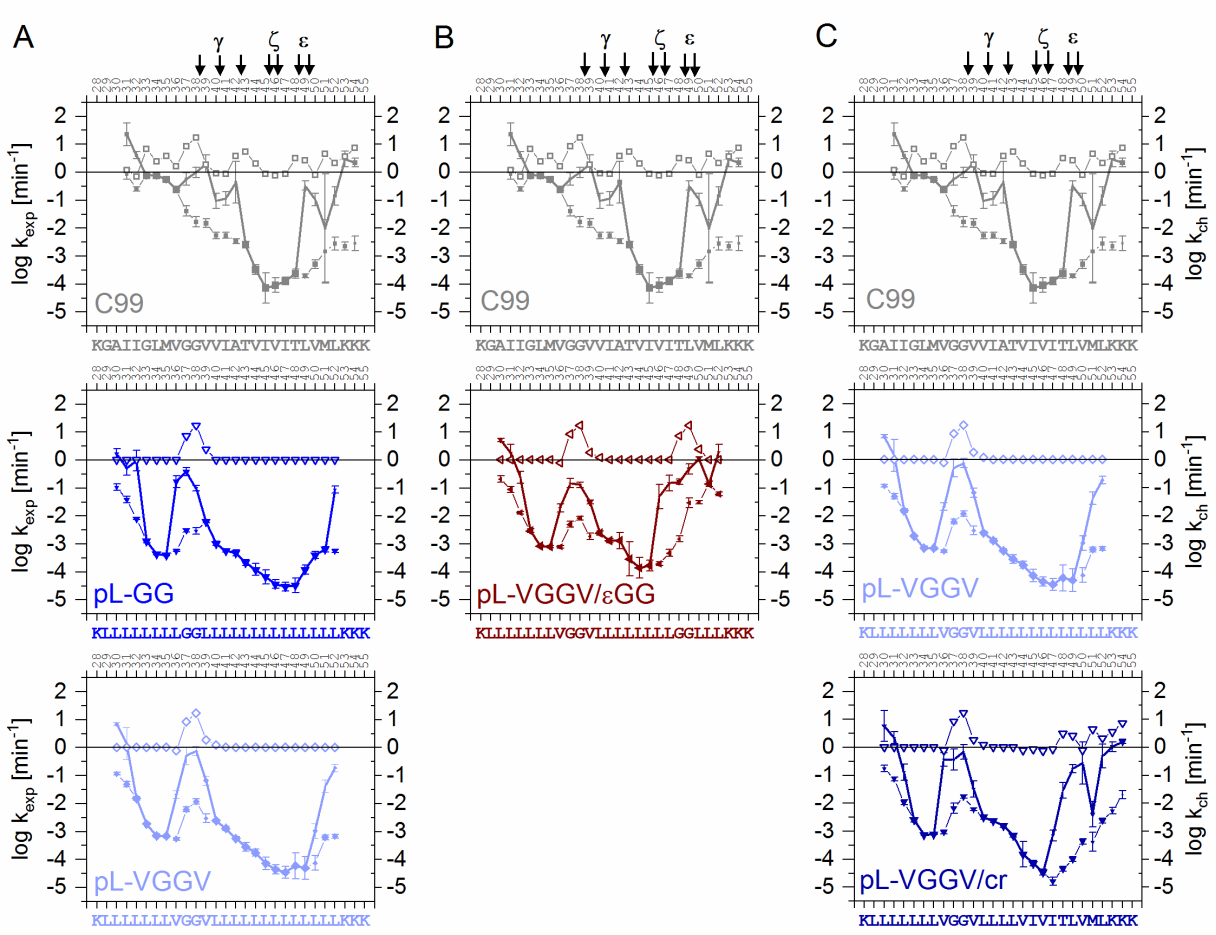

Figure S5. DHX rate constants of TMD peptides. Rate constants k_{exp} of constructs whose ΔG values are depicted in Fig. 2 **(A)**, Fig. 3 **(B)**, or Fig. 4 **(C)**. Shown are k_{exp} of individual amide deuterons (filled symbols, N = 3 independent DHX reactions, log k_{exp} ± error of fit) and the respective amide-specific intrinsic chemical exchange rate constants k_{ch} that describe the exchange kinetics in the unfolded state [11] (emtpy symbols). Note that diverging values of k_{exp} and k_{ch} indicate folded regions that are partially protected from exchange. At some positions k_{exp} exceeds k_{ch}, indicating that the reference values determined in aqueous solution [11] slightly underestimate k_{ch} in 80% TFE (see: Methods). Within regions of biphasic DHX, more positive values denote $k_{exp,A}$. Values characterizing single (k_{exp}, $k_{exp,A}$) or double ($k_{exp,B}$) H-bond openings are connected by thick or thin lines, respectively.

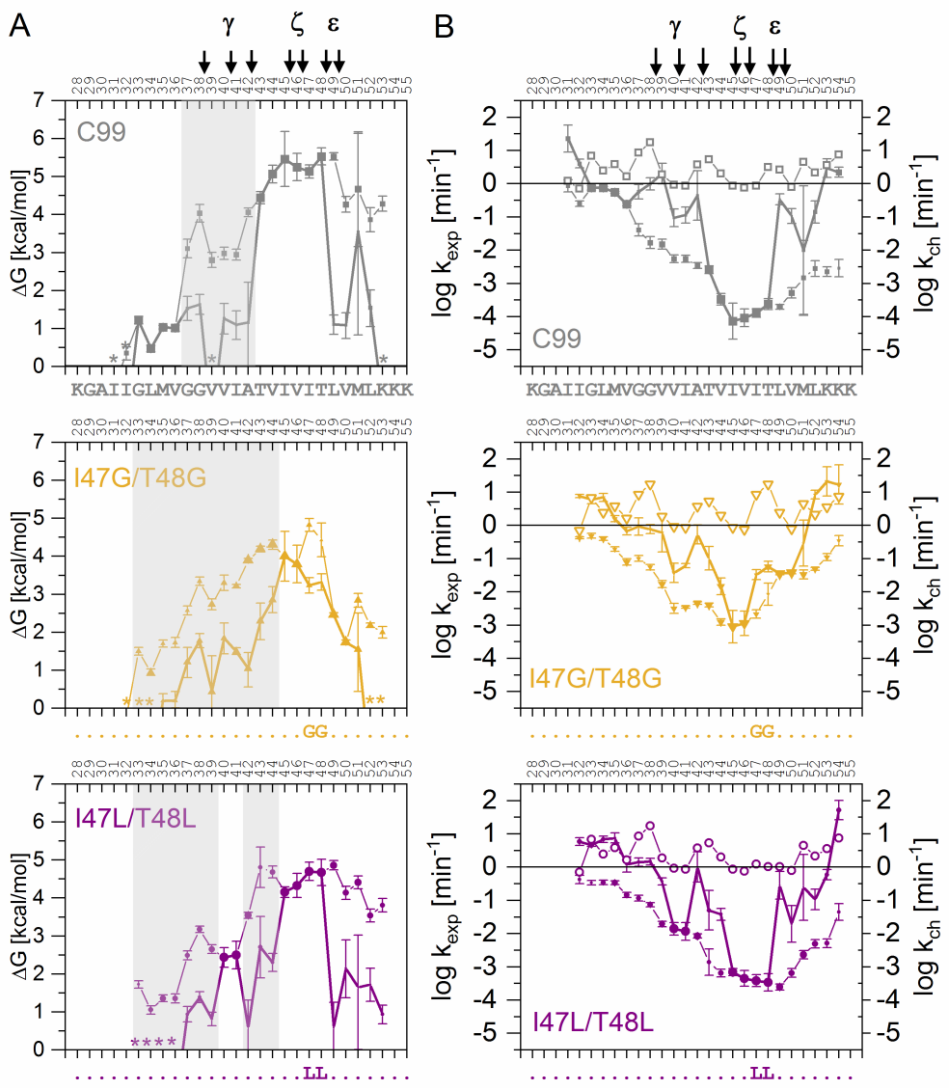
A
B
γ
ζ
ε
C99
I47G/T48G
I47L/T48L
ΔG [kcal/mol]
log k_exp [min^-1]
log k_ch [min^-1]
KGAIIGLMVGGVVIATVIVITLVMLKKK
GG
LL

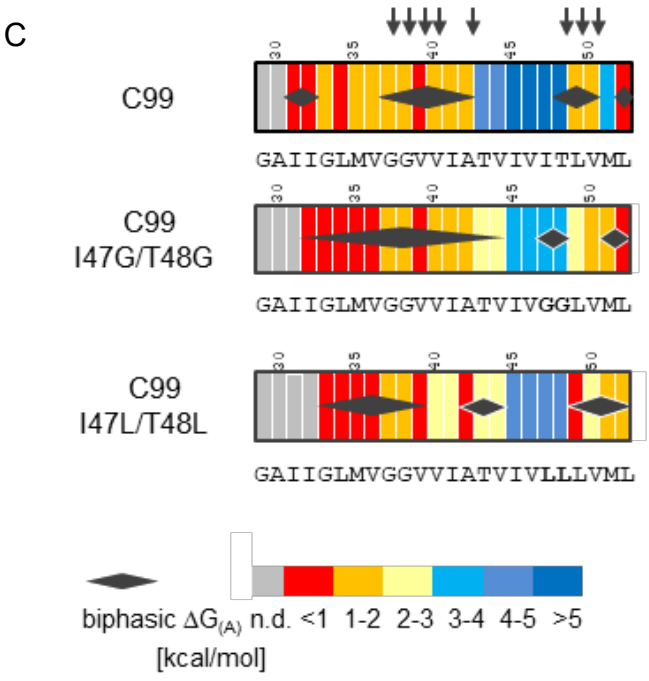
C
C99
GAIIGLMVGGVVIATVIVITLVML
C99
I47G/T48G
GAIIGLMVGGVVIATVIVGGLVML
C99
I47L/T48L
GAIIGLMVGGVVIATVIVLLLVML
biphasic ΔG(A) n.d. <1 1-2 2-3 3-4 4-5 >5
[kcal/mol]

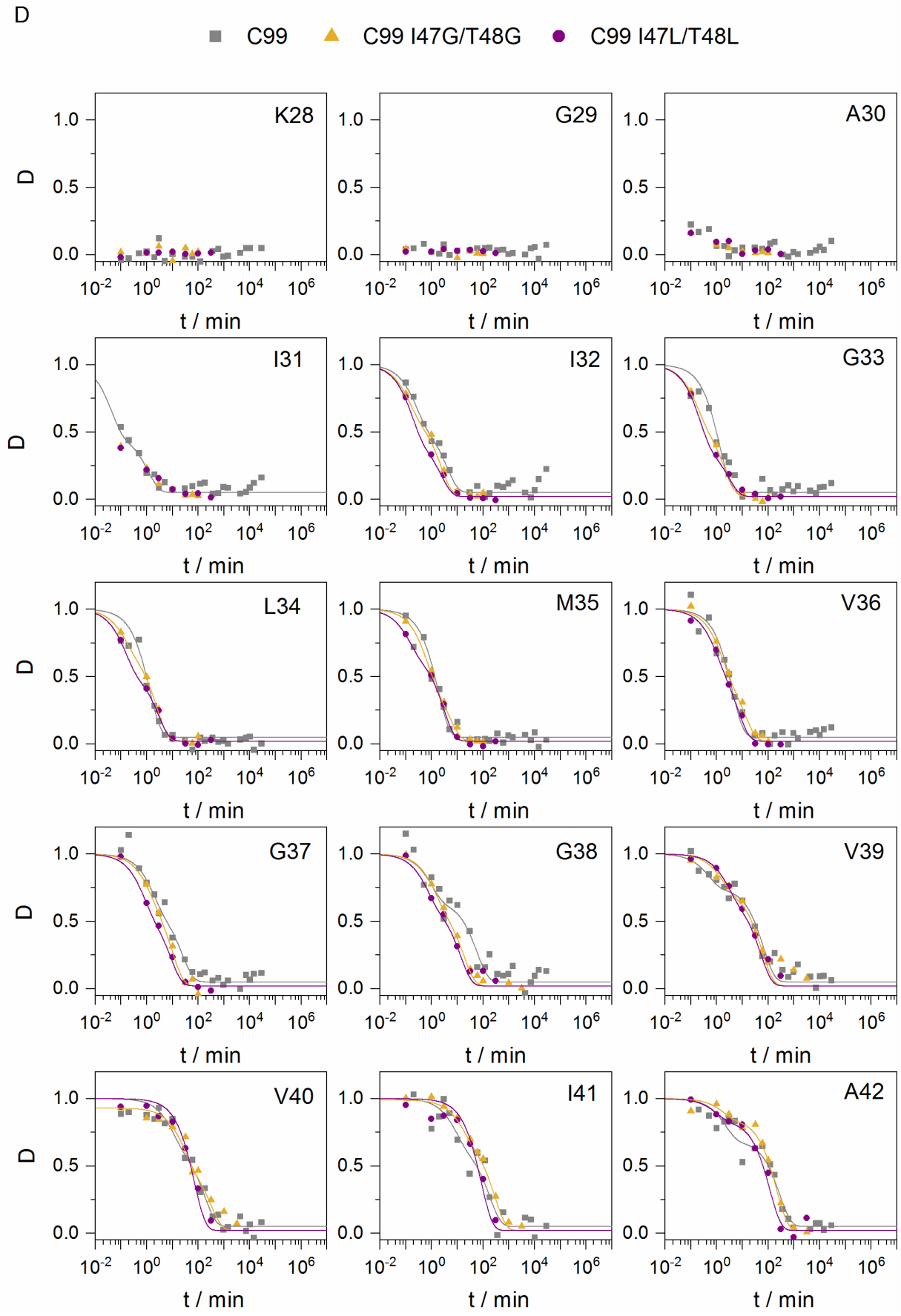
D
C99
C99 I47G/T48G
C99 I47L/T48L
K28
G29
A30
I31
I32
G33
L34
M35
V36
G37
G38
V39
V40
I41
A42
D
t / min
1.0
0.5
0.0
10^{-2}
10^{0}
10^{2}
10^{4}
10^{6}

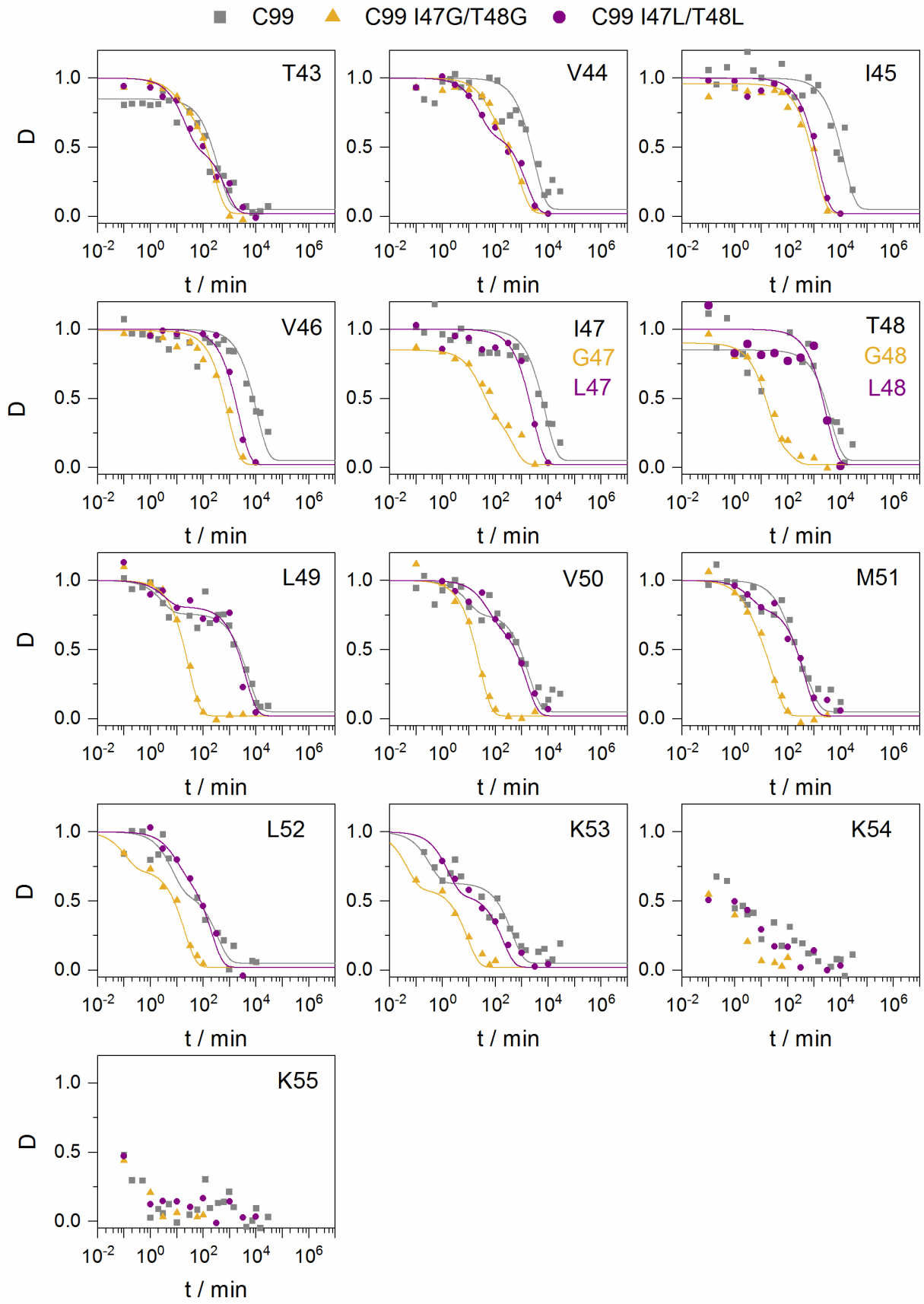
C99
C99 I47G/T48G
C99 I47L/T48L
T43
V44
I45
V46
I47
G47
L47
T48
G48
L48
L49
V50
M51
L52
K53
K54
K55
D
t / min
1.0
0.5
0.0
10^{-2} 10^{0} 10^{2} 10^{4} 10^{6}

Figure S6. Conformational flexibility of C99 I47G/T48G and I47L/T48L mutants. (A) Amide H-bond stabilities ΔG. Within areas of biphasic DHX, lower and higher values correspond to ΔG_A and ΔG_B, respectively, with the sizes of the data points approximating the deuteron populations A and B. Asterisks denote residues where the calculated ΔG_A <0 or where the apparent $k_{exp,A}$ exceeds the chemical exchange rate (see: Methods); thus reflecting extremely facile single H-bond opening. Thick and thin lines connect the values of single and double H-bond openings, respectively. The sequences feature two additional Lys residues at the N-terminus not shown here (Table S1). Aβ numbering is used and main cleavage sites are indicated. Error bars correspond to standard confidence intervals (calculated from the errors of fit in k_{exp} determination, in some cases smaller than the symbols, N=3 independent DHX reactions). **(B)** Exchange rate constants k_{exp} (filled symbols, N = 3, log k_{exp} ± error of fit) and chemical exchange rate constants k_{ch} (empty symbols). At some positions k_{exp} exceeds k_{ch}, indicating that the reference values determined in aqueous solution [11,12] slightly underestimate k_{ch} in 80% TFE (see: Methods). Within regions of biphasic DHX, more positive values denote $k_{exp,A}$. Values characterizing single H-bond openings (k_{exp}, $k_{exp,A}$) are connected by thick lines. **(C)** Heat map summarizing the color-coded ΔG_A values of single H-bond openings, the occurence of double openings (diamonds) and canonical γ-secretase cleavage sites (arrows). **(D)** Residue-specific amide DHX kinetics where the calculated deuterium contents D of the respective amides are plotted against the exchange period t. Wt C99 data are reproduced from Fig. S1.

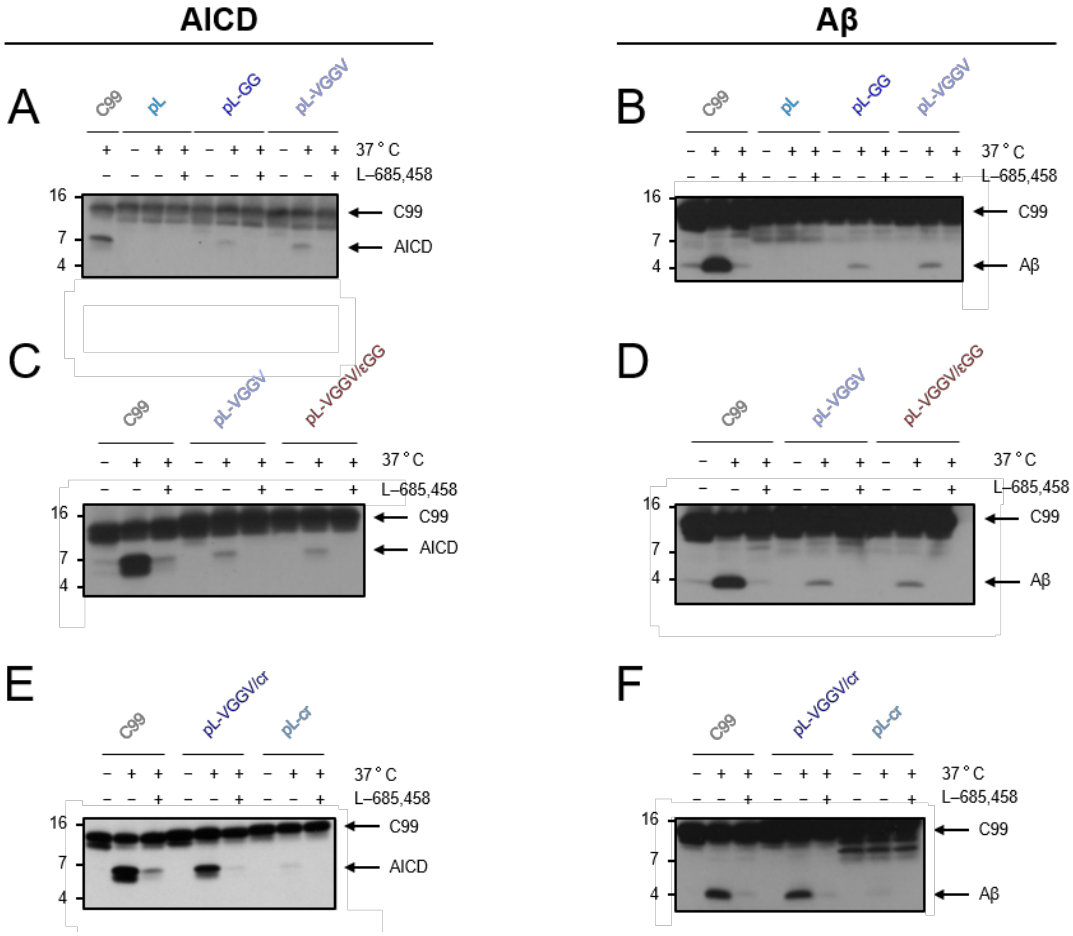

Figure S7. Cleavage detected *in vitro* is γ-secretase dependent. (A - F) Cleavage efficiency of the different constructs after incubation with CHAPSO-solubilized HEK293 membrane fractions at 37°C. To exclude γ-secretase independent cleavage additional samples, incubated at 4°C, or at 37°C in the presence of the specific γ-secretase inhibitor L-685,458 (0.5 µM), are shown for all constructs used in this paper. Levels of AICD (left panel) and Aβ (right panel) were analyzed by immunoblotting.

Supplemental References

1 Zheng, J., Strutzenberg, T., Pascal, B. D. & Griffin, P. R. Protein dynamics and conformational changes explored by hydrogen/deuterium exchange mass spectrometry. *Curr Opin Struct Biol* **58**, 305-313, doi:10.1016/j.sbi.2019.06.007 (2019).

2 Pester, O. *et al.* The Backbone Dynamics of the Amyloid Precursor Protein Transmembrane Helix Provides a Rationale for the Sequential Cleavage Mechanism of γ-Secretase. *J. Am. Chem. Soc.* **135**, 1317-1329 (2013).

3 Teilum, K., Kragelund, B. B. & Poulsen, F. M. *Application of Hydrogen Exchange Kinetics to Studies of Protein Folding*. Vol. Part I (Wiley-VCH, 2005).

4 Stelzer, W., Scharnag, C., Leurs, U., Rand, K. D. & Langosch, D. The impact of the 'Austrian' mutation of the amyloid precursor protein transmembrane helix is communicated to the hinge region. *Chemistry Select* **1**, 4408-4412 (2016).

5 Gotz, A. *et al.* Increased H-Bond Stability Relates to Altered epsilon-Cleavage Efficiency and Abeta Levels in the I45T Familial Alzheimer's Disease Mutant of APP. *Sci Rep* **9**, 5321, doi:10.1038/s41598-019-41766-1 (2019).

6 Yin, Y. I. *et al.* γ-Secretase Substrate Concentration Modulates the Abeta42/Abeta40 Ratio: IMPLICATIONS FOR ALZHEIMER DISEASE. *J Biol Chem* **282**, 23639-23644, doi:10.1074/jbc.M704601200 (2007).

7 Gotz, A. *et al.* Modulating hinge flexibility in the APP transmembrane domain alters γ-secretase cleavage. *Biophys. J.* **116**, 1-18 (2019).

8 Stelzer, W. & Langosch, D. Conformationally Flexible Sites within the Transmembrane Helices of Amyloid Precursor Protein and Notch1 Receptor. *Biochemistry* **58**, 3065-3068, doi:10.1021/acs.biochem.9b00505 (2019).

9 Barrett, P. J. *et al.* The amyloid precursor protein has a flexible transmembrane domain and binds cholesterol. *Science* **336**, 1168-1171, doi:336/6085/1168 [pii] 10.1126/science.1219988 (2012).

10 Humphrey, W., Dalke, A. & Schulten, K. VMD: visual molecular dynamics. *Journal of molecular graphics* **14**, 33-38, 27-38 (1996).

11 Englander, S. W. Hydrogen exchange and mass spectrometry: A historical perspective. *J Am Soc Mass Spectrom* **17**, 1481-1489, doi:10.1016/j.jasms.2006.06.006 (2006).

12 Bai, Y., Milne, J. S., Mayne, L. & Englander, S. W. Primary Structure Effects on Peptide Group Hydrogen Exchange. *Proteins-Structure Function and Genetics* **17**, 75-86 (1993).

3 Discussion

3.1 Substrate Requirements of γ-Secretase: The Role of a Flexible TM-N

Uncovering substrate requirements for γ-secretase is necessary to improve our understanding of one of the key enzymes in AD pathogenesis and of intramembrane proteolysis in general. However, still little is known about how substrates, and what features of the substrate, are being recognized by γ-secretase. Only a few rather general requirements (see chapter 1.1.1.4.1) have been identified for γ-secretase (Struhl and Adachi, 2000, Xia and Wolfe, 2003, Hemming et al., 2008, Laurent et al., 2015, Bolduc et al., 2016, Yan et al., 2017). Substrates are typically type I membrane proteins (Xia and Wolfe, 2003) with a short ECD (Struhl and Adachi, 2000, Hemming et al., 2008, Laurent et al., 2015, Bolduc et al., 2016), and a permissive TMD and ICD (Hemming et al., 2008). It has been proposed, not only for γ-secretase but for IMPs in general, that a certain flexibility of the substrate is required for the interaction with the enzyme, the access to the active site, and for the presentation of the scissile bond (Lemberg and Martoglio, 2002, Tian et al., 2002, Strisovsky et al., 2009, Moin and Urban, 2012, Scharnagl et al., 2014, Langosch et al., 2015, Stelzer et al., 2016). Motifs containing potentially helix-destabilizing residues, like a GG-hinge motif (Fluhrer et al., 2012) or a short asparagine-proline motif (Ye et al., 2000), can be found in substrates of other aspartyl proteases (signal peptide peptidase (SPP), signal peptide peptidase-like 2a and b) (Lemberg and Martoglio, 2002, Fluhrer et al., 2012, Spitz et al., 2020), the rhomboid proteases (Urban and Freeman, 2003, Akiyama and Maegawa, 2007, Moin and Urban, 2012), and the site-2-metalloprotease (Ye et al., 2000, Linser et al., 2015).

Several studies suggested that the G37/G38-motif present in the TMD of APP may act as a hinge region (Barrett et al., 2012, Dominguez et al., 2014, Lemmin et al., 2014, Scharnagl et al., 2014, Götz and Scharnagl, 2018). A hinge describes a flexible region which facilitates certain motions of the TMD, conferring flexibility to an otherwise rigid TMD (Hayward and Lee, 2002, Götz and Scharnagl, 2018, Högel et al., 2018, Götz et al., 2019a). It was hypothesized that this GG-hinge motif might provide the flexibility needed (Pester et al., 2013a, Dominguez et al., 2014, Lemmin et al., 2014) to allow the TMD to bend and access the active site (Tian et al., 2002, Scharnagl et al., 2014, Langosch et al., 2015, Langosch and Steiner, 2017). Such a role for helix-stabilizing amino acids had been proposed also for substrates of rhomboid proteases (Strisovsky et al., 2009).

The results presented in this thesis confirmed that the GG-motif in APP indeed acts as a flexible hinge motif. Mutating one of the glycines (G38) in this GG-hinge affected the flexibility of the APP TMD and reduced the cleavability of the two hinge-constructs analyzed. The analysis of the intrahelical H-bond strength and MD simulations revealed that the G38L mutation reduced the flexibility in the vicinity of the hinge, while the G38P mutation increased it. Additionally, circular dichroism spectroscopy and nuclear magnetic resonance (NMR) spectroscopy demonstrated an increased helicity for the G38L mutant on the one hand, and a reduced helical conformation for the G38P mutation on the other hand. Importantly, both mutations did not change the initial contact between substrate and enzyme, as shown by substrate docking simulations. One of the major contact regions of all substrates was the PS1-NTF, which is in good agreement with earlier studies identifying PS1-NTF as the primary contact site of C99 (Fukumori and Steiner, 2016). Thus, the data provide further proof that flexibility is important for substrate cleavage, but flexibility does not appear to play a role for the initial contact of substrate and enzyme.

Before a γ-secretase substrate is cleaved, it interacts with several exosites until it can access the active site and is finally cleaved (Fukumori et al., 2020). It has been proposed that a flexible TMD enables the substrate to translocate from these exosites to the active center (Tian et al., 2002, Scharnagl et al., 2014, Langosch et al., 2015, Stelzer et al., 2016) and the findings presented here further support this idea. However, it became evident that only a certain degree of flexibility is necessary. The G38P substrate was even more flexible than the WT, resulting in an increase in the potential conformations the substrate could adopt. This might hamper the binding to and further interaction with the γ-secretase complex, contributing to the decreased cleavability observed for this construct.

Initially, a few studies, showing that the exchange of one of the glycines in this motif had differential effects, seemed to contradict an important role of the GG-hinge motif of APP (Fukumori and Steiner, 2016, Higashide et al., 2017, Yan et al., 2017). One of these studies showed that exchanging one of the helix-destabilizing glycines by an unnatural amino acid, *para*-benzoyl-L-phenylalanine (Bpa), increased the cleavability of the resulting substrates (Fukumori and Steiner, 2016). However, it must be considered that Bpa does not occur naturally in proteins so that this result is difficult to interpret. Yan and colleagues showed that exchanging either of the glycines by an alanine, did not affect the cleavability of these substrates. On the

other hand, exchanging both glycines to prolines, which are known to introduce a kink in TMD helices (von Heijne, 1991), decreased the cleavability (Yan et al., 2017). In line with this, another study showed that exchanging the G37 by alanine slightly increased the cleavability of the C99-based substrate (Higashide et al., 2017). Interestingly, alanine is a helix-forming amino acid which, nevertheless, has been shown to form a rather flexible helix (Bright and Sansom, 2003). In the light of the findings presented here, demonstrating that a certain flexibility is important for substrate cleavage, the latter two studies by Yan *et al*. and Higashide *et al*. now appear to be in good agreement with the findings presented here and may even provide further proof that flexibility is indeed crucial for cleavage by γ-secretase.

Further, molecular dynamic simulations reveal that both G38 mutations analyzed here differentially altered the bending and twisting motions of the TMD, as well as the predominant relative orientation of the TM-C harboring the ε-site. Together, the changed motions and the different orientation of the TM-C most likely affected the presentation of the scissile bond at the active site. An effect of the two hinge mutations on the conformational flexibility as well as the relative orientation of the two parts of the TMD (TM-N and TM-C) could be confirmed by a recent study examining the structure of several C99 mutants by NMR spectroscopy (Silber et al., 2020). Additionally, the G38P mutation introduced a permanent kink of the TMD, as presented here, which presumably affected the interaction with the enzyme, as well as the presentation of the scissile bond even further. Thus, the reduced cleavability of both constructs can be explained by the changes in the flexibility and the relative orientation of the ε-cleavage sites, induced by the GG-hinge mutations. Altogether, the GG-hinge confers a certain flexibility and appears to be crucial for the correct positioning of the scissile bond at the active site. These findings confirmed a previous hypothesis that changes in the flexibility of the TMD may lead to an altered presentation of ε-sites at the active center of γ-secretase (Stelzer et al., 2016, Götz and Scharnagl, 2018, Tang et al., 2019).

Interestingly, the results presented here clearly showed that the processivity of the G38L construct was increased in contrast to the WT, whereas the G38P mutation slightly reduced the processivity. In case of the G38L construct the reduced flexibility may already impair the translocation to the active site and the presentation of the scissile bonds. However, once the scissile bonds are positioned and the initial cleavage occurred the increased helicity in TM-N appears to promote the sequential cleavage (trimming) of the G38L construct, resulting in the

generation of short Aβ species (mainly Aβ37). Alternatively, a helical TMD may induce skipping of the γ- and ζ-cleavage sites, resulting in the production of the short Aβ species. However, it appears to be less likely that γ-secretase, instead of following its usual cleavage pattern, skips a stretch of about 8-12 amino acids. In fact, that a helical TMD promotes trimming is supported by a study in which mutating the helix-destabilizing G37 into a helix-forming alanine also increased the processivity of the C99-based substrate (Higashide et al., 2017). In line with this, recently developed γ-secretase inhibitors, mimicking the substrate TMD, have been shown to require a helical conformation in the N-terminus (Bhattarai et al., 2020). Since also the TM-N of APP and Notch-1 is in a helical conformation when bound to γ-secretase (Zhou et al., 2019, Yang et al., 2019), it appears that these inhibitors are already in a conformation suitable for the interaction with γ-secretase (Bhattarai et al., 2020, Wolfe, 2020), arguing that a helical conformation of the TM-N seems to be important. A helical conformation within TM-N may facilitate a proper positioning of the scissile bonds or promote enzyme-substrate-interactions critical for the cleavage, which takes place mainly in TM-C.

Overall, a certain flexibility appears to be needed for the interaction with the enzyme and for the presentation of the scissile bond, however, a helical conformation of the substrate TMD promotes the processivity. That conformational flexibility of a substrate is generally important for its recognition and for the catalysis has been suggested by several groups (Henzler-Wildman et al., 2007, Boehr et al., 2009, Ma and Nussinov, 2010, Nashine et al., 2010). It is possible that γ-secretase utilizes some sort of conformational sampling at the different steps of substrate recruitment and processing to differentiate between substrates and non-substrates (**Publication 1**).

Further analysis of a C99-based construct with a TMD consisting only of leucines (polyLeu-TMD) demonstrated that this construct was virtually uncleaved by γ-secretase. This construct proved to be very stable, as can be deduced from the increased H-bond strength in comparison to the natural C99-TMD. Thus, exchanging only the TMD, of the γ-secretase substrate C99, by a TMD with helix-stabilizing leucines converted this construct into a non-substrate of γ-secretase. It is possible that due to the rigid polyLeu-TMD the construct either fails to translocate to the active site or to properly present the scissile bond at the active site and as a result, this construct is not cleaved by γ-secretase. Again, this underlined the importance of flexibility for substrate recruitment and cleavage by γ-secretase.

Reintroducing only the GG-hinge motif back into the TM-N of the polyLeu-TMD increased the flexibility around the hinge motif but also a few residues more C-terminal and was sufficient to transform this non-substrate into a substrate of γ-secretase. These experiments clearly demonstrate that the presence of a flexible region in the TM-N of APP is a sufficient substrate requirement for γ-secretase cleavage of C99 (**Publication 2**). A certain flexibility of the TM-N may even be a substrate requirement for a subgroup of γ-secretase substrates, since APP is not the only substrate harboring a GG-hinge motif in its TMD. About 17 % of all substrates (see Table 1 in the appendix) known so far have such a motif with two or even three consecutive glycines in their TMD. Substrates without a GG-hinge may feature other helix-destabilizing motifs, which provide the flexibility needed for substrate recruitment and cleavage. For instance, Notch-1 harbors a poly-alanine stretch in its TM-N which has been suggested to form a hinge region in the Notch-1 TMD, similar to the GG-hinge in C99 (Stelzer and Langosch, 2019). The importance of a flexible region in the TM-N of Notch-1 is supported by a study showing that mutating either of the first two alanines of the poly-alanine stretch in Notch-1 reduced the cleavability of the mutant constructs (Xu et al., 2016). Another study showed that replacing one of the four alanines in the alanine stretch by the helix-destabilizing residue valine (Lyu et al., 1990, Lyu et al., 1991) enhanced the cleavability for three of these constructs (Tanii et al., 2006). The exchange of two leucines in the TMD, close to the alanine stretch, by two alanines also increased the cleavability of the resulting Notch-1-based substrate (Vooijs et al., 2004). Together, these studies provide further proof for the hypothesis that γ-secretase substrates require a flexible TM-N. In line with this, further analysis presented here show that Notch-1 and two other γ-secretase substrates, N-Cadherin and ErbB4, indeed feature flexible regions in their TM-N. The presence of a flexible motif within the TMD of γ-secretase substrates may reflect the need for a substrate to bend in order to access the active site, as well as for the presentation of the scissile bond, as suggested previously (Tian et al., 2002, Scharnagl et al., 2014, Langosch et al., 2015, Stelzer et al., 2016).

Indeed, this may even be extended to IMPs in general since helix-destabilizing residues in the substrate's TMD have so far been shown to affect proteolysis by three of the four IMP families (Ye et al., 2000, Lemberg and Martoglio, 2002, Urban and Freeman, 2003, Akiyama and Maegawa, 2007, Fluhrer et al., 2012, Moin and Urban, 2012, Spitz et al., 2020). Several groups reported that replacing helix-breaking residues in the TMD of different IMPs substrates by potentially helix-stabilizing amino acids did decrease or even abolish the cleavability of the

resulting constructs (Ye et al., 2000, Lemberg and Martoglio, 2002, Akiyama and Maegawa, 2007, Strisovsky et al., 2009, Fluhrer et al., 2012, Spitz et al., 2020). Three of these studies demonstrated that exchanging only the potentially flexible motif almost or completely abolished the cleavage of the mutant constructs (Ye et al., 2000, Strisovsky et al., 2009, Spitz et al., 2020). In line with this, it has been shown that introducing helix-breaking residues into substrates of IMPs increased their cleavability (Urban and Freeman, 2003, Akiyama and Maegawa, 2007, Moin and Urban, 2012, Spitz et al., 2020). Three studies even showed that introducing one or two helix-breaking amino acids into a non-cleavable construct of SPP or a rhomboid protease facilitated the cleavage of the original non-cleavable construct (Lemberg and Martoglio, 2002, Urban and Freeman, 2003, Moin and Urban, 2012). Interestingly, it could be demonstrated also for a rhomboid protease that exchanging the TMD of a cleavable construct by a polyLeu-TMD completely abolished the cleavage (Maegawa et al., 2005). Further analysis would, however, be needed to conclude whether helix-destabilizing residues are a common (sufficient) substrate requirement of IMPs and whether further requirements are to be identified.

The rhomboid proteases are the only IMP family for which a prevalent recognition motif has been identified (Strisovsky et al., 2009). Initially, it was demonstrated that a motif in the TMD of the rhomboid substrate Spitz, containing several potentially helix-destabilizing amino acids, was necessary and sufficient for cleavage (Urban and Freeman, 2003). Based on this, it was proposed that rhomboids recognize a common conformation in their substrates and that this motif may be a universal recognition motif for rhomboid proteases (Urban and Freeman, 2003). Later, a recognition motif has been identified, which determined the cleavage site and proved to be more important than helix-destabilizing residues (Strisovsky et al., 2009). This recognition motif, however, resembled more a region featuring certain properties. The study demonstrated a preference for small residues directly N-terminal of the scissile bond (P1 position) and for hydrophobic, and preferentially large residues four amino acids N-terminal (P4) as well as two amino acids C-terminal of the cleavage site (P2') (Strisovsky et al., 2009). However, not all proteins containing this motif were indeed cleaved by one of the rhomboid proteases analyzed in this study and, furthermore, the motif is not present in all rhomboid substrates (Strisovsky et al., 2009). Thus, this motif does not appear to be a substrate requirement for all rhomboid proteases (Tatsuta et al., 2007, Strisovsky et al., 2009, Schäfer et al., 2010, Ha et al., 2013). Instead, it appears that both, certain sequence requirements and a flexible TMD, are important

for cleavage by rhomboid proteases (Freeman, 2014), and still further requirements may exist (Strisovsky et al., 2009).

3.2 Substrate Requirements of γ-Secretase: The Role of the TM-C

The cleavage sites of soluble proteases preferentially reside within flexible regions, or regions prone to unfolding (Hubbard, 1998, Belushkin et al., 2014). In line with this, proteases typically recognize and bind their substrates in an extended β-strand conformation (Tyndall et al., 2005). IMPs, on the other hand, cleave their substrates within the TMD, which assumes an α-helical structure within the hydrophobic environment of the lipid bilayer (Popot and Engelman, 2000). However, α-helices are generally not susceptible to cleavage (Hubbard, 1998, Madala et al., 2010). Thus, in order to be cleaved by γ-secretase the local helical structure around the cleavage sites needs to unwind first (Ye et al., 2000, Clemente et al., 2018, Brown et al., 2018, Yang et al., 2019, Zhou et al., 2019). For γ-secretase and for IMPs in general it has been suggested that helix-destabilizing amino acids or a certain conformational flexibility may facilitate the unwinding and the exposure of the scissile bond (Ye et al., 2000, Lemberg and Martoglio, 2002, Lu et al., 2011, Brown et al., 2018, Clemente et al., 2018, Steiner et al., 2020). Indeed, several potentially destabilizing residues are found N-terminally of the initial cleavage site in the γ-secretase substrates C99, Notch-1, and TREM2 which may facilitate unfolding (Steiner et al., 2020). Further, TREM2 has recently been reported to be cleaved within a flexible region in its TMD (Steiner et al., 2020). Interestingly, introducing a mutation which stabilized the region around the initial cleavage site abolished the cleavage at the original cleavage site and shifted the cleavage to another, newly formed, flexible region (Steiner et al., 2020). In line with this, introducing potentially helix-stabilizing or -destabilizing residues near the initial cleavage site of C99 decreased or increased the cleavability, respectively (Fernandez et al., 2016, Sato et al., 2009). Similar findings have been reported for the cleavage of a Notch1-based substrate, where helix-stabilizing mutations close to the initial cleavage site also decreased the cleavability of the resulting construct (Vooijs et al., 2004, Xu et al., 2016).

At a first glance, these data suggest that a flexible TM-C is required for substrate cleavage by γ-secretase. However, the results presented here and by two other groups clearly show that the TMD of C99 is rather rigid in the vicinity of the cleavage site (Pester et al., 2013b, Götz et al., 2019b, Stelzer and Langosch, 2019). As shown here, increasing the flexibility in the TM-C of the polyLeu-TMD substrate, harboring the GG-hinge in the TM-N, by adding a second

GG-hinge at the initial cleavage sites did not improve the cleavability any further. Thus, this did not support an important role of flexibility in the TM-C for substrate cleavage. Instead, specific interactions of the TM-C with the enzyme appear to be more important. Indeed, the C-terminal cleavage region was sufficient to render the non-cleavable polyLeu-TMD into a substrate of γ-secretase. More importantly, introducing the C-terminal cleavage region, together with the hinge in the TM-N, into the non-cleavable polyLeu-TMD resulted in a cleavage efficiency higher than just the total of both efficiencies. Consequently, combining both, the N-terminal hinge and the C-terminal cleavage region, was sufficient to restore cleavability of the natural TMD of C99. This suggested that the flexible region in the TM-N and the natural APP cleavage region in the TM-C are sufficient substrate requirements for C99/γ-secretase and that they cooperate for efficient cleavage (**Publication 2**). Importantly, the insights gained from the cell-free system could be recapitulated in a cellular model, providing proof that the results presented here also hold true in a more complex cellular context and further supporting the relevance of these findings.

At first, the result obtained with the polyLeu-TMD construct harboring a second hinge at the initial cleavage site, as presented here, appear to be in contrast with the results presented by Fernandez and colleagues (Fernandez et al., 2016). In this study, introducing two potentially helix-destabilizing glycines at position 47 and 48 increased the cleavability of the C99-based construct, while exchanging the natural residues by two potentially helix-stabilizing leucine decrease the cleavability. Remarkably, analysis of the H-bond strength of these two constructs used by Fernandez and colleagues, as presented here, revealed an increased flexibility around the ε-sites for the I47G/T48G but also a slight increase for the I47L/T48L substrate. This could be explained by the removal of the H-bond from T48, which has been shown to have a stabilizing effect (Scharnagl et al., 2014). Interestingly, both mutations also affected the flexibility in TM-N. While the LL-mutation stabilized the region between residues V39 and I41, the I47G/T48G substrate further destabilized the TM-N. Thus, these data provide further proof that flexibility in the TM-C is not necessary for cleavage by γ-secretase, rather they again support an important role for flexibility within TM-N.

In line with this, the introduction of potentially helix-destabilizing glycines within the cleavage region (Xu et al., 2016) or C-terminal of the cleavage region (Sato et al., 2009), have been shown to decrease the cleavability of the respective C99-based substrates. Further support is

provided by deuterium hydrogen exchange (DHX) and MD studies reporting that APP FAD mutations near the cleavage sites did actually destabilize the helix close to the GG-hinge of APP, but not around the cleavage (Stelzer et al., 2016, Götz and Scharnagl, 2018). Along the same lines, also the two hinge mutations G38L and G38P presented in this thesis only increased the flexibility around the hinge motif, while the region around the initial cleavage site proved to be in a stable helical conformation. These findings are in good agreement with earlier findings (Pester et al., 2013a, Pester et al., 2013b, Scharnagl et al., 2014). Whether flexibility in the TM-C is generally not necessary for cleavage by γ-secretase, remains to be investigated, since the TM-C of Notch-1 was reported to be more flexible than the TM-C of C99 (Stelzer and Langosch, 2019). On the other hand, introducing helix-destabilizing residues at or near the cleavage site of substrates of other aspartate IMPs also did not increase the cleavability of the respective substrates (Yücel et al., 2019, Spitz et al., 2020). Together, this indicates that specific interactions between the substrates TM-C and the enzyme are far more important than flexibility in the TM-C (**Publication 2**).

Specifically, the TM-C may be needed for docking of the region surrounding the scissile bond at the active center and for the formation of a β-sheet upon interaction with the γ-secretase. The two recent structures of γ-secretase in complex with two of its substrates, C83 and Notch-1, uncovered the formation of a β-strand downstream of the cleavage sites (Yang et al., 2019, Zhou et al., 2019). This β-strand interacted with two newly formed β-strands of PS1 to form a β-sheet, which proved to be important for stabilizing the substrate and bringing the scissile bond into position (Zhou et al., 2019). Such a β-sheet may not only be formed for the initial cleavage, but for all the subsequent cleavages (stepwise trimming) of C99 (Yang et al., 2019). Interestingly, the region N-terminal of the initial cleavage sites of C99 is particularly rich in β-branched residues (threonine, isoleucine, and valine). Generally, β-branched residues have a high β-sheet forming propensity (Li and Deber, 1992, Kim and Berg, 1993, Minor and Kim, 1994, Smith et al., 1994) and consequently tend to form β-strands rather than α-helices. After the initial cleavage has taken place, a high content of β-branched residues in the TM-C of C99 might thus facilitate the formation of a β-sheet prior to each subsequent cleavage, thereby stabilizing the substrate and positioning the scissile bond. Additionally, β-branched residues may facility the unfolding of the helix required for cleavage. Therefore, the important role of the TM-C for cleavability might further be explained by the relatively high number of β-branched residues in the TM-C of C99. Together, this suggests that β-branched residues in

the TM-C may be an important requirement for C99. In accordance with this, one study demonstrated that the TM-C of C99 is not in a helical conformation and that extending the α-helix inhibited the cleavage (Sato et al., 2009). The presence of β-branched residues in the TM-C might even be a more common substrate requirement for γ-secretase, since also other substrates have a high content of β-branched residues in the C-terminal half of their TMD (compare Table 2 in the appendix). More data would, however, be needed to draw this conclusion.

Finally, the analysis of the AICD species generated from the C99-based polyLeu-TMD constructs demonstrated that all substrates presented here shifted the initial ε-cleavage site. Consequently, the N-terminal hinge and the C-terminal cleavage region are important for cleavability but are not decisive for ε-site specificity. Thus, the cleavability of C99 is determined by a certain flexibility in its TM-N facilitating the translocation to the active site, by specific interactions of its TM-C with the enzyme required for docking to the active site and formation of a β-sheet, as well as the cooperation of TM-N and TM-C in this process. Interestingly, the processivity of all generated polyLeu-TMD substrates was greatly enhanced, as seen for the G38L mutant presented here. The Aβ species generated from the polyLeu-TMD substrates were even shorter than the Aβ species detected for the G38L, where only one leucine has been introduced. Interestingly, all polyLeu-based substrates mainly generated Aβ species that were even shorter than those usually generated from C99 WT. Again, indicating that once the substrate has reached the active site a helical TMD appears to promote its trimming.

3.3 Conclusions

Altogether, the results presented in this thesis clearly demonstrated that the GG-motif in C99 acts as a flexible hinge facilitating certain motions of the TMD conveying the flexibility needed for the interaction with γ-secretase. Not only does this flexibility seem to be necessary for the translocation from the exosites to the active site, further, the results presented here uncovered that mutating this GG-hinge affected the relative orientation of the initial cleavage site. Consequently, the flexibility provided by the hinge enables a correct positioning of the scissile bond. In fact, the presence of a flexible region in the TM-N of C99 proved to be a sufficient substrate requirement for the γ-secretase cleavage of C99. It appears likely, that γ-secretase utilizes some sort of conformational sampling during substrate recruitment and cleavage to distinguish between substrates and non-substrates. Whether a certain flexibility of the TM-N is a general substrate requirement for γ-secretase substrates, or if this may be unique to APP still requires further investigation.

The cleavage by γ-secretase, however, does not require the TM-C to be flexible, rather specific interactions between the substrates TM-C and the enzyme appeared to be far more critical. Indeed, the TM-C may promote the formation of a cleavage competent state by facilitating docking of the scissile bond at the active center and the formation of a β-sheet after the initial cleavage has occurred, which helps to stabilize the substrate and to bring the scissile bond into position (Yang et al., 2019, Zhou et al., 2019), as well as for the inevitable unfolding of the helix prior to cleavage. Consequently, β-branched residues in the TM-C may be an important requirement for C99. However, once C99 has reached the active site and the scissile bond has been positioned and cleaved, further trimming is promoted by a helical conformation of the C99-TMD.

Taken together, this work demonstrated that the flexible region in the TM-N and the natural cleavage domain in the TM-C of C99 are sufficient substrate requirements for γ-secretase cleavage of C99 and that they cooperate for efficient cleavage. The cleavability of C99, on the one hand, was determined by the flexibility in the TM-N and possibly by specific interactions of its TM-C with γ-secretase, while a helical TMD facilitated further trimming. In sum, this work provides important insights into how γ-secretase distinguishes between substrates and non-substrates, and further uncovers features determining the cleavability as well as the processivity of C99.

4 Material and Methods

The following section contains a brief description of the methods and equipment used in this thesis. Whenever specialized equipment was necessary this is stated explicitly in the text, otherwise common laboratory equipment and solutions have been used.

4.1 Antibodies

Table 1: Antibodies used in this thesis for immunoblotting (IB) and immunoprecipitation (IP).

Antibody	Epitope	Species	IB	IP	Source/Reference
Y188	APP-CTF[1]	Rb[2]	1:4000	-	Abcam
2D8	Aβ, AA 1-16	R[2]	1:10	-	(Shirotani et al., 2007)
4G8	Aβ, AA 17-24	M	-	1:250	Covance
Penta-His	His_6-peptide	M	1:2000	-	Qiagen

AA: Amino acids; **M**: Mouse; **Rb**: Rabbit; **R**: Rat
[1] Exact epitope not specified by the manufacturer
[2] Monoclonal antibody

4.2 Molecular Biological Methods

4.2.1 Plasmids and Primer

In order to express and purify C99-based GG-hinge constructs in *E.coli* cells, the desired mutations were introduced (compare 4.2.2) into the WT C100-His_6 (Met-C99-His_6) construct (in pQE60 vector). This WT C100-His_6 construct already existed in the laboratory and was used without further modifications. The polyLeu-based C99 construct on the other hand, were kindly provided by Prof. Lichtenthaler and featured an N-terminal HA-tag and two FLAG-tags at the C-terminus (in pcDNA3.1). In a first step, the polyLeu-based constructs had to be recloned into the pQE60 vector. After a PCR using the primers 1 and 2, NcoI/BamHI restriction digest, and ligation of the construct into the pQE60 vector, the resulting constructs featured an N-terminal Met (M1 in C100) and His_6-tag at the C-terminus (connected via a GSRS linker), similar to the C100 WT. Due to inefficient expression in the pQE60 vector the polyLeu-based constructs had to be recloned into the pET-21d(+) vector, following PCR with primers 1 and 3 and NcoI/HindIII restriction digest. All three primers used are listed in the following table.

Number	Name	Sequence
1	NcoI-C99_for	CGCCCATGGATGCAGAATTCCGAC
2	C99-BamHI_rev	CTTTGAGCAGATGCAGAACGGATCCGCG
3	C99-HindIII_rev	GCAAGCTTAGTGATGGTGATGGTGATG

4.2.2 Site-Directed Mutagenesis

Desired point mutations were introduced into C99 WT by using site-directed mutagenesis. The primer used for the generation of the GG-hinge mutants G38L and G38P are listed below. The mutated amino acids are depicted in bold letters.

Primer	Sequence
G38L_for	CAATCATTGGACTCATGGTGGGC**CTG**GTTG
G38L_rev	GATCACTGTCGCTATGACAAC**CAG**GCC
G38P_for	CAATCATTGGACTCATGGTGGGC**CCG**GTTG
G38P_rev	GATCACTGTCGCTATGACAAC**CGG**GCC

The reagents needed for the site-directed mutagenesis are listed in the table below.

Reagent	Amount for 1 reaction
Plasmid DNA	10 ng
Forward primer	0.5 µl
Reverse primer	0.5 µl
dNTP-Mix (10mM)	1 µl
10x Reaction buffer	2 µl
Pfu Turbo-Polymerase	1 µl
H_2O	ad 20 µl

To allow the reaction to take place, the samples were incubated in a PCR cycler following the program below.

Step	Duartion	Temperature	Number of Cycles
Initial denaturation	5 min	95 °C	1
Denaturation	30 s	95 °C	
Annealing	1 min	55 °C	14
Elongation	9 min	68 °C	
Final elongation	10 min	68 °C	1

Finally, each sample was incubated with 1 µl *DpnI* (1 h at 37°C), thereby digesting the methylated parental DNA and leaving the newly generated mutant DNA intact.

4.2.3 Transformation of DNA into *E.coli* Bacteria

LB medium 1 % Bacto-Tryptone; 0.5 % yeast extract; 17.25 mM NaCl

For the transformation of DNA into competent *E.coli* bacteria (BL21(DE3)$_{RIL}$ or Rosetta (DE3)) the bacteria were thawed on ice and 60 µl of competent cells were incubated together with 10 µl of *DpnI*-digested DNA (20 min on ice). This was followed by a second incubation step at 42 °C for 60 s. Next, 500 µl of LB medium was added to the cells and the samples were incubated for another 30 min (37 °C, while shaking). Finally, 200 µl were plated onto LB-agar plates (containing the appropriate selection antibiotic) and incubated at 37 °C overnight.

4.3 Expression of WT and Mutant C100-His$_6$ Proteins

LB medium 1 % Bacto-Tryptone; 0.5 % yeast extract; 17.25 mM NaCl

Ampicillin medium LB medium 100 µg/ml ampicillin (1000x stock in 50 % ethanol)

IPTG 1 M IPTG in H2O

Tris-Puffer 2 M Tris-HCl (pH 8.5)

The C99 and GG-hinge constructs analyzed in this thesis were expressed in *E. coli* BL21(DE3$_{RIL}$) cells, while the polyLeu-based constructs were expressed in *E.coli* Rosetta (DE3) cells. To this end, a pre culture (50 ml ampicillin medium) was prepared with the respective cells and incubated at 37 °C overnight, while shaking. Next, the culture was adjusted to an OD_{600} of 0.2 with ampicillin medium to yield 200 ml in total. Once an OD_{600} of 0.5 was

reached the expression was induced by addition of IPTG (1 mM) and the cultures were incubated for another 3.5h (37 °C, shaking). The cells were collected via centrifugation (10 min, 600 rpm, 4 °C) and the pellet was kept at -20 °C until further use.

4.4 Purification of WT and Mutant C100-His_6 Proteins

TE-buffer	20 mM Tris-HCl (pH 7.5); 1 mM EDTA, 1 x PI (cOmplete, Roche)
Urea-buffer	20 mM Tris-HCl (pH 8.5); 6 M urea; 1 % Triton X-100; 1 % SDS; 1 mM $CaCl_2$; 100 mM NaCl, 1 x PI (cOmplete EDTA-free, Roche)
Binding-Buffer	20 mM Tris-HCl (pH 7.5); 150 mM NaCl
Triton washing buffer	20 mM Tris-HCl (pH 8.5); 300 mM NaCl; 1 % Triton X-100
SDS washing buffer	20 mM Tris-HCl (pH 8.5); 300 mM NaCl; 0.2 % SDS
Imidazole washing buffer	20 mM Tris-HCl (pH 8.5); 300 mM NaCl; 0.2 % SDS; 20 mM imidazole
Elution buffer	20 mM Tris-HCl (pH 8.5); 300 mM NaCl; 0.2 % SDS; 100 mM imidazole
Final elution buffer	20 mM Tris-HCl (pH 8.5); 300 mM NaCl; 0.2 % SDS; 500 mM imidazole

The recombinant C100-His_6 substrates used for the cell-free cleavage analysis were purified via Ni^{2+}-NTA-agarose. To this end, the cell pellets (compare section 4.3) were resuspended with TE-buffer, sonicated on ice (30 s pulse, 60 s break) and centrifuged (10 min, 12000 rpm, 4 °C) twice. After the second centrifugation step, the cells were resuspended in urea-buffer and incubated overnight (4 °C, shaking). Next, the samples were centrifuged once more (10 min, 12000 rpm, 4 °C) and the amount of C100-His_6 present in each sample was determined. Prior to the incubation with the Ni^{2+}-NTA-agarose (Qiagen) the agarose was washed three times with Tris/HCL (20 mM, pH 7.5) and centrifuged after each washing step (2 min, 600 g, 4 °C). The samples were diluted with binding buffer (1:5), the washed agarose (50 % suspension) was added, and the samples were incubated for 2 h (RT) while shaking. To elute the C100-His_6 constructs from the beads the samples were centrifuged (5 min, 600 g, 4 °C) and the beads were loaded onto a column (Poly-Prep® Chromatography Columns, Bio-Rad) with Triton washing buffer (for 100 µl of agarose beads 200 µl of buffer were added). Next, the beads were washed four times with the Triton washing buffer, four times with the SDS washing buffer, and three times with the imidazole washing buffer. Next, the constructs were eluted by adding elution

buffer in five consecutive steps. Any remaining protein was eluted from the beads by the singular addition of final elution buffer. For each step, the volume of buffer added was always twice the volume of the agarose loaded onto the column. Finally, the protein concentration was measured and adjusted to 6.6 µm. All samples were stored at 4 °C. The different fractions were analyzed via SDS-polyacrylamide gel electrophoresis (SDS-PAGE) and immunoblotting (compare section 4.5.3 and 4.5.6) using antibodies Y188 or Penta-His for detection.

4.5 Protein Biochemical Methods

4.5.1 Preparation of γ-Secretase Containing Membrane Fractions

Hypotonic buffer	15 mM Sodium-Citrate (pH 6.4); 1 x PI (cOmplete, Roche)

Membranes containing γ-secretase were prepared from HEK293 cells which were scraped when the cells were 90% confluent, centrifuged (5 min, 1,000 g, 4 °C), and lysed with 1 ml hypotonic buffer per 10 cm dish. The OD_{600} was adjusted (OD_{600} = 2) and the cells were incubated for 10 min on ice. Next, the samples were frozen in liquid nitrogen (5 min), thawed (on ice), and centrifuged (15 min, 1,000 g, 4 °C). The supernatant was again centrifuged (45 min, 16,000 g, 4 °C) and the resulting membrane pellet was either directly processed or frozen in liquid nitrogen and stored until further use (-80 °C).

4.5.2 Cell-free γ-Secretase Cleavage Assay Using CHAPSO Solubilized Membrane Fractions

CHAPSO buffer	1% (w/v) CHAPSO; 150 mM Citrate buffer (pH 6.4); 1 x PI (cOmplete, Roche)
Citrate buffer	1.5 M Sodium-Citrate (pH 6.4)
Assay buffer (2x)	150 mM Sodium-Citrate (pH 6.4); 1 mg/ml Phosphatidylcholine; 20 mM DTT; 0.2 mg/ml BSA; 1 x PI (cOmplete, Roche)
C100-His_6 substrate	6.6µM; 0.1 % SDS; 3.3 µM DTT

Prior to the cell-free cleavage assay, the membrane pellet (see chapter 4.5.1) was resuspended in CHAPSO buffer (100 µl/10 cm dish) and incubated for 20 min (on ice). Next, the samples were cleared from all insoluble components by centrifugation (30 min, 100,000 g, 4 °C) and the supernatant (CHAPSO membrane lysate) was frozen in liquid nitrogen and stored at -80 °C or directly used for the cleavage assay.

For the cleavage assay, the purified C100-His_6 constructs were incubated together with the CHAPSO membrane lysate and the following components at 37 °C for 16 h, while shaking:

Reagent	Amount for 1 sample
Citrate buffer	5 µl
Assay buffer (2x)	10 µl
Membrane lysate	5 µl
C100-His_6	0.5 µl
Inhibitor/DMSO	0.5 µl

Two additional samples, incubated at 4 °C or at 37 °C and in the presence of the γ-secretase inhibitor L-685,458 (InSolution™ γ-Secretase inhibitor X, Merck Millipore), served as controls for each construct. Following this incubation step, the cleavage products were analyzed via immunoblotting and the signal was quantified with the image reader LAS-4000 (Fujifilm Life Science, USA).

4.5.3 Protein Analysis via SDS-PAGE and Immunoblotting

4x Laemmli-sample buffer 188 mM Tris-HCl (pH 6.8); 6 % SDS; 30 % glycerol; 7.5 % β-mercaptoethanol; 6 M urea; bromophenol blue

Subjecting samples to SDS-PAGE allows for a separation of the proteins by size. Subsequently, the proteins were transferred onto a membrane via immunoblotting (see chapter 4.5.6) and visualized using specific antibodies (compare chapter 4.1). To this end, samples were prepared using the 4x Laemmli-sample buffer. For the various analyses different gels and buffers had to be used as described below.

4.5.4 Tris-Glycine Gels

4x Separation gel buffer 1.5 M Tris-HCl pH 8.8; 0.4 % SDS
4x Stacking gel buffer 0.5 M Tris-HCl pH 6.8; 0.4 % SDS
Tris-Glycine-Running buffer 25 mM Tris-HCL; 200 mM Glycine; 0.1 % SDS

These gels were used for the analysis of purified His_6-tagged proteins (see chapter 4.4). The table below summarizes the reagents needed for two Tris-Glycine gels.

Reagent	Separation gel (15 %)	Stacking gel
4x Stacking gel buffer	-	1.25 ml
4x Separation gel buffer	5.85 ml	-
H_2O	8.8 ml	3.4 ml
Acryl-/Bisacrylamide (37.5:1: 40 %)	8.8 ml	0.5 ml
10% APS	45 µl	15 µl
TEMED	45 µl	15 µl

4.5.5 Tris-Tricine Gels

Tris-Tricine running buffer 100 mM Tris; 100 mM Tricine; 0.1 % SDS

In order to analyze and quantify the amount of cleavage products (ACID, Aβ) generated in the cell-free cleavage assay (compare section 4.5.2) commercial Tris-Tricine gels (10-20 %, Invitrogen) have been used.

4.5.6 Immunoblotting

Tris-Glycine blotting buffer 25 mM Tris-HCl; 200 mM Glycine
Blocking buffer 0.2 % I-Block (Tropix); 0.1 % Tween20 in PBS
TBS-Tween buffer 100 mM Tris-HCl (pH 7.4); 150 mM NaCl; 0.1 % Tween20

Following separation of the proteins via SDS-PAGE, the proteins were transferred onto a nitrocellulose membrane. Therefore, the gels and the membranes were placed into a blotting chamber filled with Tris-Glycine blotting buffer and blotted for 1 h (400 mA). In order to achieve good signals, especially for small proteins (AICD, Aβ), the membrane was boiled for 5 min in PBS. Next, the membrane was blocked for 1 h in blocking buffer (RT) and then incubated (4 °C, overnight) with the primary antibody (compare chapter 4.1). The membranes were washed three times with TBS-Tween buffer (15 min, RT) prior to and after the incubation with the HRP-coupled secondary antibody (1 h, RT). Primary and secondary antibodies were always diluted in blocking buffer. After the final washing step, ECL solution (Pierce™ ECL Western-Blotting Substrate, Thermo Scientific) was added to the membranes and the signal from the HRP was detected either using a radiographic film or via a CCD camera (LAS-4000 Image Reader, Fujifilm Life Sciences). Finally, the images from the image reader were analyzed using the Multi-Gauge (V3.0) software.

For the detection of small proteins (AICD, Aβ) nitrocellulose membrane with a pore size of 0.2 µm were used. For all other proteins, nitrocellulose membranes with 0.45 µm pore size were used.

4.5.7 Immunoprecipitation

IP-MS buffer	0.1 % N-octyl glucoside, 140 mM NaCl, and 10 mM Tris (pH 8.0)

Prior to the analysis using the mass spectrometer, the cleavage products generated in the cell-free assay had to be immunoprecipitated (IP). After overnight incubation of the cell-free assay, specific antibodies were added to the sample. For the IP of AICD species 1µl Y188 antibody and 15µl protein A-Sepharose and for the IP of Aβ species 4µl 4G8 antibody and 12µl protein G-Sepharose were added to the sample and incubated for 16 h at 4 °C while shaking. Next, the beads were washed (3 times with IP-MS buffer and 3 times with ddH_2O) and centrifuged in between the washing steps (1000 g, 4 °C, 1 min). After the last washing step, the remaining fluid was removed using a pipet tip, where the tip had been compressed beforehand. The samples were either directly prepared for further analysis or had been stored at -20 °C.

4.5.8 Mass Spectrometry Analysis of AICD and Aβ Species

MS-matrix	50 % Acetonitril, 0.3 % trichloracetic acid in H_2O, saturated with α-Cyano-4-hydroxycinnamic acid

After immunoprecipitation, the samples were analyzed on a 4800 MALDI-TOF/TOF Analyzer (Applied Biosystems/MDS SCIEX). The MS-matrix was prepared as follows: acetonitrile was mixed with trichloracetic acid (1:2) and saturated with α-Cyano-4-hydroxycinnamic acid. The MS-matrix was incubated for 15 min at 37 °C, while shaking. To elute the peptides, 10 µl MS-matrix were added to the samples, which were briefly stirred. Next, 0.4 µl of the supernatant were spotted (3 times) onto the MALDI-plate which was subsequently analyzed on the MALDI-TOF/TOF Analyzer. Data were analyzed using the DataExplorer™ (V4.8, Applied Biosystems) software.

5 References

Abramov, E., Dolev, I., Fogel, H., Ciccotosto, G. D., Ruff, E. & Slutsky, I. 2009. Amyloid-β as a positive endogenous regulator of release probability at hippocampal synapses. *Nature Neuroscience,* 12**,** 1567-76.

Akiyama, Y. & Maegawa, S. 2007. Sequence features of substrates required for cleavage by GlpG, an Escherichia coli rhomboid protease. *Molecular Microbiology,* 64**,** 1028-1037.

Alzforum Mutations

Alzheimer, A. 1907. Über eine eigenartige Erkrankung der Hirnrinde. *Allgemeine Zeitschrift fur Psychiatrie und Psychisch-gerichtliche Medizin,* 64**,** 146-148.

Andersson, E. R., Sandberg, R. & Lendahl, U. 2011. Notch signaling: simplicity in design, versatility in function. *Development,* 138**,** 3593-3612.

Asai, M., Hattori, C., Szabó, B., Sasagawa, N., Maruyama, K., Tanuma, S. & Ishiura, S. 2003. Putative function of ADAM9, ADAM10, and ADAM17 as APP α-secretase. *Biochemical and Biophysical Research Communications,* 301**,** 231-5.

Atwood, C. S., Bowen, R. L., Smith, M. A. & Perry, G. 2003. Cerebrovascular requirement for sealant, anti-coagulant and remodeling molecules that allow for the maintenance of vascular integrity and blood supply. *Brain Research Reviews,* 43**,** 164-78.

Avci, D., Fuchs, S., Schrul, B., Fukumori, A., Breker, M., Frumkin, I., Chen, C.-Y., Biniossek, Martin l., Kremmer, E., Schilling, O., Steiner, H., Schuldiner, M. & Lemberg, Marius k. 2014. The yeast ER-intramembrane protease Ypf1 refines nutrient sensing by regulating transporter abundance. *Molecular Cell,* 56**,** 630-640.

Bai, X.-C., Rajendra, E., Yang, G., Shi, Y. & Scheres, S. H. W. 2015a. Sampling the conformational space of the catalytic subunit of human γ-secretase. *eLife,* 4**,** e11182.

Bai, X. C., Yan, C., Yang, G., Lu, P., Ma, D., Sun, L., Zhou, R., Scheres, S. H. W. & Shi, Y. 2015b. An atomic structure of human γ-secretase. *Nature,* 525**,** 212-217.

Bammens, L., Chávez-Gutiérrez, L., Tolia, A., Zwijsen, A. & De Strooper, B. 2011. Functional and topological analysis of PEN-2, the fourth subunit of the γ-secretase complex. *Journal of Biological Chemistry,* 286**,** 12271-82.

Barrett, P. J., Song, Y., Van Horn, W. D., Hustedt, E. J., Schafer, J. M., Hadziselimovic, A., Beel, A. J. & Sanders, C. R. 2012. The amyloid precursor protein has a flexible transmembrane domain and binds cholesterol. *Science,* 336**,** 1168-71.

Beard, H. A., Barniol-Xicota, M., Yang, J. & Verhelst, S. H. L. 2019. Discovery of cellular roles of intramembrane proteases. *ACS Chemical Biology,* 14**,** 2372-2388.

Beel, A. J. & Sanders, C. R. 2008. Substrate specificity of γ-secretase and other intramembrane proteases. *Cellular and Molecular Life Sciences,* 65**,** 1311-1334.

Beher, D., Clarke, E. E., Wrigley, J. D., Martin, A. C., Nadin, A., Churcher, I. & Shearman, M. S. 2004. Selected non-steroidal anti-inflammatory drugs and their derivatives target γ-secretase at a novel site. Evidence for an allosteric mechanism. *Journal of Biological Chemistry,* 279**,** 43419-26.

Beher, D., Fricker, M., Nadin, A., Clarke, E. E., Wrigley, J. D. J., Li, Y.-M., Culvenor, J. G., Masters, C. L., Harrison, T. & Shearman, M. S. 2003. In vitro characterization of the presenilin-dependent γ-secretase complex using a novel affinity ligand. *Biochemistry,* 42**,** 8133-8142.

Beher, D., Wrigley, J. D., Nadin, A., Evin, G., Masters, C. L., Harrison, T., Castro, J. L. & Shearman, M. S. 2001. Pharmacological knock-down of the presenilin 1 heterodimer by a novel γ-secretase inhibitor: implications for presenilin biology. *Journal of Biological Chemistry,* 276**,** 45394-402.

Belushkin, A. A., Vinogradov, D. V., Gelfand, M. S., Osterman, A. L., Cieplak, P. & Kazanov, M. D. 2014. Sequence-derived structural features driving proteolytic processing. *Proteomics,* 14**,** 42-50.

Ben-Shem, A., Fass, D. & Bibi, E. 2007. Structural basis for intramembrane proteolysis by rhomboid serine proteases. *Proceedings of the National Academy of Sciences,* 104**,** 462-466.

Benilova, I., Gallardo, R., Ungureanu, A. A., Castillo Cano, V., Snellinx, A., Ramakers, M., Bartic, C., Rousseau, F., Schymkowitz, J. & De Strooper, B. 2014. The Alzheimer disease protective mutation A2T modulates kinetic and thermodynamic properties of amyloid-beta (Abeta) aggregation. *Journal of Biological Chemistry,* 289**,** 30977-89.

Bhattarai, S., Devkota, S., Meneely, K. M., Xing, M., Douglas, J. T. & Wolfe, M. S. 2020. Design of substrate transmembrane mimetics as structural probes for γ-secretase. *Journal of the American Chemical Society,* 142**,** 3351-3355.

Black, P. H. 1980. Shedding from normal and cancer-cell surfaces. *The New England Journal of Medicine,* 303**,** 1415-6.

Boehr, D. D., Nussinov, R. & Wright, P. E. 2009. The role of dynamic conformational ensembles in biomolecular recognition. *Nature Chemical Biology,* 5**,** 789-96.

Bolduc, D. M., Montagna, D. R., Gu, Y., Selkoe, D. J. & Wolfe, M. S. 2016. Nicastrin functions to sterically hinder γ-secretase–substrate interactions driven by substrate transmembrane domain. *Proceedings of the National Academy of Sciences,* 113**,** E509-E518.

Boyartchuk, V. L., Ashby, M. N. & Rine, J. 1997. Modulation of Ras and a-factor function by carboxyl-terminal proteolysis. *Science,* 275**,** 1796-800.

Brady, O. A., Zhou, X. & Hu, F. 2014. Regulated intramembrane proteolysis of the frontotemporal lobar degeneration risk factor, TMEM106B, by signal peptide peptidase-like 2a (SPPL2a). *Journal of Biological Chemistry,* 289**,** 19670-80.

Bright, J. N. & Sansom, M. S. P. 2003. The flexing/twirling helix: exploring the flexibility about molecular hinges formed by proline and glycine motifs in transmembrane helices. *The Journal of Physical Chemistry B,* 107**,** 627-636.

Brookmeyer, R., Gray, S. & Kawas, C. 1998. Projections of Alzheimer's disease in the United States and the public health impact of delaying disease onset. *American Journal of Public Health,* 88**,** 1337-42.

Brothers, H. M., Gosztyla, M. L. & Robinson, S. R. 2018. The physiological roles of amyloid-β peptide hint at new ways to treat alzheimer's disease. *Frontiers in Aging Neuroscience,* 10**,** 118-118.

Brown, M. C., Abdine, A., Chavez, J., Schaffner, A., Torres-Arancivia, C., Lada, B., Jiji, R. D., Osman, R., Cooley, J. W. & Ubarretxena-Belandia, I. 2018. Unwinding of the substrate transmembrane helix in intramembrane proteolysis. *Biophysical Journal,* 114**,** 1579-1589.

Brown, M. S., Ye, J., Rawson, R. B. & Goldstein, J. L. 2000. Regulated intramembrane proteolysis: a control mechanism conserved from bacteria to humans. *Cell,* 100**,** 391-8.

Burns, A., Jacoby, R. & Levy, R. 1991. Progression of cognitive impairment in Alzheimer's disease. *Journal of the American Geriatrics Society,* 39**,** 39-45.

Bursavich, M. G., Harrison, B. A. & Blain, J. F. 2016. γ-Secretase modulators: new alzheimer's drugs on the horizon? *Journal of Medicinal Chemistry,* 59**,** 7389-409.

Busciglio, J., Gabuzda, D. H., Matsudaira, P. & Yankner, B. A. 1993. Generation of β-amyloid in the secretory pathway in neuronal and nonneuronal cells. *Proceedings of the National Academy of Sciences of the United States of America,* 90**,** 2092-2096.

Buxbaum, J. D., Liu, K. N., Luo, Y., Slack, J. L., Stocking, K. L., Peschon, J. J., Johnson, R. S., Castner, B. J., Cerretti, D. P. & Black, R. A. 1998. Evidence that tumor necrosis

factor α converting enzyme is involved in regulated α-secretase cleavage of the Alzheimer amyloid protein precursor. *Journal of Biological Chemistry,* 273**,** 27765-7.

Cai, H., Wang, Y., Mccarthy, D., Wen, H., Borchelt, D. R., Price, D. L. & Wong, P. C. 2001. BACE1 is the major β-secretase for generation of Aβ peptides by neurons. *Nature Neuroscience,* 4**,** 233-4.

Cao, X. & Südhof, T. C. 2001. A transcriptionally active complex of APP with Fe65 and histone acetyltransferase Tip60. *Science,* 293**,** 115-20.

Capell, A., Beher, D., Prokop, S., Steiner, H., Kaether, C., Shearman, M. S. & Haass, C. 2005. γ-Secretase complex assembly within the early secretory pathway. *Journal of Biological Chemistry,* 280**,** 6471-8.

Capell, A., Grünberg, J., Pesold, B., Diehlmann, A., Citron, M., Nixon, R., Beyreuther, K., Selkoe, D. J. & Haass, C. 1998. The proteolytic fragments of the Alzheimer's disease-associated presenilin-1 form heterodimers and occur as a 100-150-kDa molecular mass complex. *Journal of Biological Chemistry,* 273**,** 3205-3211.

Chartier-Harlin, M.-C., Crawford, F., Houlden, H., Warren, A., Hughes, D., Fidani, L., Goate, A., Rossor, M., Roques, P., Hardy, J. & Mullan, M. 1991. Early-onset Alzheimer's disease caused by mutations at codon 717 of the β-amyloid precursor protein gene. *Nature,* 353**,** 844-846.

Checler, F., Sunyach, C., Pardossi-Piquard, R., Sévalle, J., Vincent, B., Kawarai, T., Girardot, N., St George-Hyslop, P. & Da Costa, C. A. 2007. The γ/η-secretase-derived APP intracellular domain fragments regulate p53. *Current Alzheimer Research,* 4**,** 423-6.

Chen, C.-Y., Malchus, N. S., Hehn, B., Stelzer, W., Avci, D., Langosch, D. & Lemberg, M. K. 2014. Signal peptide peptidase functions in ERAD to cleave the unfolded protein response regulator XBP1u. *EMBO Journal,* 33**,** 2492-2506.

Chêne, G., Beiser, A., Au, R., Preis, S. R., Wolf, P. A., Dufouil, C. & Seshadri, S. 2015. Gender and incidence of dementia in the Framingham Heart Study from mid-adult life. *Alzheimers Dement,* 11**,** 310-320.

Chou, P. Y. & Fasman, G. D. 1974. Conformational parameters for amino acids in helical, β-sheet, and random coil regions calculated from proteins. *Biochemistry,* 13**,** 211-222.

Chow, V. W., Mattson, M. P., Wong, P. C. & Gleichmann, M. 2010. An overview of APP processing enzymes and products. *Neuromolecular medicine,* 12**,** 1-12.

Chyung, J. H., Raper, D. M. & Selkoe, D. J. 2005. γ-Secretase exists on the plasma membrane as an intact complex that accepts substrates and effects intramembrane cleavage. *Journal of Biological Chemistry,* 280**,** 4383-92.

Chyung, J. H. & Selkoe, D. J. 2003. Inhibition of receptor-mediated endocytosis demonstrates generation of amyloid β-protein at the cell surface. *Journal of Biological Chemistry,* 278**,** 51035-43.

Citron, M., Oltersdorf, T., Haass, C., Mcconlogue, L., Hung, A. Y., Seubert, P., Vigo-Pelfrey, C., Lieberburg, I. & Selkoe, D. J. 1992. Mutation of the β-amyloid precursor protein in familial Alzheimer's disease increases β-protein production. *Nature,* 360**,** 672-4.

Clemente, N., Abdine, A., Ubarretxena-Belandia, I. & Wang, C. 2018. Coupled transmembrane substrate docking and helical unwinding in intramembrane proteolysis of amyloid precursor protein. *Scientific Reports,* 8**,** 12411.

Cook, D. G., Forman, M. S., Sung, J. C., Leight, S., Kolson, D. L., Iwatsubo, T., Lee, V. M. & Doms, R. W. 1997. Alzheimer's Aβ(1-42) is generated in the endoplasmic reticulum/intermediate compartment of NT2N cells. *Nature Medicine,* 3**,** 1021-3.

Coric, V., Salloway, S., Van Dyck, C. H., Dubois, B., Andreasen, N., Brody, M., Curtis, C., Soininen, H., Thein, S., Shiovitz, T., Pilcher, G., Ferris, S., Colby, S., Kerselaers, W., Dockens, R., Soares, H., Kaplita, S., Luo, F., Pachai, C., Bracoud, L., Mintun, M., Grill, J. D., Marek, K., Seibyl, J., Cedarbaum, J. M., Albright, C., Feldman, H. H. & Berman,

R. M. 2015. Targeting prodromal Alzheimer disease with avagacestat: a randomized clinical trial. *Journal of the American Medical Association Neurology,* 72**,** 1324-1333.

Crump, C. J., Johnson, D. S. & Li, Y.-M. 2013. Development and mechanism of γ-secretase modulators for Alzheimer's disease. *Biochemistry,* 52**,** 3197-3216.

Cullen, N., Janelidze, S., Palmqvist, S., Stomrud, E., Mattsson-Carlgren, N. & Hansson, O. 2021. Association of CSF Aβ38 levels with risk of Alzheimer disease-related decline. *Neurology*.

Cummings, J. L., Morstorf, T. & Zhong, K. 2014. Alzheimer's disease drug-development pipeline: few candidates, frequent failures. *Alzheimer's Research and Therapy,* 6**,** 37.

Cummings, J. L., Tong, G. & Ballard, C. 2019. Treatment combinations for Alzheimer's disease: current and future pharmacotherapy options. *Journal of Alzheimer's Disease,* 67**,** 779-794.

De Strooper, B., Annaert, W., Cupers, P., Saftig, P., Craessaerts, K., Mumm, J. S., Schroeter, E. H., Schrijvers, V., Wolfe, M. S., Ray, W. J., Goate, A. & Kopan, R. 1999. A presenilin-1-dependent γ-secretase-like protease mediates release of Notch intracellular domain. *Nature,* 398**,** 518-522.

De Strooper, B., Saftig, P., Craessaerts, K., Vanderstichele, H., Guhde, G., Annaert, W., Von Figura, K. & Van Leuven, F. 1998. Deficiency of presenilin-1 inhibits the normal cleavage of amyloid precursor protein. *Nature,* 391**,** 387-390.

De Strooper, B., Umans, L., Van Leuven, F. & Van Den Berghe, H. 1993. Study of the synthesis and secretion of normal and artificial mutants of murine amyloid precursor protein (APP): cleavage of APP occurs in a late compartment of the default secretion pathway. *Journal of Cell Biology,* 121**,** 295-304.

Dehury, B., Tang, N., Blundell, T. L. & Kepp, K. P. 2019a. Structure and dynamics of γ-secretase with presenilin 2 compared to presenilin 1. *RSC Advances,* 9**,** 20901-20916.

Dehury, B., Tang, N. & Kepp, K. P. 2019b. Molecular dynamics of C99-bound γ-secretase reveal two binding modes with distinct compactness, stability, and active-site retention: implications for Aβ production. *Biochemical Journal,* 476**,** 1173-1189.

Devkota, S., Williams, T. D. & Wolfe, M. S. 2021. Familial Alzheimer's disease mutations in amyloid protein precursor alter proteolysis by γ-secretase to increase amyloid β-peptides of >45 residues. *Journal of Biological Chemistry***,** 100281.

Di Fede, G., Catania, M., Morbin, M., Rossi, G., Suardi, S., Mazzoleni, G., Merlin, M., Giovagnoli, A. R., Prioni, S., Erbetta, A., Falcone, C., Gobbi, M., Colombo, L., Bastone, A., Beeg, M., Manzoni, C., Francescucci, B., Spagnoli, A., Cantù, L., Del Favero, E., Levy, E., Salmona, M. & Tagliavini, F. 2009. A recessive mutation in the APP gene with dominant-negative effect on amyloidogenesis. *Science,* 323**,** 1473-7.

Dimitrov, M., Alattia, J. R., Lemmin, T., Lehal, R., Fligier, A., Houacine, J., Hussain, I., Radtke, F., Dal Peraro, M., Beher, D. & Fraering, P. C. 2013. Alzheimer's disease mutations in APP but not γ-secretase modulators affect ε-cleavage-dependent AICD production. *Nature Communications,* 4**,** 2246.

Doerfler, P., Shearman, M. S. & Perlmutter, R. M. 2001a. Presenilin-dependent γ-secretase activity modulates thymocyte development. *Proceedings of the National Academy of Sciences of the United States of America,* 98**,** 9312-7.

Doerfler, P., Shearman, M. S. & Perlmutter, R. M. 2001b. Presenilin-dependent γ-secretase activity modulates thymocyte development. *Proceedings of the National Academy of Sciences,* 98**,** 9312-9317.

Dominguez, L., Foster, L., Straub, J. E. & Thirumalai, D. 2016. Impact of membrane lipid composition on the structure and stability of the transmembrane domain of amyloid precursor protein. *Proceedings of the National Academy of Sciences of the United States of America,* 113**,** E5281-7.

Dominguez, L., Meredith, S. C., Straub, J. E. & Thirumalai, D. 2014. Transmembrane fragment structures of amyloid precursor protein depend on membrane surface curvature. *Journal of the American Chemical Society,* 136**,** 854-7.

Donoviel, D. B., Hadjantonakis, A. K., Ikeda, M., Zheng, H., Hyslop, P. S. & Bernstein, A. 1999. Mice lacking both presenilin genes exhibit early embryonic patterning defects. *Genes and Development,* 13**,** 2801-10.

Doody, R. S., Raman, R., Farlow, M., Iwatsubo, T., Vellas, B., Joffe, S., Kieburtz, K., He, F., Sun, X., Thomas, R. G., Aisen, P. S., Siemers, E., Sethuraman, G. & Mohs, R. 2013. A phase 3 trial of semagacestat for treatment of Alzheimer's disease. *The New England Journal of Medicine,* 369**,** 341-50.

Dougherty, J. J., Wu, J. & Nichols, R. A. 2003. β-Amyloid regulation of presynaptic nicotinic receptors in rat hippocampus and neocortex. *Journal of Neuroscience,* 23**,** 6740-7.

Dyrks, T., Weidemann, A., Multhaup, G., Salbaum, J. M., Lemaire, H. G., Kang, J., Müller-Hill, B., Masters, C. L. & Beyreuther, K. 1988. Identification, transmembrane orientation and biogenesis of the amyloid A4 precursor of Alzheimer's disease. *EMBO Journal,* 7**,** 949-57.

Edbauer, D., Winkler, E., Haass, C. & Steiner, H. 2002. Presenilin and nicastrin regulate each other and determine amyloid β-peptide production via complex formation. *Proceedings of the National Academy of Sciences,* 99**,** 8666-8671.

Edbauer, D., Winkler, E., Regula, J. T., Pesold, B., Steiner, H. & Haass, C. 2003. Reconstitution of γ-secretase activity. *Nature Cell Biology,* 5**,** 486-8.

Elad, N., De Strooper, B., Lismont, S., Hagen, W., Veugelen, S., Arimon, M., Horré, K., Berezovska, O., Sachse, C. & Chávez-Gutiérrez, L. 2015. The dynamic conformational landscape of γ-secretase. *Journal of Cell Science,* 128**,** 589-598.

Escamilla-Ayala, A., Wouters, R., Sannerud, R. & Annaert, W. 2020. Contribution of the Presenilins in the cell biology, structure and function of γ-secretase. *Seminars in Cell and Developmental Biology,* 105**,** 12-26.

Esch, F. S., Keim, P. S., Beattie, E. C., Blacher, R. W., Culwell, A. R., Oltersdorf, T., Mcclure, D. & Ward, P. J. 1990. Cleavage of amyloid β peptide during constitutive processing of its precursor. *Science,* 248**,** 1122-4.

Esler, W. P., Kimberly, W. T., Ostaszewski, B. L., Diehl, T. S., Moore, C. L., Tsai, J. Y., Rahmati, T., Xia, W., Selkoe, D. J. & Wolfe, M. S. 2000. Transition-state analogue inhibitors of γ-secretase bind directly to presenilin-1. *Nature Cell Biology,* 2**,** 428-34.

Esler, W. P., Kimberly, W. T., Ostaszewski, B. L., Ye, W., Diehl, T. S., Selkoe, D. J. & Wolfe, M. S. 2002. Activity-dependent isolation of the presenilin– γ-secretase complex reveals nicastrin and a γ substrate. *Proceedings of the National Academy of Sciences,* 99**,** 2720-2725.

Esparza, T. J., Zhao, H., Cirrito, J. R., Cairns, N. J., Bateman, R. J., Holtzman, D. M. & Brody, D. L. 2013. Amyloid-β oligomerization in Alzheimer dementia versus high-pathology controls. *Annals of Neurology,* 73**,** 104-19.

Estus, S., Golde, T. E. & Younkin, S. G. 1992. Normal processing of the Alzheimer's disease amyloid β protein precursor generates potentially amyloidogenic carboxyl-terminal derivatives. *Annals of the New York Academy of Sciences,* 674**,** 138-48.

Evans, D. A., Funkenstein, H. H., Albert, M. S., Scherr, P. A., Cook, N. R., Chown, M. J., Hebert, L. E., Hennekens, C. H. & Taylor, J. O. 1989. Prevalence of Alzheimer's disease in a community population of older persons. Higher than previously reported. *Journal of the American Medical Association,* 262**,** 2551-6.

FDA 2021. FDA grants accelerated approval for Alzheimer’s drug. FDA News Release.

Feng, L., Yan, H., Wu, Z., Yan, N., Wang, Z., Jeffrey, P. D. & Shi, Y. 2007. Structure of a site-2 protease family intramembrane metalloprotease. *Science,* 318**,** 1608-1612.

Fernandez, M. A., Biette, K. M., Dolios, G., Seth, D., Wang, R. & Wolfe, M. S. 2016. Transmembrane Substrate Determinants for γ-Secretase Processing of APP CTFβ. *Biochemistry,* 55**,** 5675-5688.

Fleig, L., Bergbold, N., Sahasrabudhe, P., Geiger, B., Kaltak, L. & Lemberg, Marius k. 2012. Ubiquitin-dependent intramembrane rhomboid protease promotes ERAD of membrane proteins. *Molecular Cell,* 47**,** 558-569.

Fluhrer, R., Martin, L., Klier, B., Haug-Kröper, M., Grammer, G., Nuscher, B. & Haass, C. 2012. The α-helical content of the transmembrane domain of the British dementia protein-2 (Bri2) determines its processing by signal peptide peptidase-like 2b (SPPL2b). *Journal of Biological Chemistry,* 287**,** 5156-63.

Frackowiak, J., Wisniewski, H. M., Wegiel, J., Merz, G. S., Iqbal, K. & Wang, K. C. 1992. Ultrastructure of the microglia that phagocytose amyloid and the microglia that produce β-amyloid fibrils. *Acta Neuropathologica,* 84**,** 225-33.

Fraering, P. C., Lavoie, M. J., Ye, W., Ostaszewski, B. L., Kimberly, W. T., Selkoe, D. J. & Wolfe, M. S. 2004. Detergent-dependent dissociation of active γ-secretase reveals an interaction between PEN-2 and PS1-NTF and offers a model for subunit organization within the complex. *Biochemistry,* 43**,** 323-333.

Francis, R., Mcgrath, G., Zhang, J., Ruddy, D. A., Sym, M., Apfeld, J., Nicoll, M., Maxwell, M., Hai, B., Ellis, M. C., Parks, A. L., Xu, W., Li, J., Gurney, M., Myers, R. L., Himes, C. S., Hiebsch, R., Ruble, C., Nye, J. S. & Curtis, D. 2002. APH-1 and PEN-2 are required for Notch pathway signaling, γ-secretase cleavage of βAPP, and presenilin protein accumulation. *Developmental Cell,* 3**,** 85-97.

Freeman, M. 2014. The rhomboid-like superfamily: molecular mechanisms and biological roles. *Annual Review of Cell and Developmental Biology,* 30**,** 235-54.

Fukumori, A., Feilen, L. P. & Steiner, H. 2020. Substrate recruitment by γ-secretase. *Seminars in Cell and Developmental Biology,* 105**,** 54-63.

Fukumori, A., Fluhrer, R., Steiner, H. & Haass, C. 2010. Three-amino acid spacing of presenilin endoproteolysis suggests a general stepwise cleavage of γ-secretase-mediated intramembrane proteolysis. *Journal of Neuroscience,* 30**,** 7853-7862.

Fukumori, A. & Steiner, H. 2016. Substrate recruitment of γ-secretase and mechanism of clinical presenilin mutations revealed by photoaffinity mapping. *EMBO Journal,* 35**,** 1628-1643.

Funamoto, S., Sasaki, T., Ishihara, S., Nobuhara, M., Nakano, M., Watanabe-Takahashi, M., Saito, T., Kakuda, N., Miyasaka, T., Nishikawa, K., Saido, T. C. & Ihara, Y. 2013. Substrate ectodomain is critical for substrate preference and inhibition of γ-secretase. *Nature Communications,* 4**,** 2529.

Galasko, D. R., Graff-Radford, N., May, S., Hendrix, S., Cottrell, B. A., Sagi, S. A., Mather, G., Laughlin, M., Zavitz, K. H., Swabb, E., Golde, T. E., Murphy, M. P. & Koo, E. H. 2007. Safety, tolerability, pharmacokinetics, and Aβ levels after short-term administration of R-flurbiprofen in healthy elderly individuals. *Alzheimer Disease and Associated Disorders,* 21**,** 292-9.

Gao, Y. & Pimplikar, S. W. 2001. The γ-secretase-cleaved C-terminal fragment of amyloid precursor protein mediates signaling to the nucleus. *Proceedings of the National Academy of Sciences of the United States of America,* 98**,** 14979-84.

Gatz, M., Reynolds, C. A., Fratiglioni, L., Johansson, B., Mortimer, J. A., Berg, S., Fiske, A. & Pedersen, N. L. 2006. Role of genes and environments for explaining Alzheimer disease. *Archives of General Psychiatry,* 63**,** 168-74.

Geling, A., Steiner, H., Willem, M., Bally-Cuif, L. & Haass, C. 2002. A γ-secretase inhibitor blocks Notch signaling in vivo and causes a severe neurogenic phenotype in zebrafish. *EMBO reports,* 3**,** 688-694.

Glenner, G. G. & Wong, C. W. 1984a. Alzheimer's disease and Down's syndrome: sharing of a unique cerebrovascular amyloid fibril protein. *Biochemical and Biophysical Research Communications,* 122**,** 1131-5.

Glenner, G. G. & Wong, C. W. 1984b. Alzheimer's disease: initial report of the purification and characterization of a novel cerebrovascular amyloid protein. *Biochemical and Biophysical Research Communications,* 120**,** 885-90.

Goate, A., Chartier-Harlin, M. C., Mullan, M., Brown, J., Crawford, F., Fidani, L., Giuffra, L., Haynes, A., Irving, N., James, L. & Et Al. 1991. Segregation of a missense mutation in the amyloid precursor protein gene with familial Alzheimer's disease. *Nature,* 349**,** 704-6.

Golde, T., Estus, S., Younkin, L., Selkoe, D. & Younkin, S. 1992. Processing of the amyloid protein precursor to potentially amyloidogenic derivatives. *Science,* 255**,** 728-730.

Goldgaber, D., Lerman, M. I., Mcbride, O. W., Saffiotti, U. & Gajdusek, D. C. 1987. Characterization and chromosomal localization of a cDNA encoding brain amyloid of Alzheimer's disease. *Science,* 235**,** 877-80.

Goldstein, J. L., Rawson, R. B. & Brown, M. S. 2002. Mutant mammalian cells as tools to delineate the sterol regulatory element-binding protein pathway for feedback regulation of lipid synthesis. *Archives of Biochemistry and Biophysics,* 397**,** 139-48.

Gosztyla, M. L., Brothers, H. M. & Robinson, S. R. 2018. Alzheimer's Amyloid-β is an Antimicrobial Peptide: A Review of the Evidence. *Journal of Alzheimer's Disease,* 62**,** 1495-1506.

Götz, A., Högel, P., Silber, M., Chaitoglou, I., Luy, B., Muhle-Goll, C., Scharnagl, C. & Langosch, D. 2019a. Increased H-bond stability relates to altered ε-cleavage efficiency and Aβ levels in the I45T familial Alzheimer's disease mutant of APP. *Scientific Reports,* 9**,** 5321.

Götz, A., Mylonas, N., Högel, P., Silber, M., Heinel, H., Menig, S., Vogel, A., Feyrer, H., Huster, D., Luy, B., Langosch, D., Scharnagl, C., Muhle-Goll, C., Kamp, F. & Steiner, H. 2019b. Modulating hinge flexibility in the APP transmembrane domain alters γ-secretase cleavage. *Biophysical Journal,* 116**,** 2103-2120.

Götz, A. & Scharnagl, C. 2018. Dissecting conformational changes in APP's transmembrane domain linked to ε-efficiency in familial Alzheimer's disease. *PLOS ONE,* 13**,** e0200077.

Goutte, C., Tsunozaki, M., Hale, V. A. & Priess, J. R. 2002. APH-1 is a multipass membrane protein essential for the Notch signaling pathway in Caenorhabditis elegans embryos. *Proceedings of the National Academy of Sciences of the United States of America,* 99**,** 775-9.

Gratuze, M., Leyns, C. E. G. & Holtzman, D. M. 2018. New insights into the role of TREM2 in Alzheimer's disease. *Molecular Neurodegeneration,* 13**,** 66.

Greenfield, J. P., Tsai, J., Gouras, G. K., Hai, B., Thinakaran, G., Checler, F., Sisodia, S. S., Greengard, P. & Xu, H. 1999. Endoplasmic reticulum and trans-Golgi network generate distinct populations of Alzheimer β-amyloid peptides. *Proceedings of the National Academy of Sciences of the United States of America,* 96**,** 742-7.

Gu, Y., Chen, F., Sanjo, N., Kawarai, T., Hasegawa, H., Duthie, M., Li, W., Ruan, X., Luthra, A., Mount, H. T., Tandon, A., Fraser, P. E. & St George-Hyslop, P. 2003. APH-1 interacts with mature and immature forms of presenilins and nicastrin and may play a role in maturation of presenilin.nicastrin complexes. *Journal of Biological Chemistry,* 278**,** 7374-80.

Gu, Y., Misonou, H., Sato, T., Dohmae, N., Takio, K. & Ihara, Y. 2001. Distinct intramembrane cleavage of the β-amyloid precursor protein family resembling γ-secretase-like cleavage of Notch. *Journal of Biological Chemistry,* 276**,** 35235-8.

Gunawardena, S. & Goldstein, L. S. B. 2001. Disruption of axonal transport and neuronal viability by amyloid precursor protein mutations in Drosophila. *Neuron,* 32**,** 389-401.

Güner, G. & Lichtenthaler, S. F. 2020. The substrate repertoire of γ-secretase/presenilin. *Seminars in Cell and Developmental Biology,* 105**,** 27-42.

Ha, Y., Akiyama, Y. & Xue, Y. 2013. Structure and mechanism of rhomboid protease. *Journal of Biological Chemistry,* 288**,** 15430-15436.

Haapasalo, A. & Kovacs, D. M. 2011. The many substrates of presenilin/γ-secretase. *Journal of Alzheimer's Disease,* 25**,** 3-28.

Haass, C., Hung, A. Y., Schlossmacher, M. G., Teplow, D. B. & Selkoe, D. J. 1993. β-Amyloid peptide and a 3-kDa fragment are derived by distinct cellular mechanisms. *Journal of Biological Chemistry,* 268**,** 3021-4.

Haass, C., Kaether, C., Thinakaran, G. & Sisodia, S. 2012. Trafficking and proteolytic processing of APP. *Cold Spring Harbor Perspectives in Medicine* 2**,** a006270.

Haass, C., Koo, E. H., Mellon, A., Hung, A. Y. & Selkoe, D. J. 1992a. Targeting of cell-surface β-amyloid precursor protein to lysosomes: alternative processing into amyloid-bearing fragments. *Nature,* 357**,** 500-3.

Haass, C., Lemere, C. A., Capell, A., Citron, M., Seubert, P., Schenk, D., Lannfelt, L. & Selkoe, D. J. 1995. The Swedish mutation causes early-onset Alzheimer's disease by β-secretase cleavage within the secretory pathway. *Nature Medicine,* 1**,** 1291-6.

Haass, C., Schlossmacher, M. G., Hung, A. Y., Vigo-Pelfrey, C., Mellon, A., Ostaszewski, B. L., Lieberburg, I., Koo, E. H., Schenk, D., Teplow, D. B. & Et Al. 1992b. Amyloid β-peptide is produced by cultured cells during normal metabolism. *Nature,* 359**,** 322-5.

Haass, C. & Selkoe, D. J. 1993. Cellular processing of β-amyloid precursor protein and the genesis of amyloid β-peptide. *Cell,* 75**,** 1039-42.

Haass, C. & Selkoe, D. J. 2007. Soluble protein oligomers in neurodegeneration: lessons from the Alzheimer's amyloid β-peptide. *Nature Reviews Molecular Cell Biology,* 8**,** 101-12.

Hadland, B. K., Manley, N. R., Su, D.-M., Longmore, G. D., Moore, C. L., Wolfe, M. S., Schroeter, E. H. & Kopan, R. 2001. γ-Secretase inhibitors repress thymocyte development. *Proceedings of the National Academy of Sciences,* 98**,** 7487-7491.

Hampton, S. E., Dore, T. M. & Schmidt, W. K. 2018. Rce1: mechanism and inhibition. *Critical Reviews in Biochemistry and Molecular Biology,* 53**,** 157-174.

Hansen, D. V., Hanson, J. E. & Sheng, M. 2018. Microglia in Alzheimer's disease. *Journal of Cell Biology,* 217**,** 459-472.

Hardy, J. & Allsop, D. 1991. Amyloid deposition as the central event in the aetiology of Alzheimer's disease. *Trends in Pharmacological Sciences,* 12**,** 383-8.

Hardy, J. & Selkoe, D. J. 2002. The amyloid hypothesis of Alzheimer's disease: progress and problems on the road to therapeutics. *Science,* 297**,** 353-356.

Hardy, J. A. & Higgins, G. A. 1992. Alzheimer's disease: the amyloid cascade hypothesis. *Science,* 256**,** 184-5.

Hartmann, T., Bieger, S. C., Brühl, B., Tienari, P. J., Ida, N., Allsop, D., Roberts, G. W., Masters, C. L., Dotti, C. G., Unsicker, K. & Beyreuther, K. 1997. Distinct sites of intracellular production for Alzheimer's disease Aβ40/42 amyloid peptides. *Nature Medicine,* 3**,** 1016-20.

Hatami, A., Monjazeb, S., Milton, S. & Glabe, C. G. 2017. Familial Alzheimer's disease mutations within the amyloid precursor protein alter the aggregation and conformation of the amyloid-β peptide. *Journal of Biological Chemistry,* 292**,** 3172-3185.

Hayward, S. & Lee, R. A. 2002. Improvements in the analysis of domain motions in proteins from conformational change: DynDom version 1.50. *Journal of Molecular Graphics and Modelling,* 21**,** 181-3.

Hébert, S. S., Serneels, L., Dejaegere, T., Horré, K., Dabrowski, M., Baert, V., Annaert, W., Hartmann, D. & De Strooper, B. 2004. Coordinated and widespread expression of γ-

secretase in vivo: evidence for size and molecular heterogeneity. *Neurobiology of Disease,* 17**,** 260-272.

Hébert, S. S., Serneels, L., Tolia, A., Craessaerts, K., Derks, C., Filippov, M. A., Müller, U. & De Strooper, B. 2006. Regulated intramembrane proteolysis of amyloid precursor protein and regulation of expression of putative target genes. *EMBO Reports* 7**,** 739-45.

Hemming, M. L., Elias, J. E., Gygi, S. P. & Selkoe, D. J. 2008. Proteomic profiling of γ-secretase substrates and mapping of substrate requirements. *PLOS Biology,* 6**,** e257.

Henzler-Wildman, K. A., Lei, M., Thai, V., Kerns, S. J., Karplus, M. & Kern, D. 2007. A hierarchy of timescales in protein dynamics is linked to enzyme catalysis. *Nature,* 450**,** 913-6.

Herreman, A., Hartmann, D., Annaert, W., Saftig, P., Craessaerts, K., Serneels, L., Umans, L., Schrijvers, V., Checler, F., Vanderstichele, H., Baekelandt, V., Dressel, R., Cupers, P., Huylebroeck, D., Zwijsen, A., Van Leuven, F. & De Strooper, B. 1999. Presenilin 2 deficiency causes a mild pulmonary phenotype and no changes in amyloid precursor protein processing but enhances the embryonic lethal phenotype of presenilin 1 deficiency. *Proceedings of the National Academy of Sciences of the United States of America,* 96**,** 11872-7.

Herreman, A., Serneels, L., Annaert, W., Collen, D., Schoonjans, L. & De Strooper, B. 2000. Total inactivation of γ-secretase activity in presenilin-deficient embryonic stem cells. *Nature Cell Biology,* 2**,** 461-2.

Herreman, A., Van Gassen, G., Bentahir, M., Nyabi, O., Craessaerts, K., Mueller, U., Annaert, W. & De Strooper, B. 2003. γ-Secretase activity requires the presenilin-dependent trafficking of nicastrin through the Golgi apparatus but not its complex glycosylation. *Journal of Cell Science,* 116**,** 1127-36.

Higashide, H., Ishihara, S., Nobuhara, M., Ihara, Y. & Funamoto, S. 2017. Alanine substitutions in the GXXXG motif alter C99 cleavage by γ-secretase but not its dimerization. *Journal of Neurochemistry,* 140**,** 955-962.

Hitzenberger, M. & Zacharias, M. 2019a. Structural modeling of γ-secretase Aβn complex formation and substrate processing. *ACS Chemical Neuroscience,* 10**,** 1826-1840.

Hitzenberger, M. & Zacharias, M. 2019b. Uncovering the binding mode of γ-secretase inhibitors. *ACS Chemical Neuroscience,* 10**,** 3398-3403.

Högel, P., Götz, A., Kuhne, F., Ebert, M., Stelzer, W., Rand, K. D., Scharnagl, C. & Langosch, D. 2018. Glycine perturbs local and global conformational flexibility of a transmembrane helix. *Biochemistry,* 57**,** 1326-1337.

Hollingworth, P., Harold, D., Sims, R., Gerrish, A., Lambert, J.-C., Carrasquillo, M. M., Abraham, R., Hamshere, M. L., Pahwa, J. S., Moskvina, V., Dowzell, K., Jones, N., Stretton, A., Thomas, C., Richards, A., Ivanov, D., Widdowson, C., Chapman, J., Lovestone, S., Powell, J.*, et al.* 2011. Common variants at ABCA7 , MS4A6A/MS4A4E , EPHA1 , CD33 and CD2AP are associated with Alzheimer's disease. *Nature Genetics,* 43**,** 429-435.

Holtzman, D. M., Morris, J. C. & Goate, A. M. 2011. Alzheimer's disease: the challenge of the second century. *Science Translational Medicine,* 3**,** 77sr1.

Hori, Y., Hashimoto, T., Wakutani, Y., Urakami, K., Nakashima, K., Condron, M. M., Tsubuki, S., Saido, T. C., Teplow, D. B. & Iwatsubo, T. 2007. The Tottori (D7N) and English (H6R) familial Alzheimer disease mutations accelerate Aβ fibril formation without increasing protofibril formation. *Journal of Biological Chemistry,* 282**,** 4916-4923.

Hubbard, S. J. 1998. The structural aspects of limited proteolysis of native proteins. *Biochimica et Biophysica Acta - Protein Structure and Molecular Enzymology,* 1382**,** 191-206.

Hyman, B. T., Phelps, C. H., Beach, T. G., Bigio, E. H., Cairns, N. J., Carrillo, M. C., Dickson, D. W., Duyckaerts, C., Frosch, M. P., Masliah, E., Mirra, S. S., Nelson, P. T., Schneider, J. A., Thal, D. R., Thies, B., Trojanowski, J. Q., Vinters, H. V. & Montine, T. J. 2012.

National Institute on Aging–Alzheimer's Association guidelines for the neuropathologic assessment of Alzheimer's disease. *Alzheimer's and Dementia,* 8**,** 1-13.

Ikezu, T., Trapp, B. D., Song, K. S., Schlegel, A., Lisanti, M. P. & Okamoto, T. 1998. Caveolae, plasma membrane microdomains for α-secretase-mediated processing of the amyloid precursor protein *Journal of Biological Chemistry,* 273**,** 10485-10495.

Imbimbo, B. P., Giardino, L., Sivilia, S., Giuliani, A., Gusciglio, M., Pietrini, V., Del Giudice, E., D'arrigo, A., Leon, A., Villetti, G. & Calzà, L. 2010. CHF5074, a novel γ-secretase modulator, restores hippocampal neurogenesis potential and reverses contextual memory deficit in a transgenic mouse model of Alzheimer's disease. *Journal of Alzheimer's Disease,* 20**,** 159-73.

Iqbal, K., Wiśniewski, H. M., Shelanski, M. L., Brostoff, S., Liwnicz, B. H. & Terry, R. D. 1974. Protein changes in senile dementia. *Brain Research* 77**,** 337-43.

Iwatsubo, T., Odaka, A., Suzuki, N., Mizusawa, H., Nukina, N. & Ihara, Y. 1994. Visualization of Aβ42(43) and Aβ40 in senile plaques with end-specific Aβ monoclonals: Evidence that an initially deposited species is Aβ42(43). *Neuron,* 13**,** 45-53.

Jakel, L., Boche, D., Nicoll, J. a. R. & Verbeek, M. M. 2019. Aβ43 in human Alzheimer's disease: effects of active Aβ42 immunization. *Acta Neuropathologica Communications,* 7**,** 141.

Jarrett, J. T., Berger, E. P. & Lansbury, P. T., Jr. 1993. The carboxy terminus of the β amyloid protein is critical for the seeding of amyloid formation: implications for the pathogenesis of Alzheimer's disease. *Biochemistry,* 32**,** 4693-7.

Jonsson, T., Atwal, J. K., Steinberg, S., Snaedal, J., Jonsson, P. V., Bjornsson, S., Stefansson, H., Sulem, P., Gudbjartsson, D., Maloney, J., Hoyte, K., Gustafson, A., Liu, Y., Lu, Y., Bhangale, T., Graham, R. R., Huttenlocher, J., Bjornsdottir, G., Andreassen, O. A., Jonsson, E. G., Palotie, A., Behrens, T. W., Magnusson, O. T., Kong, A., Thorsteinsdottir, U., Watts, R. J. & Stefansson, K. 2012. A mutation in APP protects against Alzheimer's disease and age-related cognitive decline. *Nature,* 488**,** 96-9.

Jung, J. I., Ran, Y., Cruz, P. E., Rosario, A. M., Ladd, T. B., Kukar, T. L., Koo, E. H., Felsenstein, K. M. & Golde, T. E. 2014. Complex relationships between substrate sequence and sensitivity to alterations in γ-secretase processivity induced by γ-secretase modulators. *Biochemistry,* 53**,** 1947-1957.

Jurisch-Yaksi, N., Sannerud, R. & Annaert, W. 2013. A fast growing spectrum of biological functions of γ-secretase in development and disease. *Biochimica et Biophysica Acta* 1828**,** 2815-27.

Kaether, C., Lammich, S., Edbauer, D., Ertl, M., Rietdorf, J., Capell, A., Steiner, H. & Haass, C. 2002. Presenilin-1 affects trafficking and processing of βAPP and is targeted in a complex with nicastrin to the plasma membrane. *Journal of Cell Biology,* 158**,** 551-561.

Kaether, C., Schmitt, S., Willem, M. & Haass, C. 2006. Amyloid precursor protein and Notch intracellular domains are generated after transport of their precursors to the cell surface. *Traffic,* 7**,** 408-415.

Kakuda, N., Funamoto, S., Yagishita, S., Takami, M., Osawa, S., Dohmae, N. & Ihara, Y. 2006. Equimolar production of amyloid β-protein and amyloid precursor protein intracellular domain from β-carboxyl-terminal fragment by γ-secretase. *Journal of Biological Chemistry,* 281**,** 14776-86.

Kamenetz, F., Tomita, T., Hsieh, H., Seabrook, G., Borchelt, D., Iwatsubo, T., Sisodia, S. & Malinow, R. 2003. APP processing and synaptic function. *Neuron,* 37**,** 925-37.

Kang, J., Lemaire, H. G., Unterbeck, A., Salbaum, J. M., Masters, C. L., Grzeschik, K. H., Multhaup, G., Beyreuther, K. & Müller-Hill, B. 1987. The precursor of Alzheimer's disease amyloid A4 protein resembles a cell-surface receptor. *Nature,* 325**,** 733-6.

Kapeller, M., Gal-Oz, R., Grover, N. B. & Doljanski, F. 1973. Natural shedding of carbohydrate-containing macromolecules from cell surfaces. *Experimental Cell Research,* 79**,** 152-8.

Kidd, M. 1963. Paired helical filaments in electron microscopy of Alzheimer's disease. *Nature,* 197**,** 192-3.

Kidd, M. 1964. Alzheimer's disease - an electron microscopical study. *Brain,* 87**,** 307-20.

Kim, C. A. & Berg, J. M. 1993. Thermodynamic β-sheet propensities measured using a zinc-finger host peptide. *Nature,* 362**,** 267-70.

Kim, S. H. & Sisodia, S. S. 2005. A sequence within the first transmembrane domain of PEN-2 is critical for PEN-2-mediated endoproteolysis of presenilin 1. *Journal of Biological Chemistry,* 280**,** 1992-2001.

Kim, S. H., Yin, Y. I., Li, Y. M. & Sisodia, S. S. 2004. Evidence that assembly of an active γ-secretase complex occurs in the early compartments of the secretory pathway. *Journal of Biological Chemistry,* 279**,** 48615-9.

Kim, W. Y. & Shen, J. 2008. Presenilins are required for maintenance of neural stem cells in the developing brain. *Molecular Neurodegeneration,* 3**,** 2.

Kimberly, W. T., Lavoie, M. J., Ostaszewski, B. L., Ye, W., Wolfe, M. S. & Selkoe, D. J. 2003. γ-Secretase is a membrane protein complex comprised of presenilin, nicastrin, APH-1, and PEN-2. *Proceedings of the National Academy of Sciences of the United States of America,* 100**,** 6382-7.

Kimberly, W. T., Xia, W., Rahmati, T., Wolfe, M. S. & Selkoe, D. J. 2000. The transmembrane aspartates in presenilin 1 and 2 are obligatory for γ-secretase activity and amyloid β-protein generation. *Journal of Biological Chemistry,* 275**,** 3173-8.

Kimura, A., Hata, S. & Suzuki, T. 2016. Alternative selection of β-Site APP-cleaving enzyme 1 (BACE1) cleavage sites in amyloid β-protein precursor (APP) harboring protective and pathogenic mutations within the Aβ sequence. *Journal of Biological Chemistry,* 291**,** 24041-24053.

Kinoshita, A., Whelan, C. M., Berezovska, O. & Hyman, B. T. 2002. The γ-secretase-generated carboxyl-terminal domain of the amyloid precursor protein induces apoptosis via Tip60 in H4 cells. *Journal of Biological Chemistry,* 277**,** 28530-6.

Koffie, R. M., Meyer-Luehmann, M., Hashimoto, T., Adams, K. W., Mielke, M. L., Garcia-Alloza, M., Micheva, K. D., Smith, S. J., Kim, M. L., Lee, V. M., Hyman, B. T. & Spires-Jones, T. L. 2009. Oligomeric amyloid β associates with postsynaptic densities and correlates with excitatory synapse loss near senile plaques. *Proceedings of the National Academy of Sciences,* 106**,** 4012-4017.

Kong, R., Chang, S., Xia, W. & Wong, S. T. C. 2015. Molecular dynamics simulation study reveals potential substrate entry path into γ-secretase/presenilin-1. *Journal of Structural Biology,* 191**,** 120-129.

Koo, E. H. & Squazzo, S. L. 1994. Evidence that production and release of amyloid β-protein involves the endocytic pathway. *Journal of Biological Chemistry,* 269**,** 17386-9.

Kornilova, A. Y., Bihel, F., Das, C. & Wolfe, M. S. 2005. The initial substrate-binding site of γ-secretase is located on presenilin near the active site. *Proceedings of the National Academy of Sciences of the United States of America,* 102**,** 3230-3235.

Kounnas, M. Z., Danks, A. M., Cheng, S., Tyree, C., Ackerman, E., Zhang, X., Ahn, K., Nguyen, P., Comer, D., Mao, L., Yu, C., Pleynet, D., Digregorio, P. J., Velicelebi, G., Stauderman, K. A., Comer, W. T., Mobley, W. C., Li, Y.-M., Sisodia, S. S., Tanzi, R. E. & Wagner, S. L. 2010. Modulation of γ-secretase reduces β-amyloid deposition in a transgenic mouse model of Alzheimer's disease. *Neuron,* 67**,** 769-780.

Kretner, B., Fukumori, A., Kuhn, P. H., Pérez-Revuelta, B. I., Lichtenthaler, S. F., Haass, C. & Steiner, H. 2013. Important functional role of residue x of the presenilin GxGD protease

active site motif for APP substrate cleavage specificity and substrate selectivity of γ-secretase. *Journal of Neurochemistry,* 125**,** 144-56.

Kretner, B., Trambauer, J., Fukumori, A., Mielke, J., Kuhn, P. H., Kremmer, E., Giese, A., Lichtenthaler, S. F., Haass, C., Arzberger, T. & Steiner, H. 2016. Generation and deposition of Aβ43 by the virtually inactive presenilin-1 L435F mutant contradicts the presenilin loss-of-function hypothesis of Alzheimer's disease. *EMBO Molecular Medicine,* 8**,** 458-65.

Kuentzel, S. L., Ali, S. M., Altman, R. A., Greenberg, B. D. & Raub, T. J. 1993. The Alzheimer β-amyloid protein precursor/protease nexin-II is cleaved by secretase in a trans-Golgi secretory compartment in human neuroglioma cells. *Biochemical Journal,* 295 (Pt 2)**,** 367-78.

Kuhn, P.-H., Wang, H., Dislich, B., Colombo, A., Zeitschel, U., Ellwart, J. W., Kremmer, E., Roßner, S. & Lichtenthaler, S. F. 2010. ADAM10 is the physiologically relevant, constitutive α-secretase of the amyloid precursor protein in primary neurons. *EMBO Journal,* 29**,** 3020-3032.

Kuhn, P. H., Voss, M., Haug-Kröper, M., Schröder, B., Schepers, U., Bräse, S., Haass, C., Lichtenthaler, S. F. & Fluhrer, R. 2015. Secretome analysis identifies novel signal Peptide peptidase-like 3 (Sppl3) substrates and reveals a role of Sppl3 in multiple Golgi glycosylation pathways. *Molecular and Cellular Proteomics,* 14**,** 1584-98.

Kukar, T. L., Ladd, T. B., Robertson, P., Pintchovski, S. A., Moore, B., Bann, M. A., Ren, Z., Jansen-West, K., Malphrus, K., Eggert, S., Maruyama, H., Cottrell, B. A., Das, P., Basi, G. S., Koo, E. H. & Golde, T. E. 2011. Lysine 624 of the amyloid precursor protein (APP) is a critical determinant of amyloid β peptide length: support for a sequential model of γ-secretase intramembrane proteolysis and regulation by ther amyloid β presursor protein (APP) juxtamembrane region. *Journal of Biological Chemistry,* 286**,** 39804-39812.

Kunkle, B. W., Grenier-Boley, B., Sims, R., Bis, J. C., Damotte, V., Naj, A. C., Boland, A., Vronskaya, M., Van Der Lee, S. J., Amlie-Wolf, A., Bellenguez, C., Frizatti, A., Chouraki, V., Martin, E. R., Sleegers, K., Badarinarayan, N., Jakobsdottir, J., Hamilton-Nelson, K. L., Moreno-Grau, S., Olaso, R.*, et al.* 2019. Genetic meta-analysis of diagnosed Alzheimer's disease identifies new risk loci and implicates Aβ, tau, immunity and lipid processing. *Nature Genetics,* 51**,** 414-430.

Lal, M. & Caplan, M. 2011. Regulated intramembrane proteolysis: signaling pathways and biological functions. *Physiology (Bethesda),* 26**,** 34-44.

Lambert, M. P., Barlow, A. K., Chromy, B. A., Edwards, C., Freed, R., Liosatos, M., Morgan, T. E., Rozovsky, I., Trommer, B., Viola, K. L., Wals, P., Zhang, C., Finch, C. E., Krafft, G. A. & Klein, W. L. 1998. Diffusible, nonfibrillar ligands derived from Aβ1-42 are potent central nervous system neurotoxins. *Proceedings of the National Academy of Sciences of the United States of America,* 95**,** 6448-53.

Lammich, S., Kojro, E., Postina, R., Gilbert, S., Pfeiffer, R., Jasionowski, M., Haass, C. & Fahrenholz, F. 1999. Constitutive and regulated α-secretase cleavage of Alzheimer's amyloid precursor protein by a disintegrin metalloprotease. *Proceedings of the National Academy of Sciences of the United States of America,* 96**,** 3922-7.

Lammich, S., Okochi, M., Takeda, M., Kaether, C., Capell, A., Zimmer, A. K., Edbauer, D., Walter, J., Steiner, H. & Haass, C. 2002. Presenilin-dependent intramembrane proteolysis of CD44 leads to the liberation of its intracellular domain and the secretion of an Aβ-like peptide. *Journal of Biological Chemistry,* 277**,** 44754-9.

Langosch, D., Scharnagl, C., Steiner, H. & Lemberg, M. K. 2015. Understanding intramembrane proteolysis: from protein dynamics to reaction kinetics. *Trends in Biochemical Sciences,* 40**,** 318-327.

Langosch, D. & Steiner, H. 2017. Substrate processing in intramembrane proteolysis by γ-secretase - the role of protein dynamics. *Biological Chemistry,* 398**,** 441-453.

Lastun, V. L., Grieve, A. G. & Freeman, M. 2016. Substrates and physiological functions of secretase rhomboid proteases. *Seminars in Cell and Developmental Biology,* 60**,** 10-18.

Laurent, S. A., Hoffmann, F. S., Kuhn, P.-H., Cheng, Q., Chu, Y., Schmidt-Supprian, M., Hauck, S. M., Schuh, E., Krumbholz, M., Rübsamen, H., Wanngren, J., Khademi, M., Olsson, T., Alexander, T., Hiepe, F., Pfister, H.-W., Weber, F., Jenne, D., Wekerle, H., Hohlfeld, R., Lichtenthaler, S. F. & Meinl, E. 2015. γ-Secretase directly sheds the survival receptor BCMA from plasma cells. *Nature Communications,* 6**,** 7333.

Lavoie, M. J., Fraering, P. C., Ostaszewski, B. L., Ye, W., Kimberly, W. T., Wolfe, M. S. & Selkoe, D. J. 2003. Assembly of the γ-secretase complex involves early formation of an intermediate subcomplex of APH-1 and Nicastrin. *Journal of Biological Chemistry,* 278**,** 37213-22.

Leblanc, A. C., Chen, H. Y., Autilio-Gambetti, L. & Gambetti, P. 1991. Differential APP gene expression in rat cerebral cortex, meninges, and primary astroglial, microglial and neuronal cultures. *FEBS Letters,* 292**,** 171-8.

Lee, J. R., Urban, S., Garvey, C. F. & Freeman, M. 2001. Regulated intracellular ligand transport and proteolysis control EGF signal activation in Drosophila. *Cell,* 107**,** 161-171.

Lee, S. F., Shah, S., Li, H., Yu, C., Han, W. & Yu, G. 2002. Mammalian APH-1 interacts with presenilin and Nicastrin and is required for intramembrane proteolysis of amyloid-β precursor protein and Notch. *Journal of Biological Chemistry,* 277**,** 45013-9.

Leem, J. Y., Vijayan, S., Han, P., Cai, D., Machura, M., Lopes, K. O., Veselits, M. L., Xu, H. & Thinakaran, G. 2002. Presenilin 1 is required for maturation and cell surface accumulation of Nicastrin. *Journal of Biological Chemistry,* 277**,** 19236-40.

Lemberg, M. K. & Martoglio, B. 2002. Requirements for signal peptide peptidase-catalyzed intramembrane proteolysis. *Molecular Cell,* 10**,** 735-744.

Lemmin, T., Dimitrov, M., Fraering, P. C. & Dal Peraro, M. 2014. Perturbations of the straight transmembrane α-helical structure of the amyloid precursor protein affect its processing by γ-secretase. *Journal of Biological Chemistry,* 289**,** 6763-74.

Levy-Lahad, E., Wasco, W., Poorkaj, P., Romano, D. M., Oshima, J., Pettingell, W. H., Yu, C. E., Jondro, P. D., Schmidt, S. D., Wang, K. & Et Al. 1995a. Candidate gene for the chromosome 1 familial Alzheimer's disease locus. *Science,* 269**,** 973-7.

Levy-Lahad, E., Wijsman, E. M., Nemens, E., Anderson, L., Goddard, K. A., Weber, J. L., Bird, T. D. & Schellenberg, G. D. 1995b. A familial Alzheimer's disease locus on chromosome 1. *Science,* 269**,** 970-3.

Lewcock, J. W., Schlepckow, K., Di Paolo, G., Tahirovic, S., Monroe, K. M. & Haass, C. 2020. Emerging Microglia Biology Defines Novel Therapeutic Approaches for Alzheimer's Disease. *Neuron,* 108**,** 801-821.

Li, S. & Selkoe, D. J. 2020. A mechanistic hypothesis for the impairment of synaptic plasticity by soluble Aβ oligomers from Alzheimer's brain. *Journal of Neurochemistry,* 154**,** 583-597.

Li, S. C. & Deber, C. M. 1992. Glycine and β-branched residues support and modulate peptide helicity in membrane environments. *FEBS Letters,* 311**,** 217-20.

Li, S. C. & Deber, C. M. 1994. A measure of helical propensity for amino acids in membrane environments. *Nature Structural and Molecular Biology,* 1**,** 558.

Li, Y.-M., Lai, M.-T., Xu, M., Huang, Q., Dimuzio-Mower, J., Sardana, M. K., Shi, X.-P., Yin, K.-C., Shafer, J. A. & Gardell, S. J. 2000. Presenilin 1 is linked with γ-secretase activity in the detergent solubilized state. *Proceedings of the National Academy of Sciences,* 97**,** 6138-6143.

Li, Y., Lu, S. H., Tsai, C. J., Bohm, C., Qamar, S., Dodd, R. B., Meadows, W., Jeon, A., Mcleod, A., Chen, F., Arimon, M., Berezovska, O., Hyman, B. T., Tomita, T., Iwatsubo, T., Johnson, C. M., Farrer, L. A., Schmitt-Ulms, G., Fraser, P. E. & St George-Hyslop, P. H. 2014. Structural interactions between inhibitor and substrate docking sites give insight into mechanisms of human PS1 complexes. *Structure (London, England : 1993),* 22**,** 125-35.

Lichtenthaler, S. F., Haass, C. & Steiner, H. 2011. Regulated intramembrane proteolysis--lessons from amyloid precursor protein processing. *Journal of Neurochemistry,* 117**,** 779-96.

Linser, R., Salvi, N., Briones, R., Rovó, P., De Groot, B. L. & Wagner, G. 2015. The membrane anchor of the transcriptional activator SREBP is characterized by intrinsic conformational flexibility. *Proceedings of the National Academy of Sciences,* 112**,** 12390-12395.

Lippa, C. F., Saunders, A. M., Smith, T. W., Swearer, J. M., Drachman, D. A., Ghetti, B., Nee, L., Pulaski-Salo, D., Dickson, D., Robitaille, Y., Bergeron, C., Crain, B., Benson, M. D., Farlow, M., Hyman, B. T., George-Hyslop, S. P., Roses, A. D. & Pollen, D. A. 1996. Familial and sporadic Alzheimer's disease: neuropathology cannot exclude a final common pathway. *Neurology,* 46**,** 406-12.

Liu, Q., Zerbinatti, C. V., Zhang, J., Hoe, H. S., Wang, B., Cole, S. L., Herz, J., Muglia, L. & Bu, G. 2007. Amyloid precursor protein regulates brain apolipoprotein E and cholesterol metabolism through lipoprotein receptor LRP1. *Neuron,* 56**,** 66-78.

Lleó, A., Berezovska, O., Herl, L., Raju, S., Deng, A., Bacskai, B. J., Frosch, M. P., Irizarry, M. & Hyman, B. T. 2004. Nonsteroidal anti-inflammatory drugs lower Aβ42 and change presenilin 1 conformation. *Nature Medicine,* 10**,** 1065-1066.

Lobo, A., Launer, L. J., Fratiglioni, L., Andersen, K., Di Carlo, A., Breteler, M. M., Copeland, J. R., Dartigues, J. F., Jagger, C., Martinez-Lage, J., Soininen, H. & Hofman, A. 2000. Prevalence of dementia and major subtypes in Europe: A collaborative study of population-based cohorts. Neurologic diseases in the Elderly Research Group. *Neurology,* 54**,** S4-9.

Long, J. M. & Holtzman, D. M. 2019. Alzheimer disease: an update on pathobiology and treatment strategies. *Cell,* 179**,** 312-339.

López, A. R., Dimitrov, M., Gerber, H., Braman, V., Hacker, D. L., Wurm, F. M. & Fraering, P. C. 2015. Production of active glycosylation-deficient γ-secretase complex for crystallization studies. *Biotechnology and Bioengineering,* 112**,** 2516-26.

Lorent, K., Overbergh, L., Moechars, D., De Strooper, B., Van Leuven, F. & Van Den Berghe, H. 1995. Expression in mouse embryos and in adult mouse brain of three members of the amyloid precursor protein family, of the α-2-macroglobulin receptor/low density lipoprotein receptor-related protein and of its ligands apolipoprotein E, lipoprotein lipase, α-2-macroglobulin and the 40,000 molecular weight receptor-associated protein. *Neuroscience,* 65**,** 1009-25.

Lu, J. X., Yau, W. M. & Tycko, R. 2011. Evidence from solid-state NMR for nonhelical conformations in the transmembrane domain of the amyloid precursor protein. *Biophysical Journal,* 100**,** 711-719.

Lu, P., Bai, X.-C., Ma, D., Xie, T., Yan, C., Sun, L., Yang, G., Zhao, Y., Zhou, R., Scheres, S. H. W. & Shi, Y. 2014. Three-dimensional structure of human γ-secretase. *Nature,* 512**,** 166-170.

Lue, L. F., Kuo, Y. M., Roher, A. E., Brachova, L., Shen, Y., Sue, L., Beach, T., Kurth, J. H., Rydel, R. E. & Rogers, J. 1999. Soluble amyloid β peptide concentration as a predictor of synaptic change in Alzheimer's disease. *American Journal of Pathology,* 155**,** 853-62.

Luo, W. J., Wang, H., Li, H., Kim, B. S., Shah, S., Lee, H. J., Thinakaran, G., Kim, T. W., Yu, G. & Xu, H. 2003. PEN-2 and APH-1 coordinately regulate proteolytic processing of presenilin 1. *Journal of Biological Chemistry,* 278**,** 7850-4.

Lyu, P., Liff, M., Marky, L. & Kallenbach, N. 1990. Side chain contributions to the stability of α-helical structure in peptides. *Science,* 250**,** 669-673.

Lyu, P. C., Sherman, J. C., Chen, A. & Kallenbach, N. R. 1991. α-Helix stabilization by natural and unnatural amino acids with alkyl side chains. *Proceedings of the National Academy of Sciences,* 88**,** 5317-5320.

Ma, B. & Nussinov, R. 2010. Enzyme dynamics point to stepwise conformational selection in catalysis. *Current Opinion in Chemical Biology,* 14**,** 652-9.

Madala, P. K., Tyndall, J. D., Nall, T. & Fairlie, D. P. 2010. Update 1 of: Proteases universally recognize β strands in their active sites. *Chemical Reviews,* 110**,** Pr1-31.

Maegawa, S., Ito, K. & Akiyama, Y. 2005. Proteolytic action of GlpG, a rhomboid protease in the Escherichia coli cytoplasmic membrane. *Biochemistry,* 44**,** 13543-52.

Malik, M., Parikh, I., Vasquez, J. B., Smith, C., Tai, L., Bu, G., Ladu, M. J., Fardo, D. W., Rebeck, G. W. & Estus, S. 2015. Genetics ignite focus on microglial inflammation in Alzheimer's disease. *Molecular Neurodegeneration,* 10**,** 52.

Maloney, J. A., Bainbridge, T., Gustafson, A., Zhang, S., Kyauk, R., Steiner, P., Van Der Brug, M., Liu, Y., Ernst, J. A., Watts, R. J. & Atwal, J. K. 2014. Molecular mechanisms of Alzheimer disease protection by the A673T allele of amyloid precursor protein. *J Biol Chem,* 289**,** 30990-1000.

Manolaridis, I., Kulkarni, K., Dodd, R. B., Ogasawara, S., Zhang, Z., Bineva, G., O'reilly, N., Hanrahan, S. J., Thompson, A. J., Cronin, N., Iwata, S. & Barford, D. 2013. Mechanism of farnesylated CAAX protein processing by the intramembrane protease Rce1. *Nature,* 504**,** 301-305.

Masters, C. L., Simms, G., Weinman, N. A., Multhaup, G., Mcdonald, B. L. & Beyreuther, K. 1985. Amyloid plaque core protein in Alzheimer disease and Down syndrome. *Proceedings of the National Academy of Sciences of the United States of America,* 82**,** 4245-9.

Matsumura, N., Takami, M., Okochi, M., Wada-Kakuda, S., Fujiwara, H., Tagami, S., Funamoto, S., Ihara, Y. & Morishima-Kawashima, M. 2014. γ-Secretase associated with lipid rafts: multiple interactive pathways in the stepwise processing of β-carboxyl-terminal fragment. *Journal of Biological Chemistry,* 289**,** 5109-21.

Mawuenyega, K. G., Sigurdson, W., Ovod, V., Munsell, L., Kasten, T., Morris, J. C., Yarasheski, K. E. & Bateman, R. J. 2010. Decreased clearance of CNS β-amyloid in Alzheimer's disease. *Science,* 330**,** 1774.

Mazaheri, F., Snaidero, N., Kleinberger, G., Madore, C., Daria, A., Werner, G., Krasemann, S., Capell, A., Trumbach, D., Wurst, W., Brunner, B., Bultmann, S., Tahirovic, S., Kerschensteiner, M., Misgeld, T., Butovsky, O. & Haass, C. 2017. TREM2 deficiency impairs chemotaxis and microglial responses to neuronal injury. *EMBO Reports* 18**,** 1186-1198.

Mc Donald, J. M., Savva, G. M., Brayne, C., Welzel, A. T., Forster, G., Shankar, G. M., Selkoe, D. J., Ince, P. G., Walsh, D. M., Medical Research Council Cognitive, F. & Ageing, S. 2010. The presence of sodium dodecyl sulphate-stable Aβ dimers is strongly associated with Alzheimer-type dementia. *Brain,* 133**,** 1328-41.

Mclean, C. A., Cherny, R. A., Fraser, F. W., Fuller, S. J., Smith, M. J., Beyreuther, K., Bush, A. I. & Masters, C. L. 1999. Soluble pool of Aβ amyloid as a determinant of severity of neurodegeneration in Alzheimer's disease. *Annals of Neurology,* 46**,** 860-6.

Meckler, X. & Checler, F. 2016. Presenilin 1 and Presenilin 2 Target γ-Secretase Complexes to Distinct Cellular Compartments. *Journal of Biological Chemistry,* 291**,** 12821-12837.

Mentrup, T., Cabrera-Cabrera, F., Fluhrer, R. & Schröder, B. 2020. Physiological functions of SPP/SPPL intramembrane proteases. *Cellular and Molecular Life Sciences,* 77**,** 2959-2979.

Minor, D. L., Jr. & Kim, P. S. 1994. Measurement of the β-sheet-forming propensities of amino acids. *Nature,* 367**,** 660-3.

Mitani, Y., Yarimizu, J., Saita, K., Uchino, H., Akashiba, H., Shitaka, Y., Ni, K. & Matsuoka, N. 2012. Differential effects between γ-secretase inhibitors and modulators on cognitive function in amyloid precursor protein-transgenic and nontransgenic mice. *Journal of Neuroscience,* 32**,** 2037-50.

Miyashita, N., Straub, J. E., Thirumalai, D. & Sugita, Y. 2009. Transmembrane structures of amyloid precursor protein dimer predicted by replica-exchange molecular dynamics simulations. *Journal of the American Chemical Society,* 131**,** 3438-9.

Moin, S. M. & Urban, S. 2012. Membrane immersion allows rhomboid proteases to achieve specificity by reading transmembrane segment dynamics. *eLife,* 1**,** e00173.

Moniruzzaman, M., Ishihara, S., Nobuhara, M., Higashide, H. & Funamoto, S. 2018. Glycosylation status of Nicastrin influences catalytic activity and substrate preference of γ-secretase. *Biochemical and Biophysical Research Communications,* 502**,** 98-103.

Moore, B. D., Martin, J., De Mena, L., Sanchez, J., Cruz, P. E., Ceballos-Diaz, C., Ladd, T. B., Ran, Y., Levites, Y., Kukar, T. L., Kurian, J. J., Mckenna, R., Koo, E. H., Borchelt, D. R., Janus, C., Rincon-Limas, D., Fernandez-Funez, P. & Golde, T. E. 2017. Short Aβ peptides attenuate Aβ42 toxicity in vivo. *Journal of Experimental Medicine,* 215**,** 283-301.

Morris, J. C., Storandt, M., Miller, J. P., Mckeel, D. W., Price, J. L., Rubin, E. H. & Berg, L. 2001. Mild cognitive impairment represents early-stage Alzheimer disease. *Archives of Neurology,* 58**,** 397-405.

Mucke, L., Masliah, E., Yu, G. Q., Mallory, M., Rockenstein, E. M., Tatsuno, G., Hu, K., Kholodenko, D., Johnson-Wood, K. & Mcconlogue, L. 2000. High-level neuronal expression of Aβ1-42 in wild-type human amyloid protein precursor transgenic mice: synaptotoxicity without plaque formation. *Journal of Neuroscience,* 20**,** 4050-8.

Mullan, M., Crawford, F., Axelman, K., Houlden, H., Lilius, L., Winblad, B. & Lannfelt, L. 1992. A pathogenic mutation for probable Alzheimer's disease in the APP gene at the N-terminus of β-amyloid. *Nature Genetics,* 1**,** 345-7.

Müller, T., Concannon, C. G., Ward, M. W., Walsh, C. M., Tirniceriu, A. L., Tribl, F., Kögel, D., Prehn, J. H. & Egensperger, R. 2007. Modulation of gene expression and cytoskeletal dynamics by the amyloid precursor protein intracellular domain (AICD). *Molecular Biology of the Cell,* 18**,** 201-10.

Munter, L. M., Botev, A., Richter, L., Hildebrand, P. W., Althoff, V., Weise, C., Kaden, D. & Multhaup, G. 2010. Aberrant amyloid precursor protein (APP) processing in hereditary forms of Alzheimer disease caused by APP familial Alzheimer disease mutations can be rescued by mutations in the APP GxxxG motif. *Journal of Biological Chemistry,* 285**,** 21636-43.

Murray, B., Sorci, M., Rosenthal, J., Lippens, J., Isaacson, D., Das, P., Fabris, D., Li, S. & Belfort, G. 2016. A2T and A2V Aβ peptides exhibit different aggregation kinetics, primary nucleation, morphology, structure, and LTP inhibition. *Proteins,* 84**,** 488-500.

Murrell, J., Farlow, M., Ghetti, B. & Benson, M. D. 1991. A mutation in the amyloid precursor protein associated with hereditary Alzheimer's disease. *Science,* 254**,** 97-9.

Nadezhdin, K. D., Bocharova, O. V., Bocharov, E. V. & Arseniev, A. S. 2011. Structural and dynamic study of the transmembrane domain of the amyloid precursor protein. *Acta Naturae,* 3**,** 69-76.

Nakayama, K., Ohkawara, T., Hiratochi, M., Koh, C. S. & Nagase, H. 2008. The intracellular domain of amyloid precursor protein induces neuron-specific apoptosis. *Neuroscience Letters,* 444**,** 127-31.

Naruse, S., Thinakaran, G., Luo, J. J., Kusiak, J. W., Tomita, T., Iwatsubo, T., Qian, X., Ginty, D. D., Price, D. L., Borchelt, D. R., Wong, P. C. & Sisodia, S. S. 1998. Effects of PS1 deficiency on membrane protein trafficking in neurons. *Neuron,* 21**,** 1213-21.

Nashine, V. C., Hammes-Schiffer, S. & Benkovic, S. J. 2010. Coupled motions in enzyme catalysis. *Current Opinion in Chemical Biology,* 14**,** 644-51.

Nelson, P. T., Alafuzoff, I., Bigio, E. H., Bouras, C., Braak, H., Cairns, N. J., Castellani, R. J., Crain, B. J., Davies, P., Tredici, K. D., Duyckaerts, C., Frosch, M. P., Haroutunian, V., Hof, P. R., Hulette, C. M., Hyman, B. T., Iwatsubo, T., Jellinger, K. A., Jicha, G. A., Kövari, E., Kukull, W. A., Leverenz, J. B., Love, S., Mackenzie, I. R., Mann, D. M., Masliah, E., Mckee, A. C., Montine, T. J., Morris, J. C., Schneider, J. A., Sonnen, J. A., Thal, D. R., Trojanowski, J. Q., Troncoso, J. C., Wisniewski, T., Woltjer, R. L. & Beach, T. G. 2012. Correlation of Alzheimer disease neuropathologic changes with cognitive status: a review of the literature. *Journal of Neuropathology and Experimental Neurology,* 71**,** 362-381.

Nilsberth, C., Westlind-Danielsson, A., Eckman, C. B., Condron, M. M., Axelman, K., Forsell, C., Stenh, C., Luthman, J., Teplow, D. B., Younkin, S. G., Näslund, J. & Lannfelt, L. 2001. The 'Arctic' APP mutation (E693G) causes Alzheimer's disease by enhanced Aβ protofibril formation. *Nature Neuroscience,* 4**,** 887-93.

Nochlin, D., Van Belle, G., Bird, T. D. & Sumi, S. M. 1993. Comparison of the severity of neuropathologic changes in familial and sporadic Alzheimer's disease. *Alzheimer Disease and Associated Disorders,* 7**,** 212-22.

Nordstedt, C., Caporaso, G. L., Thyberg, J., Gandy, S. E. & Greengard, P. 1993. Identification of the Alzheimer β/A4 amyloid precursor protein in clathrin-coated vesicles purified from PC12 cells. *Journal of Biological Chemistry,* 268**,** 608-12.

O'neil, K. & Degrado, W. 1990. A thermodynamic scale for the helix-forming tendencies of the commonly occurring amino acids. *Science,* 250**,** 646-651.

Okochi, M., Fukumori, A., Jiang, J., Itoh, N., Kimura, R., Steiner, H., Haass, C., Tagami, S. & Takeda, M. 2006. Secretion of the Notch-1 Aβ-like peptide during Notch signaling. *Journal of Biological Chemistry,* 281**,** 7890-8.

Okochi, M., Steiner, H., Fukumori, A., Tanii, H., Tomita, T., Tanaka, T., Iwatsubo, T., Kudo, T., Takeda, M. & Haass, C. 2002. Presenilins mediate a dual intramembranous γ-secretase cleavage of Notch-1. *EMBO Journal,* 21**,** 5408-16.

Okochi, M., Tagami, S., Yanagida, K., Takami, M., Kodama, T. S., Mori, K., Nakayama, T., Ihara, Y. & Takeda, M. 2013. γ-Secretase modulators and presenilin 1 mutants act differently on presenilin/γ-secretase function to cleave Aβ42 and Aβ43. *Cell Reports,* 3**,** 42-51.

Olsson, F., Schmidt, S., Althoff, V., Munter, L. M., Jin, S., Rosqvist, S., Lendahl, U., Multhaup, G. & Lundkvist, J. 2014. Characterization of intermediate steps in amyloid β (Aβ) production under near-native conditions. *Journal of Biological Chemistry,* 289**,** 1540-50.

Ossenkoppele, R., Jansen, W. J., Rabinovici, G. D., Knol, D. L., Van Der Flier, W. M., Van Berckel, B. N. M., Scheltens, P., Visser, P. J. & Group, A. T. a. P. S. 2015. Prevalence of Amyloid PET Positivity in Dementia Syndromes: A Meta-analysis. *Journal of the American Medical Association,* 313**,** 1939-1950.

Ousson, S., Saric, A., Baguet, A., Losberger, C., Genoud, S., Vilbois, F., Permanne, B., Hussain, I. & Beher, D. 2013. Substrate determinants in the C99 juxtamembrane domains differentially affect γ-secretase cleavage specificity and modulator pharmacology. *Journal of Neurochemistry,* 125**,** 610-619.

Ozaki, T., Li, Y., Kikuchi, H., Tomita, T., Iwatsubo, T. & Nakagawara, A. 2006. The intracellular domain of the amyloid precursor protein (AICD) enhances the p53-mediated apoptosis. *Biochemical and Biophysical Research Communications,* 351**,** 57-63.

Page, R. M., Gutsmiedl, A., Fukumori, A., Winkler, E., Haass, C. & Steiner, H. 2010. β-amyloid precursor protein mutants respond to γ-secretase modulators. *Journal of Biological Chemistry,* 285**,** 17798-17810.

Panza, F., Lozupone, M., Seripa, D. & Imbimbo, B. P. 2019. Amyloid-β immunotherapy for Alzheimer disease: is it now a long shot? *Annals of Neurology,* 85**,** 303-315.

Paresce, D. M., Ghosh, R. N. & Maxfield, F. R. 1996. Microglial cells internalize aggregates of the Alzheimer's disease amyloid β-protein via a scavenger receptor. *Neuron,* 17**,** 553-65.

Paris, D., Townsend, K., Quadros, A., Humphrey, J., Sun, J., Brem, S., Wotoczek-Obadia, M., Delledonne, A., Patel, N., Obregon, D. F., Crescentini, R., Abdullah, L., Coppola, D., Rojiani, A. M., Crawford, F., Sebti, S. M. & Mullan, M. 2004. Inhibition of angiogenesis by Aβ peptides. *Angiogenesis,* 7**,** 75-85.

Parvathy, S., Karran, E. H., Turner, A. J. & Hooper, N. M. 1998. The secretases that cleave angiotensin converting enzyme and the amyloid precursor protein are distinct from tumour necrosis factor-α convertase. *FEBS Letters,* 431**,** 63-5.

Pasternak, S. H., Bagshaw, R. D., Guiral, M., Zhang, S., Ackerley, C. A., Pak, B. J., Callahan, J. W. & Mahuran, D. J. 2003. Presenilin-1, Nicastrin, amyloid precursor protein, and γ-secretase activity are co-localized in the lysosomal membrane. *Journal of Biological Chemistry,* 278**,** 26687-94.

Peacock, M. L., Warren, J. T., Jr., Roses, A. D. & Fink, J. K. 1993. Novel polymorphism in the A4 region of the amyloid precursor protein gene in a patient without Alzheimer's disease. *Neurology,* 43**,** 1254-6.

Pérez-Revuelta, B. I., Fukumori, A., Lammich, S., Yamasaki, A., Haass, C. & Steiner, H. 2010. Requirement for small side chain residues within the GxGD-motif of presenilin for γ-secretase substrate cleavage. *Journal of Neurochemistry,* 112**,** 940-950.

Pester, O., Barrett, P. J., Hornburg, D., Hornburg, P., Pröbstle, R., Widmaier, S., Kutzner, C., Dürrbaum, M., Kapurniotu, A., Sanders, C. R., Scharnagl, C. & Langosch, D. 2013a. The backbone dynamics of the amyloid precursor protein transmembrane helix provides a rationale for the sequential cleavage mechanism of γ-secretase. *Journal of the American Chemical Society,* 135**,** 1317-29.

Pester, O., Götz, A., Multhaup, G., Scharnagl, C. & Langosch, D. 2013b. The cleavage domain of the amyloid precursor protein transmembrane helix does not exhibit above-average backbone dynamics. *ChemBioChem,* 14**,** 1943-8.

Petit, D., Hitzenberger, M., Lismont, S., Zoltowska, K. M., Ryan, N. S., Mercken, M., Bischoff, F., Zacharias, M. & Chávez-Gutiérrez, L. 2019. Extracellular interface between APP and Nicastrin regulates Aβ length and response to γ-secretase modulators. *EMBO Journal,* 38**,** e101494.

Podlisny, M. B., Citron, M., Amarante, P., Sherrington, R., Xia, W., Zhang, J., Diehl, T., Levesque, G., Fraser, P., Haass, C., Koo, E. H., Seubert, P., St George-Hyslop, P., Teplow, D. B. & Selkoe, D. J. 1997. Presenilin proteins undergo heterogeneous endoproteolysis between Thr291 and Ala299 and occur as stable N- and C-terminal fragments in normal and Alzheimer brain tissue. *Neurobiology of Disease,* 3**,** 325-37.

Popot, J. L. & Engelman, D. M. 2000. Helical membrane protein folding, stability, and evolution. *Annual Review of Biochemistry,* 69**,** 881-922.

Prokop, S., Shirotani, K., Edbauer, D., Haass, C. & Steiner, H. 2004. Requirement of PEN-2 for stabilization of the presenilin N-/C-terminal fragment heterodimer within the γ-Secretase Complex *Journal of Biological Chemistry,* 279**,** 23255-23261.

Puzzo, D., Privitera, L., Fa, M., Staniszewski, A., Hashimoto, G., Aziz, F., Sakurai, M., Ribe, E. M., Troy, C. M., Mercken, M., Jung, S. S., Palmeri, A. & Arancio, O. 2011. Endogenous amyloid-β is necessary for hippocampal synaptic plasticity and memory. *Annals of Neurology,* 69**,** 819-830.

Puzzo, D., Privitera, L., Leznik, E., Fà, M., Staniszewski, A., Palmeri, A. & Arancio, O. 2008. Picomolar amyloid-β positively modulates synaptic plasticity and memory in hippocampus. *Journal of Neuroscience,* 28**,** 14537-45.

Qi-Takahara, Y., Morishima-Kawashima, M., Tanimura, Y., Dolios, G., Hirotani, N., Horikoshi, Y., Kametani, F., Maeda, M., Saido, T. C., Wang, R. & Ihara, Y. 2005. Longer forms of amyloid β protein: implications for the mechanism of intramembrane cleavage by γ-secretase. *Journal of Neuroscience,* 25**,** 436-45.

Quint, S., Widmaier, S., Minde, D., Hornburg, D., Langosch, D. & Scharnagl, C. 2010. Residue-specific side-chain packing determines the backbone dynamics of transmembrane model helices. *Biophysical Journal,* 99**,** 2541-9.

Ran, Y., Hossain, F., Pannuti, A., Lessard, C. B., Ladd, G. Z., Jung, J. I., Minter, L. M., Osborne, B. A., Miele, L. & Golde, T. E. 2017. γ-Secretase inhibitors in cancer clinical trials are pharmacologically and functionally distinct. *EMBO Molecular Medicine,* 9**,** 950-966.

Rawson, R. B., Zelenski, N. G., Nijhawan, D., Ye, J., Sakai, J., Hasan, M. T., Chang, T. Y., Brown, M. S. & Goldstein, J. L. 1997. Complementation cloning of S2P, a gene encoding a putative metalloprotease required for intramembrane cleavage of SREBPs. *Molecular Cell,* 1**,** 47-57.

Ren, Z., Schenk, D., Basi, G. S. & Shapiro, I. P. 2007. Amyloid β-protein precursor juxtamembrane domain regulates specificity of γ-secretase-dependent cleavages. *Journal of Biological Chemistry,* 282**,** 35350-35360.

Rizzo, P., Osipo, C., Foreman, K., Golde, T., Osborne, B. & Miele, L. 2008. Rational targeting of Notch signaling in cancer. *Oncogene,* 27**,** 5124-31.

Robakis, N. K., Ramakrishna, N., Wolfe, G. & Wisniewski, H. M. 1987. Molecular cloning and characterization of a cDNA encoding the cerebrovascular and the neuritic plaque amyloid peptides. *Proceedings of the National Academy of Sciences of the United States of America,* 84**,** 4190-4.

Robertson, A. L., Headey, S. J., Ng, N. M., Wijeyewickrema, L. C., Scanlon, M. J., Pike, R. N. & Bottomley, S. P. 2016. Protein unfolding is essential for cleavage within the α-helix of a model protein substrate by the serine protease, thrombin. *Biochimie,* 122**,** 227-234.

Rogaev, E. I., Sherrington, R., Rogaeva, E. A., Levesque, G., Ikeda, M., Liang, Y., Chi, H., Lin, C., Holman, K., Tsuda, T. & Et Al. 1995. Familial Alzheimer's disease in kindreds with missense mutations in a gene on chromosome 1 related to the Alzheimer's disease type 3 gene. *Nature,* 376**,** 775-8.

Rogers, K., Felsenstein, K. M., Hrdlicka, L., Tu, Z., Albayya, F., Lee, W., Hopp, S., Miller, M.-J., Spaulding, D., Yang, Z., Hodgdon, H., Nolan, S., Wen, M., Costa, D., Blain, J.-F., Freeman, E., De Strooper, B., Vulsteke, V., Scrocchi, L., Zetterberg, H., Portelius, E., Hutter-Paier, B., Havas, D., Ahlijanian, M., Flood, D., Leventhal, L., Shapiro, G., Patzke, H., Chesworth, R. & Koenig, G. 2012. Modulation of γ-secretase by EVP-0015962 reduces amyloid deposition and behavioral deficits in Tg2576 mice. *Molecular Neurodegeneration,* 7**,** 61-61.

Rynearson, K. D., Ponnusamy, M., Prikhodko, O., Xie, Y., Zhang, C., Nguyen, P., Hug, B., Sawa, M., Becker, A., Spencer, B., Florio, J., Mante, M., Salehi, B., Arias, C., Galasko, D., Head, B. P., Johnson, G., Lin, J. H., Duddy, S. K., Rissman, R. A., Mobley, W. C., Thinakaran, G., Tanzi, R. E. & Wagner, S. L. 2021. Preclinical validation of a potent γ-secretase modulator for Alzheimer's disease prevention. *Journal of Experimental Medicine,* 218**,** e20202560.

Saito, T., Suemoto, T., Brouwers, N., Sleegers, K., Funamoto, S., Mihira, N., Matsuba, Y., Yamada, K., Nilsson, P., Takano, J., Nishimura, M., Iwata, N., Van Broeckhoven, C., Ihara, Y. & Saido, T. C. 2011. Potent amyloidogenicity and pathogenicity of Aβ43. *Nature Neuroscience,* 14**,** 1023-32.

Sakai, J., Duncan, E. A., Rawson, R. B., Hua, X., Brown, M. S. & Goldstein, J. L. 1996. Sterol-regulated release of SREBP-2 from cell membranes requires two sequential cleavages, one within a transmembrane segment. *Cell,* 85**,** 1037-1046.

Sambamurti, K., Shioi, J., Anderson, J. P., Pappolla, M. A. & Robakis, N. K. 1992. Evidence for intracellular cleavage of the Alzheimer's amyloid precursor in PC12 cells. *Journal of Neuroscience Research,* 33**,** 319-29.

Sannerud, R., Esselens, C., Ejsmont, P., Mattera, R., Rochin, L., Tharkeshwar, A. K., De Baets, G., De Wever, V., Habets, R., Baert, V., Vermeire, W., Michiels, C., Groot, A. J., Wouters, R., Dillen, K., Vints, K., Baatsen, P., Munck, S., Derua, R., Waelkens, E., Basi, G. S., Mercken, M., Vooijs, M., Bollen, M., Schymkowitz, J., Rousseau, F., Bonifacino, J. S., Van Niel, G., De Strooper, B. & Annaert, W. 2016. Restricted location of PSEN2/γ-secretase determines substrate specificity and generates an intracellular Aβ pool. *Cell,* 166**,** 193-208.

Sastre, M., Steiner, H., Fuchs, K., Capell, A., Multhaup, G., Condron, M. M., Teplow, D. B. & Haass, C. 2001. Presenilin-dependent γ-secretase processing of β-amyloid precursor protein at a site corresponding to the S3 cleavage of Notch. *EMBO Reports* 2**,** 835-41.

Sato, C., Morohashi, Y., Tomita, T. & Iwatsubo, T. 2006. Structure of the catalytic pore of γ-secretase probed by the accessibility of substituted cysteines. *Journal of Neuroscience,* 26**,** 12081-8.

Sato, C., Takagi, S., Tomita, T. & Iwatsubo, T. 2008. The C-terminal PAL motif and transmembrane domain 9 of presenilin 1 are involved in the formation of the catalytic pore of the γ-secretase. *Journal of Neuroscience,* 28**,** 6264-6271.

Sato, T., Diehl, T. S., Narayanan, S., Funamoto, S., Ihara, Y., De Strooper, B., Steiner, H., Haass, C. & Wolfe, M. S. 2007. Active γ-secretase complexes contain only one of each component. *Journal of Biological Chemistry,* 282**,** 33985-93.

Sato, T., Tang, T.-C., Reubins, G., Fei, J. Z., Fujimoto, T., Kienlen-Campard, P., Constantinescu, S. N., Octave, J.-N., Aimoto, S. & Smith, S. O. 2009. A helix-to-coil transition at the ε-cut site in the transmembrane dimer of the amyloid precursor protein is required for proteolysis. *Proceedings of the National Academy of Sciences,* 106**,** 1421-1426.

Schäfer, A., Zick, M., Kief, J., Steger, M., Heide, H., Duvezin-Caubet, S., Neupert, W. & Reichert, A. S. 2010. Intramembrane proteolysis of Mgm1 by the mitochondrial rhomboid protease is highly promiscuous regarding the sequence of the cleaved hydrophobic segment. *Journal of Molecular Biology,* 401**,** 182-93.

Scharnagl, C., Pester, O., Hornburg, P., Hornburg, D., Götz, A. & Langosch, D. 2014. Side-chain to main-chain hydrogen bonding controls the intrinsic backbone dynamics of the amyloid precursor protein transmembrane helix. *Biophysical Journal,* 106**,** 1318-26.

Scheuner, D., Eckman, C., Jensen, M., Song, X., Citron, M., Suzuki, N., Bird, T. D., Hardy, J., Hutton, M., Kukull, W., Larson, E., Levy-Lahad, E., Viitanen, M., Peskind, E., Poorkaj, P., Schellenberg, G., Tanzi, R., Wasco, W., Lannfelt, L., Selkoe, D. & Younkin, S. 1996. Secreted amyloid β-protein similar to that in the senile plaques of Alzheimer's disease is increased in vivo by the presenilin 1 and 2 and APP mutations linked to familial Alzheimer's disease. *Nature Medicine,* 2**,** 864-70.

Schroeter, E. H., Kisslinger, J. A. & Kopan, R. 1998. Notch-1 signalling requires ligand-induced proteolytic release of intracellular domain. *Nature,* 393**,** 382-6.

Selkoe, D. J. 1991. The molecular pathology of Alzheimer's disease. *Neuron,* 6**,** 487-98.

Selkoe, D. J. & Hardy, J. 2016. The amyloid hypothesis of Alzheimer's disease at 25 years. *EMBO Molecular Medicine,* 8**,** 595-608.

Sengoku, R. 2020. Aging and Alzheimer's disease pathology. *Neuropathology,* 40**,** 22-29.

Seubert, P., Vigo-Pelfrey, C., Esch, F., Lee, M., Dovey, H., Davis, D., Sinha, S., Schlossmacher, M., Whaley, J., Swindlehurst, C. & Et Al. 1992. Isolation and quantification of soluble Alzheimer's β-peptide from biological fluids. *Nature,* 359**,** 325-7.

Shah, S., Lee, S. F., Tabuchi, K., Hao, Y. H., Yu, C., Laplant, Q., Ball, H., Dann, C. E., 3rd, Südhof, T. & Yu, G. 2005. Nicastrin functions as a γ-secretase-substrate receptor. *Cell,* 122**,** 435-47.

Shankar, G. M., Li, S., Mehta, T. H., Garcia-Munoz, A., Shepardson, N. E., Smith, I., Brett, F. M., Farrell, M. A., Rowan, M. J., Lemere, C. A., Regan, C. M., Walsh, D. M., Sabatini, B. L. & Selkoe, D. J. 2008. Amyloid-β protein dimers isolated directly from Alzheimer's brains impair synaptic plasticity and memory. *Nature Medicine,* 14**,** 837-42.

Shen, J., Bronson, R. T., Chen, D. F., Xia, W., Selkoe, D. J. & Tonegawa, S. 1997. Skeletal and CNS defects in Presenilin-1-deficient mice. *Cell,* 89**,** 629-39.

Sherrington, R., Rogaev, E. I., Liang, Y., Rogaeva, E. A., Levesque, G., Ikeda, M., Chi, H., Lin, C., Li, G., Holman, K., Tsuda, T., Mar, L., Foncin, J. F., Bruni, A. C., Montesi, M. P., Sorbi, S., Rainero, I., Pinessi, L., Nee, L., Chumakov, I., Pollen, D., Brookes, A., Sanseau, P., Polinsky, R. J., Wasco, W., Da Silva, H. A., Haines, J. L., Perkicak-Vance, M. A., Tanzi, R. E., Roses, A. D., Fraser, P. E., Rommens, J. M. & St George-Hyslop, P. H. 1995. Cloning of a gene bearing missense mutations in early-onset familial Alzheimer's disease. *Nature,* 375**,** 754-60.

Shirotani, K., Edbauer, D., Capell, A., Schmitz, J., Steiner, H. & Haass, C. 2003. γ-Secretase activity is associated with a conformational change of Nicastrin. *Journal of Biological Chemistry,* 278**,** 16474-7.

Shirotani, K., Edbauer, D., Kostka, M., Steiner, H. & Haass, C. 2004a. Immature Nicastrin stabilizes APH-1 independent of PEN-2 and presenilin: identification of nicastrin mutants that selectively interact with APH-1. *Journal of Neurochemistry,* 89**,** 1520-1527.

Shirotani, K., Edbauer, D., Prokop, S., Haass, C. & Steiner, H. 2004b. Identification of distinct γ-secretase complexes with different APH-1 variants. *Journal of Biological Chemistry,* 279**,** 41340-5.

Shirotani, K., Tomioka, M., Kremmer, E., Haass, C. & Steiner, H. 2007. Pathological activity of familial Alzheimer's disease-associated mutant presenilin can be executed by six different γ-secretase complexes. *Neurobiology of Disease,* 27**,** 102-7.

Shoji, M., Golde, T. E., Ghiso, J., Cheung, T. T., Estus, S., Shaffer, L. M., Cai, X. D., Mckay, D. M., Tintner, R., Frangione, B. & Et Al. 1992. Production of the Alzheimer amyloid β protein by normal proteolytic processing. *Science,* 258**,** 126-9.

Siemers, E. R., Dean, R. A., Friedrich, S., Ferguson-Sells, L., Gonzales, C., Farlow, M. R. & May, P. C. 2007. Safety, tolerability, and effects on plasma and cerebrospinal fluid amyloid-β after inhibition of γ-secretase. *Clinical Neuropharmacology,* 30**,** 317-25.

Siemers, E. R., Quinn, J. F., Kaye, J., Farlow, M. R., Porsteinsson, A., Tariot, P., Zoulnouni, P., Galvin, J. E., Holtzman, D. M., Knopman, D. S., Satterwhite, J., Gonzales, C., Dean, R. A. & May, P. C. 2006. Effects of a γ-secretase inhibitor in a randomized study of patients with Alzheimer disease. *Neurology,* 66**,** 602-4.

Silber, M., Hitzenberger, M., Zacharias, M. & Muhle-Goll, C. 2020. Altered hinge conformations in APP transmembrane helix mutants may affect enzyme–substrate interactions of γ-secretase. *ACS Chemical Neuroscience,* 11**,** 4426-4433.

Sims, R., Hill, M. & Williams, J. 2020. The multiplex model of the genetics of Alzheimer's disease. *Nature Neuroscience,* 23**,** 311-322.

Sinha, S., Anderson, J. P., Barbour, R., Basi, G. S., Caccavello, R., Davis, D., Doan, M., Dovey, H. F., Frigon, N., Hong, J., Jacobson-Croak, K., Jewett, N., Keim, P., Knops, J., Lieberburg, I., Power, M., Tan, H., Tatsuno, G., Tung, J., Schenk, D., Seubert, P., Suomensaari, S. M., Wang, S., Walker, D., Zhao, J., Mcconlogue, L. & John, V. 1999. Purification and cloning of amyloid precursor protein β-secretase from human brain. *Nature,* 402**,** 537-40.

Sisodia, S. S. 1992. β-Amyloid precursor protein cleavage by a membrane-bound protease. *Proceedings of the National Academy of Sciences of the United States of America,* 89**,** 6075-6079.

Sisodia, S. S., Koo, E. H., Beyreuther, K., Unterbeck, A. & Price, D. L. 1990. Evidence that β-amyloid protein in Alzheimer's disease is not derived by normal processing. *Science,* 248**,** 492-5.

Slack, B. E., Ma, L. K. & Seah, C. C. 2001. Constitutive shedding of the amyloid precursor protein ectodomain is up-regulated by tumour necrosis factor-α converting enzyme. *Biochemical Journal,* 357**,** 787-94.

Slunt, H. H., Thinakaran, G., Von Koch, C., Lo, A. C., Tanzi, R. E. & Sisodia, S. S. 1994. Expression of a ubiquitous, cross-reactive homologue of the mouse β-amyloid precursor protein (APP). *Journal of Biological Chemistry,* 269**,** 2637-44.

Smith, C. K., Withka, J. M. & Regan, L. 1994. A thermodynamic scale for the β-sheet forming tendencies of the amino acids. *Biochemistry,* 33**,** 5510-7.

Somavarapu, A. K. & Kepp, K. P. 2017. Membrane dynamics of γ-secretase provides a molecular basis for β-amyloid binding and processing. *ACS Chemical Neuroscience,* 8**,** 2424-2436.

Soscia, S. J., Kirby, J. E., Washicosky, K. J., Tucker, S. M., Ingelsson, M., Hyman, B., Burton, M. A., Goldstein, L. E., Duong, S., Tanzi, R. E. & Moir, R. D. 2010. The Alzheimer's disease-associated amyloid β-protein is an antimicrobial peptide. *PLOS ONE,* 5**,** e9505.

Spitz, C., Schlosser, C., Guschtschin-Schmidt, N., Stelzer, W., Menig, S., Götz, A., Haug-Kröper, M., Scharnagl, C., Langosch, D., Muhle-Goll, C. & Fluhrer, R. 2020. Non-canonical shedding of TNFα by SPPL2a is determined by the conformational flexibility of its transmembrane helix. *iScience,* 23.

Steiner, A., Schlepckow, K., Brunner, B., Steiner, H., Haass, C. & Hagn, F. 2020. γ-Secretase cleavage of the Alzheimer risk factor TREM2 is determined by its intrinsic structural dynamics. *EMBO Journal,* 39**,** e104247.

Steiner, H., Duff, K., Capell, A., Romig, H., Grim, M. G., Lincoln, S., Hardy, J., Yu, X., Picciano, M., Fechteler, K., Citron, M., Kopan, R., Pesold, B., Keck, S., Baader, M., Tomita, T., Iwatsubo, T., Baumeister, R. & Haass, C. 1999a. A loss of function mutation of presenilin-2 interferes with amyloid β-peptide production and Notch signaling. *Journal of Biological Chemistry,* 274**,** 28669-73.

Steiner, H., Fukumori, A., Tagami, S. & Okochi, M. 2018. Making the final cut: pathogenic amyloid-β peptide generation by γ-secretase. *Cell Stress,* 2**,** 292-310.

Steiner, H., Kostka, M., Romig, H., Basset, G., Pesold, B., Hardy, J., Capell, A., Meyn, L., Grim, M. L., Baumeister, R., Fechteler, K. & Haass, C. 2000. Glycine 384 is required for presenilin-1 function and is conserved in bacterial polytopic aspartyl proteases. *Nature Cell Biology,* 2**,** 848-51.

Steiner, H., Romig, H., Pesold, B., Philipp, U., Baader, M., Citron, M., Loetscher, H., Jacobsen, H. & Haass, C. 1999b. Amyloidogenic function of the Alzheimer's disease-associated presenilin 1 in the absence of endoproteolysis. *Biochemistry,* 38**,** 14600-5.

Steiner, H., Winkler, E., Edbauer, D., Prokop, S., Basset, G., Yamasaki, A., Kostka, M. & Haass, C. 2002. PEN-2 is an integral component of the γ-secretase complex required for coordinated expression of presenilin and Nicastrin. *Journal of Biological Chemistry,* 277**,** 39062-5.

Stelzer, W. & Langosch, D. 2019. Conformationally flexible sites within the transmembrane helices of amyloid precursor protein and Notch1 receptor. *Biochemistry,* 58**,** 3065-3068.

Stelzer, W., Scharnagl, C., Leurs, U., Rand, K. D. & Langosch, D. 2016. The impact of the 'Austrian' mutation of the amyloid precursor protein transmembrane helix is communicated to the hinge region. *ChemistrySelect,* 1**,** 4408-4412.

Strisovsky, K., Sharpe, H. J. & Freeman, M. 2009. Sequence-specific intramembrane proteolysis: identification of a recognition motif in rhomboid substrates. *Molecular Cell,* 36**,** 1048-1059.

Struhl, G. & Adachi, A. 1998. Nuclear access and action of notch in vivo. *Cell,* 93**,** 649-60.

Struhl, G. & Adachi, A. 2000. Requirements for presenilin-dependent cleavage of Notch and other transmembrane proteins. *Molecular Cell,* 6**,** 625-636.

Sun, L., Li, X. & Shi, Y. 2016. Structural biology of intramembrane proteases: mechanistic insights from rhomboid and S2P to γ-secretase. *Current Opinion in Structural Biology,* 37**,** 97-107.

Sun, L., Zhao, L., Yang, G., Yan, C., Zhou, R., Zhou, X., Xie, T., Zhao, Y., Wu, S., Li, X. & Shi, Y. 2015. Structural basis of human γ-secretase assembly. *Proceedings of the National Academy of Sciences,* 112**,** 6003-6008.

Suzuki, N., Cheung, T. T., Cai, X. D., Odaka, A., Otvos, L., Jr., Eckman, C., Golde, T. E. & Younkin, S. G. 1994. An increased percentage of long amyloid β protein secreted by familial amyloid β protein precursor (β APP717) mutants. *Science,* 264**,** 1336-40.

Szaruga, M., Munteanu, B., Lismont, S., Veugelen, S., Horré, K., Mercken, M., Saido, T. C., Ryan, N. S., De Vos, T., Savvides, S. N., Gallardo, R., Schymkowitz, J., Rousseau, F., Fox, N. C., Hopf, C., De Strooper, B. & Chávez-Gutiérrez, L. 2017. Alzheimer's-causing mutations shift Aβ length by destabilizing γ-secretase-Aβn interactions. *Cell,* 170**,** 443-456.e14.

Takami, M., Nagashima, Y., Sano, Y., Ishihara, S., Morishima-Kawashima, M., Funamoto, S. & Ihara, Y. 2009. γ-Secretase: successive tripeptide and tetrapeptide release from the transmembrane domain of β-carboxyl terminal fragment. *Journal of Neuroscience,* 29**,** 13042-13052.

Takasugi, N., Tomita, T., Hayashi, I., Tsuruoka, M., Niimura, M., Takahashi, Y., Thinakaran, G. & Iwatsubo, T. 2003. The role of presenilin cofactors in the γ-secretase complex. *Nature,* 422**,** 438-441.

Takeo, K., Tanimura, S., Shinoda, T., Osawa, S., Zahariev, I. K., Takegami, N., Ishizuka-Katsura, Y., Shinya, N., Takagi-Niidome, S., Tominaga, A., Ohsawa, N., Kimura-Someya, T., Shirouzu, M., Yokoshima, S., Yokoyama, S., Fukuyama, T., Tomita, T. & Iwatsubo, T. 2014. Allosteric regulation of γ-secretase activity by a phenylimidazole-type γ-secretase modulator. *Proceedings of the National Academy of Sciences,* 111**,** 10544-10549.

Tamaoka, A., Odaka, A., Ishibashi, Y., Usami, M., Sahara, N., Suzuki, N., Nukina, N., Mizusawa, H., Shoji, S. & Kanazawa, I. 1994. APP717 missense mutation affects the ratio of amyloid β protein species (Aβ1-42/43 and Aβ1-40) in familial Alzheimer's disease brain. *Journal of Biological Chemistry,* 269**,** 32721-4.

Tanaka, S., Shiojiri, S., Takahashi, Y., Kitaguchi, N., Ito, H., Kameyama, M., Kimura, J., Nakamura, S. & Ueda, K. 1989. Tissue-specific expression of three types of β-protein precursor mRNA: enhancement of protease inhibitor-harboring types in Alzheimer's disease brain. *Biochemical and Biophysical Research Communications,* 165**,** 1406-14.

Tang, B. L. 2020. Enhancing α-secretase processing for Alzheimer's disease-a view on SFRP1. *Brain sciences,* 10**,** 122.

Tang, T. C., Kienlen-Campard, P., Hu, Y., Perrin, F., Opsomer, R., Octave, J. N., Constantinescu, S. N. & Smith, S. O. 2019. Influence of the familial Alzheimer's

disease-associated T43I mutation on the transmembrane structure and γ-secretase processing of the C99 peptide. *Journal of Biological Chemistry,* 294**,** 5854-5866.

Tanii, H., Jiang, J., Fukumori, A., Tagami, S., Okazaki, Y., Okochi, M. & Takeda, M. 2006. Effect of valine on the efficiency and precision at S4 cleavage of the Notch-1 transmembrane domain. *Journal of Neuroscience Research,* 84**,** 918-25.

Tanzi, R. E., Gusella, J. F., Watkins, P. C., Bruns, G. A., St George-Hyslop, P., Van Keuren, M. L., Patterson, D., Pagan, S., Kurnit, D. M. & Neve, R. L. 1987. Amyloid β protein gene: cDNA, mRNA distribution, and genetic linkage near the Alzheimer locus. *Science,* 235**,** 880-4.

Tanzi, R. E., Mcclatchey, A. I., Lamperti, E. D., Villa-Komaroff, L., Gusella, J. F. & Neve, R. L. 1988. Protease inhibitor domain encoded by an amyloid protein precursor mRNA associated with Alzheimer's disease. *Nature,* 331**,** 528-530.

Tatsuta, T., Augustin, S., Nolden, M., Friedrichs, B. & Langer, T. 2007. m-AAA protease-driven membrane dislocation allows intramembrane cleavage by rhomboid in mitochondria. *EMBO Journal,* 26**,** 325-335.

Terry, R. D. 1963. The fine structure of neurofibrillary tangles in Alzheimer's disease. *Journal of Neuropathology and Experimental Neurology,* 22**,** 629-42.

Terry, R. D. 1995. Biologic differences between early- and late-onset Alzheimer disease. *Alzheimer Disease and Associated Disorders,* 9 Suppl 1**,** S26-7.

Thinakaran, G., Borchelt, D. R., Lee, M. K., Slunt, H. H., Spitzer, L., Kim, G., Ratovitsky, T., Davenport, F., Nordstedt, C., Seeger, M., Hardy, J., Levey, A. I., Gandy, S. E., Jenkins, N. A., Copeland, N. G., Price, D. L. & Sisodia, S. S. 1996. Endoproteolysis of presenilin 1 and accumulation of processed derivatives in vivo. *Neuron,* 17**,** 181-90.

Thinakaran, G., Kitt, C. A., Roskams, A. J., Slunt, H. H., Masliah, E., Von Koch, C., Ginsberg, S. D., Ronnett, G. V., Reed, R. R., Price, D. L. & Et Al. 1995. Distribution of an APP homolog, APLP2, in the mouse olfactory system: a potential role for APLP2 in axogenesis. *Journal of Neuroscience,* 15**,** 6314-26.

Thinakaran, G., Regard, J. B., Bouton, C. M., Harris, C. L., Price, D. L., Borchelt, D. R. & Sisodia, S. S. 1998. Stable association of presenilin derivatives and absence of presenilin interactions with APP. *Neurobiology of Disease,* 4**,** 438-53.

Tian, G., Sobotka-Briner, C. D., Zysk, J., Liu, X., Birr, C., Sylvester, M. A., Edwards, P. D., Scott, C. D. & Greenberg, B. D. 2002. Linear non-competitive inhibition of solubilized human γ-secretase by pepstatin A methylester, L685458, sulfonamides, and benzodiazepines. *Journal of Biological Chemistry,* 277**,** 31499-31505.

Timmer, J. C., Zhu, W., Pop, C., Regan, T., Snipas, S. J., Eroshkin, A. M., Riedl, S. J. & Salvesen, G. S. 2009. Structural and kinetic determinants of protease substrates. *Nature Structural and Molecular Biology,* 16**,** 1101-1108.

Tolia, A., Chávez-Gutiérrez, L. & De Strooper, B. 2006. Contribution of presenilin transmembrane domains 6 and 7 to a water-containing cavity in the γ-secretase complex. *Journal of Biological Chemistry,* 281**,** 27633-42.

Tolia, A., Horré, K. & De Strooper, B. 2008. Transmembrane domain 9 of presenilin determines the dynamic conformation of the catalytic site of γ-secretase. *Journal of Biological Chemistry,* 283**,** 19793-803.

Tomita, S., Kirino, Y. & Suzuki, T. 1998. Cleavage of Alzheimer's amyloid precursor protein (APP) by secretases occurs after O-glycosylation of APP in the protein secretory pathway: identification of intracellular compartments in which APP cleavage occurs without using toxic agents that interfere with protein metabolism. *Journal of Biological Chemistry,* 273**,** 6277-6284.

Toyn, J. H., Boy, K. M., Raybon, J., Meredith, J. E., Robertson, A. S., Guss, V., Hoque, N., Sweeney, F., Zhuo, X., Clarke, W., Snow, K., Denton, R. R., Zuev, D., Thompson, L. A., Morrison, J., Grace, J., Berisha, F., Furlong, M., Wang, J.-S., Lentz, K. A.,

Padmanabha, R., Cook, L., Wei, C., Drexler, D. M., Macor, J. E., Albright, C. F., Gasior, M., Olson, R. E., Hong, Q., Soares, H. D., Abutarif, M. & Ahlijanian, M. K. 2016. Robust translation of γ-secretase modulator pharmacology across preclinical species and human subjects. *Journal of Pharmacology and Experimental Therapeutics,* 358**,** 125-137.

Trambauer, J., Fukumori, A. & Steiner, H. 2020. Pathogenic Aβ generation in familial Alzheimer's disease: novel mechanistic insights and therapeutic implications. *Current Opinion in Neurobiology,* 61**,** 73-81.

Tsruya, R., Wojtalla, A., Carmon, S., Yogev, S., Reich, A., Bibi, E., Merdes, G., Schejter, E. & Shilo, B. Z. 2007. Rhomboid cleaves Star to regulate the levels of secreted Spitz. *EMBO Journal,* 26**,** 1211-20.

Tyndall, J. D. A., Nall, T. & Fairlie, D. P. 2005. Proteases universally recognize β strands in their active sites. *Chemical Reviews,* 105**,** 973-1000.

Uemura, K., Lill, C. M., Li, X., Peters, J. A., Ivanov, A., Fan, Z., Destrooper, B., Bacskai, B. J., Hyman, B. T. & Berezovska, O. 2009. Allosteric modulation of PS1/γ-secretase conformation correlates with amyloid β42/40 ratio. *PLOS ONE,* 4**,** e7893.

Urban, S. & Freeman, M. 2003. Substrate specificity of rhomboid intramembrane proteases is governed by helix-breaking residues in the substrate transmembrane domain. *Molecular Cell,* 11**,** 1425-34.

Urban, S., Lee, J. R. & Freeman, M. 2001. Drosophila rhomboid-1 defines a family of putative intramembrane serine proteases. *Cell,* 107**,** 173-82.

Vassar, R., Bennett, B. D., Babu-Khan, S., Kahn, S., Mendiaz, E. A., Denis, P., Teplow, D. B., Ross, S., Amarante, P., Loeloff, R., Luo, Y., Fisher, S., Fuller, J., Edenson, S., Lile, J., Jarosinski, M. A., Biere, A. L., Curran, E., Burgess, T., Louis, J. C., Collins, F., Treanor, J., Rogers, G. & Citron, M. 1999. β-Secretase cleavage of Alzheimer's amyloid precursor protein by the transmembrane aspartic protease BACE. *Science,* 286**,** 735-41.

Von Heijne, G. 1991. Proline kinks in transmembrane α-helices. *Journal of Molecular Biology,* 218**,** 499-503.

Vooijs, M., Schroeter, E. H., Pan, Y., Blandford, M. & Kopan, R. 2004. Ectodomain shedding and intramembrane cleavage of mammalian Notch proteins is not regulated through oligomerization. *Journal of Biological Chemistry,* 279**,** 50864-73.

Wahlster, L., Arimon, M., Nasser-Ghodsi, N., Post, K. L., Serrano-Pozo, A., Uemura, K. & Berezovska, O. 2013. Presenilin-1 adopts pathogenic conformation in normal aging and in sporadic Alzheimer's disease. *Acta Neuropathologica,* 125**,** 187-199.

Wan, C., Fu, J., Wang, Y., Miao, S., Song, W. & Wang, L. 2012. Exosome-related multi-pass transmembrane protein TSAP6 is a target of rhomboid protease RHBDD1-induced proteolysis. *PLOS ONE,* 7**,** e37452.

Wang, J., Beher, D., Nyborg, A. C., Shearman, M. S., Golde, T. E. & Goate, A. 2006a. C-terminal PAL motif of presenilin and presenilin homologues required for normal active site conformation. *Journal of Neurochemistry,* 96**,** 218-27.

Wang, J., Brunkan, A. L., Hecimovic, S., Walker, E. & Goate, A. 2004. Conserved "PAL" sequence in presenilins is essential for γ-secretase activity, but not required for formation or stabilization of γ-secretase complexes. *Neurobiology of Disease,* 15**,** 654-66.

Wang, J., Dickson, D. W., Trojanowski, J. Q. & Lee, V. M. 1999. The levels of soluble versus insoluble brain Aβ distinguish Alzheimer's disease from normal and pathologic aging. *Experimental Neurology,* 158**,** 328-37.

Wang, X., Cui, J., Li, W., Zeng, X., Zhao, J. & Pei, G. 2015. γ-Secretase modulators and inhibitors induce different conformational changes of presenilin 1 revealed by FLIM and FRET. *Journal of Alzheimer's Disease,* 47**,** 927-937.

Wang, Y., Zhang, Y. & Ha, Y. 2006b. Crystal structure of a rhomboid family intramembrane protease. *Nature,* 444**,** 179-80.

Ward, M. W., Concannon, C. G., Whyte, J., Walsh, C. M., Corley, B. & Prehn, J. H. 2010. The amyloid precursor protein intracellular domain(AICD) disrupts actin dynamics and mitochondrial bioenergetics. *Journal of Neurochemistry,* 113**,** 275-84.

Weggen, S. & Beher, D. 2012. Molecular consequences of amyloid precursor protein and presenilin mutations causing autosomal-dominant Alzheimer's disease. *Alzheimer's Research and Therapy,* 4**,** 9.

Weggen, S., Eriksen, J. L., Das, P., Sagi, S. A., Wang, R., Pietrzik, C. U., Findlay, K. A., Smith, T. E., Murphy, M. P., Bulter, T., Kang, D. E., Marquez-Sterling, N., Golde, T. E. & Koo, E. H. 2001. A subset of NSAIDs lower amyloidogenic Aβ42 independently of cyclooxygenase activity. *Nature,* 414**,** 212-216.

Weggen, S., Eriksen, J. L., Sagi, S. A., Pietrzik, C. U., Golde, T. E. & Koo, E. H. 2003a. Aβ42-lowering nonsteroidal anti-inflammatory drugs preserve intramembrane cleavage of the amyloid precursor protein (APP) and ErbB-4 receptor and signaling through the APP intracellular domain. *Journal of Biological Chemistry,* 278**,** 30748-30754.

Weggen, S., Eriksen, J. L., Sagi, S. A., Pietrzik, C. U., Ozols, V., Fauq, A., Golde, T. E. & Koo, E. H. 2003b. Evidence that nonsteroidal anti-inflammatory drugs decrease amyloid β42 production by direct modulation of γ-secretase activity. *Journal of Biological Chemistry,* 278**,** 31831-31837.

Weidemann, A., Eggert, S., Reinhard, F. B. M., Vogel, M., Paliga, K., Baier, G., Masters, C. L., Beyreuther, K. & Evin, G. 2002. A novel ε-cleavage within the transmembrane domain of the Alzheimer amyloid precursor protein demonstrates homology with Notch processing. *Biochemistry,* 41**,** 2825-2835.

Weihofen, A., Binns, K., Lemberg, M. K., Ashman, K. & Martoglio, B. 2002. Identification of signal peptide peptidase, a presenilin-type aspartic protease. *Science,* 296**,** 2215-8.

Welander, H., Frånberg, J., Graff, C., Sundström, E., Winblad, B. & Tjernberg, L. O. 2009. Aβ43 is more frequent than Aβ40 in amyloid plaque cores from Alzheimer disease brains. *Journal of Neurochemistry,* 110**,** 697-706.

WHO. 2020. *Dementia* [Online]. Available: https://www.who.int/news-room/fact-sheets/detail/dementia [Accessed 17.12.2020].

Wilson, R. S., Segawa, E., Boyle, P. A., Anagnos, S. E., Hizel, L. P. & Bennett, D. A. 2012. The natural history of cognitive decline in Alzheimer's disease. *Psychology Aging,* 27**,** 1008-17.

Wolfe, M. S. 2009. Intramembrane-cleaving proteases. *Journal of Biological Chemistry,* 284**,** 13969-13973.

Wolfe, M. S. 2020. Substrate recognition and processing by γ-secretase. *Biochimica et Biophysica Acta - Biomembranes,* 1862**,** 183016.

Wolfe, M. S., Citron, M., Diehl, T. S., Xia, W., Donkor, I. O. & Selkoe, D. J. 1998. A substrate-based difluoro ketone selectively inhibits Alzheimer's γ-secretase activity. *Journal of Medicinal Chemistry,* 41**,** 6-9.

Wolfe, M. S., Xia, W., Ostaszewski, B. L., Diehl, T. S., Kimberly, W. T. & Selkoe, D. J. 1999. Two transmembrane aspartates in presenilin-1 required for presenilin endoproteolysis and γ-secretase activity. *Nature,* 398**,** 513-7.

Wong, G. T., Manfra, D., Poulet, F. M., Zhang, Q., Josien, H., Bara, T., Engstrom, L., Pinzon-Ortiz, M., Fine, J. S., Lee, H. J., Zhang, L., Higgins, G. A. & Parker, E. M. 2004. Chronic treatment with the γ-secretase inhibitor LY-411,575 inhibits β-amyloid peptide production and alters lymphopoiesis and intestinal cell differentiation. *Journal of Biological Chemistry,* 279**,** 12876-82.

Wong, P. C., Zheng, H., Chen, H., Becher, M. W., Sirinathsinghji, D. J., Trumbauer, M. E., Chen, H. Y., Price, D. L., Van Der Ploeg, L. H. & Sisodia, S. S. 1997. Presenilin 1 is

required for Notch1 and DII1 expression in the paraxial mesoderm. *Nature,* 387**,** 288-92.

Wouters, R., Michiels, C., Sannerud, R., Kleizen, B., Dillen, K., Vermeire, W., Ayala, A. E., Demedts, D., Schekman, R. & Annaert, W. 2021. Assembly of γ-secretase occurs through stable dimers after exit from the endoplasmic reticulum. *Journal of Cell Biology,* 220.

Wu, J., Anwyl, R. & Rowan, M. J. 1995. β-amyloid-(1–40) increases long-term potentiation in rat hippocampus in vitro. *European Journal of Pharmacology,* 284**,** R1-R3.

Wu, Z., Yan, N., Feng, L., Oberstein, A., Yan, H., Baker, R. P., Gu, L., Jeffrey, P. D., Urban, S. & Shi, Y. 2006. Structural analysis of a rhomboid family intramembrane protease reveals a gating mechanism for substrate entry. *Nature Structural and Molecular Biology,* 13**,** 1084-1091.

Xia, W. & Wolfe, M. S. 2003. Intramembrane proteolysis by presenilin and presenilin-like proteases. *Journal of Cell Science,* 116**,** 2839-44.

Xie, T., Yan, C., Zhou, R., Zhao, Y., Sun, L., Yang, G., Lu, P., Ma, D. & Shi, Y. 2014. Crystal structure of the γ-secretase component Nicastrin. *Proceedings of the National Academy of Sciences,* 111**,** 13349-13354.

Xu, T.-H., Yan, Y., Kang, Y., Jiang, Y., Melcher, K. & Xu, H. E. 2016. Alzheimer's disease-associated mutations increase amyloid precursor protein resistance to γ-secretase cleavage and the Aβ42/Aβ40 ratio. *Cell Discovery,* 2**,** 16026.

Yamasaki, A., Eimer, S., Okochi, M., Smialowska, A., Kaether, C., Baumeister, R., Haass, C. & Steiner, H. 2006. The GxGD motif of presenilin contributes to catalytic function and substrate identification of γ-secretase. *Journal of Neuroscience,* 26**,** 3821-3828.

Yamazaki, T., Koo, E. H. & Selkoe, D. J. 1996. Trafficking of cell-surface amyloid β-protein precursor. II. Endocytosis, recycling and lysosomal targeting detected by immunolocalization. *Journal of Cell Science,* 109**,** 999-1008.

Yan, R., Bienkowski, M. J., Shuck, M. E., Miao, H., Tory, M. C., Pauley, A. M., Brashier, J. R., Stratman, N. C., Mathews, W. R., Buhl, A. E., Carter, D. B., Tomasselli, A. G., Parodi, L. A., Heinrikson, R. L. & Gurney, M. E. 1999. Membrane-anchored aspartyl protease with Alzheimer's disease β-secretase activity. *Nature,* 402**,** 533-7.

Yan, Y., Xu, T. H., Melcher, K. & Xu, H. E. 2017. Defining the minimum substrate and charge recognition model of γ-secretase. *Acta Pharmacologica Sinica,* 38**,** 1412-1424.

Yanagida, K., Okochi, M., Tagami, S., Nakayama, T., Kodama, T. S., Nishitomi, K., Jiang, J., Mori, K., Tatsumi, S., Arai, T., Ikeuchi, T., Kasuga, K., Tokuda, T., Kondo, M., Ikeda, M., Deguchi, K., Kazui, H., Tanaka, T., Morihara, T., Hashimoto, R., Kudo, T., Steiner, H., Haass, C., Tsuchiya, K., Akiyama, H., Kuwano, R. & Takeda, M. 2009. The 28-amino acid form of an APLP1-derived Aβ-like peptide is a surrogate marker for Aβ42 production in the central nervous system. *EMBO Molecular Medicine,* 1**,** 223-35.

Yang, D. S., Tandon, A., Chen, F., Yu, G., Yu, H., Arawaka, S., Hasegawa, H., Duthie, M., Schmidt, S. D., Ramabhadran, T. V., Nixon, R. A., Mathews, P. M., Gandy, S. E., Mount, H. T., St George-Hyslop, P. & Fraser, P. E. 2002. Mature glycosylation and trafficking of Nicastrin modulate its binding to presenilins. *Journal of Biological Chemistry,* 277**,** 28135-42.

Yang, G., Zhou, R., Guo, X., Yan, C., Lei, J. & Shi, Y. 2021. Structural basis of γ-secretase inhibition and modulation by small molecule drugs. *Cell,* 184**,** 521-533.e14.

Yang, G., Zhou, R., Zhou, Q., Guo, X., Yan, C., Ke, M., Lei, J. & Shi, Y. 2019. Structural basis of Notch recognition by human γ-secretase. *Nature,* 565**,** 192-197.

Ye, J., Davé, U. P., Grishin, N. V., Goldstein, J. L. & Brown, M. S. 2000. Asparagine-proline sequence within membrane-spanning segment of SREBP triggers intramembrane cleavage by Site-2 protease. *Proceedings of the National Academy of Sciences,* 97**,** 5123-5128.

Yin, Y. I., Bassit, B., Zhu, L., Yang, X., Wang, C. & Li, Y. M. 2007. γ-Secretase substrate concentration modulates the Aβ42/Aβ40 ratio: implications for Alzheimer disease. *Journal of Biological Chemistry,* 282**,** 23639-44.

Yoshikai, S., Sasaki, H., Doh-Ura, K., Furuya, H. & Sakaki, Y. 1990. Genomic organization of the human amyloid β-protein precursor gene. *Gene,* 87**,** 257-63.

Yu, C., Kim, S. H., Ikeuchi, T., Xu, H., Gasparini, L., Wang, R. & Sisodia, S. S. 2001. Characterization of a presenilin-mediated amyloid precursor protein carboxyl-terminal fragment γ. Evidence for distinct mechanisms involved in γ-secretase processing of the APP and Notch1 transmembrane domains. *Journal of Biological Chemistry,* 276**,** 43756-60.

Yu, G., Chen, F., Levesque, G., Nishimura, M., Zhang, D. M., Levesque, L., Rogaeva, E., Xu, D., Liang, Y., Duthie, M., St George-Hyslop, P. H. & Fraser, P. E. 1998. The presenilin 1 protein is a component of a high molecular weight intracellular complex that contains β-catenin. *Journal of Biological Chemistry,* 273**,** 16470-5.

Yu, G., Nishimura, M., Arawaka, S., Levitan, D., Zhang, L., Tandon, A., Song, Y. Q., Rogaeva, E., Chen, F., Kawarai, T., Supala, A., Levesque, L., Yu, H., Yang, D. S., Holmes, E., Milman, P., Liang, Y., Zhang, D. M., Xu, D. H., Sato, C., Rogaev, E., Smith, M., Janus, C., Zhang, Y., Aebersold, R., Farrer, L. S., Sorbi, S., Bruni, A., Fraser, P. & St George-Hyslop, P. 2000. Nicastrin modulates presenilin-mediated Notch/glp-1 signal transduction and βAPP processing. *Nature,* 407**,** 48-54.

Yu, Y., Logovinsky, V., Schuck, E., Kaplow, J., Chang, M.-K., Miyagawa, T., Wong, N. & Ferry, J. 2014. Safety, tolerability, pharmacokinetics, and pharmacodynamics of the novel γ-secretase modulator, E2212, in healthy human subjects. *The Journal of Clinical Pharmacology,* 54**,** 528-536.

Yücel, S. S., Stelzer, W., Lorenzoni, A., Wozny, M., Langosch, D. & Lemberg, M. K. 2019. The metastable XBP1u transmembrane domain defines determinants for intramembrane proteolysis by signal peptide peptidase. *Cell Reports,* 26**,** 3087-3099.e11.

Zhang, J., Ye, W., Wang, R., Wolfe, M. S., Greenberg, B. D. & Selkoe, D. J. 2002. Proteolysis of chimeric β-amyloid precursor proteins containing the Notch transmembrane domain yields amyloid β-like peptides. *Journal of Biological Chemistry,* 277**,** 15069-15075.

Zhang, M., Haapasalo, A., Kim, D. Y., Ingano, L. A., Pettingell, W. H. & Kovacs, D. M. 2006. Presenilin/γ-secretase activity regulates protein clearance from the endocytic recycling compartment. *FASEB Journal,* 20**,** 1176-8.

Zhang, X., Hoey, R. J., Lin, G., Koide, A., Leung, B., Ahn, K., Dolios, G., Paduch, M., Ikeuchi, T., Wang, R., Li, Y.-M., Koide, S. & Sisodia, S. S. 2012. Identification of a tetratricopeptide repeat-like domain in the Nicastrin subunit of γ-secretase using synthetic antibodies. *Proceedings of the National Academy of Sciences,* 109**,** 8534-8539.

Zhang, Y. W., Wang, R., Liu, Q., Zhang, H., Liao, F. F. & Xu, H. 2007. Presenilin/γ-secretase-dependent processing of β-amyloid precursor protein regulates EGF receptor expression. *Proceedings of the National Academy of Sciences of the United States of America,* 104**,** 10613-8.

Zhang, Z., Nadeau, P., Song, W., Donoviel, D., Yuan, M., Bernstein, A. & Yankner, B. A. 2000. Presenilins are required for γ-secretase cleavage of β-APP and transmembrane cleavage of Notch-1. *Nature Cell Biology,* 2**,** 463-465.

Zhao, G., Cui, M. Z., Mao, G., Dong, Y., Tan, J., Sun, L. & Xu, X. 2005. γ-Cleavage is dependent on ζ-cleavage during the proteolytic processing of amyloid precursor protein within its transmembrane domain. *Journal of Biological Chemistry,* 280**,** 37689-97.

Zhao, G., Mao, G., Tan, J., Dong, Y., Cui, M. Z., Kim, S. H. & Xu, X. 2004. Identification of a new presenilin-dependent ζ-cleavage site within the transmembrane domain of amyloid precursor protein. *Journal of Biological Chemistry,* 279**,** 50647-50.

Zhao, H., Zhu, J., Cui, K., Xu, X., O'brien, M., Wong, K. K., Kesari, S., Xia, W. & Wong, S. T. 2009. Bioluminescence imaging reveals inhibition of tumor cell proliferation by Alzheimer's amyloid β protein. *Cancer Cell International* 9**,** 15.

Zheng, X., Liu, D., Roychaudhuri, R., Teplow, D. B. & Bowers, M. T. 2015. Amyloid beta-Protein Assembly: Differential Effects of the Protective A2T Mutation and Recessive A2V Familial Alzheimer's Disease Mutation. *ACS Chem Neurosci,* 6**,** 1732-40.

Zhou, R., Yang, G., Guo, X., Zhou, Q., Lei, J. & Shi, Y. 2019. Recognition of the amyloid precursor protein by human γ-secretase. *Science,* 363.

Appendix

I. Additional Data

Table 1: TMD-Sequence of γ-secretase substrates featuring a GG-/GGG-hinge. The substrates are taken from the list of γ-secretase substrates published by Güner and Lichtenthaler (2020) and the TMD sequence is taken from the UniProt database. GG-/GGG-hinge motifs are highlighted in bold.

Nr.	UniProt code	Substrate	TMD sequence
1	P51693	APLP1	AVSGLLIMGA**GGG**SLIVLSMLLL
2	P05067	APP	GAIIGLMV**GG**VVIATVIVITLVML
3	Q6PDJ1	CACHD1	VGPVA**GG**IMGCIMVLVLAVYA
4	Q8R5M8	CADM1	AVI**GG**VVAVVVFAMLCLLIIL
5	P12830	E-Cadherin	IL**GG**ILALLILILLLLLF
6	P29317	EphA2	I**GG**VAVGVVLLLVLAGVGFFI
7	Q15303	ErbB4	LIAAGVI**GG**LFILVIVGLTFAVYV
8	P48551	IFNaR2	I**GG**IITVFLIALVLTSTIVTL
9	P08069	IGF1R	LIIALPVAVLLIV**GG**LVIMLYVFH
10	P27930	IL1R2	ASSTFSWGIVLAPLSLAFLVL**GG**IWM
11	P08887	IL6Rα	TFLVA**GG**SLAFGTLLCIAIVL
12	Q76MJ5	IRE2	QDLLAASLTAVLL**GG**WILFVM
13	Q9JKF6	Nectin-1	II**GG**VAGSVLLVLIVVGGIIV
16	P32507	Nectin-2	II**GG**IIAAIIATAVAGTGILI
14	Q9JLB9	Nectin-3	IIASVV**GG**ALFLVLVSILAGV
15	Q9H3W5	NLRR3	LMACL**GG**LLGIIGVICLISCL
17	Q15109	RAGE	LALGIL**GG**LGTAALLIGVILW
18	Q7TSK2	SEZ6	LAAAIFLPLVAMVLLV**GG**VYL
19	Q9BYH1	SEZ6L	LAIFIPVLIISLLL**GG**AYIYI
20	P18827	Syndecan-1	GVIA**GG**LVGLIFAVCLVGFML
21	P34741	Syndecan-2	VLAAVIA**GG**VIGFLFAIFLILLLVY
22	O75056	Syndecan-3	AVIV**GG**VVGALFAAFLVTLLI
23	O60939	VGSCb2	VIVGASV**GG**FLAVVILVLMVV
24	Q8IWT1	VGSCb4	TLIILAVV**GG**VIGLLILILLI
25	P98156	VLDLR	AAWAILPLLLLVMAAV**GG**YLMW

Table 2: Content of β-branched residues (T, V, and I) in the TM-C of all known γ-secretase substrates. The substrates are taken from the list of γ-secretase substrates published by Güner and Lichtenthaler (2020) and the TMD sequence is taken from the UniProt database. All threonines (T), valines (V), and isoleucines (I) are highlighted in red and the number of β-branched residues within the TM-C (TVI content) is listed, as well as the relative amount of β-branched residues within the TM-C of each substrate (percent TVI).

Nr.	UniProt code	Substrate	TM-C	TVI content	Percent TVI
1	Q63155	DCC	VLVVVIVAVI	8	80,00
2	P54753	EphB3	VVAVVVIAIV	8	80,00
3	Q92859	Neogenin	IVVVVIIAVF	8	80,00
4	P35613	CD147	VLVLVTIIFI	7	70,00
5	O75509	DR6	VLVVIVVCSI	7	70,00
6	P54763	EphB2	LIAVVVIAIV	7	70,00
7	P54760	EphB4	LVLVVIVVAV	7	70,00
8	Q9JKF6	Nectin-1	VLIVVGGIIV	7	70,00
9	Q6UX71	PLXDC2	IVATAILVTV	7	70,00
10	P05067	APP	IATVIVITLVML	8	66,67
11	P16422	EpCAM	AVVAGIVVLVI	7	63,64
12	Q99523	Sortilin	LVTVVAGVLIV	7	63,64
13	P35070	βcellulin	VFIILVIGVC	6	60,00
14	P52800	EphrinB2	IIITLVVLLL	6	60,00
15	P48551	IFNaR2	LVLTSTIVTL	6	60,00
16	P14778	IL1R1	VIIVCSVFIY	6	60,00
17	P56974	Neuregulin-2	LVVGIVCVVA	6	60,00
18	Q86YL7	Podoplanin	GFIGAIIVVV	6	60,00
19	Q810F0	PRiMA	LVFLTVLVII	6	60,00
20	Q9UIK5	TMEFF2	AVICVVVLCI	6	60,00
21	P33151	VE-cadherin	ITVITLLIFL	6	60,00
22	O60939	VGSCb2	AVVILVLMVV	6	60,00
23	Q06481	APLP2	IATVIVISLVML	7	58,33
24	D3ZZK3	EphA4	VVILIAAFVIS	6	54,55
25	Q9NZR2	LRP1B	ITTLVIGLVLC	6	54,55
26	O75581	LRP6	TIFVSGTVYFI	6	54,55
27	P28828	PTPμ	VIIFLGVVLVM	6	54,55
28	Q15262	PTPkappa	ILLLLVVILIV	6	54,55
29	Q91XX1	PCDH γ-C3	AVTVLGVIIFKVY	7	53,85
30	Q15303	ErbB4	LVIVGLTFAVYV	6	50,00
31	P01892	HLA-A2	VITGAVVAAVMW	6	50,00
32	Q8NFT8	DNER	LMLIILIVGI	5	50,00
33	P98172	EphrinB1	VIFLLIIIFL	5	50,00
34	Q61851	FGFR3	ILVVAAVILC	5	50,00
35	Q9Z2W9	GluR3	IGVSVVLFLV	5	50,00

Nr.	UniProt code	Substrate	TM-C	TVI content	Percent TVI
36	O75460	Ire1α	IGWVAFIITY	5	50,00
37	Q9Y6J6	KCNE2	FSFIIVAILV	5	50,00
38	P10586	LAR	ILIVIAILLF	5	50,00
39	O15146	MUSK	FVLLTITTLY	5	50,00
40	Q589G5	Protogenin	CILICILILI	5	50,00
41	P32507	PVRL2	TAVAGTGILI	5	50,00
42	Q6UXD5	SEZ6L2	VIVLGSGVYI	5	50,00
43	Q62656	Ptprz1	ICLVVLVGILIYW	6	46,15
44	Q6DR98	Neuregulin-1	VVGIMCVVAYC	5	45,45
45	P08138	p75-NTR	VVVGLVAYIAF	5	45,45
46	P16882	GHR	GVAVMLFVVIFS	5	41,67
47	P14925	PAM	PVLVLLAIVMFI	5	41,67
48	I6LBW6	PCDH γ A1	IFLAFVIVLLVL	5	41,67
49	O94985	Alcadein a	LVFMIILGVF	4	40,00
50	Q9H4D0	Alcadein g	MLVFVVAMGV	4	40,00
51	Q9BQT9	Alcadein β	LVLMVVLGLV	4	40,00
52	Q6PDJ1	CACHD1	IMVLVLAVYA	4	40,00
53	Q90762	Cadherin-6B	LVTVVLFAAL	4	40,00
54	P16070	CD44	ALILAVCIAV	4	40,00
55	Q4VA61	DSCAML1	TLGVALLFVV	4	40,00
56	P54756	EphA5	LLAVVIGVLL	4	40,00
57	Q15375	EphA7	IILVFMVFGF	4	40,00
58	P08887	IL6Rα	GTLLCIAIVL	4	40,00
59	P06213	IR	VVIGSIYLFL	4	40,00
60	P19022	N-Cadherin	LILVLMFVVW	4	40,00
61	Q9JLB9	Nectin-3	LVLVSILAGV	4	40,00
62	Q9H3W5	NLRR3	IGVICLISCL	4	40,00
63	O35516	Notch2	ILFFILLGVI	4	40,00
64	Q9Y6N7	ROBO1	IILMVFSIWL	4	40,00
65	Q8WY21	SorCS1	FVGLAVFVIY	4	40,00
66	Q8IWT1	VGSCb4	IGLLILILLI	4	40,00
67	P41217	CD200	VILLVLISILLYW	5	38,46
68	Q14118	Dystroglycan	ILLIAGIIAMICY	5	38,46
69	P16150	CD43	AVIVLVALLLL	4	36,36
70	P15941	MUC1	VALAIVYLIAL	4	36,36
71	P09758	TROP2	ALVAGMAVLVI	4	36,36
72	P14209	CD99	VAVAGAISSFIA	4	33,33
73	P08069	IGF1R	VGGLVIMLYVFH	4	33,33
74	Q07954	LRP1	LLVLVAGVVFWY	4	33,33
75	P35590	Tie1	CLTILAALLTLV	4	33,33
76	P07147	TYRP1	VALIFGTASYLI	4	33,33
77	Q63722	Jagged1	WVCCLVTAFYWCV	4	30,77
78	Q91XY5	PCDH γ A3	CIFLAFVIVLLAL	4	30,77
79	P11117	ACP2	LFLLIVLLLT	3	30,00

Nr.	UniProt code	Substrate	TM-C	TVI content	Percent TVI
80	P30530	AXL	CVLILALFLV	3	30,00
81	P78310	CAR	ALALIGLIIF	3	30,00
82	Q9H2A7	CXCL16	ILTAALSYVL	3	30,00
83	Q9ERC8	DSCAM	VLLLFVLLLV	3	30,00
84	P29317	EphA2	LVLAGVGFFI	3	30,00
85	O15197	EphB6	FLLLAAITVL	3	30,00
86	Q9Y624	F11R	LGILVFGIWF	3	30,00
87	Q9Y219	Jagged2	SVLWLACVVL	3	30,00
88	Q9UEF7	Klotho	SIISLSLIFY	3	30,00
89	Q12866	MER	LILYISLAIR	3	30,00
90	P40967	Pmel17	MAVVLASLIY	3	30,00
91	Q13308	PTK7	IIAVLGLMFY	3	30,00
92	Q15109	RAGE	AALLIGVILW	3	30,00
93	Q7TSK2	SEZ6	MVLLVGGVYL	3	30,00
94	O75056	Syndecan-3	FAAFLVTLLI	3	30,00
95	Q06418	TYRO3	VTAAALALIL	3	30,00
96	P35916	VEGFR3	VFFWVLLLLI	3	30,00
97	Q61483	Delta1	LLLGCAAVVVC	3	27,27
98	P15382	KCNE1	FFTLGIMLSYI	3	27,27
99	P11627	L1	LLLVLLILCFI	3	27,27
100	Q8CJ26	NRADD	VILGLLAYVAF	3	27,27
101	P17948	VEGF-R1	TLFWLLLTLFI	3	27,27
102	Q07699	VGSCb1	IWLVAEMIYCY	3	27,27
103	P34741	Syndecan-2	LFAIFLILLLVY	3	25,00
104	P04629	TRKA	LSTLLLVL	2	25,00
105	P12830	E-Cadherin	ILILLLLLF	2	22,22
106	Q8R5M8	CADM1	FAMLCLLIIL	2	20,00
107	P78423	CX3CL1	FCLGVAMFTY	2	20,00
108	Q92896	GLG1	ILFLIGLMCG	2	20,00
109	Q76MJ5	Ire1 ß	LLGGWILFVM	2	20,00
110	P0DI97	Neurexin-1-β	LCILILLYAM	2	20,00
111	Q63376	Neurexin-2-β	LCILILLYAM	2	20,00
112	Q9HDB5	Neurexin-3-β	LCILILLYAM	2	20,00
113	P0CC10	NGL-3	MAAVMLVAFY	2	20,00
114	Q01705	Notch1	LFFVGCGVLL	2	20,00
115	Q767I8	PCDH a4	SLLVLTLLLY	2	20,00
116	Q9NPG4	PCDH12	GLILALFMSI	2	20,00
117	Q9BYH1	SEZ6L	LLLGGAYIYI	2	20,00
118	Q92673	SorLA	LSLGVGFAIL	2	20,00
119	P18827	Syndecan-1	FAVCLVGFML	2	20,00
120	P11344	Tyrosinase	LTALLAGLVS	2	20,00
121	P29812	TYRP2	VGLFVLLAFL	2	20,00
122	Q9JK00	VGSCb3	LWLLIEMIYC	2	20,00
123	P51693	APLP1	GSLIVLSMLLL	2	18,18

Nr.	UniProt code	Substrate	TM-C	TVI content	Percent TVI
124	Q02223	BCMA	SLAVFVLMFLL	2	18,18
125	Q03167	βglycan	ALLTGALWYIY	2	18,18
126	P01130	LDLR	VFLCLGVFLLW	2	18,18
127	P98156	VLDLR	VMAAVGGYLMW	2	18,18
128	P15209	Tkrb	VGFCLLVMLLLL	2	16,67
129	P27930	IL1R2	LSLAFLVLGGIWM	2	15,38
130	Q14114	ApoER2	ALLCMSGYLI	1	10,00
131	P09581	CSF1R	LVLLLLLLLY	1	10,00
132	P22455	FGFR4	AVLLLLAGLY	1	10,00
133	Q99K10	Neuroligin-1	LNILAFAALY	1	10,00
134	Q69ZK9	Neuroligin-2	LNILAFAALY	1	10,00
135	Q8VHY0	NG2	LALILPLLFY	1	10,00
136	Q61982	Notch3	LLALGALLVL	1	10,00
137	P31695	Notch4	LLALGALLVL	1	10,00
138	P08F94	Polyductin	SWLALSCLVC	1	10,00
139	P78324	SIRPα	ALLMAALYLV	1	10,00
140	P19438	TNFR1	CLLSLLFIGL	1	10,00
141	Q9NZC2	TREM2	KILAASALWA	1	10,00
142	Q6EMK4	Vasorin	LAALAAVGAA	1	10,00
143	Q14126	Desmoglein-2	LLLLLVPLLLLM	1	8,33
144	Q14626	IL11RA	AGALALGLWL	0	0,00
145	Q6E0K3	Megalin[1]	-	-	-
146	P08581	MET	LLLLLGFFLWL	0	0,00
147	P70180	NPR-C	AGLLMAFYFF	0	0,00
148	Q6P1B4	Pianp[1]	-	-	-
149	P98161	Polycystin-1[2]	-	-	-

[1] No TMD sequence available on UniProt.

[2] This protein has multiple TMDs and it is not clear where γ-secretase cleaves this protein.

II. List of Abbreviations

A	Alanine, one letter code
AA	Amino acid
AD	Alzheimer's disease
ADAM	A Disintegrin and metalloprotease
AICD	APP intracellular domain
AK	Alzheimer Krankheit
APH-1	Anterior pharynx defective-1
APH-1aL	Anterior pharynx defective 1a, long splice variant
APH-1aS	Anterior pharynx defective 1a, short splice variant
APLP	APP-like protein
ApoE	Apolipoprotein E
APP	Amyloid precursor protein
APS	Ammonium persulfate
Aβ	Amyloid-β
BACE	Beta-site APP cleaving enzyme
Bpa	*Para*-benzoyl-L-phenylalanine
BSA	Bovine serum albumin
βx	β-strand x
Caax	C: Cystein, a: aliphatic amino acids, X: other amino acid
CD44	Cluster of differentiation 44
CHAPSO	3-([3-Cholamidopropyl]dimethylammonio)-2-hydroxy-1-propansulfonat
cryo-EM	Cryogenic electron microscopy
CTF	C-terminal fragment
CTFα	C-terminal fragment of APP, generated via cleavage by α-secretase
CTFβ	C-terminal fragment of APP, generated via cleavage by β-secretase
DHX	Deuterium hydrogen exchange
DMSO	Dimethylsulfoxid
DTT	Dithiothreitol
ECD	Extracellular domain
ER	Endoplasmatic reticulum
FAD	Familiar Alzheimer´s disease
FDA	Food and Drug Administration
FTLD	Frontotemporal lobar degeneration
g	Gram or acceleration of gravity
G	Glycine, one letter code
GG	Double glycine (glycine-glycine)
GSI	γ-secretase inhibitor
GSM	γ-secretase modulator
H$_2$O	Water
HRP	Horseradish peroxidase
IB	Immunoblotting
ICD	Intracellular domain

IMP	Intramembrane protease
IP	Immunoprecipitation
IPTG	Isopropyl-β-D-thiogalactopyranosid
L	Leucine, one letter code
LB	Lysogeny broth
LE	Late endosome
LYS	Lysosomal compartment
M	Mouse
MD	Molecular dynamics
MVBs	Multivesicular bodies
NCT	Nicastrin
NFT	Neurofibrillary tangle
NICD	Notch intracellular domain
NMR	Nuclear magnetic resonance
NTA	Nitrilotriacetic acid
NTF	N-terminal fragment
OD	Optical density
P	Proline, one letter code
PD	Parkinson's disease
PEN-2	Presenilin Enhancer-2
PI	Protease inhibitor
PM	Plasma membrane
polyLeu	stretch of consequtive leucines (poly leucine)
PS	Presenilin
PS-CTF	Presenilin C-terminal fragment
PS-NTF	Presenilin N-terminal fragment
R	Rat
Ras	Rat sarcoma
Rb	Rabbit
Rce1	RAS-converting enzyme 1
RT	Room temperature
SAD	Sporadic form of AD
sAPPα	Soluble APPα, generated via cleavage by α-secretase
sAPPβ	Soluble APPβ, generated via cleavage by β-secretase
SDS	Sodium dodecyl sulfate
PAGE	Polyacrylamide gel electrophoresis
SPPL3	Signal peptide peptidase-like 3
TEMED	Tetramethylethylendiamin
TM-C	C-terminal half of the transmembrane domain
TMD	Transmembrane domain
TM-N	N-terminal half of the transmembrane domain
VEGFR1	Vascular endothelial growth factor receptor 1
WT	Wild-type

III. List of Publications

The following publications are part of this thesis:

1. Götz A, **Mylonas N,** Högel P, Silber M, Heinel H, Menig S, Vogel A, Feyrer H, Huster D, Luy B, Langosch D, Scharnagl C, Muhle-Goll C, Kamp F, Steiner H. Modulating Hinge Flexibility in the APP Transmembrane Domain Alters γ-Secretase Cleavage. *Biophys J.* 2019 Jun 4;116(11):2103-2120. doi: 10.1016/j.bpj.2019.04.030. *
2. **Werner NT**[§], Högel P[§], Güner G[§], Stelzer W, Lichtenthaler SF, Steiner H, and Langosch D. Cooperation of N- and C-terminal substrate transmembrane domain segments in intramembrane proteolysis by γ-secretase.
   [§] These authors contributed equally.
   This manuscript has been submitted to Cell Reports (15th of February 2022).

*Authors can 'use and share their works for scholarly purposes (with full acknowledgement of the original article): Include in a thesis or dissertation (provided this is not published commercially)' (https://www.elsevier.com/about/policies/copyright#Author-rights).

IV. Acknowledgements

The last few years have been a great, but also very intense and sometimes challenging journey during which I have learned a lot and grown in so many ways. I am very grateful to have had the opportunity to do a PhD in such a great environment and with all the support I received from my supervisor, my colleagues, friends, and family but also from the Graduate School of Systemic Neuroscience and the Hand and Ilse Breuer Foundation.

First of all, I would like to thank my supervisor, **Harald Steiner**, for all the support and helpful advice you gave me throughout my PhD, and for the possibility to attend several meetings and conferences. Thank you for always being available whenever needed and for giving me the opportunity to make decisions for myself and thus become confident in my abilities. Also, I am truly grateful for your support with my first author publication.

Many thanks also to **Christian Haass**, for your support and advice not only on scientific matters, for the many scientific discussions and your input. Thank you also for the opportunity to meet many great scientists during my time as a PhD Representative.

Special thanks go to my team members and colleagues, **Gabi, Edith, Johannes, Lukas, and Edgar,** for helping each other out, for all the discussions of smaller and bigger experimental problems which were always helpful. During the last few years we became like a small family, supporting each other inside and outside the lab and sharing so many things, lab stuff, food, conversations, and anecdotes. But most importantly, I want to thank you for not missing out on the fun in all of this, especially when it was a very long day or when something did not work out as planned.

I would like to thank my collaborators, **Alexander Götz, Alexander Vogel, Burkhard Luy, Christina Scharnagl, Claudia Muhle-Goll, Daniel Huster, Dieter Langosch, Gökhan Güner, Hannes Heinel, Hannes Feyrer, Mara Silber, Philipp Högel, Simon Menning, Walter Stelzer,** and **Stefan Lichtenthaler** for the productive and successful cooperation. Also, I want to thank our whole DFG FOR2290 **Forschergruppe**, our meetings and conferences were always fun and full of great discussions and fruitful conversations.

Huge thanks also to **Sabine Odoy** and **Marcel Matt**, without your support and help nothing would work in the lab.

To my thesis committee members, **Moritz Rossner** and **Marco Düring**. I really appreciate having you as my TAC members. Thank you both for all your helpful advice, your critical comments, and your insights throughout my PhD, as well as the different perspective you brought to the meetings. All of this has contributed to the progress of my PhD.

A heartfelt thanks goes to the **Hans and Ilse Breuer Foundation** for all the support I have received within the last years. The scholarship has made many things possible for me, and I am especially grateful for having had the opportunity to attend several international conferences (which was also made possible in part by the support of the GSN). At the same time, I am so grateful to be part of the **GSN** family. It was fantastic to be able to attend so many interesting workshops, to get to know many bright-minded people, as well as to be part of the Kids Brain Day. All the support I received, not only from the GSN itself, but also from all the other students has helped me grow as a scientist but also as a person.

To my awesome girls, **Isi, Laura, Moni, Babsi, and Krissi,** who were always there for me. Thank you so much for all the fun we had together, for the many places and parties we have been, for the profound talks we had, for supporting me during the wedding preparations - including the many useful tips and tricks –, as well as for your patience, for cheering me up during difficult times, and for reminding me to take everything a bit less seriously.

Life inside and outside the lab would not have been the same without many great people I got to know on my way. Together with **Alex, Julia, Susa, Karsten, Laura, Hanne, Meike, Mareike, Lukas, Johannes,** and **Georg**, we had lots of fun, many great events, but also many scientific discussions. Thank you all for sticking together, for helping everyone out, and for cheering one another up. You have made the past years a great journey ☺ Also, thanks **Mareike** and **Alex** for having been PhD Reps with me and for making organization of many scientific and social events so much fun. It wasn't always easy, but I think we did a pretty good job. ;)

My whole family**:** my grandma **Inge**, my brother **Manu** and his wife **Mona,** but especially my parents **Michaela** and **Josef**, for always being there for me when I needed them and always having an open ear and good advice for me. For always believing in me, for always cheering me up and for your never-ending support, in every way**.** For your patience and for being able to shape my life the way I want to. Thank you so much for everything, I am blessed to have you as a family. I am very grateful that I have two wonderful families now. Heike, Andreas, Andrea

and her family and Markus, I am thankful that you have lovingly taken me in and supported me in the last few years.

Georg, you are the most wonderful husband I could have ever asked for. Thank you so much for all your support, your love, and your patience over the past years, as well as for walking this path together, which often involved late nights and many scientific discussions. For all the adventures we have been on together, for making me laugh, for always surprising me, and for believing in me. I am so incredibly grateful to have you by my side, and I am looking forward to what lies ahead. We can do it!

V. Declaration of Author Contributions

Declaration of Author Contributions

Publication 1: (Götz, Mylonas, et al., 2019) 'Modulating Hinge Flexibility in the APP Transmembrane Domain Alters γ-Secretase Cleavage.'

Götz A, **Mylonas N,** Högel P, Silber M, Heinel H, Menig S, Vogel A, Feyrer H, Huster D, Luy B, Langosch D, Scharnagl C, Muhle-Goll C, Kamp F, Steiner H.

D.H., B.L., D.L., C.S., C.M.-G., and H.S. conceived the study, designed experiments, analyzed and interpreted data, and supervised research. A.G. performed all-atom and S.M. coarse-grained MD simulations. F.K. performed CD spectroscopy. N.M. performed cleavage assays. P.H. performed HDX experiments, and M.S., H.H., A.V., and H.F. performed NMR spectroscopy. A.G., S.M., F.K., N.T.M., P.H., M.S., H.H., A.V., and H.F. analyzed and interpreted data. F.K. coordinated the drafting and writing of the manuscript. F.K., C.M.-G., A.G., C.S., and H.S. wrote the manuscript with contributions of all authors.

My contribution to this publication in detail:

For this publication, I designed, generated, and purified the C99-based substrates which I investigated using the *in vitro* (cell free) assay. I performed the *in vitro* cleavage assays, analyzed the levels of cleavage products generated (AICD and Aβ) by immunoblotting and further quantified the AICD and Aβ levels. To analyze the different AICD and A*β* species via mass spectrometry, I did further cleavage assays with an additional immunoprecipitation step to capture the generated Aβ peptides. Figure 1 (B-F) comprises all the data I have contributed to this publication. Additionally, I interpreted data and commented on the manuscript.

Publication 2: Werner *et al.*, (to be submitted soon) 'Cooperation of N- and C-terminal substrate transmembrane domain segments in intramembrane proteolysis by γ-secretase.'

Nadine T. Werner[§], Philipp Högel[§], Gökhan Güner[§], Walter Stelzer, Stefan F. Lichtenthaler, Harald Steiner, and Dieter Langosch.

[§]These authors contributed equally.

NTW performed *in vitro* cleavage assays, PH and WS did DHX assays, GG performed *in cellulo* cleavage assays. DL, SL, and HS designed and supervised the project. DL wrote the manuscript together with the co-authors. All authors analysed their data, created their figures and have given approval to the final version of the manuscript.

My contribution to this publication in detail:

For this second study, I designed, generated, and purified the C99-based constructs which I investigated in this study. I performed *in vitro* (cell free) cleavage assays, analyzed the cleavage efficiency of all the different constructs via immunoblotting, and quantified the levels of cleavage products generated. I did additional *in vitro* assays in order to analyze the different AICD and Aβ species generated via mass spectrometry (matrix-assisted laser desorption/ionization time-of-flight, MALDI-TOF). Prior to the MALDI-TOF analysis I performed an immunoprecipitation step to capture the respective cleavage products (AICD or Aβ, separately). All the data I have contributed to this publication can be found in figures 2-4, B-G. Further, I interpreted the data and helped to write the manuscript.